

TWO-PHASE FLOW IN TIGHT GAS SANDS

FINAL REPORT
(April 1986-November 1989)

Prepared by

P. CHOWDIAH
D. J. SOEDER

INSTITUTE OF GAS TECHNOLOGY
3424 South State Street
Chicago, Illinois 60616

IGT Project No. 30603

for

GAS RESEARCH INSTITUTE
Contract No. 5086-211-1258

GRI PROJECT MANAGER
PAUL TROUSIL

November 1990

LEGAL NOTICE This report was prepared by Institute of Gas Technology ("IGT") as an account of work sponsored by Gas Research Institute ("GRI"). Neither GRI, members of GRI, IGT, nor any person acting on behalf of either:

- a. Makes any warranty or representation, expressed or implied, with respect to the accuracy, completeness, or usefulness of the information contained in this report, or that the use of any information, apparatus, method, or process disclosed in this report may not infringe privately owned rights, or
- b. Assumes any liability with respect to the use of, or for damages resulting from the use of, any information, apparatus, method, or process disclosed in this report.

Reference to trade names or specific commercial products, commodities, or services in this report does not represent or constitute an endorsement, recommendation, or opinion of suitability by GRI or IGT of the specific commercial product, commodity, or service.

REPORT DOCUMENTATION PAGE	1. REPORT NO.	2.	3. Recipient's Accession No.
4. Title and Subtitle TWO-PHASE FLOW IN TIGHT GAS SANDS - FINAL REPORT (DRAFT)		5. Report Date MAY 1990	
7. Author(s) P. CHOWDIAH, D. J. SOEDER		6.	
9. Performing Organization Name and Address INSTITUTE OF GAS TECHNOLOGY 3424 SOUTH STATE STREET CHICAGO, ILLINOIS 60616		8. Performing Organization Rept. No.	
12. Sponsoring Organization Name and Address GAS RESEARCH INSTITUTE 8600 WEST BRYN MAWR AVENUE CHICAGO, ILLINOIS 60631		10. Project/Task/Work Unit No. 30603-00	
		11. Contract(C) or Grant(G) No. (C) 5086-211-1258 (G)	
		13. Type of Report & Period Covered FINAL REPORT	
15. Supplementary Notes FINAL REPORT FOR THIS PROJECT		14. 4-01-86 to 11-30-89	
16. Abstract (Limit: 200 words) Analyses of 55 core samples from moderate to low-permeability sandstones in the Travis Peak Formation and underlying Cotton Valley Group in eastern Texas have been performed at IGT. Results of these analyses, as well as earlier work at IGT, demonstrate that tight gas sandstone is a distinct petrologic type, where unique correlations have been found between features of the pore geometry and matrix flow properties. Recognition and quantification of this relationship has led to an improved understanding of the nature of two-phase (gas/water) fluid flow through these rocks. Relative permeability and critical gas saturation measurements on these samples revealed the need for improved laboratory techniques for handling tight rocks. Confining stress cycling and the method of establishing partial water saturations were found to be particularly important. The results of this work should lead to better laboratory methodology for analyzing tight sands, and the pore structure studies should help to improve the correlations between reservoir quality and the geological properties of these rocks.			
17. Document Analysis a. Descriptors Tight gas sandstone, core analysis, formation evaluation, sandstone petrology, low-permeability rocks, unconventional gas			
b. Identifiers/Open-Ended Terms Travis Peak Sandstone, eastern Texas, Cotton Valley Group, Staged Field Experiments, sandstone permeability, pore geometry			
c. COSATI Field/Group			
18. Availability Statement unlimited release of approved version		19. Security Class (This Report) unclassified	21. No. of Pages 233
		20. Security Class (This Page) unclassified	22. Price

RESEARCH SUMMARY

Title Two-Phase Flow Analysis -- Final Report (Draft)

Contractor Institute of Gas Technology

GRI Contract No. 5086-211-1258

Principal Investigator Daniel J. Soeder

Report Period December 1987 - March 1989
Final Report

Objective To develop an understanding of reservoir properties and gas transport mechanisms in tight sands of interest to the Gas Research Institute (GRI) through petrography and core analysis under pressures representative of producing conditions. This report describes the results of analyses performed by the Institute of Gas Technology (IGT) on sandstone core from GRI's Staged Field Experiment wells and from other cooperative wells in eastern Texas.

Technical Perspective Reliable measurements of relative permeabilities to gas and liquid are necessary when estimating reserves and productivity in natural gas reservoirs, especially tight reservoirs. Because of the difficulties inherent in accurately measuring two-phase flow behavior in tight sands, precise laboratory measurements made under carefully reproduced in-situ net pressures and water saturations are required to evaluate the effects of pore structure and water content on gas flow. These data can reduce some of the uncertainty in wireline well log interpretation, and indicate the presence of inaccurate assumptions sometimes incorporated into numerical reservoir simulators. Work at IGT and elsewhere has shown that many of the reservoir properties that influence tight sand gas production are very different from those affecting the gas productivity of conventional, high permeability reservoirs. For example, permeability of tight sands is reduced by an increase in effective stress during drawdown, which exerts virtually no significant influence on gas productivity in a conventional reservoir. This program investigates these unique tight sand reservoir properties in an attempt to define realistic parameters for reliable log analysis and reservoir simulation, specifically for reservoirs in eastern Texas.

Results Significant results of the work are detailed below:

- The pore geometry of tight sands was discovered to fall into three major groups, defined by the nature of the flowpaths. Type 1 consists of primary porosity with pore throats clogged by authigenic clay or calcite. Type 2 is

the most common, and consists of secondary pores developed at the sites of unstable mineral grains, while primary porosity is almost totally occluded by quartz overgrowths. Flowpaths consist of narrow, crack-like or "slot" pores along the boundaries between adjoining quartz overgrowths. Type 3 consists of sand grains suspended in an all-pervasive, fine, microporous matrix of clay or carbonate. Each type was found to correlate to a particular set of petrophysical properties.

- The Travis Peak and Taylor sandstone core analysis, petrography, and mercury porosimetry data were analyzed together with earlier data from Mesaverde tight sandstone cores from the Rocky Mountains. Results indicate that generalized correlations for tight sands may be possible for rapidly and inexpensively assessing the quality of a tight sandstone reservoir using petrography and mercury porosimetry.
- Drainage experiments showed the Travis Peak samples to have critical gas saturations of the order of 10%. This is similar to values measured earlier on the tight Mesaverde sandstone.
- Both imbibition and evaporation experiments showed that water redistribution in these tight sands is very slow and difficult. As a result, neither of these methods for varying sample water saturation yielded the kind of uniform saturation needed for meaningful relative permeability measurements. Future work utilizing an x-ray imaging system will help understand water movement in these rocks better.

Technical
Approach

The technical approach is to utilize the capabilities of specialized core analysis hardware and petrography to understand the roles that different pore geometries in tight sand play with respect to relative permeability and its changes with pressure that occur during actual production from Travis Peak reservoirs. Emphasis is also placed on understanding the extent to which results obtained are dependent upon laboratory procedures and on establishing procedures such that laboratory results are valid quantitative descriptions of the in-situ reservoir. Detailed analysis of the pore geometry of the eastern Texas tight gas sandstones combined with accurate measurements of reservoir properties, is leading to a greater understanding of gas/water interaction and fluid transport phenomena in these rocks.

Project
Implications

The research performed by IGT has resulted in a much better understanding of pore geometry for tight gas sandstone reservoirs which impacts industry's ability to accurately identify potential pay zones and to accurately predict producibility. IGT has developed simple and rapid

petrographic/mercury porosimetry techniques to categorize tight gas sandstones into groups from which a better forecast of future production performance may be made. The relative permeability experiments have been pioneering because they involved extremely low permeability rock. This effort has identified numerous problems in attempting to acquire this data and also has identified topics of future research which will help overcome these obstacles. Successful future acquisition of relative permeability data for tight gas sandstones will greatly aid reservoir simulation studies and will allow producers to more accurately predict the volume and duration of gas production from their producing properties.

GRI Project Manager: Mark R. Johnson
Tight Gas Sands Geology

TABLE OF CONTENTS

	<u>Page</u>
1.0. PROGRAM OBJECTIVES	1
1.1. Overall Objective of the Program	1
1.2. Specific Objectives	1
2.0. WORK PLAN	3
3.0. WORK PERFORMED	5
4.0. DRY CORE ANALYSIS	7
4.1. Experimental and Analytical Methods	7
4.1.1. Mean Pore Width and Tortuosity	7
4.1.2. Pore Volume Compressibility	8
4.1.3. Stress Dependence of Permeability	9
4.1.4. Mercury Porosimetry	9
4.1.5. Sample Preparation	10
4.2. Mast A-1 Data	10
4.3. SFE No. 1 Data	15
4.4. SFE No. 2 Data	20
4.5. SFE No. 3 Data	24
4.5.1. Lithology	24
4.5.2. Reservoir Properties	26
5.0. PORE STRUCTURE STUDIES	31
5.1. Petrographic Methods	31
5.2. Results	33
6.0. RESERVOIR PROPERTY CORRELATIONS	47
6.1. Porosity and Permeability	47
6.2. SFE No. 3 Chip Analysis	52
7.0. TWO-PHASE FLOW STUDIES	61

TABLE OF CONTENTS, Cont.

	<u>Page</u>
7.1. Drainage Measurements	61
7.1.1. Procedure	61
7.1.2. Results	64
7.2. Desaturation by Evaporation	68
7.2.1. Mast A-1 Data	69
7.2.2. SFE No. 2 Data	71
7.2.3. Water Distribution During Evaporation	76
7.3. Imbibition Experiments	77
8.0. MAJOR ACHIEVEMENTS	81
9.0. MAJOR TECHNICAL PROBLEM AREAS	83
10.0. CONCLUSIONS	85
11.0. RECOMMENDATIONS	87
12.0. REFERENCES CITED	89
APPENDIX A. Detailed Core Analysis Data for SFE No. 3 Samples	A-1
APPENDIX B. Technical Papers Published From This Project	B-1

LIST OF FIGURES

<u>Figure No.</u>		<u>Page</u>
1	Location of GRI Tight Sand Wells in East Texas	6
2	Location of Mast A-1 Well in Eastern Texas and Cored Intervals in the Travis Peak From Which IGT Samples Were Selected	11
3	Location of IGT Samples in Core From the SFE No. 1 Well From the Upper Productive Zone and Lower Productive Zone	16
4	Location of IGT Samples in Core From the SFE No. 2 Well	21
5	Three Types of Internal Pore/Grain Structures Present in Tight Gas Sandstone	34
6	Photomicrographs of Travis Peak Sandstone From SFE No. 1 Core, 6122.8 ft Depth	36
7	Photomicrographs of Travis Peak Sandstone From SFE No. 1 Core, 7418.2 ft Depth	37
8	Photomicrographs of Travis Peak Sandstone From SFE No. 1 Core, 7419.9 ft Depth	38
9	Photomicrographs of Travis Peak Sandstone From SFE No. 1 Core, 7457.8 ft Depth	39
10	Photomicrographs of Travis Peak Sandstone From SFE No. 2 Core, 8275 ft	41
11	Photomicrographs of Travis Peak Sandstone From SFE No. 2 Well, 8730 ft	42
12	Photomicrographs of Travis Peak Sandstone from SFE No. 2 Well, 9492 ft	43
13	Photomicrographs of Travis Peak Sandstone, SFE No. 2 Well, 9875.9 ft	44
14	Gas Porosity Measured From Core Versus Depth in East Texas Tight Sandstones	48
15	Dry Gas Permeability From Core Analysis Versus Depth in East Texas Tight Sandstones	49
16	Permeability Versus Swanson Parameter for Travis Peak, Taylor and Mesaverde Cores	51

LIST OF FIGURES, Cont.

<u>Figure No.</u>		Page
17	Comparison of Porosity From Mercury Porosimetry on Core Chips with Gas Expansion Measurements	55
18	Porosity Versus Depth on SFE No. 3 Core Chips	56
19	"As-Received" Water Saturation of SFE No. 3 Core Versus Mercury Entry Pressure	57
20	Comparison of Visible Porosity With Mercury Porosimetry Data SFE No. 3 Chip Analysis	58
21	Plot Showing Routine Gas Permeability Versus Pore Geometry Type From SFE No. 3 Core	59
22	Schematic of Sample Assembly for Displacement Experiments	62
23	Relative Permeability of Gas Phase in Mast Core Versus Drainage Water Saturation	66
24	Gas-Phase Relative Permeability Data From Drainage Experiments, SFE No. 2 Samples	67
25	Apparatus Utilized for the Vacuum Saturation of Tight Sand Cores With Water	70
26	Gas Permeability of Mast 8623.2 Core Versus Water Saturation and Net Stress	73
27	Gas Permeability of Mast 9203.3 Core Versus Water Saturation and Net Stress	74
28	Gas Permeability of Mast 9954.9 Core Versus Water Saturation and Net Stress	75
29	Schematic Diagram of Water Injection Components Added to Inlet Lines on Upstream Endcaps in Coral II	78

LIST OF TABLES

<u>Table No.</u>		<u>Page</u>
1	Summary of Mast A-1 Dry Core Analyses	13
2	Stress Dependence Data for Mast A-1 Samples	14
3	Summary of Holditch Howell No. 5 (SFE No. 1) Core Analysis Results	18
4	Summary of SFE No. 2 Core Analysis Results	22
5	Summary of SFE No. 3 Core Analysis Results	28
6	SFE No. 3 Chip Analysis and Routine Core Analysis Data	53
7	Data From Drainage Experiments	65
8	Gas Phase Relative Permeability Data by the Evaporation Method, Mast A-1 Samples	72
9	Gas-Phase Permeability Data by the Evaporation Method, SFE No. 2 Samples	76

1.0. PROGRAM OBJECTIVES

1.1. Overall Objective of the Program

This project was conducted as part of the Gas Research Institute's (GRI) program for tight sand gas reservoirs, under which the research and development needed to stimulate near-term commercialization of low-permeability gas sandstones is being performed. The expected result of this project was the accurate definition of several important in-situ reservoir parameters for use in wireline log analyses as a correlation tool to better understand log responses, and as input data for numerical simulation of tight sand gas production using sophisticated computer models. The project's overall objective was to develop quantitative knowledge about gas entrainment and transport mechanisms in tight sandstones, with respect to the engineering problems involved in recovering the gas from these formations. The eventual goal of this research was to develop an improved understanding of the nature of fluid movement through low permeability porous media, which would help increase the predictability of tight gas reservoirs by allowing some aspects of reservoir quality to be assessed through relatively inexpensive and timely analyses. Techniques such as mercury porosimetry and petrographic observations of drill cuttings can be performed at the well site, and based on IGT's work, could be used to evaluate the pore structure of the target formation. By understanding the correlations between pore structure and reservoir properties, producers would be better able to rapidly assess the potential gas productivity of the various zones penetrated by the drill bit.

1.2. Specific Objectives

The specific objectives of this project were to measure reservoir properties of tight sand core samples and correlate those measurements with the observed pore structures of the rocks. The tight sand that was studied consisted primarily of the Travis Peak Sandstone of eastern Texas, selected by GRI as the target formation for a staged field experiment. Tight sandstone samples from the underlying Cotton Valley Group were also analyzed for this project. The objective of the measurements made on these cores was to obtain data in a controlled laboratory environment that accurately represented true pressure and stress conditions in the natural reservoir.

2.0. WORK PLAN

This project builds upon previous tight gas sands research funded by GRI (Contract No. 5082-260-0711) at the Institute of Gas Technology (IGT) to measure and analyze two-phase flow through low-permeability porous media. That work initially emphasized the development of laboratory procedures that would not damage the pore structure of the samples, and through use of the Computer Operated Rock Analysis Laboratory (CORAL), built a data base of detailed core analysis results on over 50 tight sand cores from the Rocky Mountains. Calculations and theoretical analyses using this data base resulted in the development of the "slot pore" model for gas transport paths in tight sands, and petrographic studies made with this model in mind led to the actual observation and photographing of slot pores in several different Rocky Mountain tight sands.

The work plan for this project called for studies similar to those carried out previously on tight sands from the Rocky Mountains, but emphasized instead the primary formation of interest to the GRI staged field experiment program, which is the Travis Peak Sandstone of eastern Texas. Comparison of the Travis Peak with the Rocky Mountain data collected earlier has provided a broader picture of reservoir properties and gas transport mechanisms in tight sands.

Specific work planned for this project included a variety of core analyses on both dry rocks and samples containing various partial water saturations. Dry core analysis on Travis Peak samples was to consist of measuring the porosity, pore volume compressibility, Klinkenberg permeability and stress-dependence of permeability under conditions of initial reservoir net stress and stress at the midpoint of reservoir drawdown. Petrographic analysis of these samples was also to be performed to assess pore structure, diagenesis, rock fabric, and the geometry of grain contacts that support the rock against stress. These studies utilize thin-section observations under both standard and reflectance fluorescent microscopes, X-ray diffraction to determine clay fraction composition, mercury porosimetry to obtain pore size distribution and capillary entry pressure, and scanning electron microscopy (SEM) to observe the contents of pores. The pore structure studies were to be

integrated with the dry core analysis data for the purpose of achieving a basic understanding of gas entrainment and transport mechanisms in the subject formation.

Work planned for this project also included core analysis measurements on selected tight sandstone samples at various partial water saturations. Particular emphasis was to be placed on the microscopic distribution (imbibition/drainage) of water in the sample pores. Initially, experiments involving drainage and evaporation procedures for sample desaturation were planned for measurement of gas-phase relative permeability. Later, experiments involving a true imbibition process were also included in the plan. Because of the complexity, experimental state, and time-consuming nature of these wet core analyses, the work plans called for only a very limited number of samples to undergo this full suite of measurements.

3.0. WORK PERFORMED

Work performed under this project included single- and two-phase flow studies, and petrographic studies on core samples from the Mast A-1 and SFE Nos. 1 and 2 wells in the Travis Peak Formation, East Texas. Cores from the Taylor Sandstone in the Cotton Valley Group, underlying the Travis Peak, were studied as well from the SFE No. 3 well, also in East Texas. The locations of these wells are shown in Figure 1. Detailed results of work specific to the first three of these wells have been published in earlier reports.¹⁻³ For the purpose of this report, the results have been divided into several topics listed below.

- **Dry Core Analysis:** This includes permeability, porosity, and other reservoir property measurements made on humidity-dried samples under representative reservoir net confining stress, as well as mercury porosimetry results. The main purpose of the dry core analyses was to provide a data base for correlation of reservoir properties with mercury porosimetry and with petrographic information. This data base was also needed for choosing samples for special studies such as two-phase flow.
- **Petrographic Studies:** Observations from thin sections provided information on pore structure, which is an important parameter in any predictive correlation for tight sands.
- **Reservoir Property Correlations:** Work performed in this area focused on developing correlations that use mercury porosimetry and petrographic image analysis for estimating reservoir properties. Both these techniques are rapid and relatively inexpensive, and require only small sample chips rather than core. This makes them ideal for use at the well site, possibly for analysis of drill-cuttings. As a preliminary step in studying the feasibility of this approach, measurements were made on 31 core chip samples from SFE No. 3 and compared with routine core analysis data.
- **Two-Phase Flow:** Experiments were conducted involving the use of drainage and imbibition, as well as evaporation, for changing water saturation in samples for gas phase permeability measurements. Results provided information on the feasibility and validity of these experimental techniques.

A detailed discussion of the results pertaining to these areas is presented in the following sections.

Source: Texas Bureau of Economic Geology, Austin

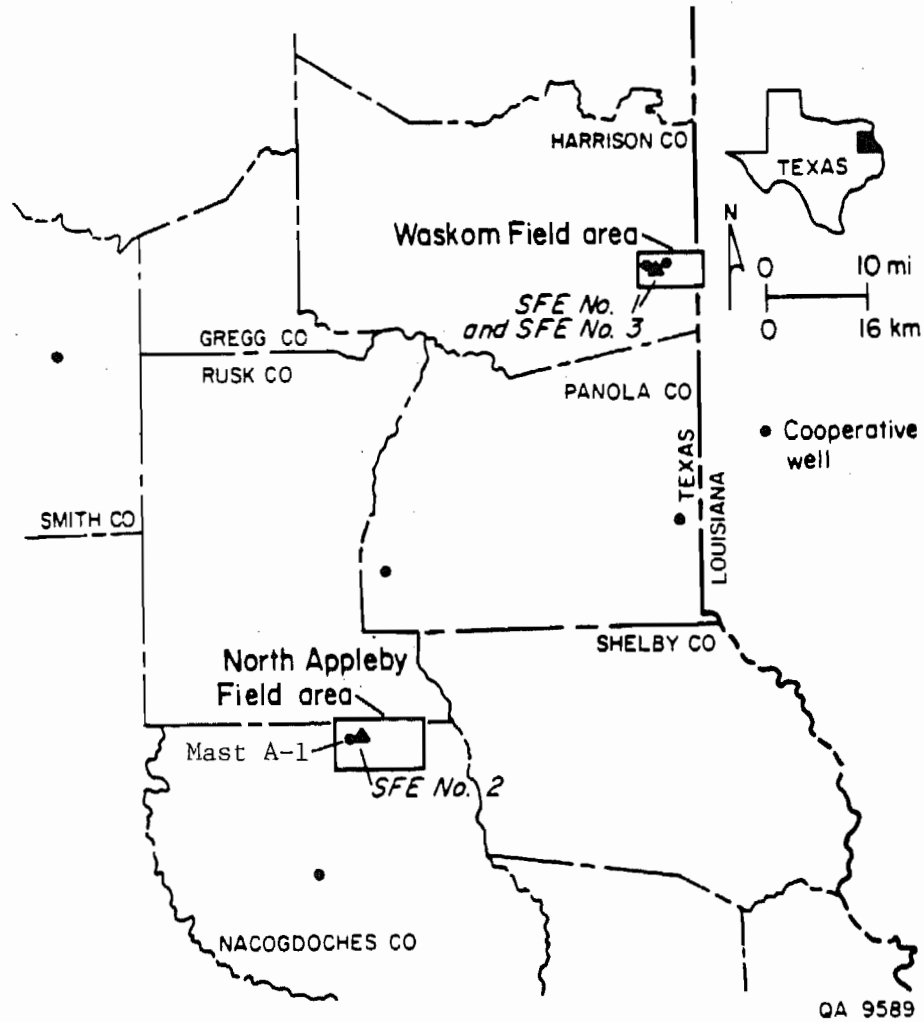


Figure 1. LOCATION OF GRI TIGHT SAND WELLS IN EAST TEXAS
(The Mast A-1 well location is shown adjacent to the SFE No. 2)

4.0. DRY CORE ANALYSIS

4.1. Experimental and Analytical Methods

Low permeability, steady-state core analysis at IGT is performed in an apparatus known as the CORAL. The CORAL system consists of four stainless steel core holders with associated high-pressure tubing and fluid supplies enclosed in an isothermal chamber. The system can operate at confining pressures up to 10,000 psi. Gas (pore) pressure is currently limited to 1500 psia by the range of the pressure transmitters in the system. The coreholders can accept either 1- or 1-1/2-inch diameter samples, though most of the samples analyzed for this report were 1 inch in diameter by about 2 inches in length.

The CORAL can measure gas flow rates as low as 10^{-6} standard cc/s, permitting gas permeability to be measured with a resolution of less than a nanodarcy. This high sensitivity is made possible by temperature control to within 0.01°F . Gas flow rates in the CORAL are measured by the pressure buildup in a small calibrated volume at the downstream end of each coreholder. Sample pore volumes are also measured in the CORAL using a "Boyle's Law" technique.

Measurements made during a CORAL run yield data at in-situ confining stress levels pertaining to

- Gas permeability (corrected for gas slippage)
- Porosity to gas
- Pore volume compressibility
- Stress dependence of permeability.

A more detailed description of the equipment and operating procedures is available in the literature referenced in this report.¹

4.1.1. Mean Pore Width and Tortuosity

Permeability data obtained in the CORAL at pore pressures ranging from 300 to 1500 psia yield values of k_{∞} and b from the Klinkenberg equation:

$$k = k_{\infty} \left(1 + \frac{b}{P} \right) \quad (1)$$

where

k = permeability at mean pore pressure of \bar{P}

k_{∞} = permeability to an ideal gas at infinite pressure

b = slip factor.

The values of b and k_{∞} can be used to calculate values of mean pore size and tortuosity representative of the sample pore space. This requires the porous medium to be modeled as a bundle of capillaries having a uniform pore size and effective length equal to the sample length multiplied by a tortuosity factor⁴. Based on prior studies indicating that pore throats in tight sands are "slot" shaped, a model incorporating slot-shaped capillaries (rather than round) has been used. The resulting equations for calculating mean pore width (\bar{w}) and tortuosity (τ) are⁴:

$$\bar{w} = \frac{16 c \mu}{b} \left(\frac{2RT}{\pi M} \right)^{1/2} \quad (2)$$

and

$$\tau = \bar{w} \left(\frac{\phi}{12k_{\infty}} \right)^{1/2} \quad (3)$$

where c is the Adzumi constant ($=0.9$); T is the temperature; R is the gas constant; μ and M are the gas viscosity and molecular weight, respectively and ϕ is the sample porosity. The primary use of these parameters is in making a comparative study of pore structure in different samples.

4.1.2. Pore Volume Compressibility

Pore volume compressibilities are calculated from measurements of gas expelled from the core during a step increase in confining stress. The step change in confining stress is generally from the initial reservoir net stress to a net stress representative of the midpoint of drawdown. Compressibility (C_{pv}) is calculated from the equation:

$$C_{pv} = \frac{1}{\Delta P_c} \frac{\Delta V_p}{V_p} \quad (4)$$

where ΔV_p is the decrease in pore volume for a confining pressure change of ΔP_c , and V_p is the sample pore volume at the initial net stress.

4.1.3. Stress Dependence of Permeability

The stress-dependence of permeability is characterized by the exponent α in the empirical equation:

$$k = k_0 (P_{net})^{-\alpha} \quad (5)$$

where k is the sample permeability at net confining stress P_{net} , with k_0 and α being constants. Values of α are calculated from Klinkenberg permeabilities measured in the CORAL at two values of net confining stress, usually "virgin" reservoir net stress and midpoint of drawdown net stress.

4.1.4. Mercury Porosimetry

The mercury porosimetry results reported here were obtained using sample chips of approximately 1 cc volume. The apparatus used was a "Micromeritics Pore Sizer" capable of a maximum pressure of 30,000 psi. The instrument software calculates pore diameters from intrusion pressure using the equation

$$d = \frac{4\gamma \cos \phi}{P} \quad (6)$$

where

d = pore diameter for a cylindrical pore, cm

γ = mercury surface tension = 485 dynes/cm

ϕ = contact angle = 130°

P = pressure, dynes/cm².

If one assumes lamellar, slot-shaped pores, the equation for pore width, w , can be written as

$$w = \frac{2\gamma \cos \phi}{P} \quad (7)$$

so that

$$w = d/2 \quad (8)$$

Parameters obtained and reported for each sample from the mercury capillary pressure data are:

- Porosity: This is based on the total volume of mercury penetrating the sample at 30,000 psi.
- Mercury Entry Pressure: This is estimated from the capillary pressure curve as the pressure corresponding to the intersection of the near-vertical and near-horizontal tangents to the curve at its "knee." The value thus obtained can be divided by a factor of 5 to estimate gas-water entry pressure.
- Median Pore Width: This is determined from the pore size distribution provided by the mercury capillary pressure data.
- Swanson Parameter: This parameter is calculated as the maximum value of the ratio of mercury saturation (S_p , percent of bulk volume) to the corresponding capillary pressure (P_c) along the capillary pressure curve. This parameter has been found useful for correlating mercury porosimetry data for tight sands with permeability in a manner suggested originally by Swanson⁵ for conventional sandstones.

4.1.5. Sample Preparation

Mast A-1 well samples received by IGT were 1.5 inch diameter horizontal plugs cut by Litton Core Research, and were used as received. For wells SFE 1, 2, and 3, horizontal plugs 1 inch diameter and 1.5 to 2 inches long were cut by IGT from whole core. All samples were dried to constant weight at 60°C under 45% relative humidity. The controlled humidity drying removes all free pore water but retains proper clay mineral hydration, thereby avoiding significant damage to clay pore structures and the associated inaccuracies in permeability measurement.⁶ The plugs were placed in thin lead sheaths after drying to prevent high-pressure gas in the pores from diffusing into the rubber confining sleeves during core analysis. As part of the sample preparation procedure, rock slices one quarter of an inch in thickness were cut from the ends of each plug to provide samples for mercury porosimetry and petrography.

4.2. Mast A-1 Data

The Mast well dry core analysis at IGT was carried out on 12 plug samples received from Litton Core Research, Incorporated, from intervals selected by Mr. Brad Robinson of Holditch Associates. The samples were horizontal plugs 1.5 inches in diameter and 2 inches long. The location of the Mast well and the intervals from which the samples were taken out of the Travis Peak core are shown in Figure 2.

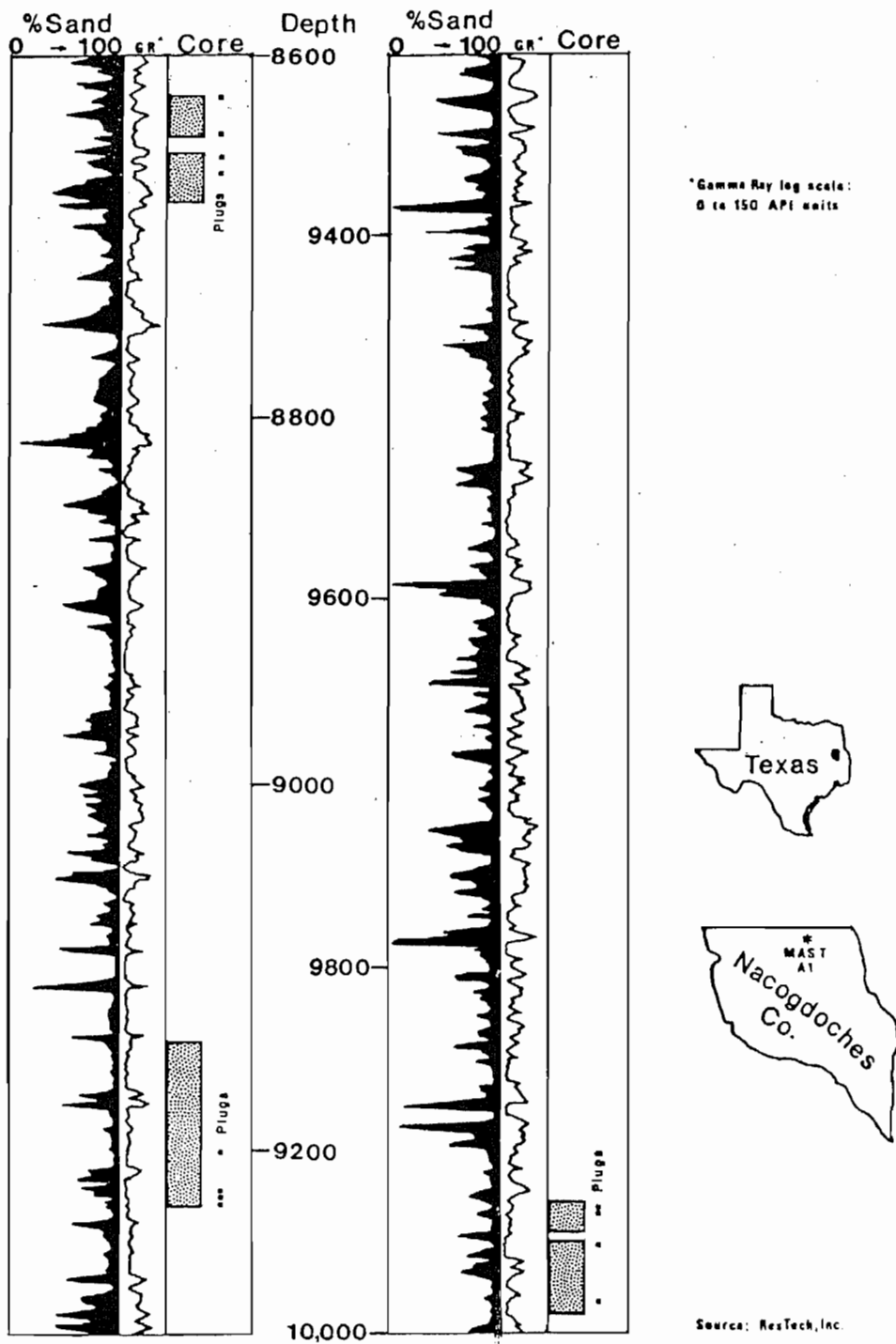


Figure 2. LOCATION OF MAST A-1 WELL IN EASTERN TEXAS AND CORED INTERVALS IN THE TRAVIS PEAK FROM WHICH IGT SAMPLES WERE SELECTED

Lithologically, the samples consisted predominantly of medium to fine sandstone, mostly uniform with little visible bedding, although a few contain finely interlaminated organic or shale zones. Some of the coaly laminae may act as flow channels, as they appeared to contain bedding plane fractures. Discontinuous and mineralized natural fractures were also visible in some of the more uniform sands. Detailed descriptions of the lithologic properties of the Mast samples are available in the literature referenced in this report.¹

Table 1 summarizes the data obtained on the Mast A-1 samples. Net stress values used were based on a confining pressure gradient of 0.85 psi/foot, with pore pressure gradients of 0.44 psi/foot for samples shallower than 9600 feet and 0.49 psi/foot for deeper samples. The table lists measurements at net stress of 1000 psi, initial reservoir net stress and a stress representative of 1/2 drawdown. For many of the samples, a repeat measurement at initial reservoir net stress was made following the measurements at 1/2 drawdown stress. Some important findings from the Mast well core analysis are summarized below. A detailed account of the results and discussion is available in the first annual report for this contract.¹

The Mast A-1 samples showed a very wide range of permeabilities, from less than a microdarcy to over 10 millidarcies. Unusually high permeability, in every case, is believed to have been the result of flow through fractures, which were clearly visible to the naked eye in some samples. The presence of fractures in these samples also manifested itself in a strong time-dependence of permeability on applying a confining stress to the samples. Permeability decreased with time over several days for most samples, though the maximum change occurred during the first 2 to 3 days after the stress change. This phenomenon resulted in problems with the Klinkenberg analysis of permeability data in many cases. Klinkenberg plots either yielded negative slopes or had data that did not lie along a straight line. Cases where the most severe time-dependent permeability behavior was observed can be identified in Table 1 by the absence of values for Klinkenberg 'b' factor (Equation 1). The permeability reported in these instances is that measured at 1500 psia pore pressure rather than the Klinkenberg permeability.

Table 2 lists values of pore volume compressibility and exponent α , for stress dependence of permeability. For cases where permeability at initial reservoir net stress was measured both before and after the sample was taken

Table 1. SUMMARY OF MAST A-1 DRY CORE ANALYSES

Plug Depth (Ft)	Net Confining Stress (psi)	Gas Porosity (%)	Permeability (K_w or K_{1500}) (microdarcy)	Klinkenberg "B" (psi)	Gas Flow Path Characteristics		Unconfined Sample Mercury Penetration Data		
					Width (micrometers)	Tortuosity (plug lengths)	Entry Pressure (psi)	Porosity (%)	Median Pore Width (μ m)
8623.2	1000	7.79	11.1	--	--	--	265	8.47	0.171
	3500	7.57	8.35	42	0.149**	5.00**			
	5500	7.50	7.06	65	0.095**	3.45**			
8645.9	1000	7.67	--	--	--	--	165	6.69	0.303
	3500	7.46	48.9	--	--	--			
	5500	7.39	34.7	23	0.264**	4.32**			
8656.3	1000	6.35	3.98	--	--	--	555	6.74	0.100
	3500	6.13	1.94	--	--	--			
	5500	6.06	0.926	149	0.063	4.61			
8666.2	1000	5.25	--	--	--	--	800	6.72	0.065
	3500	4.84	1402	--	fractured	--			
	5500	4.72	928	--	--	--			
9203.3	1000	5.10	71.0	--	--	--	65	5.54	0.476
	3800	4.81	24.66	10	0.936	11.93			
	5800	4.74	14.62	45	0.209	3.41			
	3800		19.11	44	0.210	3.04			
9226.0	1000	4.05	154	--	--	--	85	4.76	0.434
	3800	3.75	68.0	--	--	--			
	5800	3.70	39.30	16	0.575	5.09			
9229.3	1000	4.65	8.92	--	--	--	305	4.94	0.191
	3800	4.39	2.68	50	0.186	6.85			
	5800	4.32	1.33	98	0.095	4.91			
	3800		1.92	102	0.092	4.00			
9231.9	1000	3.49	45.3	--	--	--	480	3.34	0.125
	3800	3.28	3.56*	--	--	--			
	5800	3.23	0.931	169	0.056	2.95			
	3800		1.34	74	0.126	5.70			
9935.1	1000	6.30	10 ⁴	--	--	--	345	6.21	0.090
	3600	5.76	"	--	fractured	--			
	6000	5.62	"	--	--	--			
9937.7	1000	6.03	806	--	--	--	245	5.44	0.206
	3600	4.98	241	--	fractured	--			
	6000	4.90	109.3	23	0.402	2.46			
	3600		126.6	7	1.410	8.06			
9954.9	1000	5.70	149	--	--	--	120	5.66	0.271
	3600	5.27	14.25	22	0.429	7.53			
	6000	5.17	12.75	25	0.369	6.77			
	3600		13.57	26	0.353	6.36			
9984.9	1000	3.22	146	--	--	--	715	3.11	0.077
	3600	2.82	0.216	81	0.114	11.95			
	6000	2.71	0.045	290	0.032	7.15			
	3600		0.106	153	0.062	9.08			

*Permeability measured at 300 psia pore pressure

**Assumes round capillaries instead of lamellar slots based on petrographic observations.

Table 2. STRESS DEPENDENCE DATA FOR MAST A-1 SAMPLES

Depth, ft	Properties at First Excursion to Initial Reservoir Net Stress		Pore Volume Compressibility, 10^{-6} /psi	Stress Dependence, Exponent for Permeability (α)	
	Porosity, %	Permeability, μd		1st Increase of Net Stress	Decreasing Net Stress
8623.2	7.57	8.35	4.2	0.36	--
8645.9	7.46	48.9	4.9	0.75	--
8656.3	6.13	1.94	6.0	1.38	--
8666.2	4.84	14.02	12.0	0.91	--
9203.3	4.81	24.7	6.6	1.24	0.63
9226.0	3.75	68.0	7.7	1.30	--
9229.3	4.39	2.68	7.8	1.66	0.87
9231.9	3.28	9.47	6.6	3.17	0.86
9935.1	5.76	10^4	9.7	--	--
9937.7	4.98	241	6.7	1.54	0.29
9954.9	5.27	14.25	7.2	0.22	0.12
9984.9	2.82	0.216	15.2	3.05	1.66

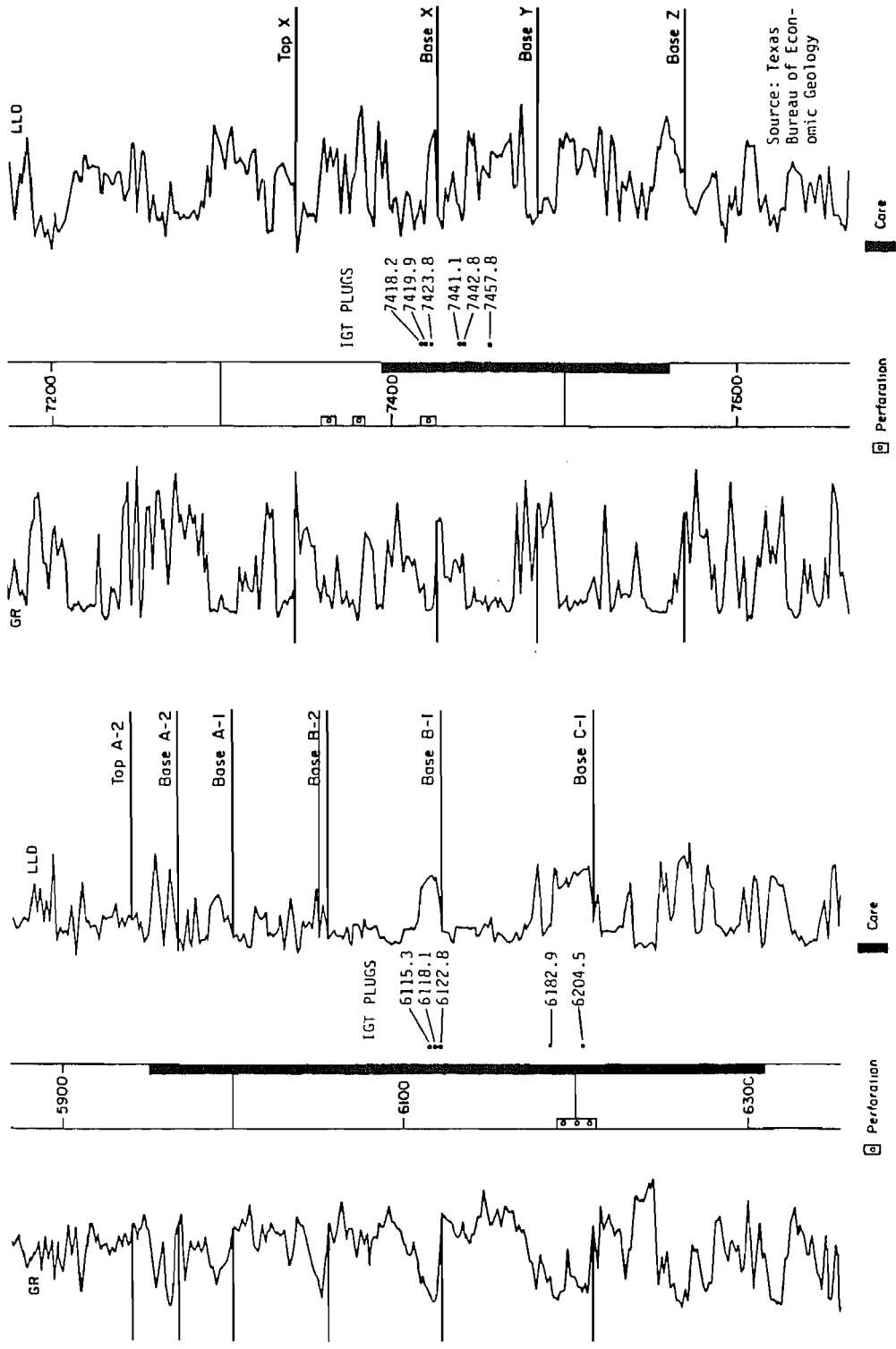
to the 1/2 drawdown net stress, two values of the stress exponent are reported. The first corresponds to the net stress increase from initial reservoir conditions to the 1/2 drawdown value. The second number corresponds to a stress decrease from 1/2 drawdown to initial reservoir conditions. The two values differ significantly. The difference is attributable to a combination of permeability hysteresis and the decrease of permeability with time observed for these samples. Low α values seem to correlate with a pore geometry containing either grain-supported primary pores (Mast 8623) or strong quartz asperity contacts in the slot pores (Mast 9954). Travis Peak pore geometry is discussed in detail in a later section.

4.3. SFE No. 1 Data

The SFE No. 1 well contains two main productive zones in the Travis Peak Formation.⁷ The "upper" zone occurs between about 5900 and 6200 feet in depth, and consists of three major sand units, informally termed the A, B, and C sands from top to bottom. The A and B sands are further subdivided into the A₂, A₁, B₂, B₁ units in order of increasing depth. IGT obtained five plug samples from the "upper" productive zone in SFE No. 1, as shown in Figure 3. Three cores were taken from the base of the B₁ sand, and two from the base of the C sand. These units consist of fluvial, upward-fining, channel-fill sandstone, with fairly sharp basal contacts as shown in the logs in Figure 3.

The "lower" productive zone in the Travis Peak Sandstone in the SFE No. 1 well occurs between about 7100 and 7600 feet in depth. Like the "upper zone", this zone also consists of three major productive sand units, informally termed the X, Y, and Z sands in order of increasing depth. IGT obtained six plug samples from the "lower" productive zone in SFE No. 1, also shown in Figure 3. Three of the plugs are from the base of the "X" sand, and three are from near the center of the underlying "Y" sand. These "lower zone" units were deposited in a sand-rich, braided stream system onto a delta platform, and consist of multiple, thin, interbedded sandstones and shales. More details concerning sample selection and lithology of plugs analyzed by IGT from the SFE No. 1 core can be found in IGT's topical report² to GRI on this well.

The net confining stress values utilized for the dry core analyses were determined from information supplied to IGT by Mr. Bill Whitehead of Holditch Associates. Initial reservoir pressures measured in the SFE No. 1 well, as



Source: Texas
Bureau of Econ-
omic Geology

Figure 3. LOCATION OF IGT SAMPLES IN CORE FROM SFE NO. 1 WELL FROM THE UPPER PRODUCTIVE ZONE AND LOWER PRODUCTIVE ZONE

reported by Holditch Associates, were 558 psia at 6117 feet (equivalent to a pore pressure gradient of only 0.09 psi/foot), 1175 psia at 6194 feet (equivalent to a pore pressure gradient of 0.19 psi/foot) and 2200 psia at 7466 feet (equivalent to a pore pressure gradient of 0.295 psi/foot). All of the measured sands in this well are significantly underpressured due to production from other wells in the field. Since this field was so extensively drawn down, it was a bit complicated to calculate representative reservoir pressures based upon data collected during Holditch Associates' well testing. Initial reservoir pressure values in the produced sands were determined from pore pressures in nearby (deeper and shallower) unproduced, "virgin" sandstones and shales. Initial reservoir pressures were calculated at 0.38 psi/foot for core samples from the "upper" productive zone, and at 0.40 psi/foot for core samples from the "lower" productive interval. These calculated initial reservoir pressure values were divided by 2 to obtain the pressures at 50% reservoir drawdown.

The confining pressure gradient utilized by other contractors during routine analysis on the SFE No. 1 core was 1.0 psi/foot. Minifrac data from Holditch Associates showed that fracture gradients in the Travis Peak sandstone units at the SFE No. 1 site range between 0.45 and 0.65 psi/foot, indicating that a confining pressure gradient on the cores of 1.0 psi/foot is not representative of initial reservoir net stresses. Based on available data, a best judgment call for a reasonable confining pressure gradient settled on about 0.75 psi/foot. It should be noted that this value is lower than the 0.925 psi/foot confining pressure gradient applied to Rocky Mountain tight sand cores, because fracture gradients in the Rockies tend to average around 0.8 psi/foot.⁸

During the dry measurements on the SFE No. 1 core, IGT found that most of the permeabilities were well above the measurement range for which IGT's equipment was designed. The response of the flow-measuring pressure transmitters to gas movement through most of these cores was much more rapid than the computer scan interval, even at very low differential pressures. This necessitated manual timing of the flow rates using a stopwatch, and resulted in flow measurements on the higher permeability samples that were at least an order of magnitude less accurate than the data routinely collected electronically. The results of the SFE No. 1 dry core analyses are summarized in Table 3. Data for the 11 samples are placed in a vertical column beneath each

Table 3. SUMMARY OF HOLDITCH HOWELL NO. 5 (SFE NO. 1) CORE ANALYSIS RESULTS

Plug Depth (feet)	6115.3	6118.1	6122.8	6189.2	6204.5	7418.2	7419.9	7423.8	7441.3	7442.8	7457.8
Informal Sand Unit	B-1	B-1	B-1	C-1	C-1	X	X	X	Y	Y	Y
Dry Gas Porosity	13.02%	14.19%	17.92%	13.53%	15.07%	9.38%	8.97%	10.10%	10.54%	10.04%	7.89%
Net Confining Stress	2300 psi	2700 psi	2700 psi	2700 psi	2700 psi	2700psi	2700 psi				
Cpv (10 ⁻⁶ /psi)	6.81	5.41	4.66	5.25	3.50	5.39	3.90	5.28	3.40	3.78	4.74
ΔNet Stress (psi)	2300-3900	2300-3900	2300-3900	2300-3400	2300-3400	2700-3400	2700-3400	2700-3400	2700-3500	2700-3500	2700-3500
<u>Dry Gas Permeability at "Unstressed" Confining Pressure</u>											
Net Stress	1500 psi	1500 psi	1500 psi	1500 psi	1000 psi						
Pore Pressure	1400 psia	1400 psia	1400 psia	1400 psia	100 psia	100 psia	100 psia	100 psia	50 psia	50 psia	50 psia
Permeability (Avg.)	1.1 md	2.5 md	No data	6.3 md	23 md	3.4 md	4.7 md	2.6 md	2.8 md	4.9 md	0.875 md
<u>Dry Gas Permeability at "Initial Net Stress" Confining Pressure</u>											
Net Stress	2300 psi	2700 psi									
Pore Pressure	500 psia	500 psia	500 psia	500 psia	100 psia	100 psia	100 psia	100 psia	50 psia	50 psia	50 psia
Permeability (Avg.)	0.313 md	2.1 md	21 md	7.7 md	18 md	39.253 μd	4.0 md	0.606 md	2.2 md	4.1 md	0.521 md
Pore Pressure					500 psia	500 psia	500 psia	500 psia	100 psia	100 psia	100 psia
Permeability (Avg.)					15 md	28.122 μd	4.3 md	0.594md	2.2 md	4.3 md	0.514 md
Pore Pressure					1000 psia	1000 psia	1000 psia	1000 psia	500 psia	500 psia	500 psia
Permeability (Avg.)					19 md	25.072 μd	4.6 md	0.587 md	2.5 md	4.7 md	0.537 md
Pore Pressure									1000 psia	1000 psia	1000 psia
Permeability (Avg)									2.4 md	4.6 md	0.547 md
<u>Dry Gas Permeability at "Midpoint of Drawdown" Net Confining Pressure</u>											
Net Stress	3900 psi	3900 psi	3900 psi	3400 psi	3500 psi	3500 psi	3500 psi				
Pore Pressure	500 psia	500 psia	500 psia	500 psia	1000 psia	1000 psia	1000 psia	1000 psia	1000 psia	1000 psia	1000 psia
Permeability (Avg)	0.285 md	2.0 md	25 md	8.6 md	17 md	21.070 μd	4.2 md	0.571 md	2.4 md	4.5 md	0.534 md
Pore Pressure	200 psia	200 psia	200 psia	200 psia	500 psia						
Permeability (Avg)	0.291 md	2.0 md	33 md	8.0 md	16 md	20.355 μd	4.4 md	0.557 md	2.4 md	4.6 md	0.519 md
Pore Pressure	100 psia										
Permeability (Avg)	0.301 md	1.9 md	25 md	7.4 md	20 md	25.015 μd	3.7 md	0.548 md	2.2 md	4.2 md	0.496 md
Pore Pressure											
Permeability (Avg)											
<u>Mercury Porosimetry Data on Unconfined Samples</u>											
Entry Pressure (psi)	35	31	14.7	19.1	15.3	65	19.8	29.6	41	No	41
Porosity (%)	13.8	13.5	16.0	12.1	13.1	10.4	8.4	10.1	8.7	Data	8.2
Median Pore Width, μm	0.185	0.294	1.202	1.389	1.771	0.309	1.302	1.220	0.363		0.579
Swanson Parameter	29.1	50.4	196.2	110.8	189.1	20.7	70.9	70.4	21.2		38.5

* Permeability data at these pressures for the plugs indicated were taken manually under conditions exceeding the design limitations of the laboratory equipment, and are less accurate than the other core samples.

** Maximum value of the ratio of Hg saturation (Sb) as a percent of bulk volume to the corresponding capillary pressure (Pc) along the capillary pressure curve. Expressed in units of 10⁻³ percent vol. per psi.

sample, as identified by depth in the uppermost line of the table. The far left column lists the analyses for which data is reported. The different rows in Table 3 are discussed below.

Porosity to gas in these rocks is surprisingly high compared to most other tight sands analyzed by IGT. Typical values for tight sand porosity have been between 5% and 10% under reservoir net stress,⁹ whereas the SFE No. 1 samples range from 8% to 18%, with over half of the 11 samples exhibiting porosities above 10%.

Pore volume compressibility, expressed as 10^{-6} volume per volume of pore space for each psi of confining pressure increase, is listed below the porosity values. Compressibilities are fairly low for the SFE No. 1 core compared to those measured by IGT⁸ on Rocky Mountain tight sands, but do fall within the range of other Travis Peak pore volume compressibilities, such as those measured on the Mast A-1 core. The lower compressibility of the Travis Peak pores, compared to Rocky Mountain tight sands, appears to be due partially to the lower porosities in the Rocky Mountain sands, and also to the greater percentage of grain-supported primary porosity in the Travis Peak pore systems.

Permeability to gas is listed in each column of Table 3 for the samples at three different confining stresses: a very low net stress equivalent to "unstressed" measurement conditions from the routine core analysis, a net stress equivalent to initial or "virgin" reservoir pressure, and a net stress equal to that experienced in the reservoir at midpoint of drawdown. As can be seen from the table, sample permeabilities are quite high for the SFE No. 1 sandstones, ranging from a few tenths of a millidarcy to several tens of millidarcies. This is significantly greater than the gas permeability typically measured by us on dry Rocky Mountain tight sands, which normally ranges between 1 and 10 microdarcies.⁹ It is also significantly higher than most of the dry permeabilities measured on cores from the other Travis Peak wells reported on here.

Because the permeabilities of the SFE No. 1 core are so high, the Klinkenberg effect ("gas slippage") is quite small. There is virtually no difference between k_{∞} values and permeabilities measured at 1000 or 1500 psia pore pressure in these rocks. Therefore, due to the inaccuracies encountered

in trying to measure such high gas flow rates with the equipment, Klinkenberg permeabilities are not reported for the SFE No. 1 dry core analyses. Instead, measured gas permeabilities are given for each of the pore pressure values employed. The tightest sample (7418.2) did yield data accurate enough to calculate k_{∞} , which is given in Table 3. Permeability data collected from the other samples at different pore pressures contained enough small inaccuracies to preclude construction of reliable Klinkenberg plots. More details on the analysis of the SFE No. 1 core can be found in the topical report² on the subject.

4.4. SFE No. 2 Data

The SFE No. 2 well contains two primary zones of interest and two secondary zones of interest, all of which were cored. As shown in Figure 4, IGT obtained two samples from the shallowest cored interval, on either side of the minifrac stress test, as well as six samples from the deepest zone of interest from core at perforated intervals. Six additional samples were collected from the intermediate, secondary zones of interest, as shown in Figure 4.

The Travis Peak in the SFE No. 2 well is similar in lithologic appearance, sedimentary structure, and geological history to the Travis Peak in the SFE No. 1 well. The SFE No. 2 cores are much lower in permeability, however. Results of the SFE No. 2 dry core analysis are summarized in Table 4. The first four columns after the sample depth give various parameters calculated from mercury porosimetry data on unconfined sample chips. Subsequent columns give information obtained from porosity and permeability measurements under net confining stress representative of reservoir conditions. For samples where data at two values of net stress are reported, the lower value corresponds to initial reservoir net stress and the higher value represents conditions at the midpoint of drawdown. Net stress values for SFE No. 2 were calculated using an average confining pressure gradient of about 0.82 psi/foot and a pore pressure gradient of about 0.47 psi/foot. The average confining pressure gradient was a best judgment call based on an overburden pressure of 1 psi/foot and a fracture gradient of about 0.62 psi/foot from data supplied by Holditch and Associates.

The porosity and permeability of the SFE No. 2 samples are comparable to those of the unfractured Mast A-1 samples, whereas the SFE No. 1 samples show

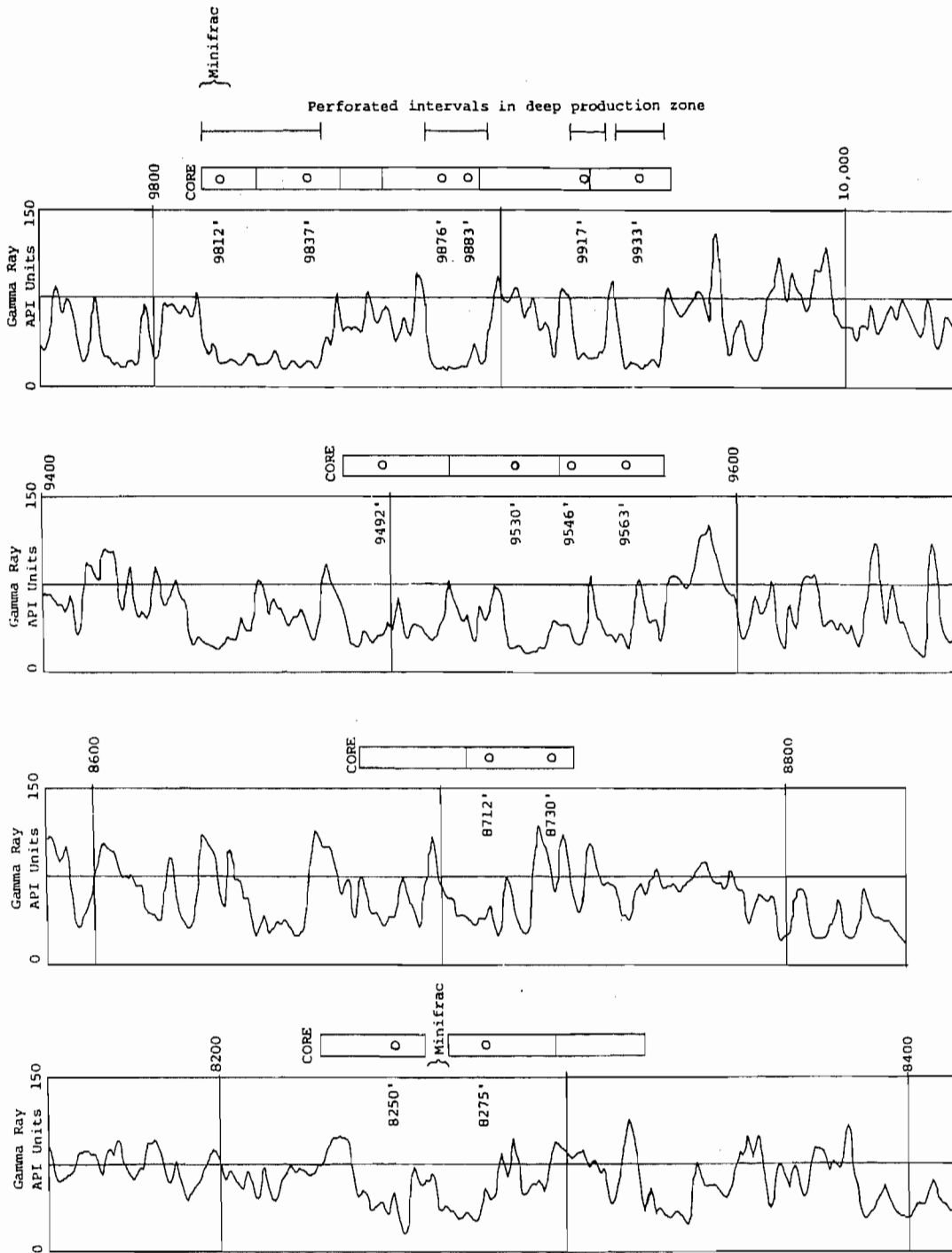


Figure 4. LOCATION OF IGT SAMPLES IN CORE FROM THE SFE #2 WELL. IGT PLUGS ARE INDICATED BY SMALL CIRCLES IN CORE INTERVALS; SAMPLE DEPTHS ARE GIVEN ALONG THE RIGHT MARGIN OF THE ACCOMPANYING GAMMA LOG STRIPS. STRESS-TESTS AND PERFORATED ZONES ARE ALSO INDICATED. SOURCE: S. A. HOLDITCH & ASSOC.

Table 4. SUMMARY OF SFE NO. 2 CORE CORE ANALYSIS RESULTS

Plug Depth (ft)	Unconfined Sample Mercury Penetration Data		Pore Parameter	Net Confining Stress (psi)	Gas Porosity (%)	Klinkenberg Permeability (μd)	Klinkenberg "b" (psi)	Gas Flow Path Characteristics		Pore Volume Compressibility (10 ⁻⁶ /psi)	Stress Dependence Exponent (α) for Permeability	
	Entry Pressure (psi)	Porosity (%)						Median Swanson	Width (μm)			Tortuosity
8250.15	473	4.76	0.073	2.04X10 ⁻³	2930 4830	4.94	1.79 1.40	125 102	0.074 0.092	3.56 4.92	5.4	0.49
8275.0	251	6.32	0.181	6.42X10 ⁻³	2930 4830	6.12	8.27 6.78	70 57	0.134 0.162	3.31 4.43	6.2	0.40
8712.0	531	5.31	0.106	3.50X10 ⁻³	2930 4830	5.26	2.57 1.68	123 103	0.075 0.090	3.15 4.62	8.0	0.85
8730.0	1353	4.45	0.034	0.6X10 ⁻³	2930 4830	4.88	0.299 0.138	475 210	0.220 0.044	2.28 7.50	11.0	1.53
9492.0	480	3.53	0.080	1.80X10 ⁻³	3920 5530	3.02	0.401 0.175	170 161	0.055 0.059	4.35 6.88	7.6	1.60
9530.7	320	5.04	0.168	5.21X10 ⁻³	3920 5530	4.73	3.86 2.32	88 73	0.107 0.128	3.38 5.23	8.2	0.98
9546.5	157	6.37	0.288	10.41X10 ⁻³	3920 5530	6.29	20.76 16.52	51 42	0.182 0.221	2.89 3.91	6.0	0.44
9562.9	1048	3.76	0.042	0.86X10 ⁻³	3920 5530	3.52	0.243 0.094	189 200	0.050 0.047	5.40 8.08	9.2	1.83
9811.55	511	4.25	0.076	1.82X10 ⁻³	3490 5770	4.55	0.476 0.271	135 147	0.069 0.063	6.14 7.42	5.24	1.12
9837.0	49	5.84	0.589	23.78X10 ⁻³	—	—	—	—	—	—	—	—
9875.95	194	4.56	0.269	7.06X10 ⁻³	3420	4.84	9.80	44	0.210	4.26	6.8	—
9882.95	243	4.17	0.231	5.57X10 ⁻³	3420	4.87	4.24	64	0.146	4.52	7.0	—
9917.4	503	3.61	0.098	2.21X10 ⁻³	3420	5.33	0.59	124	0.075	6.50	5.1	—
9932.85	217	4.71	0.232	6.69X10 ⁻³	3420	5.34	9.96	48	0.195	4.13	6.3	—

much higher porosity and permeability. As discussed in a later section, these observed variations in the range of petrophysical properties between the Travis Peak in the SFE No. 1 core on the one hand, and Mast A-1 and SFE No. 2 cores on the other can be related to fundamental differences in pore morphology of these rocks.

Mean pore width and tortuosity values for the SFE No. 2 samples in Table 4 are in the range measured for the Mast A-1 samples, and also during earlier analysis of Rocky Mountain tight sands by IGT. For most of the samples, the calculated mean pore width is higher at the higher net stress value. This is probably due to the closure of small-size pore throats as a result of the increased net stress. The average pore size for the throats that remain open is higher. The decrease in permeability is largely due to the increased tortuosity. Comparison of the mean pore width calculated from the gas slippage data with median pore widths from mercury porosimetry data shows a good correlation between the two. Though derived from data on unconfined sample chips, the variation of median pore width from mercury data is a good indicator of sample behavior under confining stress.

Pore volume compressibilities listed in Table 4 for all samples except the last four were measured for a confining pressure increase from initial reservoir net stress to half-drawdown net stress. The values reported for the last four samples are based on a step increase in net confining stress from 3000 to 3420 psi. Pore volume compressibilities for the SFE No. 2 core are somewhat larger than those measured for SFE No. 1 cores, and are of the same magnitude as those measured for the Mast A-1 samples. Pore volume compressibilities for the Travis Peak samples are generally lower than values that have been measured at IGT on Rocky Mountain tight sands⁹ from the Mesaverde formation.

The values of stress-dependence exponent for permeability (α) for the SFE No. 2 core are comparable to those measured for the Mast A-1 samples and also for tight sands from the Mesaverde formation⁹ in Colorado. The higher-permeability SFE No. 1 samples, however, had much lower stress dependence, with α values of 0.2 or less. This variation in stress dependence can be directly related to the pore morphology of the sandstones. The low stress dependence of the SFE No. 1 core is characteristic of media with grain-supported pores, whereas the high stress dependence of the SFE No. 2 and Mast

A-1 cores is typical of flow controlled by narrow slots at grain boundaries. Pore morphology of the Travis Peak sandstones, and the relationship to petrophysical properties is discussed in detail in a later section.

4.5. SFE No. 3 Data

4.5.1. Lithology

The lithology of the SFE No. 3 core samples received from the Texas Bureau of Economic Geology (BEG) are detailed below. Colors are given for wet-rock surfaces. Core plugs were also supplied to the Chemical Engineering department at the Illinois Institute of Technology for their GRI-sponsored research project.

- 9225.7-9226.15 ft: Fine, calcareous sandstone, medium gray (N5), thinly laminated. Laminations are more pronounced in upper half of core; base of core is bounded by a pebble conglomerate containing abundant shell fragments. Plug was cut at 9266 feet, just above this pebble bed.
- 9227.6-9228.2 ft: Fine sandstone, olive gray (5Y4/1), thin bedded. Top of core is bounded by calcareous sand described above, most of core consists of lightly calcareous sand, although basal part is virtually non-calcareous. A few small shells occur in middle portion of core; basal noncalcareous bed contains no shells but does have a shaly clast and shrinkage (?) cracks. Core contains a few short (0.1-0.2 feet) vertical natural fractures as well as a petal fracture. Plug was cut at 9288 feet, in shelly bed just above noncalcareous zone. An Illinois Institute of Technology (IIT) plug was cut in the lower zone.
- 9233.8-9234.65 ft: Fine calcareous sandstone, medium gray (N5) thinly to thickly laminated, with interlaminated silty shale, dark gray (N3). Shell fragments and thin zones of hash occur throughout. Interval is not bioturbated. IGT plug was cut at 9234 feet in a uniform, non-laminated, shelly bed.
- 9236.6-9237.1 ft: Fine sandstone, medium gray (N5) and medium dark gray (N6), thin-bedded, noncalcareous; and silty shale, dark gray (N3), thin bedded, noncalcareous. Individual sandstone beds contain a coarse base, composed of shell fragments. The basal part of the bed immediately above the shale contains granule-sized quartz pebbles. IGT plug was cut from uniform, fine portion of middle sandstone bed.
- 9237.2-9237.7 ft: Calcareous fine sandstone, shale and conglomerate, medium gray (N5) and dark gray (N3), thinly laminated to thin-bedded. Core consists mostly of shelly sandstone with shale clasts at the top and a basal conglomerate. IGT core plug was cut in the tightly cemented conglomerate. Plug for IIT was cut just above in fine, laminated sandstone.
- 9241.3-9242.2 ft: Fine sandstone, medium gray (N5), thin bedded to thinly laminated, stylolitic, lightly calcareous. A few pelecypod shells

and shell fragments are scattered throughout. IGT and IIT plugs were cut from lightly stylotitic, uniform, central part of the core.

- 9246.2-9246.7 ft: Fine sandstone, brownish gray (5YR4/1), thick bedded. Core consists of uniform sand with minor gravel-size quartz scattered sparsely throughout. A pyritic clast is also present, along with a near-vertical, calcite-filled joint. Overall, the core is lightly calcareous and stylolitic. IGT plug was cut perpendicular to the joint, but did intersect a stylolite in the axial direction. An additional petrographic sample was obtained from the joint.
- 9247.6-9248.7 ft: Fine sandstone with scattered shell fragments and bituminous zones, medium gray (N5), thin bedded, highly calcareous, overlain by fine sandstone containing abundant quartz pebbles scattered throughout, brownish gray (5YR4/1), thick bedded, lightly calcareous. The contact between these two units is quite sharp. An irregular, near-vertical natural fracture runs the length of the core. It is open in the calcareous sandstone, but contains abundant scattered calcite mineralization in the overlying pebble-bearing sand. IGT plug was cut horizontally in the pebble-bearing sand about 1 cm above the contact with the calcareous sand, and at about a 45° angle to the nature fracture. Pains were taken to avoid intersecting the fracture in the core plug. A plug for IIT was cut just above the IGT sample.
- 9285.6-9286.1 ft: Conglomeratic limestone, medium light gray (N6), thinly laminated to thin bedded. Core consists primarily of packstone, composed of broken oyster shell fragments with abundant coarse-sand to pea-gravel size quartz. Millimeter-size solution porosity is common throughout, but more abundant in restricted zones. A few clay clasts are also present. IGT plug was cut from one of the visibly porous zones in the core. IIT plug was taken immediately above.
- 9292.4-9294.0 ft: Fine sandstone, olive gray (5Y4/1) thick bedded, uniform, very weakly calcareous. A few sub-horizontal stylolites are present near the top of the core, and some thin carbonaceous laminae occur in a 2-cm thick zone near the base. A very irregular, compound, near-vertical natural fracture is present along the core margin; it appears to be mineralized in places. IGT plug was cut from the very uniform, central portion of the core, carefully avoiding the fracture. IIT plug was taken from same area.
- 9269.9-9298.3 ft: Fine sandstone, olive gray (5Y4/1), thick bedded, pebbly near base. Upper 0.3 feet of core consists of uniform, lightly calcareous sand, remainder is composed of shelly, moderately calcareous sand with a number of stylolitic zones. A large, light olive gray (5Y6/1), highly calcareous zone is present along the core margin from 9297.7 to 9298.0. This appears to be a patch of authigenic mineralization based on the continuity of bedding features and orientation. A number of coring-induced petal and petal-centerline fractures also occur along the core margins. IGT plug was cut at 9297 feet exactly, parallel to the slabbed face and perpendicular to a marginal petal fracture. IIT plug was cut 0.3 feet lower.

- 9305.4-9307.1 ft: Fine sandstone, olive gray (5Y4/1), thick bedded in upper portion of core, thickly laminated near base. A compound, near-vertical natural fracture occurs along the margin of the core over its entire length. Parts of the fracture are mineralized with calcite, although remainder of core is noncalcareous. Some thin carbonaceous/shaly laminae occur near the base of the core. IGT and IIT plugs were cut from the uniform, thick-bedded, upper portion of the core in a direction perpendicular to the natural fracture face.
- 9309.9-9310.6 ft: Argillaceous, carbonaceous fine sandstone, light brownish gray (5YR6/1), thinly laminated to thin bedded. Core contains numerous shaly laminations and clasts, as well as many carbonaceous or bituminous-rich beds. Shell fragments are abundant, and core is highly calcareous throughout. IGT plug was cut from a fairly uniform, non-laminated, calcareous sandstone bed near the base of the core. IIT plug was obtained from another uniform bed 0.4 feet higher in core.
- 9316.8-9317.3 ft: Fine sandstone, olive gray (5Y4/1), thinly laminated to thin bedded. A compound, calcite-mineralized natural fracture occurs along the margin of the core; it is intercepted by a coring-induced petal fracture. Other coring-induced fractures are also present on the core margins. The core itself is lightly calcareous, and the IGT plug was cut from the uniform, central portion. Care was taken to avoid intersecting any fractures in the core plug.
- 9321.1-9322.4 ft: Most of core consists of fine sandstone, olive gray (5Y4/1), thin bedded with faint, thin laminations and lightly calcareous. Basal 0.2 feet consists of sandy, carbonaceous shale, olive black (5Y2/1), thinly and irregularly laminated, noncalcareous, containing sandstone clasts 5mm to 5cm in width. A near-vertical, calcite-mineralized natural fracture runs along the core margin through the length of the sandstone lithology, and terminates at the top of the shale bed. A few shaly clasts occur in the basal portion of the sandstone. IGT plug was cut from the top part of the core, parallel to the slabbed face, and the IIT plug was cut from the center of the core perpendicular to the slabbed face to avoid intercepting the fracture.
- 9326.7-9327.7 ft: Fine sandstone, olive gray (5Y4/1), thinly laminated to thin bedded, very lightly calcareous. A few very thin carbonaceous laminae and stylolites occur in the upper portion of the core, and some small clay clasts (1-3mm) are scattered near the base. The core is fairly uniform and unfractured overall, although a few coring-induced petal fractures occur along the margin. IGT and IIT plugs were cut from uniform sandstone in the center of the core, below the stylolitic zone.

4.5.2. Reservoir Properties

IGT analyzed 16 plug samples from the 9200 to 9350 foot interval in the SFE No. 3. These were obtained from the Taylor Sandstone member of the Cotton Valley Group, underlying the Travis Peak. Although this is a different formation, the diagenetic histories between the Taylor and Travis Peak are similar

enough to permit at least some direct comparisons. From whole core samples received from the Texas BEG, 1 inch diameter plugs were cut for analysis were cut at IGT and 1.5 inch diameter plugs were cut for the IIT research project. Table 5 summarizes the results of core analysis on SFE No. 3 samples. Net-confining stresses representative of initial reservoir and half-drawdown conditions were calculated based on a confining pressure gradient of 0.75 psi/foot and pore pressure gradient of 0.38 psi/foot.

Permeabilities and porosities for the SFE No. 3 samples were in the same general range as the SFE No. 2 and the tighter Mast A-1 samples. The SFE No. 3 samples also displayed some decrease of permeability with time, but not as severe as the Mast A-1 samples. In some of the samples the phenomenon was easily noticed in the Klinkenberg plot, where it caused one or more points to deviate significantly from the straight line through the rest of the data points. Since much of the permeability decrease with time occurred during the first 2 to 3 days after the imposition of confining stress, it was always the very first permeability measurement of the series that was affected the most. In cases where such anomalous data points were observed in Klinkenberg plots, these points were dropped from the set used for calculating k_w and b . Detailed Klinkenberg plots for the SFE No. 3 samples are available in the appendix.

The calculated values of tortuosity in Table 5 show a behavior that goes against the expected increase of tortuosity with confining stress. In all cases, the calculated tortuosity was higher at the lower net confining stress. Physically, however, one would expect the closure of some pore throats at higher net stress to increase the tortuosity. This discrepancy is probably also caused by the decrease of sample permeability with time. Since the Klinkenberg data points are obtained over a period of several days, a slow decrease in sample permeability with time can manifest itself as a change in slope of the Klinkenberg plot. Since calculated values of mean pore width and tortuosity are directly dependent on, and very sensitive to the Klinkenberg slope, they are strongly influenced by this phenomenon. Similar discrepancies are apparent in the data for Mast A-1 samples. The order in which data points for each sample were measured was such that the low net stress data was first obtained while decreasing pore pressure from 1500 to 300 psi. The high net

Table 5. SUMMARY OF SFE NO. 3 CORE ANALYSIS RESULTS

Plug Depth, ft	Unconfined Sample Mercury Penetration Data				Swanson Parameter (S_w/E_c), max, %/psi	Net Confining Stress, psi	Gas Porosity, %	Klinkenberg Permeability, μd	Klinkenberg 'b', psi	Gas Flow Path Characteristics		Pore Volume Compressibility, 10^{-6} /psi	Stress Dependence Exponent for Permeability, α
	Entry Pressure, psi	Porosity, %	Median Pore Width, μm	Pore Width, μm						Width, μm	Tortuosity		
9226.0	1198	1.00	0.026	0.21 X 10^{-3}	3420	1.52	0.346	105	0.089	5.36	18.2	1.72	
					5170		0.170	233	0.041	3.44			
9228.0	528	6.15	0.098	3.34 X 10^{-3}	3420	6.91	3.63	98	0.095	3.80	4.9	0.91	
					5170		2.50	141	0.066	3.16			
9234.0	1183	1.36	0.020	0.24 X 10^{-3}	3420	1.63	0.551	81	0.114	5.70	18.1	1.75	
					5170		0.267	208	0.045	3.20			
9237.0	2004	1.21	0.012	0.082 X 10^{-3}	3420	1.52	0.161	68	0.138	12.21	10.1	2.43	
					5170		0.039	323	0.029	4.21			
9237.7	--	--	--	--	3420	0.97	3.12	46	0.203	3.26	20.6	1.63	
					5180		1.58	105	0.089	2.01			
9242.0	689	7.26	0.054	2.29 X 10^{-3}	3420	8.23	3.38	56	0.165	7.41	6.5	1.96	
					5180		1.50	234	0.041	2.71			
9246.5	412	5.84	0.120	4.00 X 10^{-3}	3420	5.62	3.77	70	0.132	4.68	6.1	1.47	
					5180		2.05	152	0.062	2.90			
9248.0	135	7.27	0.259	10.67 X 10^{-3}	3420	7.35	33.20	45	0.206	2.79	4.8	0.44	
					5180		27.69	55	0.168	2.49			
9286.0	--	--	--	--	3440	6.97	48.38	56	0.168	1.84	4.8	1.06	
					5210		31.13	79	0.119	1.62			
9293.1	252	8.07	0.175	7.81 X 10^{-3}	3440	8.84	14.69	67	0.138	3.10	4.2	0.54	
					5210		11.76	82	0.114	2.84			
9297.0	392	5.97	0.106	3.64 X 10^{-3}	3440	6.39	3.00	76	0.123	5.17	4.9	1.20	
					5210		1.82	151	0.062	3.31			
9306.0	631	3.44	0.075	1.48 X 10^{-3}	3440	3.56	0.515	119	0.078	5.94	6.4	1.97	
					5210		0.227	210	0.045	5.06			
9310.5	441	1.24	0.078	0.70 X 10^{-3}	3450	1.19	1.25	73	0.128	3.58	28.0	1.83	
					5220		0.587	139	0.068	2.74			
9317.0	1788	2.44	0.023	0.32 X 10^{-3}	3450	3.21	0.152	205	0.045	6.01	5.7	1.49	
					5220		0.082	290	0.032	5.79			
9321.1	1121	3.66	0.037	0.76 X 10^{-3}	3450	4.19	0.418	171	0.054	4.96	6.2	1.18	
					5220		0.256	229	0.041	4.74			
9327.0	317	9.43	0.157	8.25 X 10^{-3}	3450	9.88	21.28	61	0.153	3.00	4.2	0.47	
					5220		17.54	74	0.126	2.73			

stress data was then obtained while increasing pore pressure from 300 to 1500 psi. Superimposing a decrease of permeability with time on such a data set, one can see that the Klinkenberg 'b' will be underestimated for the low net stress, and overestimated for the high net stress. This scenario is in agreement with the observed discrepancy.

Most of the SFE No. 3 samples show a low pore volume compressibility similar to other East Texas tight sands analyzed thus far. The only samples that yielded high values of pore volume compressibility were the ones that had very low porosities of less than 2%. The stress dependence exponent (α) for permeability also shows values in the range encountered during analysis of Mast A-1 and SFE No. 2 samples as well as Rocky Mountain tight sands. Again, the very low porosity (<2%) samples display somewhat higher stress dependence than the rest.

Mercury porosimetry data for samples 9237.7 and 9286.0 did not yield capillary pressure curves amenable to the conventional analysis by which entry pressure and other parameters were determined for the other samples. The curves for these two samples were close to a straight line, rather than displaying the usual entry pressure, followed by a plateau region. Total penetration at 30,000 psi was approximately 1% of bulk volume for both these samples. While this value is in agreement with gas porosity for sample 9237.7, the gas porosity for 9286.0 was a much higher 6.97%. This suggests that sample 9286.0 is very heterogeneous, and the chip submitted for mercury porosimetry just happened to consist primarily of low porosity rock. Interestingly, the values of tortuosity calculated for both these samples is very low.

Porosities calculated from mercury porosimetry on unconfined chips correlate well with porosities measured using the gas expansion technique in the CORAL. Also, median pore widths calculated from the mercury porosimetry data follow the trend shown by the pore widths estimated from Klinkenberg data.

5.0. PORE STRUCTURE STUDIES

Documentation of the pore structure of tight gas sandstone samples analyzed in the laboratory at IGT has been found to be a useful procedure for understanding many of the measured petrophysical properties.⁹ This can be performed by using optical microscopy, SEM, or both. IGT has found the optical microscope to be best for observing overall pore geometry and structure, while the SEM is better for identifying pore minerals and studying the nature of grain contacts in the sample.

5.1. Petrographic Methods

Observation of rock samples with an optical microscope can be performed by either reflecting the light from the polished surface of the rock, or by slicing the sample thin enough so that the mineral components are transparent. Samples sliced in this manner are known as "thin sections," because they are ground down to a standard thickness of only 30 micrometers. To observe the pore spaces in the thin section, the rock sample is traditionally impregnated with a blue-dyed epoxy before the section is prepared. The blue epoxy fills the pore space, making most larger pores visible under the microscope. However, in tight sands containing narrow, linear fracture porosity, microporous chert, clay, or organic materials, the blue-dyed epoxy is difficult or impossible to see in a thin section. A solution to this problem was developed in 1984 by Robert Gies¹⁰ of Canadian Hunter Exploration, Ltd., in Calgary. Gies simply replaced the blue dye in the epoxy with a fluorescent dye, rhodamine-B, and studied the thin sections using incident-light fluorescence microscopy, a technique that has long had extensive medical, biological, and industrial applications. The rhodamine-B dye in the pores fluoresces strongly when illuminated by an incident light beam of a specific exciter wavelength. A dichromatic interference filter allows only the rhodamine fluorescence to reach the eyepiece of the microscope, blocking all other wavelengths. This makes the pore structure clearly visible due to the very high contrast created between the glowing epoxy and the "blacked-out" mineral grains. The incident-light approach of fluorescent microscopy also permits this technique to be applied to opaque materials such as shale and coal. In addition, the natural red color of rhodamine-B shows up under

transmitted light, preserving all of the features of the blue dye method. All tight sandstone samples at IGT are routinely impregnated with a fluorescent-dyed epoxy prior to thin sectioning.

Petrographic observations on tight sandstone cores have revealed that three main classes of pore geometry¹¹ occur in these rocks:

- 1) Grain-supported primary pores, with the throats plugged by clay, calcite or other authigenic minerals, where the rock may or may not show some development of secondary solution pores. This is the classic type of tight sand described by Wilson¹² and is basically a conventional sand made tight by precipitation of minerals in the pore throats. These sands generally exhibit low pore volume compressibility, as well as low stress-dependence of permeability.
- 2) Highly altered primary porosity, extensively filled-in with authigenic minerals, usually quartz overgrowths, coupled with significant amounts of secondary solution pore development, which makes up the bulk of the rock's porosity. Primary porosity is reduced to narrow, flat "slot" pores, which occur along the boundaries of adjoining quartz overgrowths. These slots are typically only about 0.1 micrometer in width under reservoir net stresses,⁹ and are propped open by irregular bumps or "asperities" on the faces of the adjoining overgrowths.¹³ Although most of the porosity occurs in the solution pores, the only connection between individual solution pores is commonly by way of the slots. Thus, the narrow slots provide a bottleneck for movement of pore fluids and make the rock tight. The flat, poorly supported structure of the slots is responsible for the high stress-dependence of permeability in these types of tight sands, and the narrow, uniform openings are highly susceptible to capillary blockage by imbibed water. Secondary solution pores interconnected by slots is the most common type of pore geometry observed by us in the Travis Peak and Taylor sandstones, as well as in Rocky Mountain tight sands.
- 3) Ultrafine microporosity in an all-pervading matrix composed of clay, carbonate or silica, in which sand-sized quartz grains, which may or may not be honeycombed, are suspended. This is a less common type of tight sand pore geometry that tends to exhibit a high degree of pore volume compressibility because of the lack of strong grain-to-grain support. Stress dependence of permeability may or may not be high, depending on the composition of the matrix. Calcite and silica matrices are much more stress resistant than clay, and the presence of honeycombed grains adds to the resistance by providing additional supported flowpaths. The effects of water imbibition on gas flow through this type of pore geometry are also somewhat variable; but, in general, pores of this nature are very small and easily plugged. These pores were more common in the Taylor sandstone in the SFE No. 3 core than in any of the Travis Peak samples.

Individual tight sand samples often contain more than one class of pore geometry, although a single class usually predominates. Schematic drawings

illustrating the differences between the three classes of pore geometry are shown in Figure 5.

Tight petrographic samples are impregnated at IGT using a two-stage process to insure that the epoxy fully penetrates the pore volume. The rock sample is first placed under a vacuum in a small plastic beaker to remove air and other gases from the pores. Then, while still under vacuum, the small beaker is half-filled with degassed epoxy, completely covering the rock sample. In the second stage of the process, a rubber membrane is secured over the top of the plastic beaker and the epoxy-covered sample is placed in a small pressure chamber. The epoxy is forced into the pore system under a hydraulic pressure of up to 2000 psia, well above the deduced highest capillary entry pressures for these rocks. After remaining under pressure for several hours, the rock is removed and the epoxy cured in an oven. IGT utilized a low-viscosity casting epoxy for impregnation to achieve the best results.

Once the rock has been impregnated, a flat-ground surface of the sample is glued to a flat-ground glass slide. The bulk of the sample is then trimmed away in a cut-off saw, and the thin slice remaining on the slide is ground and polished down to 30 micrometers, and then finished with a cover slip.

5.2. Results

Observations of thin sections of the Travis Peak from the SFE No. 1 well clearly indicate that a change occurs in the pore morphology with increasing depth. This was not unanticipated in view of Dutton's studies,¹⁴ which showed a strong depth correlation between quartz overgrowth volume, reduced permeability and lower porosity in the Travis Peak. In addition, IGT measurements show porosity and permeability in the SFE No. 1 core decreasing with increasing depth, and these data dovetail neatly with those obtained on the deeper Mast A-1, SFE No. 2, and SFE No. 3 cores. These differences in petrophysical properties are reflected by changes in pore morphology of the cores. Changes in pore structure and petrophysical properties with depth in the SFE No. 2 core samples are not as pronounced as those seen in the Mast and SFE No. 1 cores, and the abundant carbonate mineralization in the SFE No. 3 core makes comparisons with the others somewhat difficult. Examples of Travis Peak pore geometry are shown in the following figures.

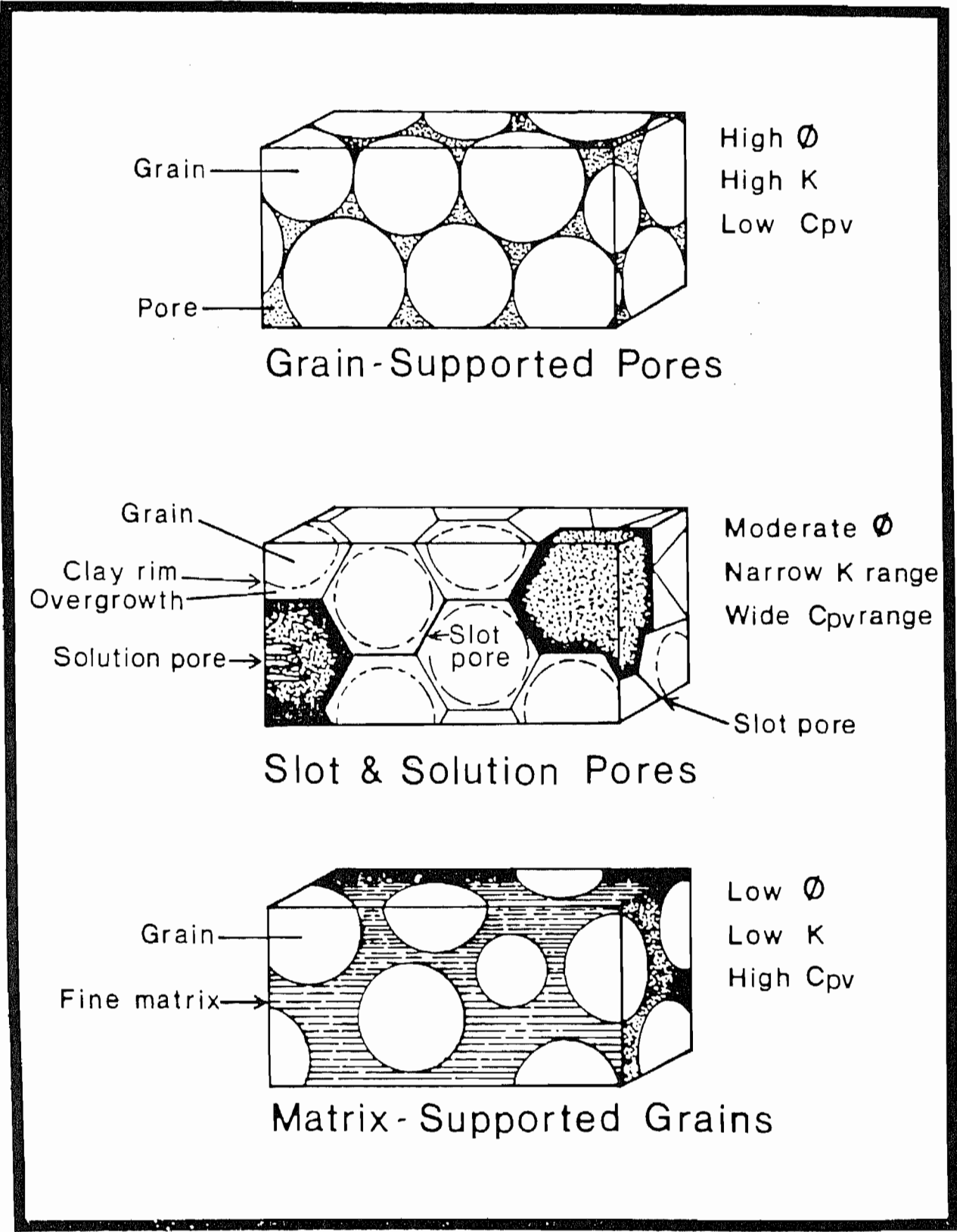


Figure 5. THREE TYPES OF INTERNAL PORE/GRAIN STRUCTURES PRESENT IN TIGHT GAS SANDSTONE

Figure 6 is a pair of photomicrographs of the 6122.8 foot sample from the SFE No. 1 core, which at 25 millidarcies exhibited the highest permeability of all the cores tested by IGT from the Travis Peak Sandstone. As can be seen in both the transmitted light and fluorescent views of the figure, this sample contains abundant primary and secondary porosity, with well-interconnected gas flowpaths resulting in high permeability.

The 7418.2 foot sample shown in Figure 7 is from 1300 feet deeper in the SFE No. 1 well than the previous sample, and displays significantly greater compaction of primary porosity. In addition, the quartz grains in this sandstone appear to have undergone some degree of pressure-solution, as evidenced by stylolitic grain boundaries. This was the only sample in the SFE No. 1 core observed to contain pressure-solution features. Significantly, it was also the tightest sample of those measured by IGT, with a permeability of only around 20 microdarcies. In comparison, the other SFE No. 1 cores had permeabilities ranging from 0.5 millidarcy to 25 millidarcies with no other sample measured approaching anywhere near the microdarcy permeabilities measured at 7418.2 feet.

Figure 8 is a pair of photomicrographs from the 7419.9 foot sample in the SFE No. 1 core, and is more representative of the Travis Peak at these depths. Much of the primary porosity has been infilled by quartz overgrowths and somewhat isolated secondary solution pores are common. Although the quartz overgrowths have not grown together to form slot pores, they have significantly obstructed primary porosity and increased the tortuosity of flowpaths visible between secondary pores. This is apparent if Figure 8 is compared to Figure 6, which was photographed at the same magnification. Surprisingly, stylolitic grain boundaries due to pressure solution are very rare in the 7419.9 foot sample, although they were fairly common in the 7418.2 foot sample only 1 1/2 feet above. Virtually all of the linear quartz grain contacts in the 7419.9 foot core are due to overgrowth precipitation, possibly of quartz derived from the pressure solution zone immediately above.

A permeability of about 0.5md was measured on the 7457.8 foot sample from the SFE No. 1 core, shown in Figure 9. This sample appears to be a mature tight gas sand, with extensive quartz overgrowths and slot pores. However, secondary porosity is not well-developed, and significantly amounts of primary porosity remain. This core, therefore, falls into a "transitional zone"

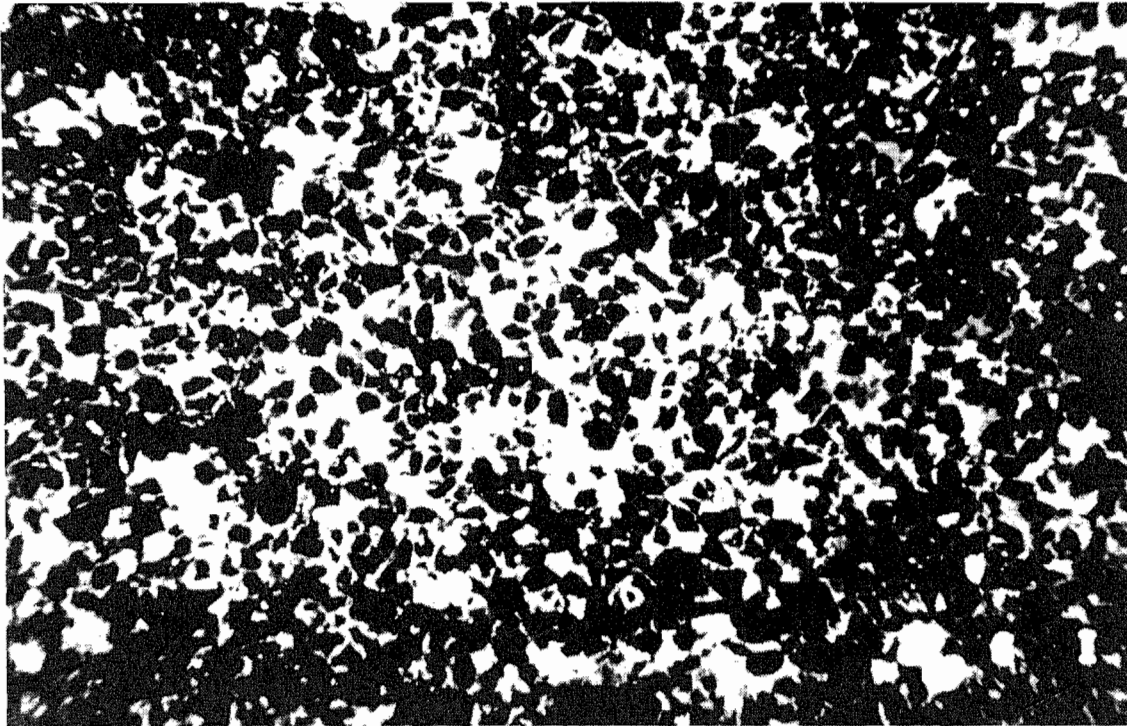
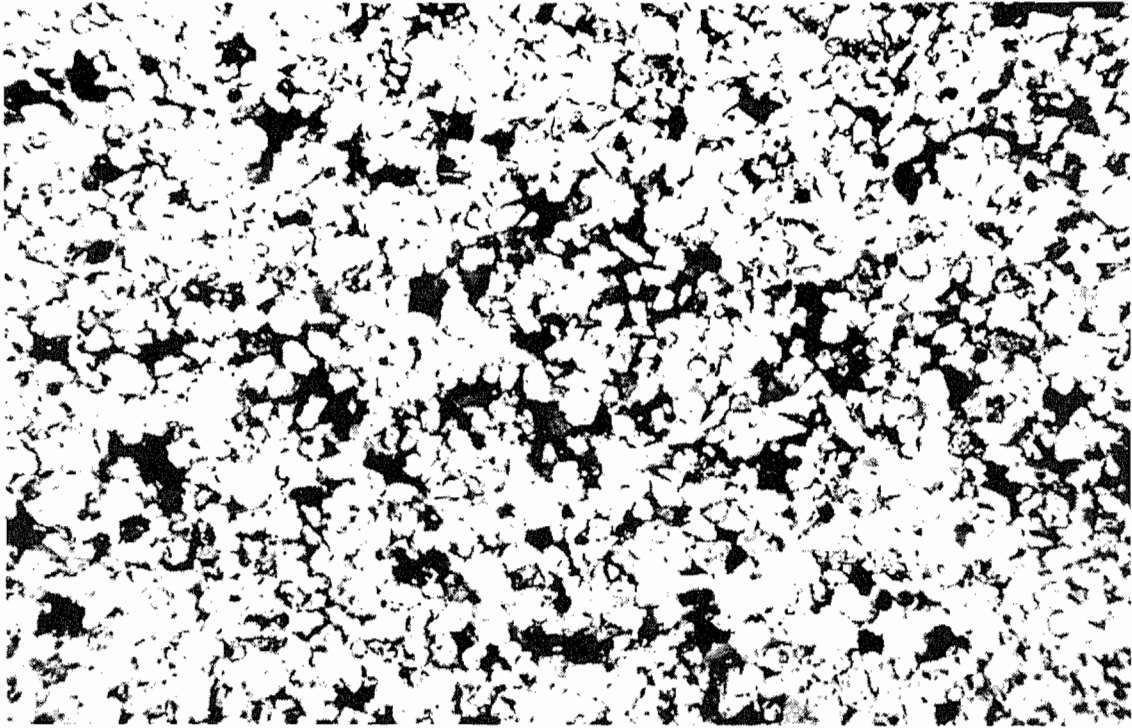


Figure 6. PHOTOMICROGRAPHS OF TRAVIS PEAK SANDSTONE FROM SFE NO. 1 CORE, 6122.8 FT. DEPTH, 30x, HEIGHT OF EACH PHOTO = 3.0mm; THIS WAS THE HIGHEST PERMEABILITY SAMPLE ANALYZED BY IGT FROM THE SFE NO. 1 CORE. UPPER PHOTO IN TRANSMITTED LIGHT SHOWS ABUNDANT PRIMARY AND SECONDARY POROSITY CONTAINING SIGNIFICANT AUTHIGENIC CLAY; LOWER PHOTO IN EPIFLUORESCENCE SHOWS THE EXTREMELY HIGH DEGREE OF INTERCONNECTION AMONG INDIVIDUAL PORES IN THIS ROCK

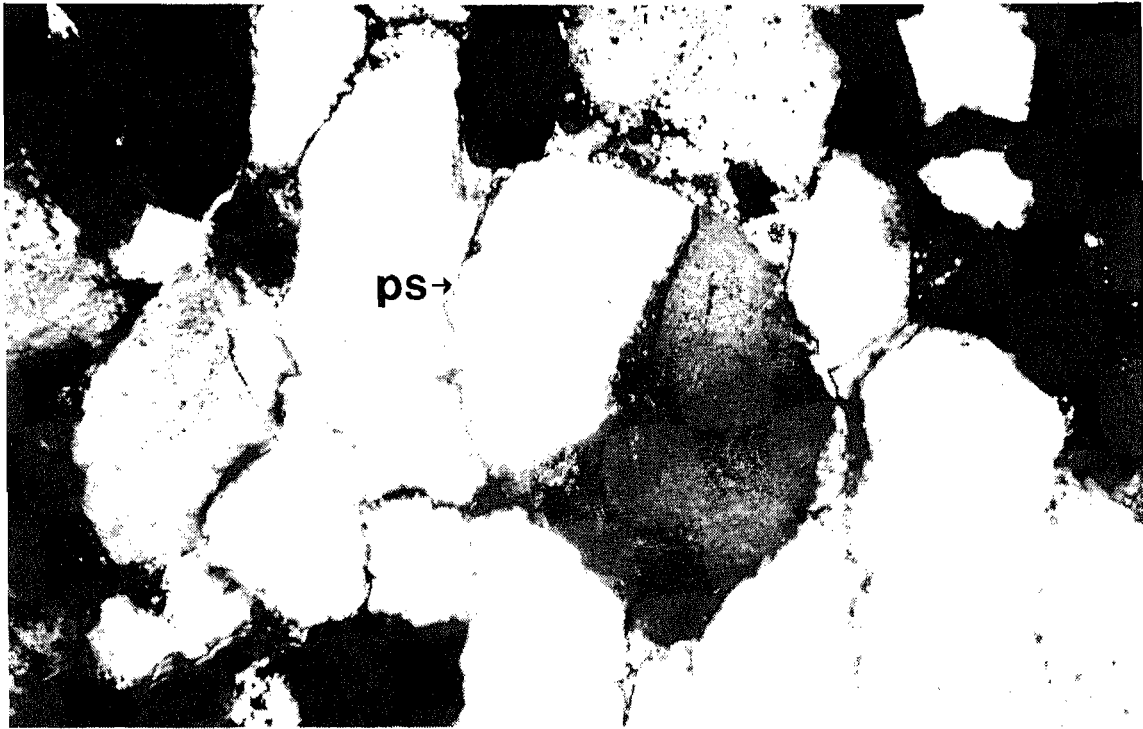


Figure 7. PHOTOMICROGRAPHS OF TRAVIS PEAK SANDSTONE FROM SFE NO. 1 CORE, 7418.2 FT. DEPTH, 200x, HEIGHT OF EACH PHOTO = 0.45mm; UPPER PHOTO IN PLANE, TRANSMITTED LIGHT THROUGH CROSSED POLARS SHOWS COMPACTED PRIMARY POROSITY AS WELL AS APPARENT PRESSURE-SOLUTION OF QUARTZ GRAINS (ps) REVEALED BY STYLOLITIC GRAIN BOUNDARIES. THE LOWER PHOTO IN EPIFLUORESCENCE SHOWS THAT MANY OF THE FLOWPATHS BETWEEN PORES RUN ALONG COMPACTED GRAIN BOUNDARIES. ARE THESE THE BEGINNINGS OF SLOT PORES?

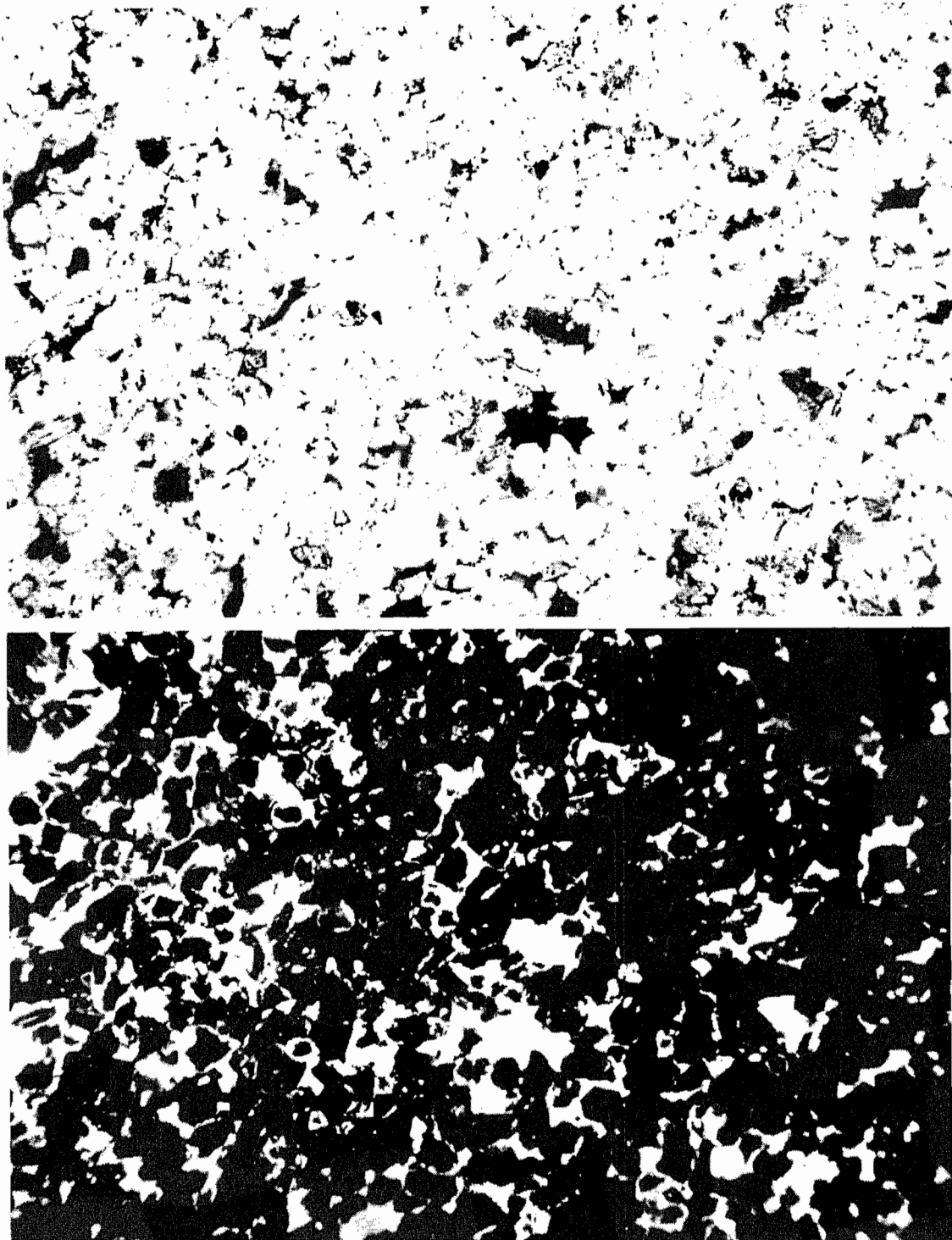


Figure 8. PHOTOMICROGRAPHS OF TRAVIS PEAK SANDSTONE FROM SFE NO. 1 CORE, 7419.9 FT. DEPTH, 30x, HEIGHT OF EACH PHOTO = 3.0mm; UPPER PHOTO IN TRANSMITTED LIGHT SHOWS FAIRLY ABUNDANT SECONDARY, CLAY-FILLED PORES AND MUCH SMALLER PRIMARY PORES OCCLUDED BY QUARTZ OVER-GROWTHS. IN SOME PARTS OF THE PHOTO, THE GRAINS ARE SO TIGHTLY INTERLOCKED THAT PRIMARY POROSITY IS ALL BUT ABSENT. THE LOWER PHOTO IN EPIFLUORESCENCE INDICATES THAT THIS SAMPLE MAY HAVE AN EARLY-STAGE SLOT PORE/SOLUTION PORE MORPHOLOGY INTERMEDIATE BETWEEN "CONVENTIONAL" AND "TIGHT" SANDSTONE

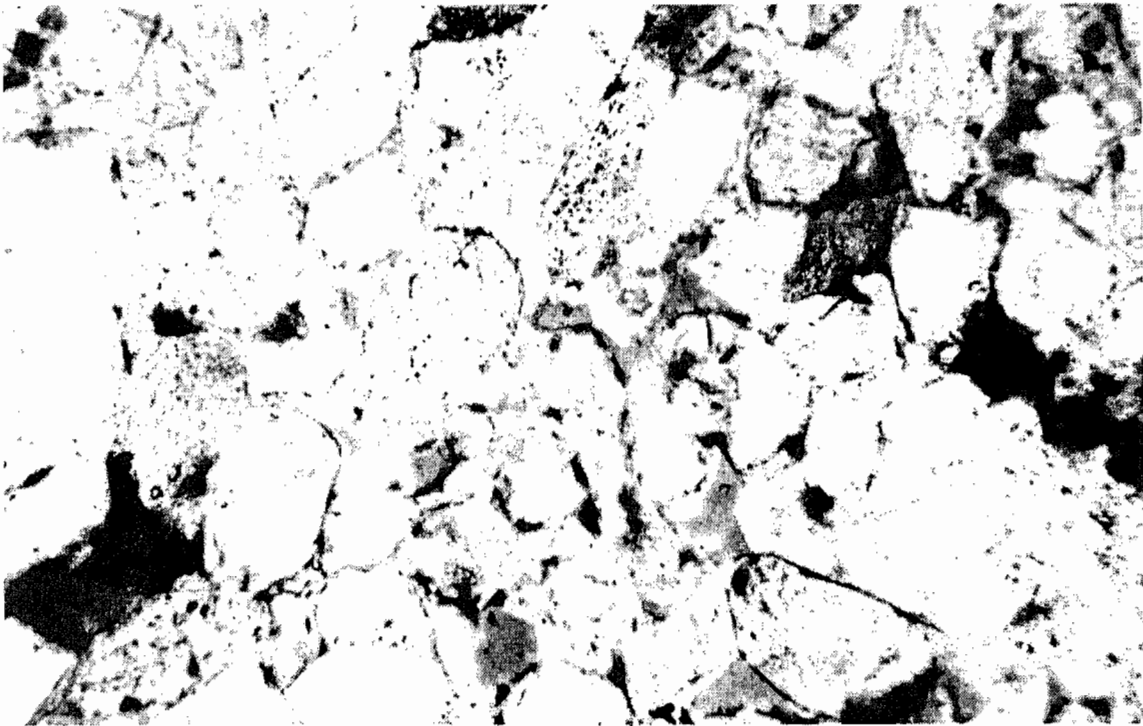
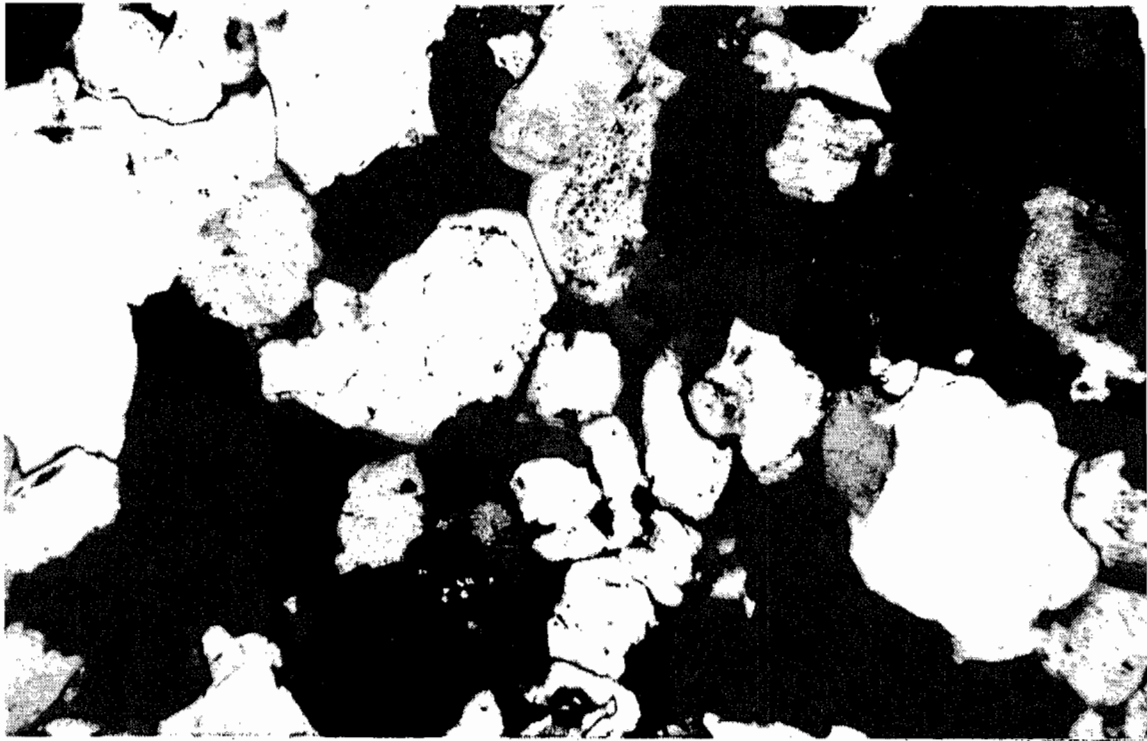


Figure 9. PHOTOMICROGRAPHS OF TRAVIS PEAK SANDSTONE FROM SFE NO. 1 CORE, 7457.8 FT. DEPTH, 100x, HEIGHT OF EACH PHOTO = 0.9mm; UPPER PHOTO THROUGH CROSSED POLARS SHOWS SLOT PORES BETWEEN ADJOINING QUARTZ OVERGROWTHS; ORIGINAL EDGES OF SOME SAND GRAINS ARE MARKED BY CLAY RIMS. ALTHOUGH THIS APPEARS TO BE A MATURE TIGHT SAND, THE LOWER PHOTO IN PLANE LIGHT REVEALS THAT QUITE A BIT OF CONNECTED PRIMARY POROSITY REMAINS, AND SECONDARY PORES ARE SOMEWHAT POORLY DEVELOPED

between conventional and tight sandstones, exhibiting features of both. Many of the other cores analyzed by IGT from the SFE No. 1 well also contain "transitional" features, providing an overview of the diagenetic processes by which conventional sandstones can be made "tight."

Figure 10 is a trio of photomicrographs from the 8275 foot sample in the SFE No. 2 core. This figure shows the solution pore/slot pore geometry common in the Travis Peak and other tight gas sands. The original grain which formed the solution pore on the right side of the photos is completely dissolved away, and a crystal of authigenic feldspar has precipitated along one edge of the pore. In contrast, the solution pore on the left side of the photos contains the skeletonized remnant of the original sand grain. Photos like these indicate that formation of secondary porosity in clastic rocks is a complex process which depends upon the mineralogy of the original grains, and may well occur at several different stages during diagenesis. The bottom, epifluorescent photo in Figure 10 also serves to illustrate the morphology of slot pores between quartz overgrowths, and the somewhat tortuous flowpaths a gas molecule must trace between solution pores when moving by way of the slots.

The 8730 foot sample from the SFE No. 2 core, shown in Figure 11, contains a very different pore geometry than that seen in the previous figure. This rock is comprised of sand grains compacted into an ultrafine porous matrix of clay and carbonate, which can be more easily seen in epifluorescence. Most of the larger, rounded dolomite rhombohedrons appear to be sedimentary in origin, rather than authigenic. This sample had one of the lowest permeabilities along with the highest stress-dependence of all the cores measured. It also had the highest pore volume compressibility of the SFE No. 2 samples analyzed by IGT.

Figure 12 shows a more common type of pore geometry in the Travis Peak from the SFE No. 2 core. It is a pair of photomicrographs from the 9492 foot sample, and shows slots formed between tightly interlocked quartz overgrowths, solution pores, and a few tiny, remnant primary pores. Many of the solution pores are shaped and bounded by the flat overgrowth surfaces, indicating that at least some of the quartz precipitation occurred after formation of secondary porosity. Dissolution of unstable silicate minerals could have provided

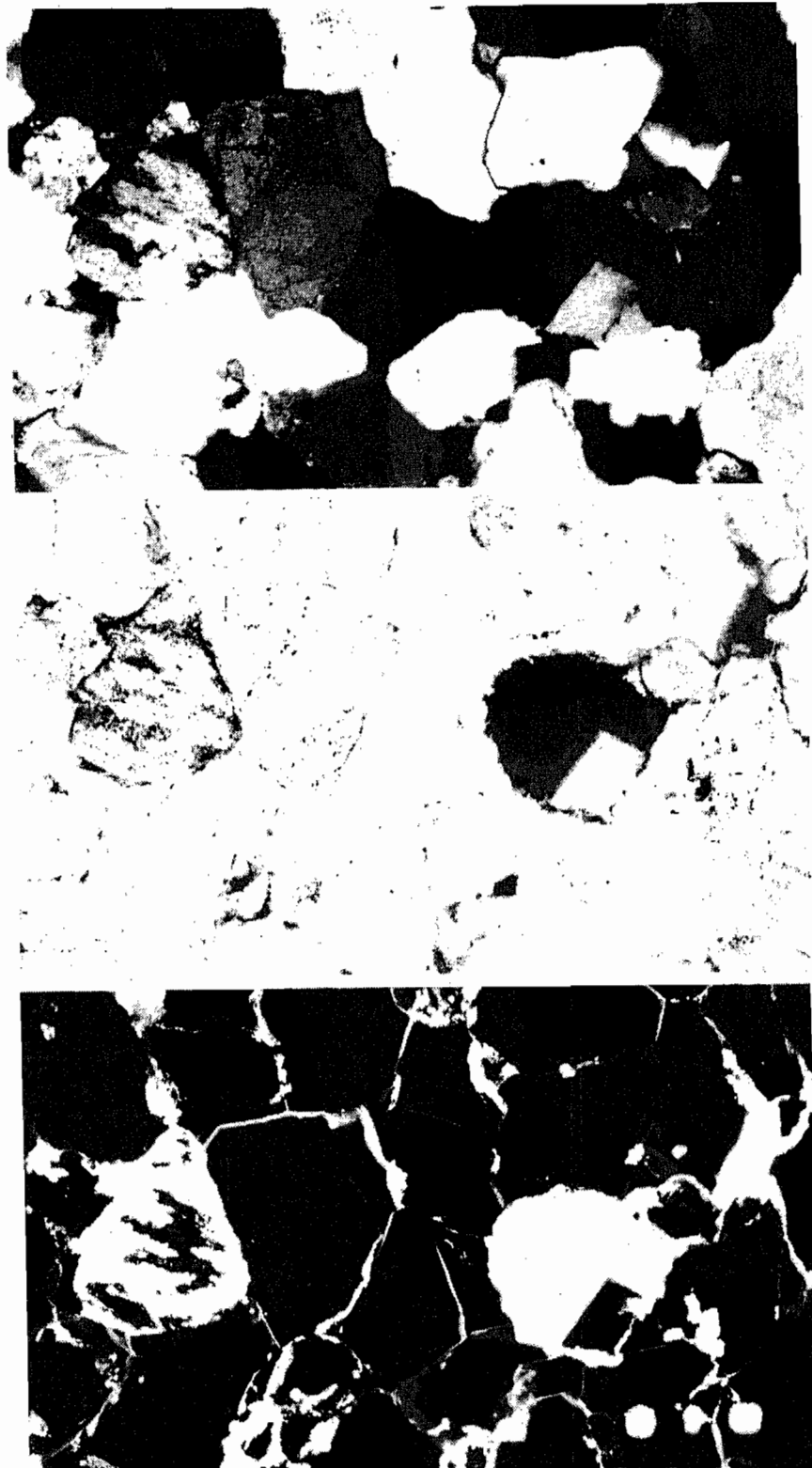


Figure 10. PHOTOMICROGRAPHS OF THE TRAVIS PEAK SANDSTONE FROM THE SFE NO. 2 CORE, 8275 FT, 100x, HEIGHT OF EACH PHOTO 0.77mm. UPPER PHOTO THROUGH CROSSED POLARS, CENTER IN PLANE LIGHT AND BOTTOM PHOTO IN EPIFLUORESCENCE. TYPICAL SOLUTION PORE/SLOT PORE MORPHOLOGY IS VISIBLE, WITH SECONDARY FELDSPAR IN PORE AT CENTER RIGHT, AND REMNANT HONEYCOMBED GRAIN IN PORE AT LEFT CENTER

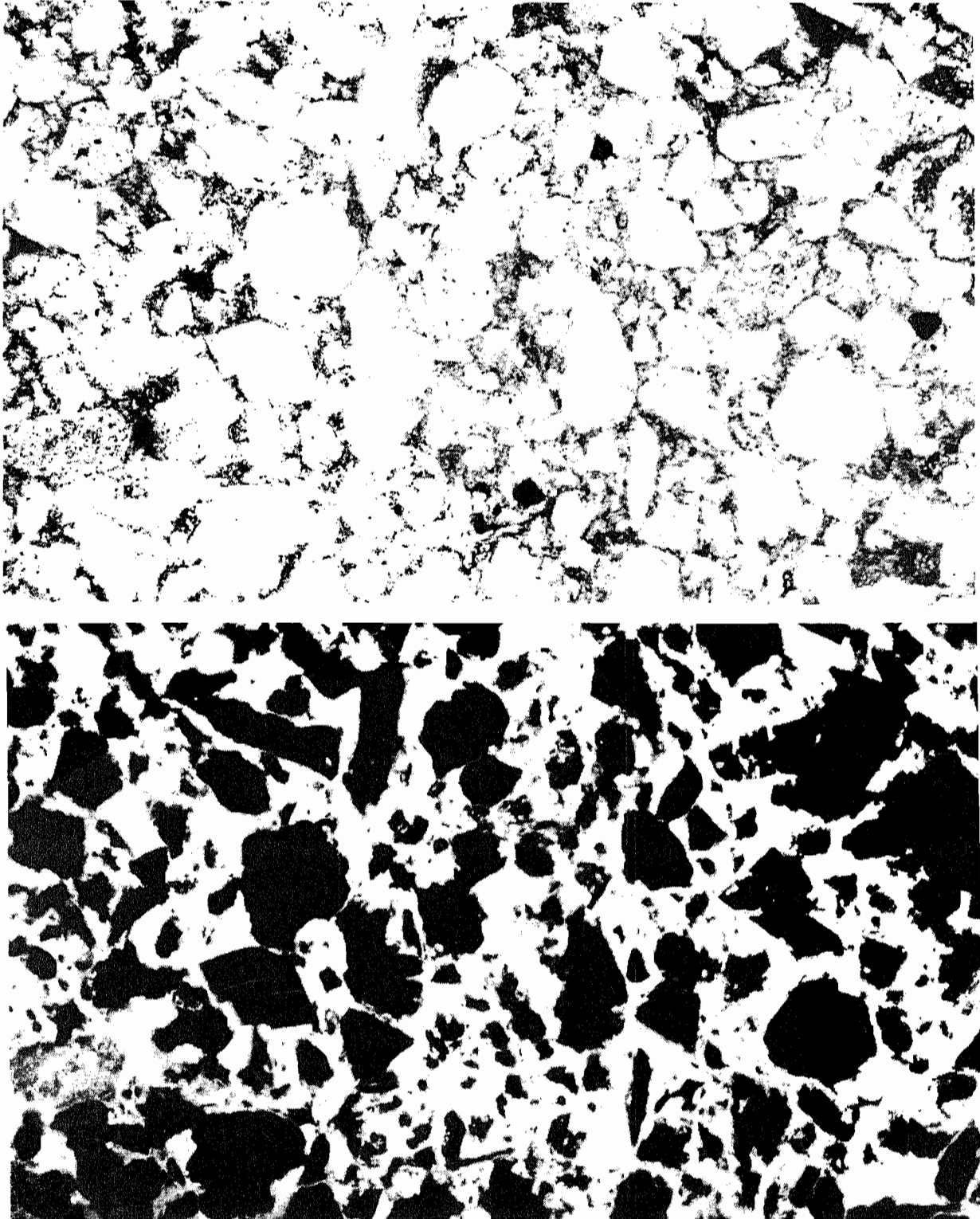


Figure 11. PHOTOMICROGRAPHS OF TRAVIS PEAK SANDSTONE FROM SFE NO. 2 WELL, 8730 FT., 100x, HEIGHT OF EACH PHOTO 0.77mm. ROCK IS COMPOSED OF SAND SIZE GRAINS SUSPENDED IN A MICROPOROUS CLAY MATRIX. UPPER PHOTO IN TRANSMITTED, PLANE LIGHT, LOWER IN EPIFLUORESCENCE

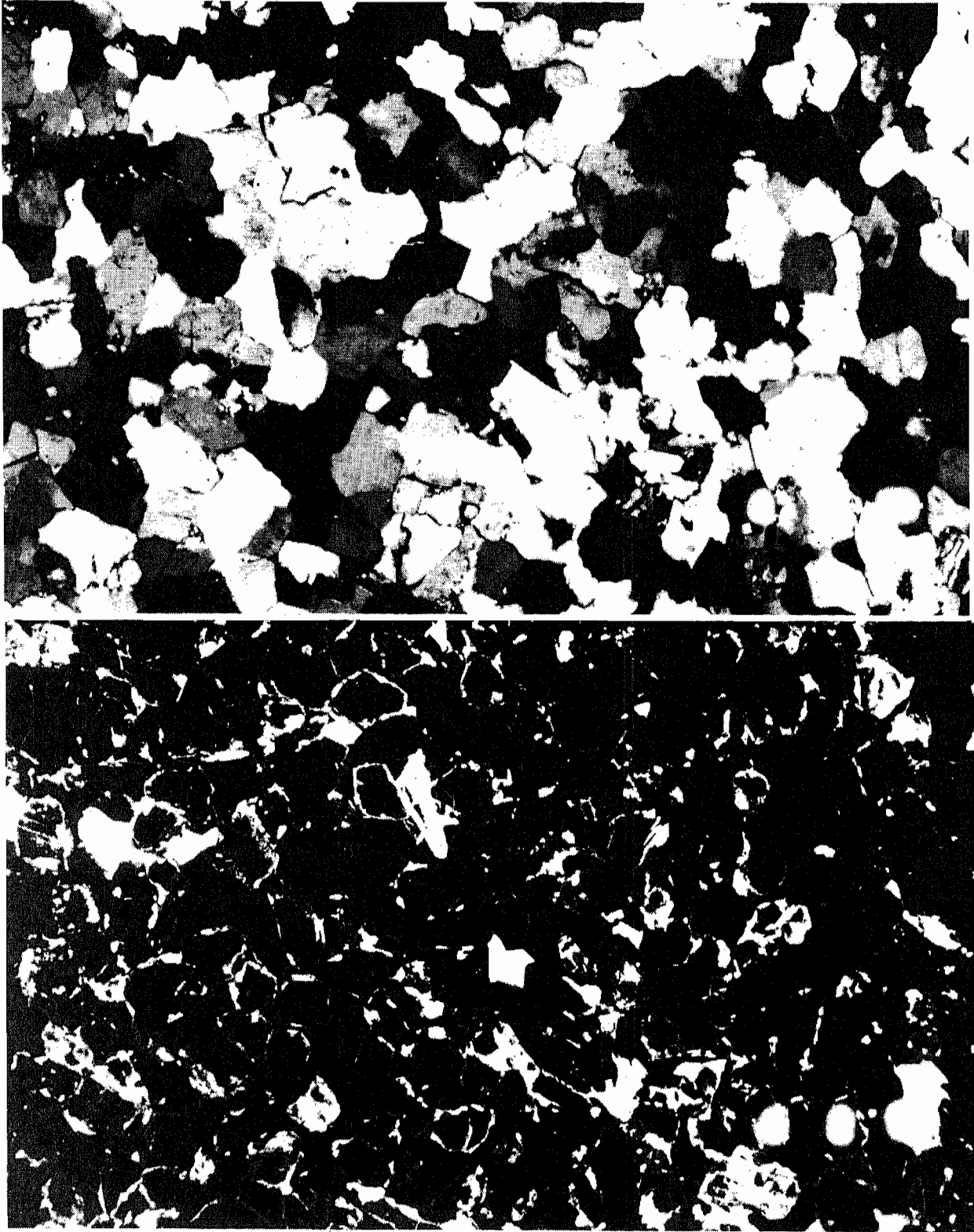


Figure 12. PHOTOMICROGRAPHS OF TRAVIS PEAK SANDSTONE FROM SFE NO. 2 WELL, 9492 FT., 40x, HEIGHT OF EACH PHOTO 1.85mm. TIGHT SLOT PORE - SOLUTION PORE GEOMETRY PREDOMINATES IN THIS SAMPLE, WITH ONLY VERY SMALL REMNANTS OF PRIMARY POROSITY. UPPER PHOTO THROUGH CROSSED POLARS, LOWER IN EPIFLUORESCENCE

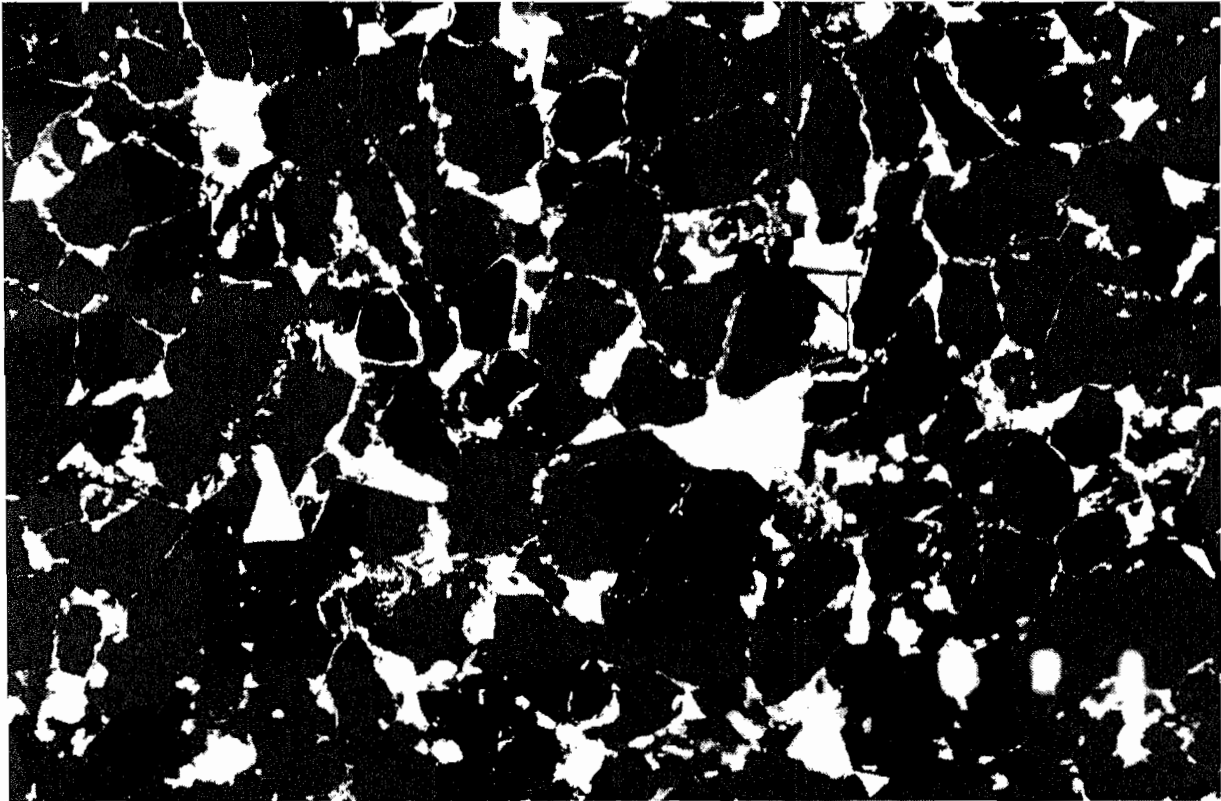
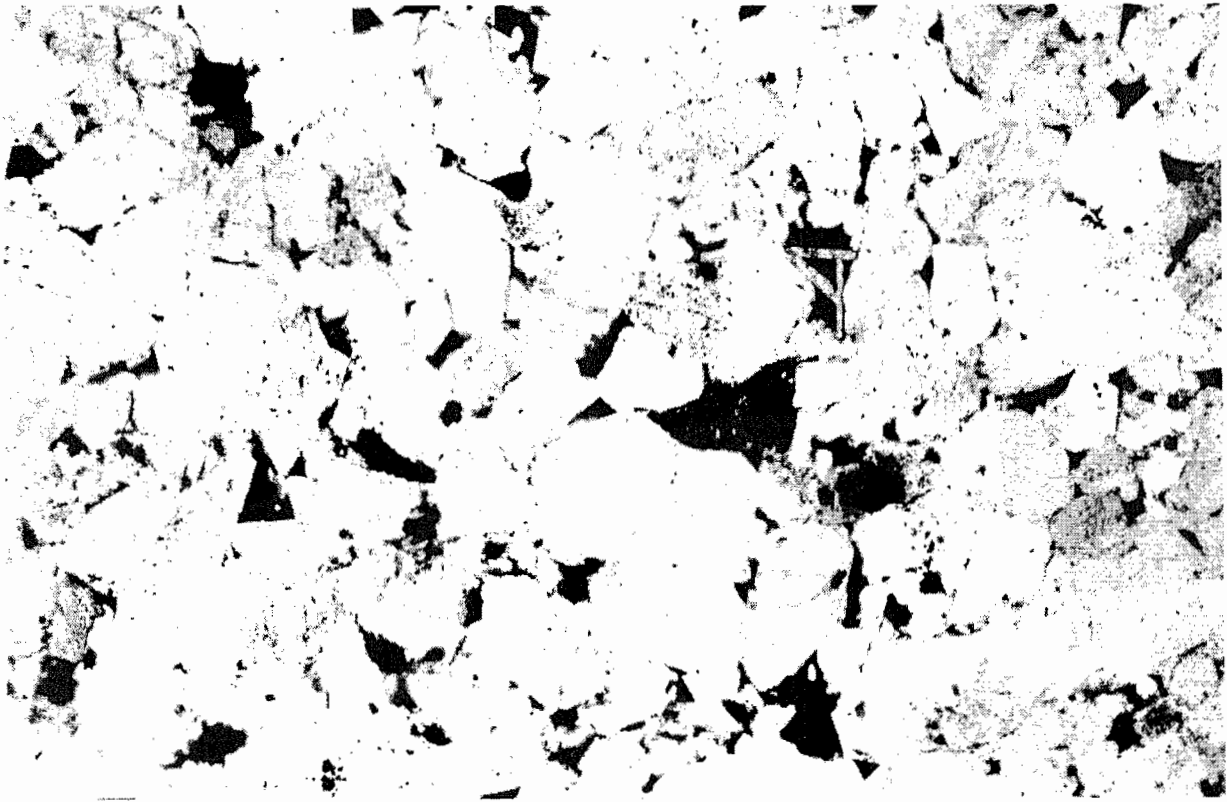


Figure 13. PHOTOMICROGRAPHS OF THE TRAVIS PEAK SANDSTONE, SFE NO. 2 WELL, 9875.9 FT., 40x, HEIGHT OF EACH PHOTO 1.85mm. UNUSUAL SLOT PORE/SOLUTION PORE GEOMETRY WITH SIGNIFICANT AMOUNTS OF REMNANT PRIMARY POROSITY PRESERVED AS WELL. UPPER PHOTO IN PLANE LIGHT, LOWER IN EPIFLUORESCENCE

a significant source for some, if not most of the silica in solution that later precipitated as quartz overgrowths.

The photomicrographs in Figure 13 show the pore geometry in the 9875.9 foot sample from SFE No. 2. This rock contains slot pores and solution pores like the previous sample, but a significant quantity of grain-supported primary porosity is present as well. The flat sides of many of the primary pores indicate that quartz overgrowths have occluded at least a portion of the original pores. A number of slot-like, linear pores along grain boundaries can be seen, and unusual lath-like crystals of an unidentified mineral, possibly quartz, are present in a solution pore at upper left center. This sample apparently represents a "transitional" lithology between conventional and tight sandstones. It is, in fact, quite similar in appearance to samples from the SFE No. 1 core, which were also identified as members of the "transitional" lithology.

SFE No. 3 cores were obtained from the Taylor Sandstone in the Cotton Valley Group, below the Travis Peak. The Taylor is much more calcareous than the Travis Peak, and consequently, one of the more common pore geometry types consists of quartz sand grains suspended in a calcite matrix. Other samples contained significant primary porosity instead of the calcite matrix; these also generally exhibited the highest permeabilities and lowest pore volume compressibilities. Interestingly, the "slot pore-solution pore" microstructure, which is predominant in the silica-rich Travis Peak is less common in the calcareous Taylor sandstone in SFE No. 3. Cracks or slot-like openings are present in many of the calcite-mineralized rocks, however, at boundaries between the calcite matrix and quartz sand grains. These cracks are not very well interconnected, and the contribution they may make to permeability is unknown. As these features were not judged to be important to fluid flow, no work was done to look for evidence (asperities that prop the slots or clays lining the slots) to determine whether the slots exist in the reservoir or are artifacts.

The pore geometry of the SFE No. 3 cores analyzed by IGT is summarized in the appendix of this report. There is no apparent trend of pore geometry type changing with depth in SFE No. 3, as was seen in the three Travis Peak cores

(Mast, SFE No. 1 and SFE No. 2) analyzed by IGT. This may be due to the relatively limited depth interval over which the SFE No. 3 cores were selected, and the abundant calcite mineralization throughout this core may have helped mask subtle differences in the pore geometry.

6.0. RESERVOIR PROPERTY CORRELATIONS

In this section we present some data correlations that should be useful in characterizing the tight gas sandstone reservoirs. In addition to correlations of porosity and permeability versus depth, we have attempted correlations of laboratory-measured reservoir parameters with mercury porosimetry data and petrographic observations. The ultimate aim of such an exercise is to develop a generalized procedure for estimating tight sand reservoir properties from relatively inexpensive mercury porosimetry and petrography on small sample chips.

6.1. Porosity and Permeability

Figure 14 is a plot of porosity at initial reservoir net stress versus depth for all the East Texas sandstone samples studied thus far at IGT. It is obvious from the plot that as depth increases to 9240 feet, there is a strong drop-off in porosity. Porosity in samples deeper than 9240 feet does not decrease at a similar rate. The plot also shows that the SFE No. 3 samples, though from a very narrow depth interval (9226 to 9327 feet) show a very wide variation in porosity. It is important to recognize that the SFE No. 3 core was from the calcareous Taylor Sandstone, not the silica-rich Travis Peak, and represents a different rock type.

Figure 15 is a plot of permeability to gas at initial reservoir net stress as a function of depth for all of the East Texas sandstone samples. The plot shows a general trend of decreasing permeability with increasing depth, which is most evident when one traces the lowest permeability measured for each depth interval. Some of the high permeabilities measured on Mast A-1 samples were due to fractures. Bearing in mind that permeability in Figure 15 is plotted on a log scale, the plot also illustrates the extremely high permeability of the SFE No. 1 samples as compared to the rest of the cores. As discussed in the section on pore structure, this difference is related to the fact that the SFE No. 1 samples generally contain a considerable amount of primary porosity, while the primary porosity has been replaced to different extents in the other Travis Peak samples with secondary porosity and a slot/solution pore type of morphology. Although primary porosity is fairly abundant in the SFE No. 3 cores, the extensive calcite mineralization of the Taylor Sandstone has kept the permeability relatively low.

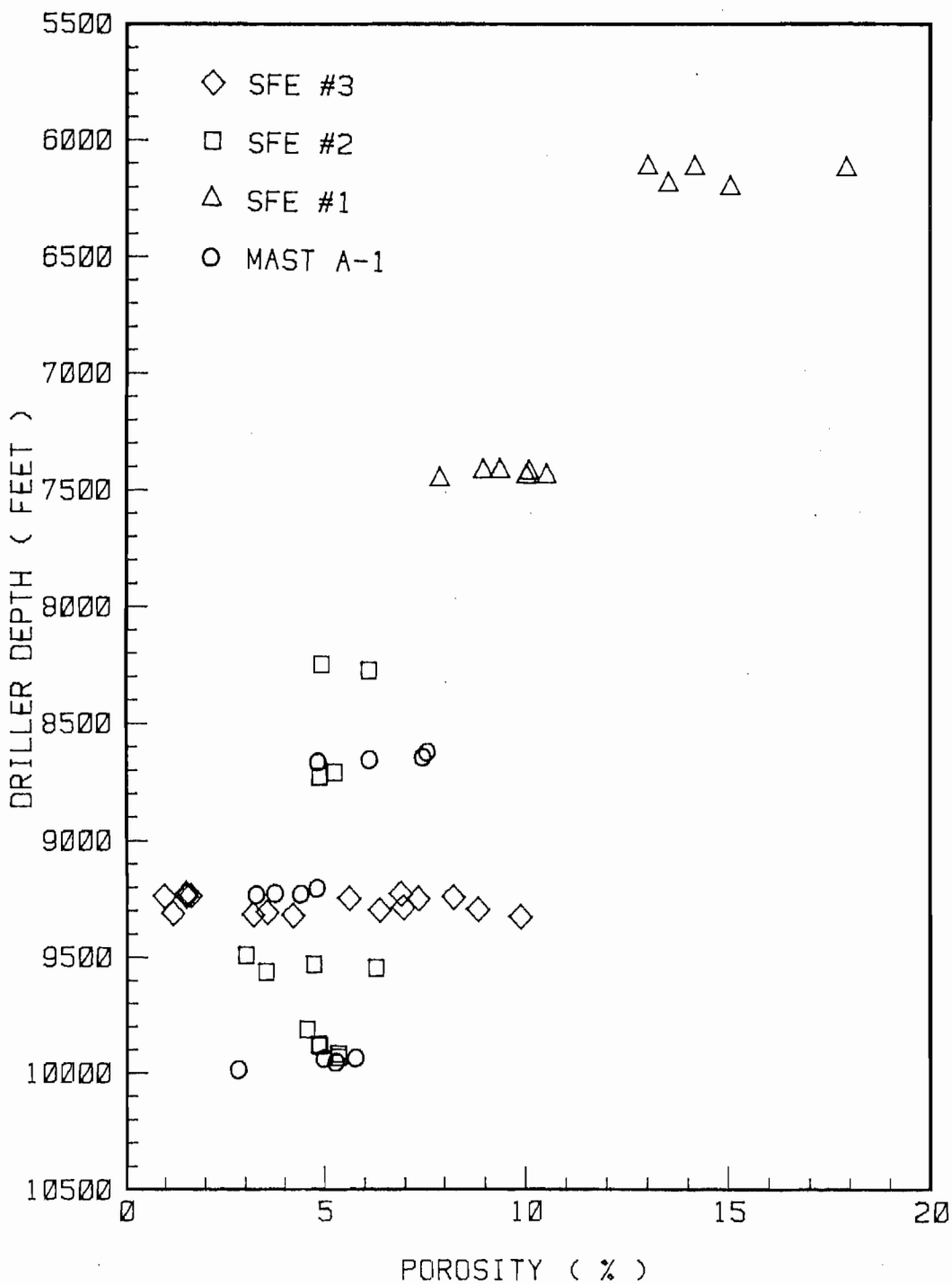


Figure 14. GAS POROSITY FROM CORE VERSUS DEPTH IN EAST TEXAS TIGHT SANDSTONES

Figure 16 is a plot showing the correlation between the "Swanson parameter" derived from mercury penetration data on unconfined samples and Klinkenberg permeability at reservoir net stress. The Swanson parameter⁵ is calculated as the maximum value of the ratio of mercury saturation (S_b) as a percent of bulk volume to the corresponding capillary pressure (P_c) along the capillary pressure curve. Figure 16 includes all of the East Texas tight sandstone data obtained at IGT, and also data from earlier analysis of samples from the Mesaverde tight sand in Colorado. All plotted Klinkenberg permeability values were measured at a net stress corresponding to the midpoint of reservoir drawdown, except for the last four SFE No. 2 samples in Table 4, for which measurements were made only at initial reservoir net stress. The Mast A-1 samples which contain visible fractures are marked by the letter "F" in Figure 16, since the measured permeabilities for these samples were anomalously high. Also shown on the plot for comparison are the correlations developed by Swanson⁵ for routine air permeability (dashed line) and brine permeability of "clean" sandstones at 1000 psi net stress (dotted line). Data for the high-permeability SFE No. 1 samples agree extremely well with Swanson's correlations. The grain-supported pore morphology in these sandstones is typical of that in conventional sandstones. Furthermore, the low stress-dependence of reservoir properties associated with such a pore geometry explains why Swanson's correlation, derived from data at a minimal confining stress, is also comparable to IGT's data measured under several thousand psi net stress.

It is seen that as one moves to samples with lower permeability, the gradual emergence of a slot pore/solution pore morphology results in larger deviations from Swanson's air permeability correlation. The low-permeability Mast A-1, SFE No.2 and SFE No. 3 samples with fully developed slot pores and secondary porosity behave in a manner similar to the Mesaverde sandstones, which also have well-developed secondary porosity connected by slots. It is possible that the observed deviation from Swanson's low net stress correlations in this permeability regime are a direct result of the high Klinkenberg effect and stress sensitivity that can be expected when narrow slots control the flow.

A few of the very low permeability SFE No. 3 samples in Figure 16 deviate somewhat from the trend set by the rest of the low permeability samples and

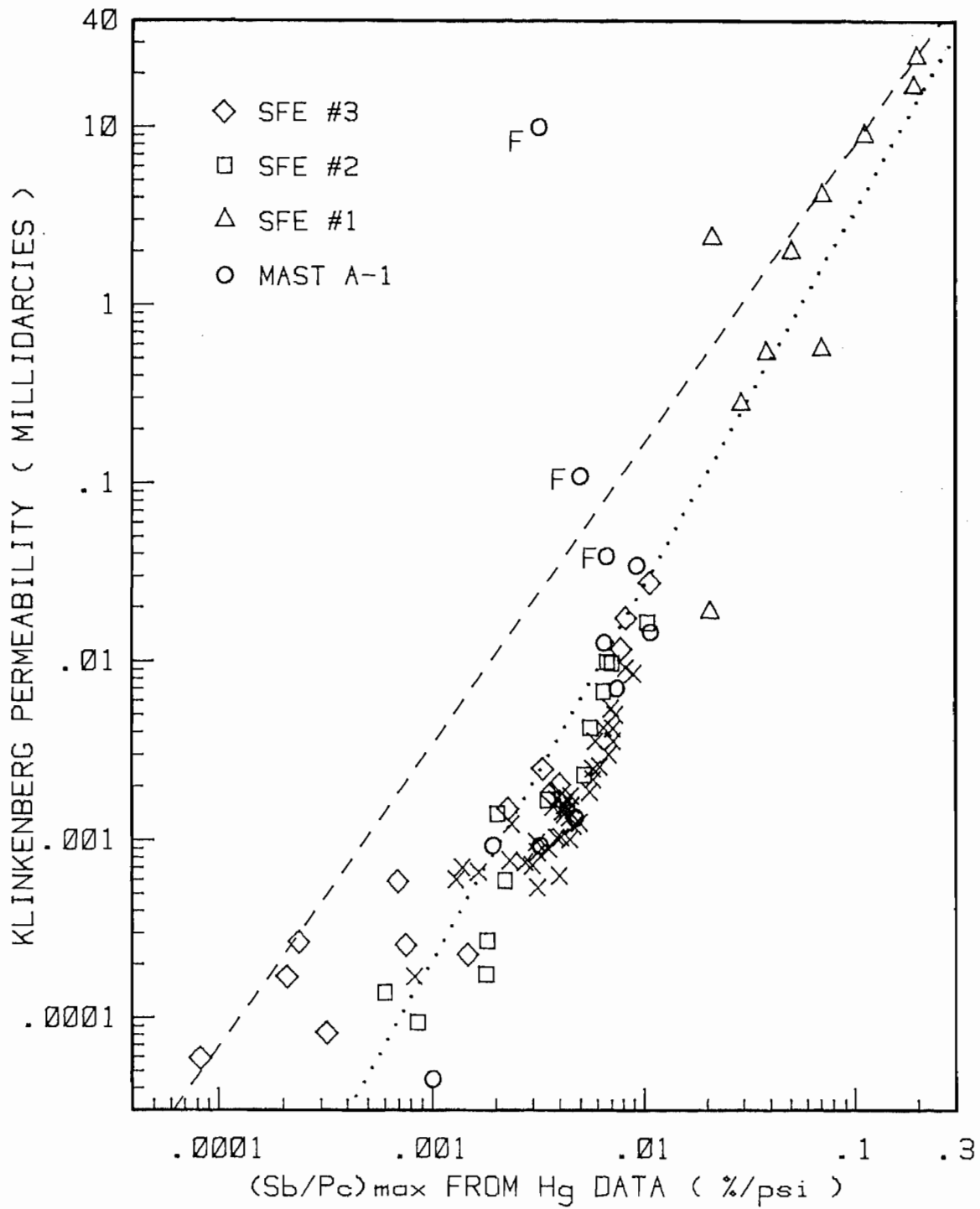


Figure 16. PERMEABILITY VERSUS SWANSON PARAMETER FOR TRAVIS PEAK, TAYLOR, AND MESAVERDE CORES (F = Fractured sample)

actually move back onto the correlation line for routine air permeability calculated by Swanson⁵. These samples are the ones (Table 5) that have a very low porosity (~ 1% to 2%) in a calcite matrix. The reason for this deviation is not yet known, but is probably related to a lower stress dependence of permeability through a microporous calcite matrix, compared to stress-sensitive slot pores between quartz overgrowths.

6.2. SFE No. 3 Chip Analysis

In order to pursue the development of techniques for using petrographic and mercury porosimetry data as predictive tools that can yield reliable results on the well site, IGT obtained 60 chip samples from the SFE No. 3 core for analysis. These samples were intended to represent drill cuttings that may be obtained at the well site for analysis during a drilling operation. The chip samples were used for mercury porosimetry data and petrographic analysis from thin sections. Image analysis software was used to calculate parameters relating to pore structure from the thin sections.

Table 6 lists petrographic and mercury porosimetry data for 31 of these samples which had been analyzed by the completion date of this contract, along with routine core analysis data on plugs collected from near the IGT chip depths as measured and reported by Core Labs. The first three columns give parameters that were obtained from thin sections. The values of visible porosity and mean pore size were obtained at IGT by the use of an image analysis program, run on a personal computer using data from a microscope camera feed, while the pore geometry parameter is a number assigned by the observer's judgment. This number classifies the sample as containing one or more of the three classes of pore geometry illustrated in Figure 5. The grain supported pore geometry has been assigned the No. 1, slot and solution pore geometry the No. 2 and the structure of matrix supported grains the No. 3. As can be seen in the table, some samples exhibited more than one type or intermediate types of pore geometry. Also listed in the table is porosity determined in the IGT Analytical Chemistry Laboratory from the volume of mercury intruded into the chip sample at 30,000 psi pressure, and the entry pressure estimated from the mercury capillary pressure curve. The helium porosity and dry sample permeability data had been measured on sample plugs from locations close to the chips by Core Labs at a confining pressure of a few hundred psi. In most cases, the match between the Core Lab and IGT data

Table 6. SFE NO. 3 CHIP ANALYSIS AND ROUTINE CORE ANALYSIS DATA

Depth	Petrographic Analysis			Mercury Data		Routine Core Analysis (Core Lab)		
	Visible Porosity, %	Mean Pore Size, μm	Pore Geometry	Mercury Porosity, %	Entry Pressure, psi	Helium Porosity, %	Dry Permeability, md	Sw %
9203.0	21.7	29.3	2	3.95	1016	3.2	0.017	58.5
9204.0	21.1	48.9	2	4.02	862	4.6	0.024	54.8
9205.3	9.2	26.0	2	6.69	647	7.2	0.016	42.9
9206.9	15.4	25.7	3	2.86	1045	8.3	0.011	41.9
9208.7	18.4	29.9	1	8.09	336	8.2	0.033	38.6
9211.0	22.8	39.6	1-2	5.88	546	8.6	0.035	36.1
9211.9	16.9	27.7	1	7.01	417	7.9	0.026	47.9
9214.3	7.8	15.2	1	1.68	1413	1.9	0.014	66.4
9216.15	14.2	16.5	1-2	8.55	430	7.5	0.025	48.2
9218.0	14.3	25.0	3	1.73	--	3.0	<0.01	81.9
9219.4	7.2	24.8	3	1.66	--	1.1	<0.01	59.1
9221.7	8.6	19.3	3	2.94	--	1.0	<0.01	77.1
9223.1	12.3	23.0	2	3.99	1370	5.0	<0.01	87.2
9224.9	18.3	26.5	2-3	4.79	683	6.4	0.025	73.7
9227.6	4.4	18.0	3	2.48	--	1.7	<0.01	81.3
9228.9	15.0	18.9	1-2	5.37	341	8.1	<0.01	49.4
9231.8	17.3	16.2	1-2	7.47	303	8.3	0.018	27.6
9233.8	3.0	10.2	3	2.88	1468	1.6	<0.01	71.2
9235.7	14.0	22.2	2	2.46	3293	3.8	0.060	70.9
9242.2	9.3	22.6	1	7.24	767	6.7	0.040	36.3
9246.7	16.4	33.1	2	5.73	383	5.9	0.019	56.0
9248.7	17.0	28.1	2	7.99	147	2.0	0.013	53.4
9251.7	14.9	26.7	1-2	7.71	292	8.4	0.064	27.6
9253.6	14.6	27.1	2	7.28	399	6.6	0.010	36.9
9257.4	11.9	24.7	2	5.13	750	4.4	0.009	39.7
9259.6	19.2	37.3	1	6.48	613	7.0	0.523	50.0
9262.2	19.2	28.4	1-2	7.39	383	7.5	0.026	29.9
9265.4	14.7	28.2	2	3.48	668	1.4	<0.01	50.4
9267.5	12.0	26.0	2	3.50	395	---	---	---
9269.5	20.1	143.8	2	10.22	1	8.8	0.217	5.9
9270.8	8.3	24.7	2	2.94	483	3.8	0.001	28.2

sets are fairly good, although discrepancies are apparent where the rocks contain small-scale variations, due to the difference in sampling depth of the plug and chip. The last column shows the "as received" water saturations reported by Core Laboratories.

Figure 17 is a plot of mercury intrusion porosity versus gas expansion (Boyle's Law) porosity from routine core analysis for SFE No. 3 samples from corresponding depths. A good correlation can be seen. Figure 18 is a plot of the same two data sets as a function of depth. These two figures illustrate that mercury porosimetry can provide very reliable porosity data. Figure 19 is a plot of "as received" water saturation reported by Core Labs, versus mercury entry pressure. A rough correlation can be observed, in the direction of increased residual water saturation in samples having a high mercury entry pressure.

Figure 20 is a plot of porosity versus depth for the SFE No. 3 chip analysis data, comparing visible porosity from thin section image analysis with values from mercury porosimetry. The visible porosity in thin sections is seen to be considerably larger than that measured during mercury porosimetry. However, the thin section values generally follow the same trend as the mercury data. The disagreement in actual values can be attributed to the fact that a two-dimensional slice is observed in thin sections, rather than the three-dimensional pore structure which actually determines porosity. However, the fact that the trends as a function of depth match closely is encouraging in that petrographic analysis can at least be used as a qualitative indicator of porosity variations. The results also suggest that it may be possible to use a conversion factor to convert petrographic porosities to actual porosities, though such factors may be specific to a formation or pore structure.

Figure 21 is a plot of routine gas permeability versus pore geometry type. For convenience, pore geometry types that have been listed as "1-2" and "2-3" in Table 6 have been plotted as 1.5 and 2.5, respectively. While a strong correlation is not apparent, the plot does display the expected tendency towards lower permeabilities in moving from a grain supported pore geometry (Type 1) to a matrix supported grain (Type 3).

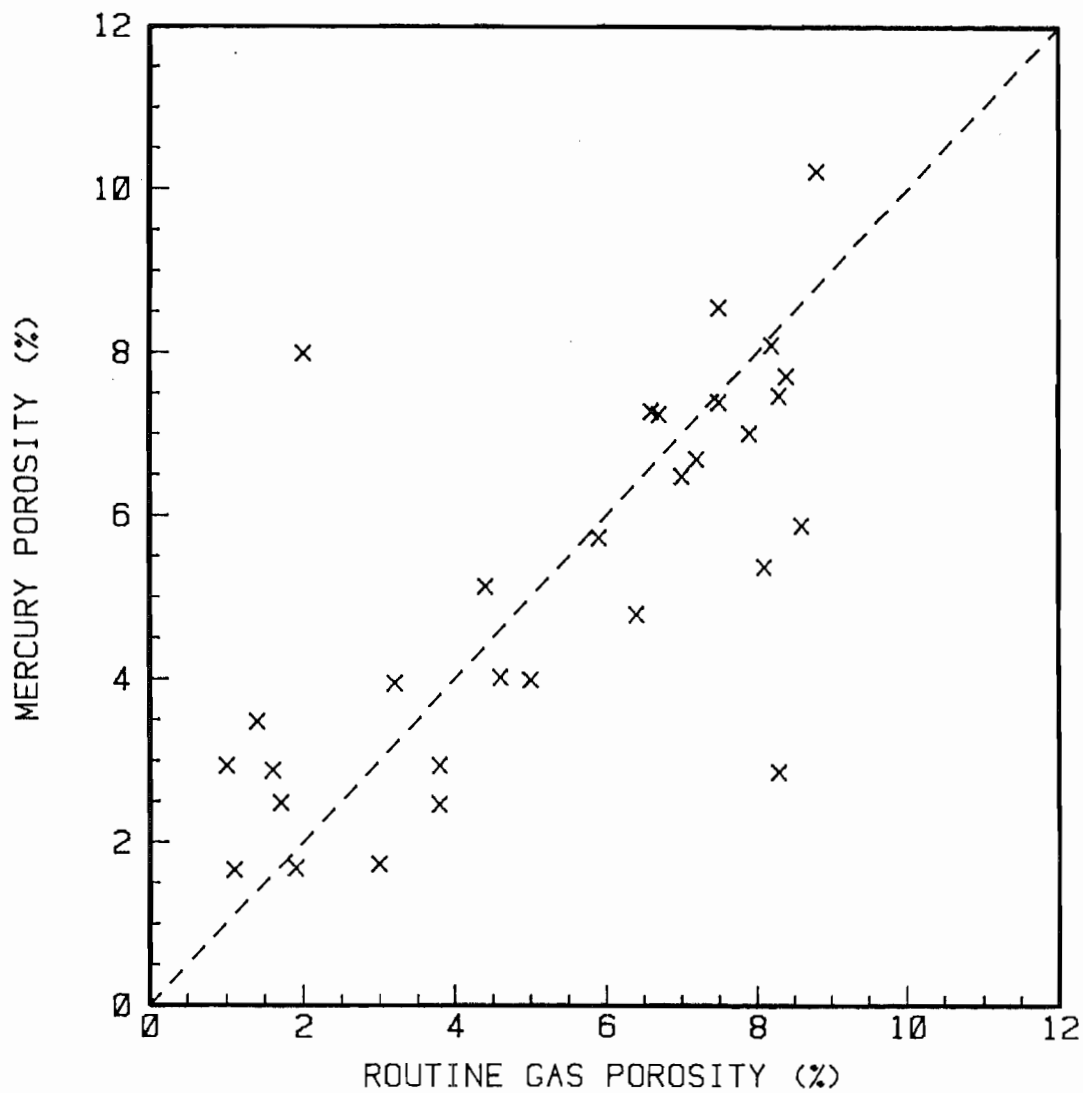


Figure 17. COMPARISON OF POROSITY FROM MERCURY POROSIMETRY ON CORE CHIPS WITH VALUES FROM ROUTINE GAS EXPANSION MEASUREMENTS ON SAMPLE PLUGS FOR SFE NO. 3

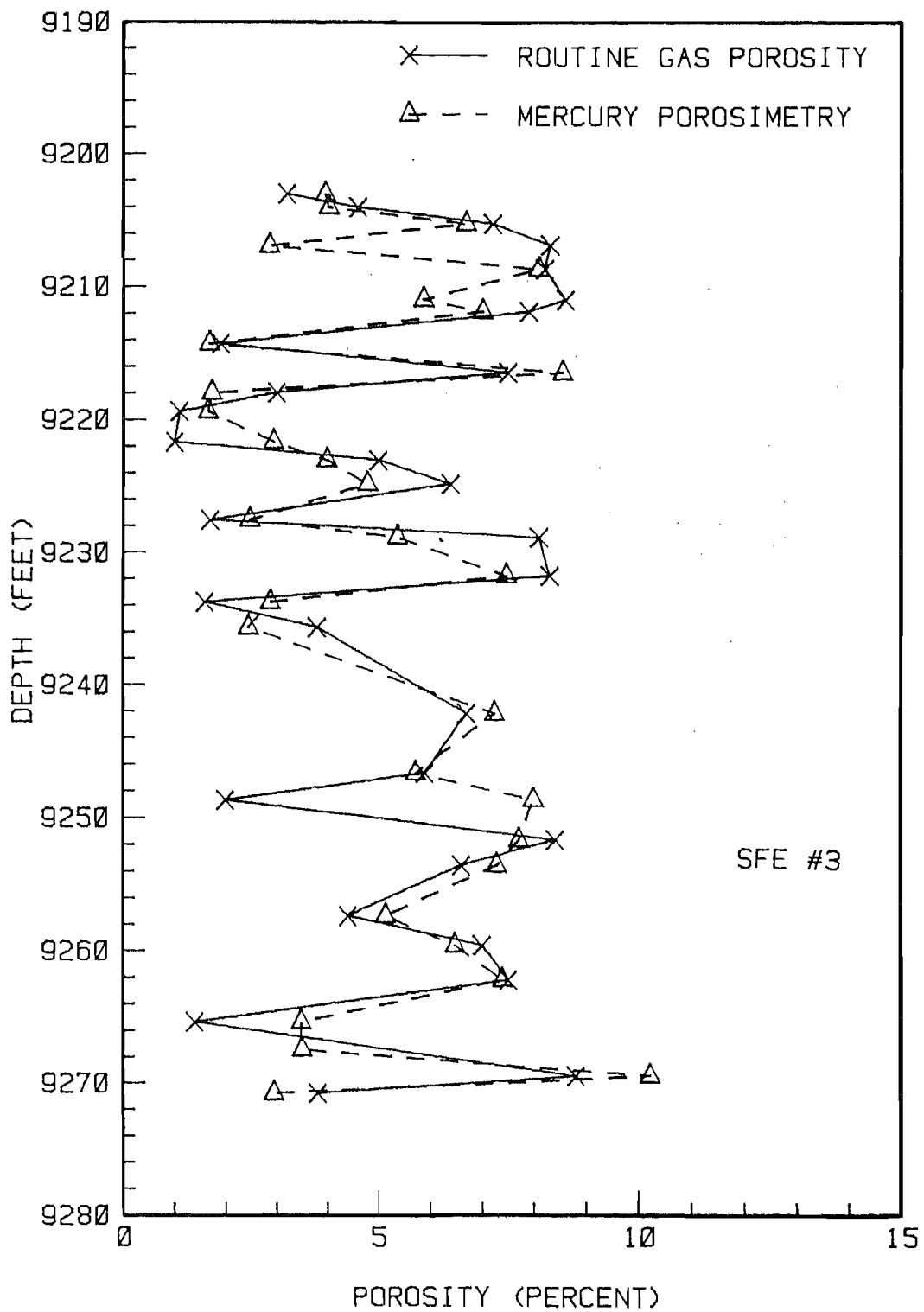


Figure 18. POROSITY VERSUS DEPTH PROFILE FROM MERCURY POROSIMETRY ON SFE NO. 3 CORE CHIPS COMPARED WITH PROFILE FROM ROUTINE CORE ANALYSIS

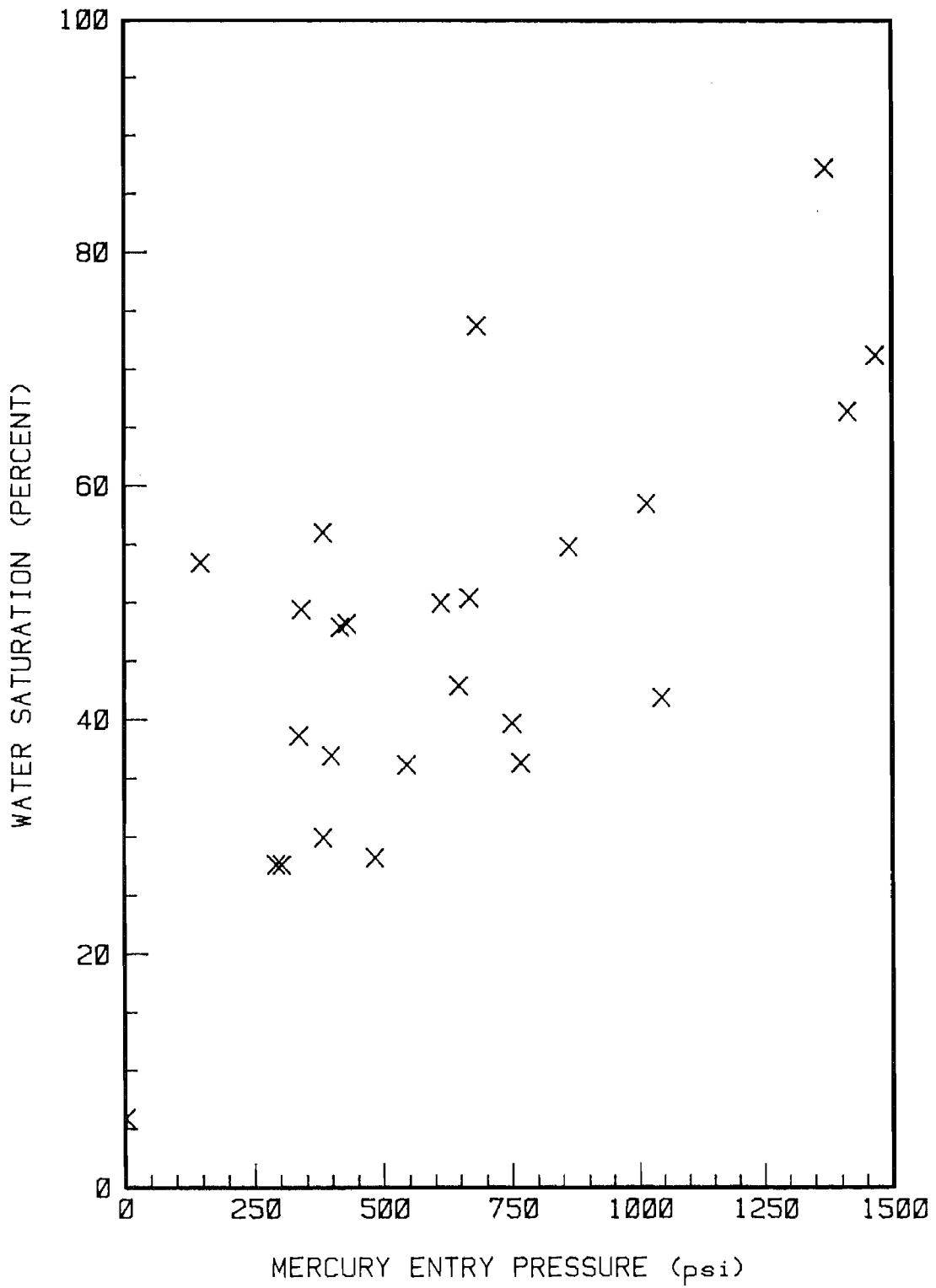


Figure 19. "AS-RECEIVED" WATER SATURATION FROM ROUTINE ANALYSIS OF SFE NO. 3 CORE VERSUS MERCURY ENTRY PRESSURE FROM CORE CHIPS AT CORRESPONDING DEPTHS

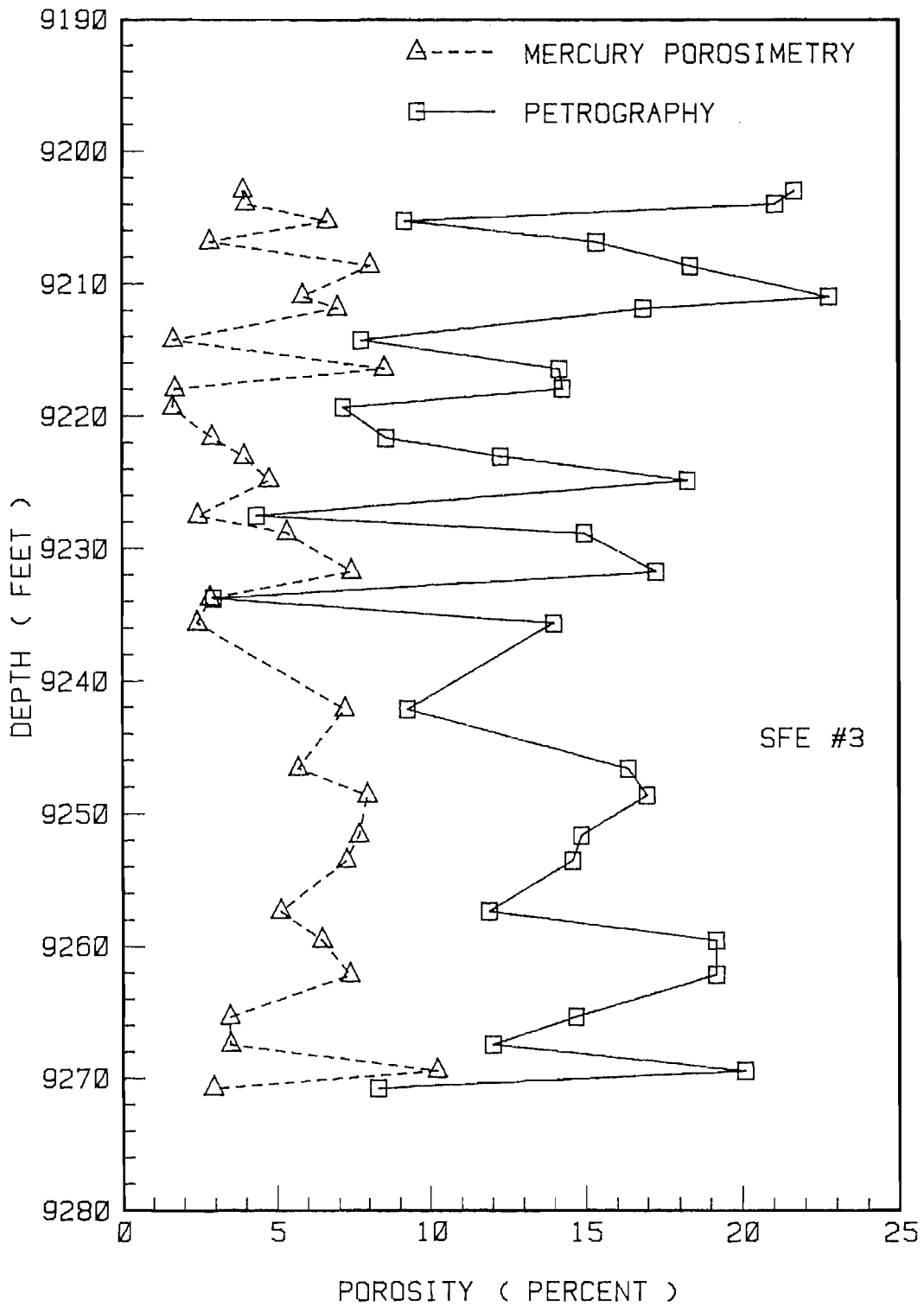


Figure 20. COMPARISON OF VISIBLE POROSITY FROM PETROGRAPHIC IMAGE ANALYSIS WITH MERCURY POROSIMETRY DATA, SFE NO. 3 CHIP ANALYSIS

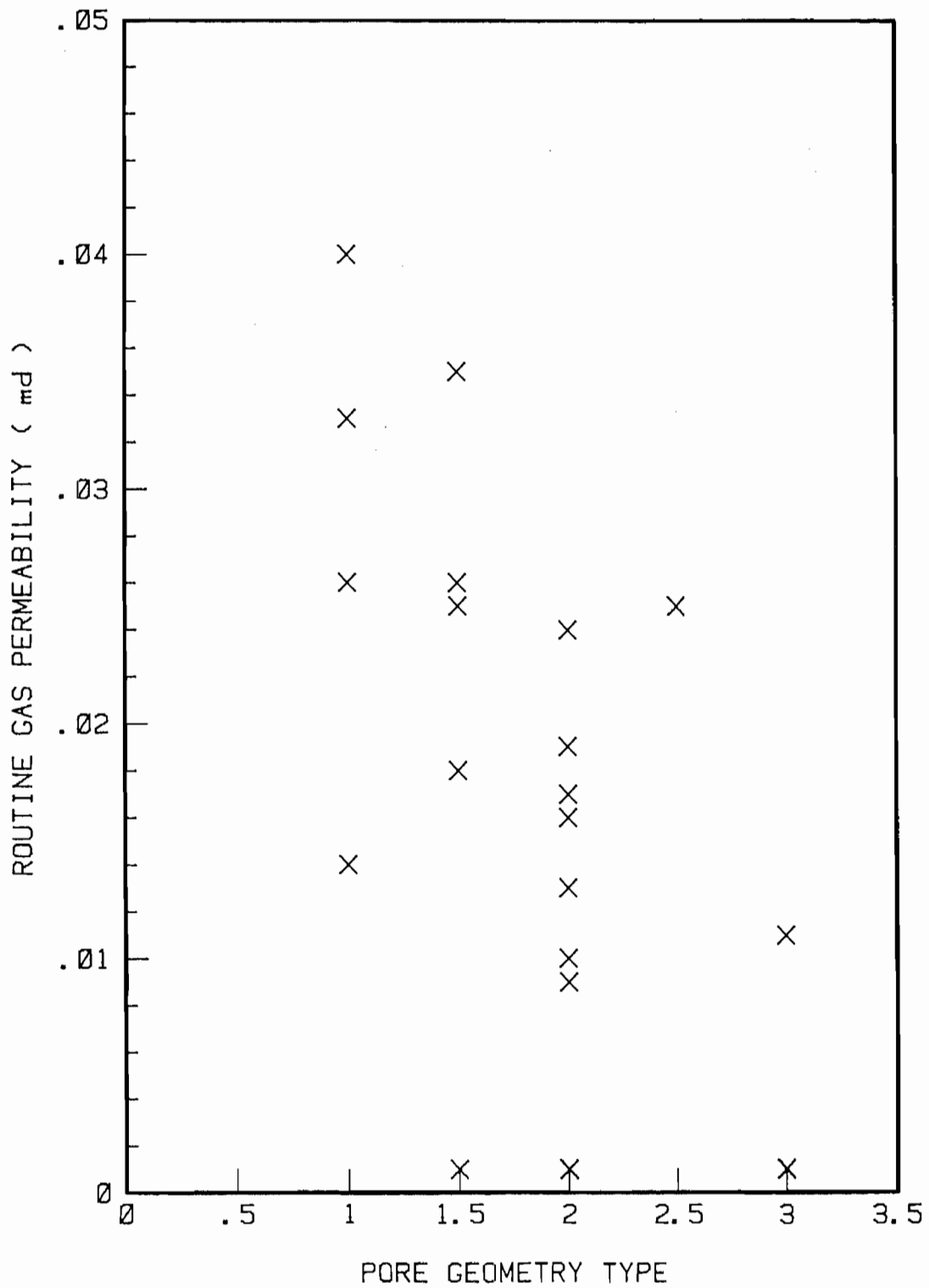


Figure 21. PLOT SHOWING ROUTINE GAS PERMEABILITY ON CORE PLUGS VERSUS PORE GEOMETRY TYPE FROM NEARBY CHIP SAMPLES, SFE NO. 3 CORE

7.0. TWO-PHASE FLOW STUDIES

Over the past several years, IGT has been directing efforts towards improving the technology of low permeability, two-phase flow core analysis. The investigators have centered around:

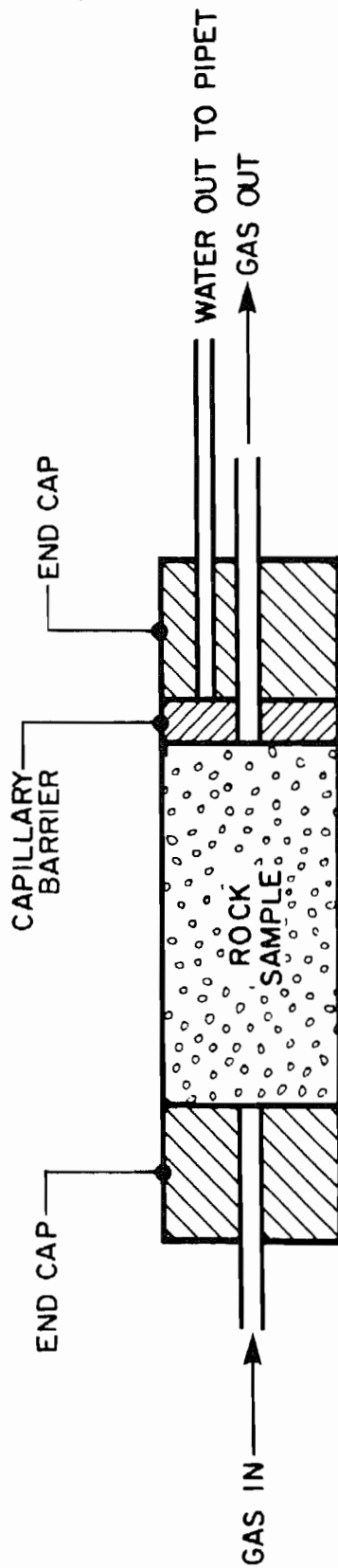
1. Developing procedures for establishing the sample water saturation in a controlled manner so that the water distribution within the pore space can be classified as either true imbibition or true drainage. It is also important, from this perspective, to be able to change pore water saturation while the samples are held in the coreholder at reservoir confining stress, in order to avoid unnecessary stress cycling and water movement caused by pore volume compression.
2. Studying the validity of the evaporation technique for varying water saturation during flow experiments. Evaporation is still the easiest method of varying water saturation in tight sand samples, and an improved understanding of pore water distribution during evaporation should lead to more meaningful uses of data obtained by this technique.

Experiments oriented toward the above goals were conducted with samples from the Travis Peak formation. The research consisted of "true drainage" experiments in the Experimental Tight Rock Apparatus (ExTRA), preliminary testing of modification to the CORAL for water imbibition experiments, and measurements using the evaporation technique. Detailed descriptions of the experiments and the results are given below.

7.1. Drainage Measurements

7.1.1. Procedure

Displacement experiments that yielded measurements of permeability to water, gas entry pressure and gas phase relative permeability under true drainage conditions were made in the Experimental Tight Rock Apparatus (ExTRA). This apparatus has been described in detail elsewhere.⁴ Figure 22 shows the schematic sample assembly and flow pattern used in the displacement experiments. A capillary barrier in contact with the downstream end of the sample plug served to separate the gas and water as they emerged from the sample, permitting measurement of flow rates of both phases. A 1-inch diameter, 1/8-inch thick disc of porous porcelain, having a gas entry pressure of approximately 5 psi, was used as the barrier. This barrier also had a negligible resistance to water flow compared to the tight sand sample. The pipet to which the water drained was open to the atmosphere, and the downstream gas monitoring system was maintained at approximately 1 psi above atmospheric



A86040318

Figure 22. SCHEMATIC DIAGRAM OF SAMPLE ASSEMBLY FOR DISPLACEMENT EXPERIMENTS

pressure so as to be below the gas entry pressure for the barrier. Water displacement was monitored by recording the level change in the collection pipet downstream of the capillary barrier. Gas flow rates were calculated from the rate of pressure buildup in an enclosed chamber.

Sample plugs approximately 1.5 inches long and 1 inch in diameter were first saturated with distilled water. This was done by evacuating a chamber containing the samples, and then filling the chamber with deaerated, distilled water in which the samples were allowed to sit for at least a day under a pressure of about 400 psi. The water-saturated sample plug was assembled in the coreholder and confined at initial reservoir net confining stress using a procedure that ensured that the coreholder end-caps were completely filled with water. The upstream end of each plug was connected to a source of gas pressure, which provided the necessary pressure drop across the plug. The approximately 0.10 cc of water contained in the flow lines associated with the upstream end cap was flowed through the sample plug for the water permeability measurement. The upstream gas pressure used to impose a pressure drop for this measurement was less than the anticipated gas entry pressure for the sample.

After all the water in the upstream flow lines had been pushed through the sample, upstream nitrogen pressure was increased in 5 to 10 psi steps until the gas entry pressure for the sample was exceeded. This was indicated by water being displaced from the sample into the pipet. This rate of displacement was always slower than the flow rate during water permeability measurements on the fully saturated sample. The critical gas saturation was obtained by noting the volume of water displaced before gas flow was detected, indicating gas breakthrough. Observation of these flow rate changes was aided by a plotting routine incorporated into the data acquisition program so that a plot of pipet level versus time was obtained on the monitor of the computer used for data acquisition.

Following gas breakthrough, water displacement and gas flow rates were monitored for at least 24 hours to allow the system to approach steady state. These data were used to calculate gas phase permeability and sample water saturation during the course of the experiment.

After the displacement step at an upstream gas pressure just above the gas entry pressure, the upstream pressure was raised by about 15 to 20 psi to displace more water from the sample. Water displacement and gas flow rates were monitored to calculate gas phase permeability and water saturation. For the SFE No. 2 samples several step increases in upstream gas pressure were imposed, resulting in final pressure gradients of up to 200 psi per inch of sample length.

7.1.2. Results

Table 7 shows the results of water permeability, gas entry pressure and critical gas saturation measurements on six samples from the Mast A-1 and SFE No. 2 wells. All measurements were at a net stress representative of initial reservoir conditions. The water permeability values are seen to be considerably smaller than the corresponding Klinkenberg permeability values reported in Tables 2 and 4. Values of critical gas saturation are generally less than 15%. Similar values were measured under drainage conditions for Rocky Mountain tight sands earlier at IGT.¹⁵ This low critical gas saturation is in contrast to values of around 40% that are obtained when evaporation is used to vary water saturation in laboratory experiments.¹⁶ Gas entry pressures reported in Table 7 follow the trend of the corresponding mercury entry pressures in Tables 2 and 4. The last column in Table 7 gives, for each sample, the factor by which mercury entry pressure needs to be divided to arrive at the measured gas entry pressure. This factor seems quite variable, and is probably a measure of the stress sensitivity of the samples, since the mercury data were obtained on unconfined sample chips. The results in Table 7 seem to correlate with petrographic observations of pore structure also. The two samples (Mast 8623.2 and SFE No. 2, 9875.95) which show the highest ratio of entry pressures (i.e., lowest stress sensitivity) showed a considerable amount of remnant primary porosity in thin sections. In contrast, the samples (Mast 9954.9 and SFE No. 2, 9917.4) with the lowest value of the ratio of entry pressures showed a predominantly slot and solution pore geometry.

Figure 23 is a plot of the drainage gas-phase relative permeability data for the two Mast A-1 samples. Figure 24 is a similar plot for the four SFE No. 2 samples. The data points on these plots correspond to the gas permeability and water saturation values at the end of a displacement step. The

Table 7. DATA FROM DRAINAGE EXPERIMENTS

Well	Depth	Net Confining Pressure, psi	Critical Gas Satn., %	Water Permeability, μd	Gas Entry Pressure, psi	Ratio of Entry Pressures, Hg/Gas
Mast A-1	8623.2	3550	7	2.56	60	4.42
	9954.9	3550	6	3.42	46	2.61
SFE No. 2	9875.95	3420	9	2.90	45	4.31
	9882.95	3420	13	1.64	85	2.86
	9917.14	3420	5	0.15	220	2.29
	9932.85	3420	12	2.62	60	3.62

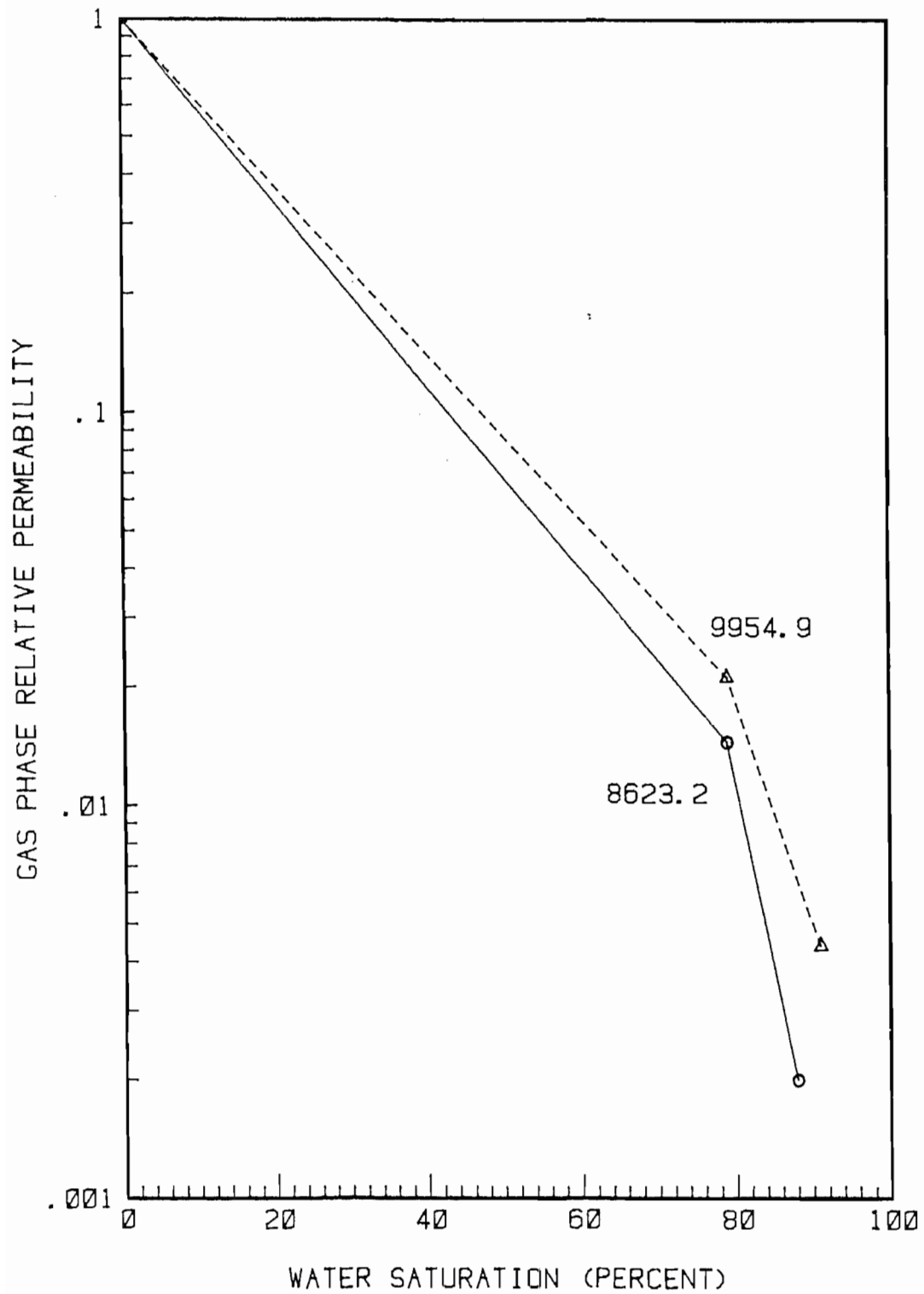


Figure 23. RELATIVE PERMEABILITY OF GAS PHASE IN MAST CORE VERSUS DRAINAGE WATER SATURATION

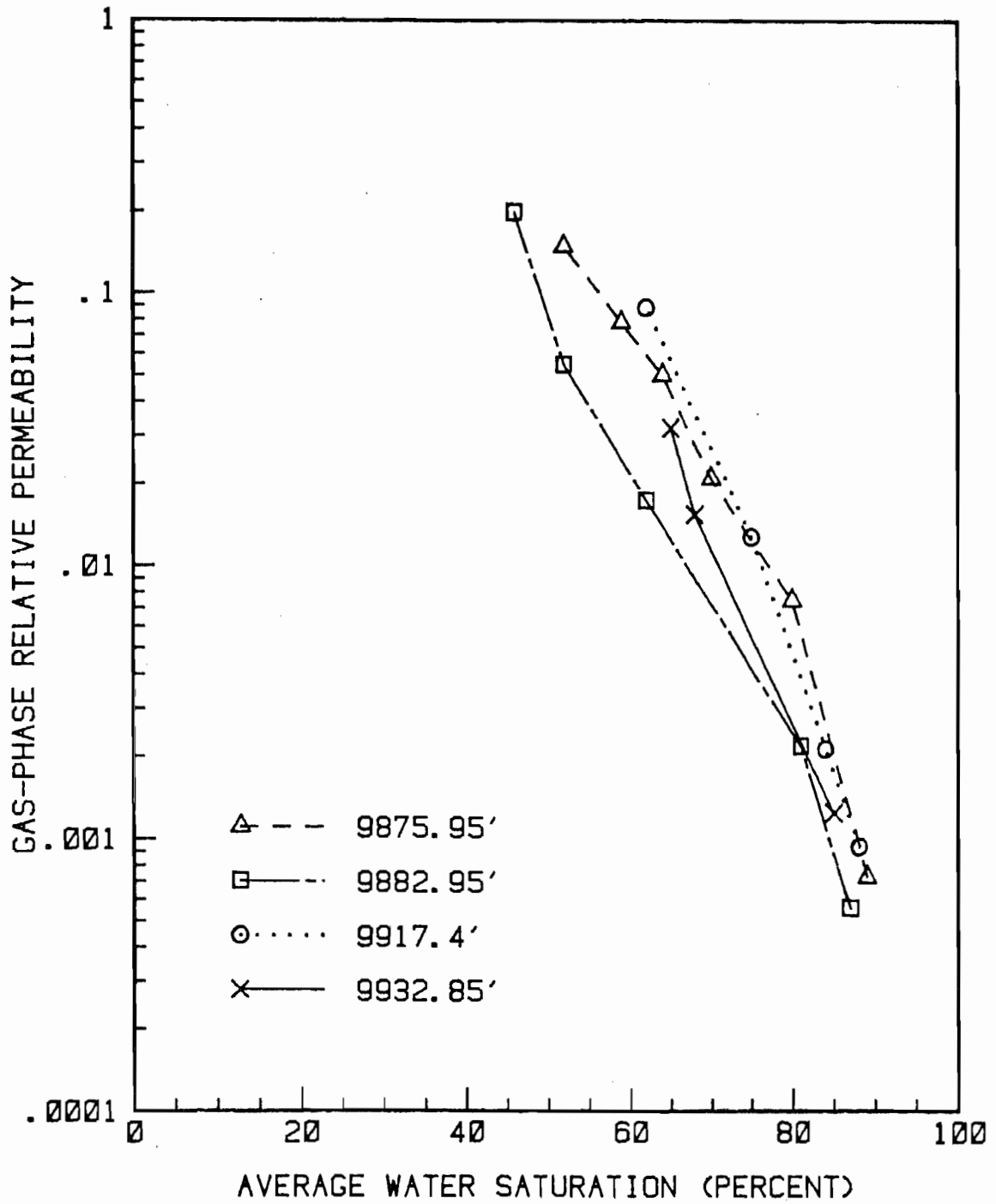


Figure 24. GAS-PHASE RELATIVE PERMEABILITY DATA FROM DRAINAGE EXPERIMENTS
SFE NO. 2 SAMPLES

absolute permeability basis used to obtain relative permeability was the dry sample permeability at the average pore pressure. Values of k_{∞} and b listed in Tables 1 and 4 for Mast A-1 and SFE No. 2 samples respectively were used for this calculation. Since significant pressure drops of up to 200 psi per inch across the sample were present during these experiments, the water saturation is not likely to have been uniform along the sample length. The water saturations reported in Figures 23 and 24 are, therefore, average water saturations. Nevertheless, the plots are believed to be representative of relative permeability curves under drainage conditions. These curves are in contrast to those obtained using evaporation to vary water saturation, presented in the next section. The evaporation data show a gas permeability shut-off at water saturations around 60% whereas the drainage data show that under drainage conditions, gas is mobile at water saturations as high as 90%.

7.2. Desaturation by Evaporation

The evaporation method of varying sample water saturation has remained the easiest and most popular way of conducting relative permeability measurements on tight sands. IGT, therefore, continue to use this technique while developing true drainage and imbibition methods. A major disadvantage of the evaporation technique is the stress-cycling the sample undergoes when it is removed from the coreholder for each saturation change. Furthermore, the water distribution in the sample resulting from the evaporation process is unknown.¹⁶ Complexities associated with water movement and distribution during the evaporation process showed up prominently during experiments with the Travis Peak samples, resulting in anomalous data in some cases. While the fact that evaporation can cause highly nonuniform saturation distributions in the sample had been speculated on earlier, the effects had not manifested themselves in the measured relative permeabilities in earlier work at IGT as they did in the present work with Travis Peak sandstones. IGT believes this to result from the fact that lead sheaths were used around the sample plugs for the first time during the Travis Peak measurements, rather than from any special characteristic of the samples themselves. The use of lead sheaths around the sample plugs during evaporation restricted evaporation to the end faces, and the resulting saturation distribution appears to be responsible for much of the unusual data observed. A detailed description of the results and their significance is given below.

7.2.1. Mast A-1 Data

Relative permeability measurements were made on four of the Mast A-1 samples listed in Table 1. As discussed earlier, many of the Mast A-1 samples contained fractures or bedding plane cracks which resulted in anomalies in the dry core analysis. Hence, the four samples chosen were those that had displayed the least anomaly during dry core analysis. These were samples 8623.2, 9203.3, 9229.3, and 9954.9.

Thin lead sheaths that had been placed around the sample plugs were retained during the relative permeability experiments. The sheaths were utilized to prevent high pressure gas in the plugs from diffusing into the elastomer confining sleeves. This had been a problem on our earlier Mesaverde core analyses, resulting in inaccurate porosities and long waits until the sleeve material reached equilibrium with the pore pressure. The metal inner sleeve was to act as a barrier to prevent this.

The Mast A-1 samples were saturated with water by using an aspirator vacuum to draw water through the samples in an apparatus shown schematically in Figure 25. Approximately 10 cc of distilled water was poured on top of each plug and was drawn into the sample by a vacuum applied to the bottom. The snug fit between the tight rubber sleeves and the smooth lead sheaths on the cores forms a very effective seal. When water appeared in the plumbing below a particular endcap, the sample isolation valve was used to shut off vacuum to the sample.

Initial water saturations established with the vacuum saturation station averaged around 80% as determined by weight. This was reduced to around 60% by evaporation before conducting the first set of gas phase permeability measurements, followed by measurements at successively lower water saturations. The time required to saturate the plugs by this technique varied from a few hours to two days, depending on the sample permeability. Interestingly, the highest permeability sample 8623.2 was the slowest at imbibing water, and also attained the lowest water saturation of the four samples. This may be related to its large pore size (low capillary pressure) and its grain-supported pore morphology, in contrast to the slot pore morphology of the other samples.

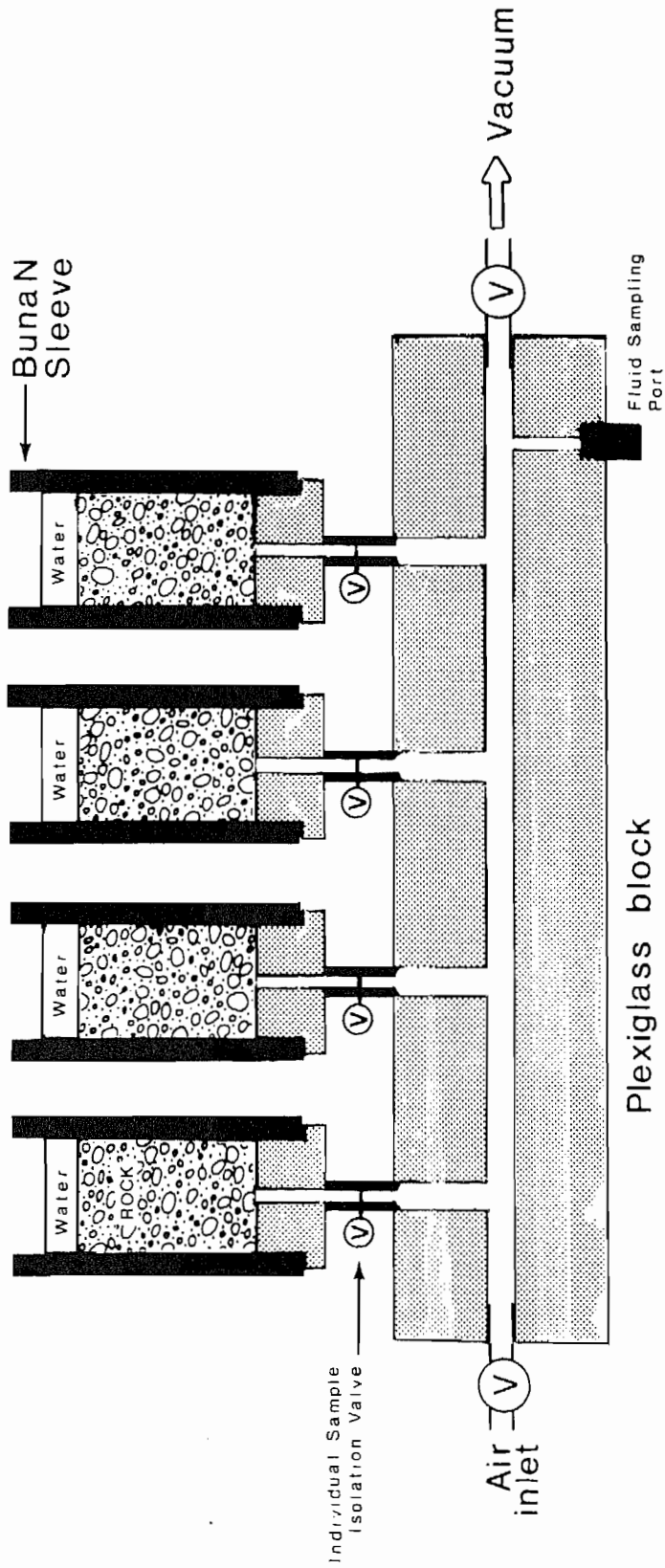


Figure 25. APPARATUS UTILIZED FOR THE VACUUM SATURATION OF TIGHT SAND CORES WITH WATER

The results of Mast A-1 gas phase permeability measurements are shown in Table 8 and Figures 26, 27, and 28. Measurements were made at a pore pressure of 1500 psia. The flow measurement at each saturation was conducted first at initial reservoir net confining stress, followed by a measurement at a higher stress representative of the midpoint of drawdown, and ending a repeat measurement at initial net stress. The values of these stresses are as reported in Table 1. A detailed description of the measurements made is available in the literature referenced in the report.¹ The Mast A-1 relative permeabilities fall off more rapidly with increased water saturation than was observed in earlier work with Rocky Mountain tight sands at IGT.¹⁶ Surprisingly, the Mast A-1 sample 9229.3 did not permit gas flow even at a water saturation as low as 30%. Similar unexpected results were obtained with SFE No. 2 samples, and as discussed in a later section, we now believe these results to be related to the fact that evaporation in the Travis Peak samples was restricted to the end faces.

7.2.2. SFE No. 2 Data

Gas phase relative permeability measurements using evaporation to vary water saturation were made on the same set of four SFE No. 2 plugs that were used in "drainage" experiments. These sample plugs also had lead sleeves sealing their curved surfaces. The samples were first saturated by placing them in a sealed vessel, evacuating the vessel (and the rock pores) with an aspirator, and then filling the vessel with deaerated, distilled water. Pressures of up to 1000 psia were used to ensure complete filling of the rock pores with water. Sample water saturation was then decreased to the desired level by evaporating off water before making gas phase permeability measurements.

Table 9 gives a summary of results obtained. All gas flow data were obtained with a 20 psi pressure drop. In all cases the sample permeability decreased with time; in one case by nearly an order of magnitude over a period of two weeks. The values reported in Table 9 are from the first measurement at each water saturation. The unusual nature of the results obtained with a lead sleeve sealing the curved surface of the sample is evident in Table 9. Sample 9917.4 yielded no flow even down to a water saturation of 40%. Sample 9882.95 yielded some gas flow at $S_w = 60\%$ but shut off completely at lower

Table 8. GAS PHASE RELATIVE PERMEABILITY DATA
BY THE EVAPORATION METHOD, MAST A-1 SAMPLES

Plug Depth, ft	Water Saturation, %	Permeability, μ d		
		Low Net Stress (1)*	High Net Stress (2)*	Low Net Stress (3)*
8623.2	60	0.034	0.007	0.015
	50	0.618	0.442	0.475
	40	1.699	1.477	1.552
	30	3.87	3.64	3.78
	0	8.58	7.37	--
9203.3	60	-----Unreliable Data at this Saturation-----		
	50	0.032	No Flow	No Flow
	40	0.505	No Flow	0.040
	30	0.93	0.304	0.661
	0	24.82	15.06	19.67
9229.3	60	-----No Flow-----		
	50	-----No Flow-----		
	40	-----No Flow-----		
	30	-----No Flow-----		
	0	2.77	1.42	2.05
9954.9	60	-----Unreliable Data at this Saturation-----		
	50	0.056	0.006	0.036
	40	1.209	0.101	0.233
	30	3.72	2.51	2.89
	0	14.46	12.96	13.81

*Number in parentheses gives the chronological order of confining stress change.
Net stresses utilized are the same as those listed in Table 1.

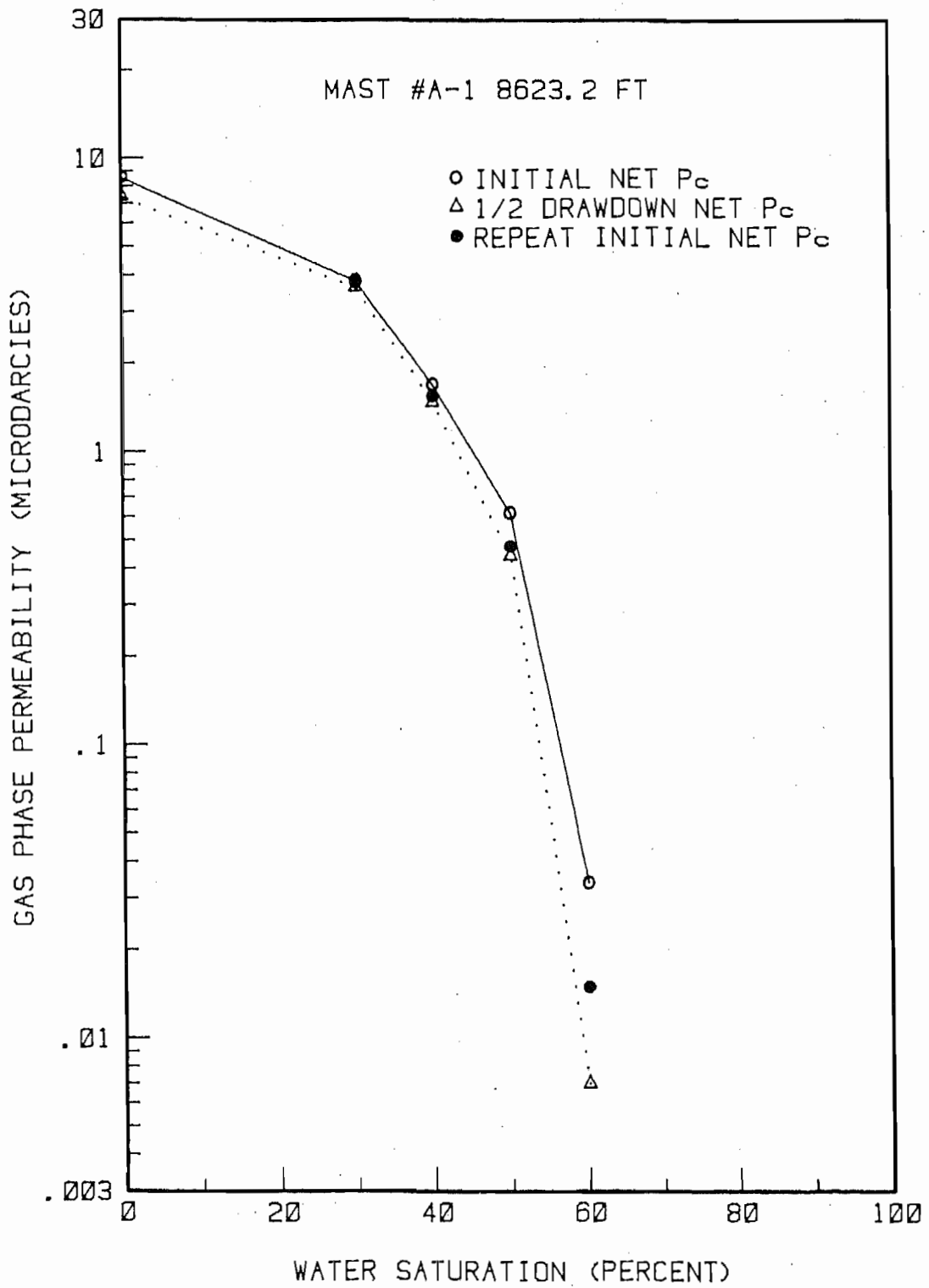


Figure 26. GAS PERMEABILITY OF MAST 8623.2 CORE VERSUS WATER SATURATION AND NET STRESS

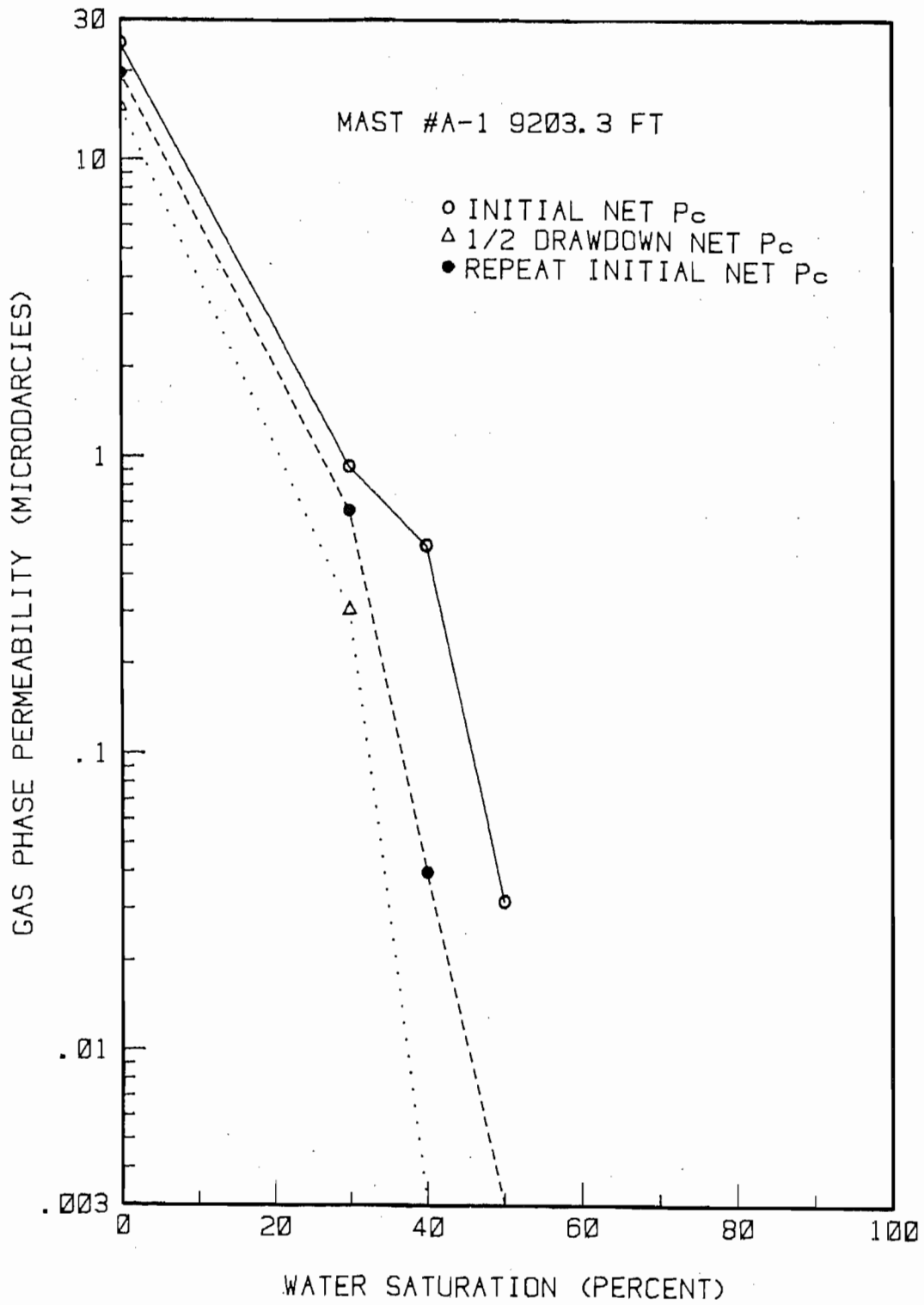


Figure 27. GAS PERMEABILITY OF MAST 9203.3 CORE VERSUS WATER SATURATION AND NET STRESS

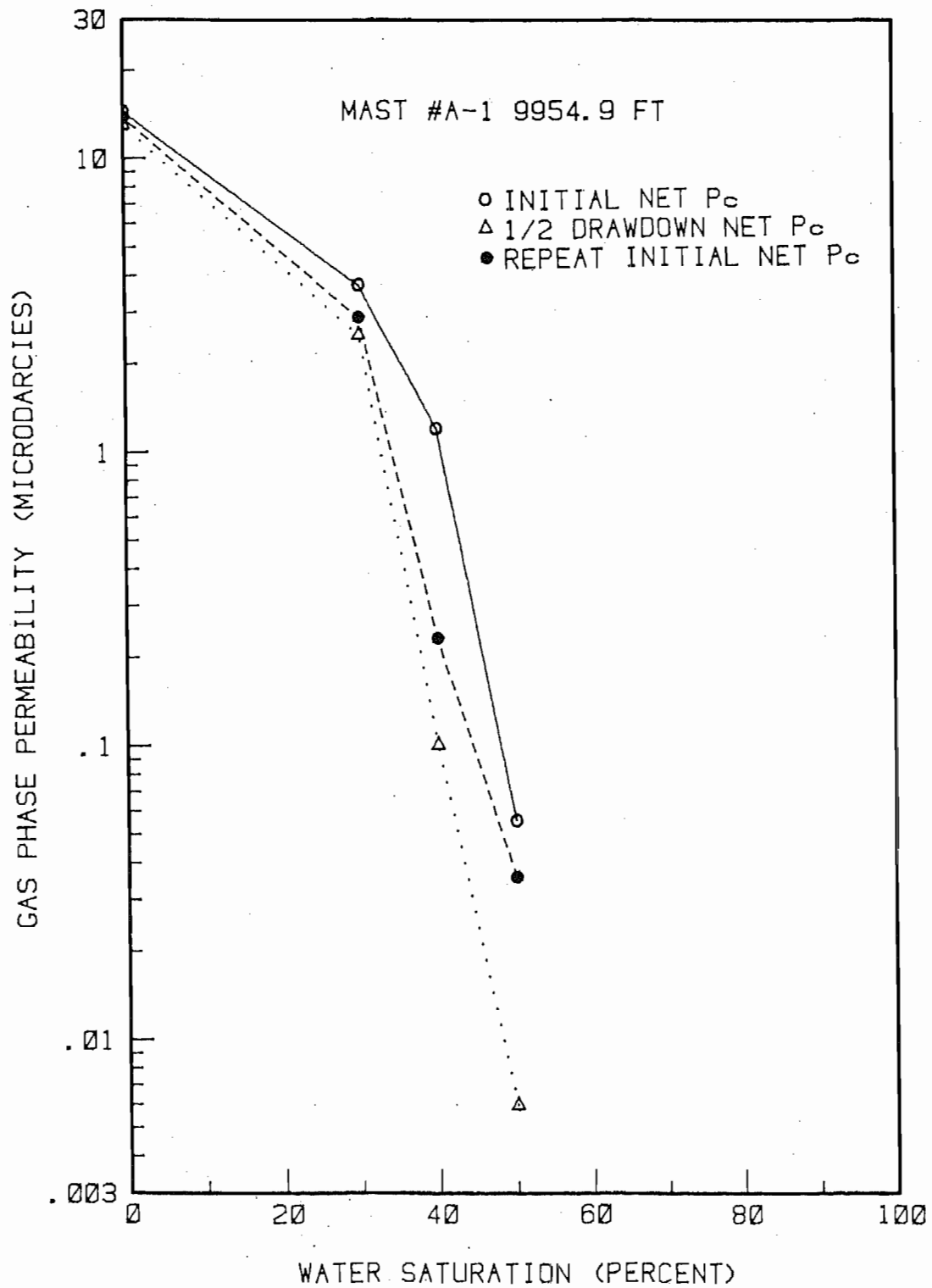


Figure 28. GAS PERMEABILITY OF MAST 9954.9 CORE VERSUS WATER SATURATION AND NET STRESS

Table 9. GAS-PHASE PERMEABILITY DATA BY THE
EVAPORATION METHOD, SFE NO. 2 SAMPLES

Water Saturation	Effective Gas Permeability (Microdarcies)			
	SFE No. 2 9875.92	SFE No. 2 9882.95	SFE No. 2 9917.4	SFE No. 2 9932.85
60%	0.014	0.0097	No Flow	0.010
50%	0.356	No Flow	No Flow	0.096
40%	0.086	No Flow	No Flow	No Flow
Dry	9.80	4.24	0.59	9.96

water saturations. Sample 9932.85 did not display the expected sharp increase in permeability to gas from $S_w = 60\%$ to $S_w = 50\%$, and shut off completely at $S_w = 40\%$. The only sample that displayed somewhat reasonable behavior was 9875.95 for the measurement at $S_w = 60\%$ and 50% . However, when evaporated down to $S_w = 40\%$, this sample also behaved anomalously, showing a gas permeability decrease rather than the expected increase. The anomalous trends noticed in the SFE No. 2 data are similar to trends noted in the Mast A-1 data. The anomalous behavior is much more pronounced in the SFE No. 2 data, however, perhaps because of the much lower porosity of these samples as compared to the Mast A-1.

7.2.3. Water Distribution During Evaporation

The Mast A-1 and SFE No. 2 relative permeability data obtained using evaporation as the desaturation technique suggest that highly nonuniform water saturations develop within the sample during the evaporation process. Evaporation, particularly from a tight sandstone, is controlled by moisture transport in the vapor phase once the region of 100% saturation retreats below the surface. This can lead to saturation profiles where water saturation is very low near the exposed surface, and near 100% in the interior of the sample. When evaporation is permitted from the curved surface of the cylindrical sample, what one is likely to end up with is a central region nearly 100% saturated, surrounded by a much drier annular region which permits gas flow. The size of this annular region increases as one evaporates off more water, so that gas permeability measurements, in effect, yield data showing the normal increase of gas phase permeability with decreasing water saturation.

On the other hand, when evaporation is restricted to the end faces of the sample plug by encasing it in a lead sleeve, it appears that this frequently results in a near 100% saturated zone in the middle extending across the

entire sample cross-section. Further desaturation would only remove water from the dry zone on the ends and decrease the thickness of the saturated zone, but a "wall of water" would still exist at the middle of the plug as a barrier to gas flow. Depending on various conditions such as the gas pressure gradient and the properties of the pore space, gas may or may not flow through the sample. In general, the behavior of the sample is likely to be very unpredictable because flow is controlled by the region of high water saturation near its middle. The decrease of gas phase permeability with time observed in the SFE No. 2 data is also probably related to the redistribution of water in the zone of high water saturation. Water movement in this zone can occur as a result of 1) pore volume compression due to confining stress and 2) compression and possible subsequent dissolution of gas trapped in isolated pockets, on application of pore pressure.

7.3. Imbibition Experiments

The CORAL apparatus was modified to permit varying saturation along a true imbibition path without removing the sample from the coreholder. The apparatus designed for this purpose is illustrated in Figure 29. This equipment was plumbed into the upstream lines of all of the four coreholders in CORAL II. It consists of the coreholder endcap connected to the downstream port of a three-way, air-actuated chromatograph valve containing minimal dead volume. One upstream part of the valve is connected to the CORAL main gas tank, while the other upstream port is connected to a small, stainless steel water reservoir. The water reservoir is also connected to the main gas tank by a line from the top. The saturation procedure starts with gas from the direct line flowing from the main gas tanks through the cores in a normal permeability mode. The small water reservoir is isolated from the gas pressure by an upstream manual valve, and by the configuration of the three-way valve. The fitting at the top of the reservoir is removed, and the volume of water needed to achieve the desired saturation in the plug sample is added to the reservoir using a high-precision syringe. The fitting is then replaced, and gas pressure from the CORAL main tank is introduced to the top of the reservoir by opening the manual valve. Once temperature stability is regained inside the CORAL (after an hour or so), the chromatograph valve is remotely activated using air pressure and the flowpath to the core switches from the direct gas line to the line leading from the bottom of the water reservoir.

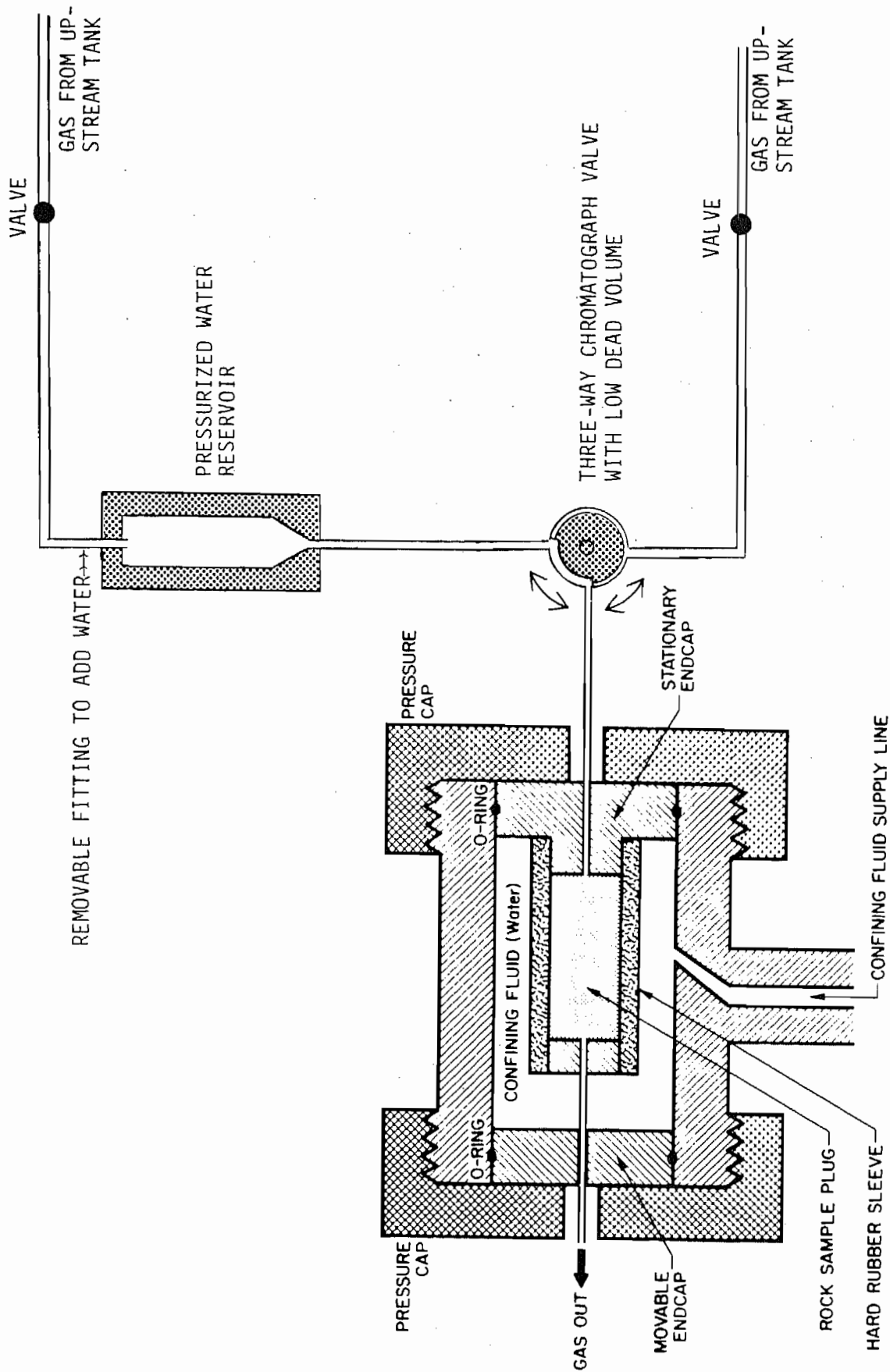


Figure 29. SCHEMATIC DIAGRAM OF WATER INJECTION COMPONENTS ADDED TO INLET LINES ON UPSTREAM END CAPS IN CORAL II. THREE-WAY VALVE PERMITS FLOW OF EITHER DRY GAS FROM TANK, OR SLUG OF WATER FROM RESERVOIR PUSHED BY GAS HEAD

The differential pressure between the gas line leading into the top of the reservoir and the lower gas pressure in the rock pores causes the water to move from the bottom of the reservoir through the lines and into the rock pores. Tests have revealed that approximately 95% of the water in the reservoir gets delivered during the first injection through dry lines, and subsequent saturation increases average about 98% to 99% delivery. Considering that the typical amount of water injected for a 10% saturation increase in a sample plug is usually less than 0.1 ml, IGT found the delivery volumes to be within acceptable limits.

Preliminary tests of the new apparatus were conducted using the same four SFE No. 2 sample plugs as used in the drainage experiments. The tests did not lead to any reliable imbibition relative permeability data, and certain unexpected phenomena were encountered. The first test was conducted beginning with dry samples. After it became evident that the injected water was not redistributing uniformly within the sample, a second test was conducted starting with the sample at irreducible water saturation (after drainage desaturation in the ExTRA). It was hoped that water injected into a sample containing irreducible water saturation would be mobile and redistribute more easily. However, the results were not significantly different from that of imbibition into a dry sample. The results suggest that the water injected into the upstream face of the rock sample did not distribute itself over the length of the sample, but stayed restricted to a narrow zone at the upstream face. This zone was near 100% water saturated and prevented the flow of gas at low-pressure gradients. Increasing the gas pressure gradient eventually resulted in gas flow when the gradient required to cause gas breakthrough in this zone was exceeded. However, this flow rate is of no use as far as calculating sample relative permeability is concerned. This is because the measured flow rate corresponds to flow through two distinct zones within the sample -- a zone of high water saturation with mobile water, followed by a zone at near irreducible water saturation. The effective sample permeability in such a case is controlled by the high water saturation zone. Furthermore, mobility of the water phase in this zone causes the sample permeability to gas to vary with the applied pressure gradient.

8.0. MAJOR ACHIEVEMENTS

The major achievements of this project are listed below:

- Measured permeability and porosity data have been correlated with petrographic observations, leading to the realization that "tight gas sand" is a unique petrologic type, and differs in many significant ways from conventional, high permeability sandstones. Results from the Travis Peak analysis clearly indicate that there is a smooth continuity between the relatively unaltered "conventional" endmember, and the very highly altered "tight" endmember. The SFE No. 1 core, in particular, exhibited petrophysical and petrological features which show various stages in the development of tight sandstones.
- Analysis of a significant number of Travis Peak and Taylor sandstone samples during this project has made it possible to compare the properties of these sandstones with those of Mesaverde tight sands from Colorado, studied earlier at IGT. This has led to the identification of certain petrological characteristics in the pore morphology, and recognition of useful indicators such as the Swanson parameter that enable a generalized evaluation of tight sands from these two widely different locations and depositional environments. As a result, pore structural studies using petrography and mercury porosimetry are emerging as important tools for predicting tight sand petrophysical properties. The present study has been a major step towards establishing relevant correlations. Such correlations are expected to be useful for estimating reservoir properties from drill cuttings at the well site.
- Gas phase relative permeability measurements made using drainage, imbibition and evaporation to vary water saturation have provided considerable insight into the applicability of these techniques for obtaining meaningful results. Results indicate that both imbibition and evaporation can give rise to severe nonuniformities in the saturation distribution.

9.0. MAJOR TECHNICAL PROBLEM AREAS

Perhaps the most important technical problem area identified during the course of this project is that of water distribution in the sample when water saturation is established by either imbibition or evaporation. Problems were encountered during gas flow measurements in both cases. The nature of the results suggest that in both cases the water did not distribute uniformly through the pores, but remained concentrated in a small region of high water saturation which tended to block gas flow. Unfortunately, the exact saturation distribution in the samples can be visualized only with the help of imaging equipment such as X-rays or microwaves. Such equipment was not available during the course of these experiments. While an improved understanding of water distribution during imbibition and evaporation needs to be pursued, caution must be exercised in using currently available relative permeability data where evaporation was used to change water saturation.

Another problem area identified is the decrease of permeability with time during measurements at in-situ net stress. This time dependence was more evident in some of the Mast A-1 samples with fractures. The major impact of this phenomenon was on the Klinkenberg data, and the values of mean pore size and tortuosity calculated therefrom. The time dependence of permeability is probably caused by a slow adjustment to confining stress, and was particularly troublesome in the steady state measurements conducted because a set of Klinkenberg permeability measurements spanned a period of several days. While there is no easy solution to this problem, it emphasizes the need to bear this phenomenon in mind during data interpretation, particularly when one is dealing with samples that contain fractures. The magnitude as well as time period of permeability change due to slow adjustment to stress can be considerable in fractured samples.

Petrographic image analysis in conjunction with mercury porosimetry shows promise as a useful tool for making reservoir property estimations. However, more work is needed in the area of converting information from two-dimensional images to values applicable to the three-dimensional rock. For example, it was found that while porosities calculated from petrographic image analysis

followed the trend of measured porosities, the petrographic porosities were considerably higher. There is a need to develop appropriate procedures and conversion factors to make quantitative results from petrography applicable to the rock.

10.0. CONCLUSIONS

The main conclusions reached from the analysis of the East Texas tight sand cores are listed below:

- Porosities and permeabilities measured on the Mast A-1, SFE No. 2 and SFE No. 3 are much lower than those measured on the SFE No. 1. There appears to be a trend toward decreasing porosity and permeability at greater depths below the top of the Travis Peak Formation which is related to increased quartz overgrowth volumes at depth.
- The Mast A-1 and SFE No. 2 cores contain the more common tight gas sandstone pore geometry, composed of secondary solution pores interconnected by slots between abutting, syntaxial quartz overgrowths. These rocks are significantly tighter than the SFE No. 1 samples, with high stress-dependence of permeability and the severe reduction in gas flow at relatively low water saturations typical of slot pore tight sands. Although quartz overgrowths and slot pores are common enough to be easily recognized in the SFE No. 1 samples, slots do not form the major flow paths for gas through these rocks. The SFE No. 3 core, from the calcareous Taylor sandstone, contained a variety of all three pore types.
- The Travis Peak in the Mast A-1 and SFE No. 2 wells represents the deeper portion of a diagenetic trend wherein the degree of pore alteration increases with depth of burial. The SFE No. 1 core represents Travis Peak from the shallower end of the trend. The SFE No. 3 core is from a different formation and does not appear to correlate with diagenetic trends in the overlying Travis Peak.
- Drainage experiments showed the Travis Peak samples to have critical gas saturations of the order of 10%. This is similar to value measured earlier for Mesaverde sandstones.
- Both imbibition and evaporation experiments showed that water redistribution in tight sands is very slow and difficult. As a result neither of these methods for varying sample water saturation yielded the kind of uniform saturation needed for meaningful relative permeability measurements. Future work utilizing an x-ray imaging system will help understand water movement in these rocks better.
- Finally, the preliminary analysis of petrographic and mercury porosimetry data conducted in this project leads us to conclude that fluorescent petrography and mercury porosimetry are useful techniques for rapidly and inexpensively assessing the quality of a tight sand reservoir. More work is needed, however, to refine these techniques and define the relevant correlations.

11.0. RECOMMENDATIONS

Some recommendations for future work, based on the results of this project, are given below.

- Development of techniques and correlations for using fluorescent petrography and mercury porosimetry as tools for rapid estimation of tight sand reservoir properties should be pursued. The comparison of Travis Peak, Taylor and Mesaverde sandstone data in this project suggests that generalized correlations applicable to tight sands from different formations may be possible. This stems from the observations that the slot and solution pore geometry seems to be the most important characteristic that gives tight sands their unique properties. Development of such a technique could provide an alternative for formation evaluation in tight sands which is faster and less expensive than time-consuming core analyses on low permeability rocks.
- Imaging techniques such as X-ray or microwave imaging should be used to study water distribution in samples during imbibition and evaporation. This would help address some of the problems encountered in this project during imbibition experiments. Also, the present work has highlighted the non-uniform saturations that are possible when evaporation takes place from a tight sand. Since evaporation is the easiest method of varying water saturation, and hence has been a popular technique, a proper understanding of resulting water saturation profiles is essential to the user of such data.

12.0. REFERENCES CITED

1. Soeder, D. J. and Chowdiah, P., "Two-Phase Flow in Tight Gas Sands, Annual Report," prepared for Gas Research Institute under Contract No. 5086-211-1258, by Institute of Gas Technology, Report GRI-87/0222, August 1987.
2. Soeder, D. J. and Chowdiah, P., "Two-Phase Flow in Tight Gas Sands -- SFE No. 1 Core," Topical Report prepared for Gas Research Institute under contract No. 5086-211-1258 by Institute of Gas Technology, Report GRI-88/0257, November 1988.
3. Chowdiah, P. and Soeder, D. J., "Two-Phase Flow in Tight Gas Sands -- SFE No. 2 Core," Topical Report prepared for Gas Research Institute under contract No. 5086-211-1258 by Institute of Gas Technology, October 1989.
4. Chowdiah, P., "Measurement and Analysis of Two-Phase Flow Through Low Permeability Media. Task 2. Experimental Research." Final Report No. GRI-86/0123-1 prepared for Gas Research Institute under Contract No. 5082-260-0711, Institute of Gas Technology, Chicago, March 1987.
5. Swanson, B. F., "A Simple Correlation Between Permeabilities and Mercury Capillary Pressures," J. Pet. Tech., 2498-504, December 1981.
6. Soeder, D. J., "Laboratory Drying Procedures and the Permeability of Tight Sandstone Core," SPE Formation Evaluation, Vol. 1, 16-22, February 1986.
7. "Advancements in Travis Peak Formation Evaluation and Hydraulic Fracture Technology: Staged Field Experiment No. 1," Report No. GRI-88/0077, compiled and edited by CER Corporation and S. A. Holditch & Associates for Gas Research Institute, Chicago, Illinois, April 1988.
8. Soeder, D. J., and Randolph, P., "Measurement and Analysis of Two-Phase Flow Through Low Permeability Media, Task 3, Final Report," prepared for Gas Research Institute under Contract No. 5082-211-0712, by Institute of Gas Technology. Report GRI-86/0160, July 1986.
9. Soeder, D. J., and Randolph, P. L., "Porosity, Permeability and Pore Structure of the Tight Mesa Verde Sandstone, Piceance Basin, Colorado," SPE Formation Evaluation, Vol. 2, 129-36, June 1987.
10. Gies, R. M., "An Improved Method for Viewing Micropores Systems in Rocks with the Polarizing Microscope," SPE Formation Evaluation, Vol. 2, 209-14, June 1987.
11. Soeder, D. J., "Reservoir Properties and the Pore Structure of Tight Gas Sands." Abstract presented at the 1984 AAPG Annual Convention, San Antonio, Texas, May 21-23, 1984. AAPG Bulletin, Vol. 68, No. 4, page 530, April 1984.
12. Wilson, M. D., "Origins of Clays Controlling Permeability in Tight Gas Sands," J. Pet. Tech., Vol. 34, No. 12, 2871-76, December 1982.

13. Ostensen, R. W., "Microcrack Permeability in Tight Gas Sandstone," Society of Pet. Engr. J., 919-26, December 1983.
14. Dutton S. P., "Diagenesis and Burial History of the Lower Cretaceous Travis Peak Formation, East Texas: Controls on Permeability in a Tight Gas Sandstone" Topical Report prepared for Gas Research Institute under Contract 5082-211-0708, by Texas Bureau of Economic Geology, Report GRI-87/0079, May 1987.
15. Chowdiah, P., "Laboratory Measurements Relevant to Two-Phase Flow in a Tight Gas Sand Matrix." Paper SPE 16945 presented at the 62nd Annual Technical Conference and Exhibition of SPE, Dallas, Texas, September 27-30, 1987
16. Chowdiah, P., "Influence of Water-Desaturation Technique and Stress on Laboratory Measurement of Hydraulic Properties of Tight Sandstones", SPE Formation Evaluation, 679-85, December 1988.

APPENDIX A.

Detailed Core Analysis Data for SFE No. 3 Samples

SFE NO. 3 CORE ANALYSIS: PORE GEOMETRY SUMMARY

<u>Plug Depth, ft</u>	<u>Pore Type</u>	<u>Petrographic Description</u>
9226.0	3	Fine quartz sand in a calcite matrix; microporosity is present in the matrix and within some of the sand grains, cracks occur at the sand/matrix boundaries.
9228.0	2	Quartz sandstone with quartz overgrowths and clay occluding primary porosity. Porosity occurs as solution pores connected by slots; some intragranular microporosity is also present.
9234.0	3	Fine quartz sand in a microporous calcite matrix. Some secondary porosity is present; cracks occur at grain/matrix boundaries.
9237.0	3	Silt-sized quartz grains in a calcite matrix. Pores are small and scattered; some microporosity is also present.
9237.7	3	Quartz conglomerate with sand grains in a carbonate matrix. Lowest porosity of samples analyzed by IGT. Cracks through grains and matrix supply flowpaths; some intragranular microporosity is also scattered throughout.
9242.0	1	Quartz sandstone containing grain-supported primary porosity partially filled with clay and dolomite rhombs.
9246.5	1.5	Quartz-lithic sandstone containing grain-supported, primary porosity partially filled with clay. Some solution porosity is also present and quartz overgrowths have formed slot pores, although these are not the main flowpaths. This represents a transitional pore geometry between types 1 and 2.
9248.0	1	Quartz-lithic sandstone with grain-supported, primary porosity partially filled with clay and carbonate. A few solution pores at sites of lithic grains are developed throughout.
9286.0	2.5	Quartz pebble conglomerate and sand in carbonate matrix, with secondary pores, microporosity and crack-like flowpaths. This pore geometry is intermediate between types 2 and 3.
9293.1	1	Quartz-lithic sandstone containing grain-supported primary porosity partially filled with clay and calcite. Secondary porosity is also common.

9297.0	2	Quartz sandstone with solution pores connected by slots; some microporosity and remnant primary porosity are scattered throughout.
9306.0	2	Quartz sandstone with well-developed overgrowths occluding primary porosity, some calcite mineralization as well, abundant secondary pores and slot-pore flowpaths.
9310.5	3	Quartz sand suspended in a calcite matrix with a few secondary pores and microporous zones; crack-like pores occur at boundaries between matrix and grains.
9317.0	2	Quartz-lithic sandstone containing secondary porosity and intragranular microporosity; flowpaths consist of slot pores.
9321.1	1.5	Very fine sandstone with significant secondary porosity and scattered microporosity. Primary porosity is partially filled with clay, but provides the major flowpaths. This pore geometry is intermediate between types 1 and 2.
9327.0	1	Quartz sandstone containing primary porosity partially filled with clay, along with some secondary porosity and abundant intragranular and intergranular microporosity.

MICROMERITICS PORE SIZER 9310

V1.04

PAGE 1

890507601

6/8/89

SFE #3 9226

2

PENETROMETER NUMBER 70522

PRESSURE PSIA	CORRECTED PRESSURE PSIA	PORE DIAMETER um	CUM. INTR. VOLUME cc/g	CUM. PORE SURFACE AREA m2/g	DIFF. INTR. VOLUME dV/:dD cc/g um	INCR. INTR. VOLUME cc/g
1.3	1.3	134.8712	0.0000	0.0000	0.0000	0.0000
2.3	2.3	77.5900	0.0001	0.0000	0.0000	0.0001
3.3	3.3	55.2083	0.0002	0.0000	0.0000	0.0001
5.0	5.0	35.9496	0.0004	0.0000	0.0000	0.0001
8.0	8.0	22.6815	0.0004	0.0000	0.0000	0.0000
10.2	10.2	17.7212	0.0005	0.0000	0.0000	0.0001
13.2	13.2	13.7454	0.0006	0.0001	0.0000	0.0001
15.0	15.0	12.0262	0.0006	0.0001	0.0000	0.0000
18.0	18.0	10.0429	0.0006	0.0001	0.0000	0.0000
20.2	20.2	8.9434	0.0006	0.0001	0.0000	0.0000
22.1	22.1	8.1724	0.0006	0.0001	0.0000	0.0000
25.1	25.1	7.2106	0.0006	0.0001	0.0000	0.0000
40.0	44.4	4.0723	0.0006	0.0001	0.0000	0.0000
61.0	65.4	2.7649	0.0006	0.0001	0.0000	0.0000
66.0	70.4	2.5686	0.0006	0.0001	0.0000	0.0000
70.0	74.4	2.4305	0.0006	0.0001	0.0000	0.0000
75.0	79.4	2.2775	0.0006	0.0001	0.0000	0.0000
81.0	85.4	2.1175	0.0006	0.0001	0.0000	0.0000
86.0	90.4	2.0004	0.0006	0.0001	0.0000	0.0000
91.0	95.4	1.8956	0.0006	0.0001	0.0000	0.0000
102.0	106.4	1.6996	0.0006	0.0001	0.0000	0.0000
130.0	134.4	1.3456	0.0006	0.0001	0.0000	0.0000
143.0	147.4	1.2269	0.0006	0.0001	0.0000	0.0000
177.0	181.4	0.9970	0.0006	0.0001	0.0000	0.0000
185.0	189.4	0.9549	0.0006	0.0001	0.0000	0.0000
204.0	208.4	0.8678	0.0006	0.0001	0.0000	0.0000
223.0	227.4	0.7953	0.0006	0.0001	0.0000	0.0000
243.0	247.4	0.7310	0.0006	0.0001	0.0000	0.0000
275.0	279.4	0.6473	0.0006	0.0001	0.0000	0.0000
283.0	287.4	0.6293	0.0006	0.0001	0.0000	0.0000
305.0	309.4	0.5845	0.0006	0.0001	0.0000	0.0000
328.0	332.4	0.5441	0.0006	0.0001	0.0000	0.0000
351.0	355.4	0.5089	0.0006	0.0001	0.0000	0.0000
388.0	392.4	0.4609	0.0007	0.0011	0.0025	0.0001
412.0	416.4	0.4343	0.0007	0.0011	0.0000	0.0000
437.0	441.4	0.4097	0.0007	0.0011	0.0000	0.0000
464.0	468.4	0.3861	0.0007	0.0011	0.0000	0.0000
477.0	481.4	0.3757	0.0007	0.0011	0.0000	0.0000
504.0	508.4	0.3557	0.0007	0.0011	0.0000	0.0000
530.0	534.4	0.3384	0.0007	0.0011	0.0000	0.0000
555.0	559.4	0.3233	0.0007	0.0011	0.0000	0.0000
583.0	587.4	0.3079	0.0007	0.0011	0.0000	0.0000

MICROMERITICS PORE SIZER 9310

V1.04

PAGE 2

890507601

SFE #3 9226

6/8/89

PENETROMETER NUMBER 70522

2

PRESSURE PSIA	CORRECTED PRESSURE PSIA	PORE DIAMETER um	CUM. INTR. VOLUME cc/g	CUM. PORE SURFACE AREA m2/g	DIFF. INTR. VOLUME dV/:dD cc/g um	INCR. INTR. VOLUME cc/g
609.0	613.4	0.2948	0.0007	0.0011	0.0000	0.0000
635.0	639.4	0.2829	0.0007	0.0011	0.0000	0.0000
662.0	666.4	0.2714	0.0007	0.0011	0.0000	0.0000
688.0	692.4	0.2612	0.0007	0.0011	0.0000	0.0000
702.0	706.4	0.2560	0.0007	0.0011	0.0000	0.0000
729.0	733.4	0.2466	0.0007	0.0011	0.0000	0.0000
757.0	761.4	0.2375	0.0007	0.0011	0.0000	0.0000
784.0	788.4	0.2294	0.0007	0.0011	0.0000	0.0000
810.0	814.4	0.2221	0.0007	0.0011	0.0000	0.0000
855.0	859.4	0.2105	0.0007	0.0011	0.0000	0.0000
853.0	857.4	0.2109	0.0007	0.0011	0.0000	0.0000
882.0	886.4	0.2040	0.0008	0.0034	0.0176	0.0001
907.0	911.4	0.1984	0.0008	0.0034	0.0000	0.0000
935.0	939.4	0.1925	0.0008	0.0034	0.0000	0.0000
963.0	967.4	0.1870	0.0008	0.0034	0.0000	0.0000
976.0	980.4	0.1845	0.0008	0.0034	0.0000	0.0000
1004.0	1008.4	0.1794	0.0008	0.0034	0.0000	0.0000
1098.0	1102.4	0.1641	0.0008	0.0034	0.0000	0.0000
1214.0	1218.4	0.1484	0.0008	0.0034	0.0000	0.0000
1313.0	1317.4	0.1373	0.0010	0.0068	0.0109	0.0001
1396.0	1400.4	0.1292	0.0011	0.0105	0.0149	0.0001
1512.0	1516.4	0.1193	0.0013	0.0183	0.0246	0.0002
1610.0	1614.3	0.1120	0.0017	0.0309	0.0503	0.0004
1697.0	1701.3	0.1063	0.0017	0.0309	0.0000	0.0000
1802.5	1806.8	0.1001	0.0021	0.0450	0.0586	0.0004
1894.0	1898.3	0.0953	0.0021	0.0450	0.0000	0.0000
1992.0	1996.3	0.0906	0.0023	0.0554	0.0519	0.0002
4976.0	4980.3	0.0363	0.0028	0.0860	0.0089	0.0005
7960.0	7964.2	0.0227	0.0033	0.1518	0.0357	0.0005
9976.0	9980.2	0.0181	0.0036	0.2231	0.0793	0.0004
14936.0	14940.2	0.0121	0.0039	0.2873	0.0403	0.0002
19920.0	19924.2	0.0091	0.0040	0.3331	0.0401	0.0001
24880.0	24884.2	0.0073	0.0042	0.4519	0.1341	0.0002
29856.0	29860.2	0.0061	0.0045	0.5976	0.2003	0.0002
19904.0	19908.2	0.0091	0.0045	0.5976	0.0000	0.0000
9984.0	9988.2	0.0181	0.0045	0.5976	0.0000	0.0000
4992.0	4996.2	0.0362	0.0045	0.5976	0.0000	0.0000
992.0	996.2	0.1816	0.0042	0.5886	0.0017	-0.0002
750.0	754.2	0.2398	0.0041	0.5863	0.0021	-0.0001
481.0	485.2	0.3727	0.0038	0.5816	0.0027	-0.0004
231.0	235.2	0.7689	0.0035	0.5799	0.0006	-0.0002
90.0	94.2	1.9192	0.0034	0.5795	0.0001	-0.0001

MICROMERITICS PORE SIZER 9310

V1.04

PAGE 3

890507601

6/8/89

SFE #3 9226

2

PENETROMETER NUMBER 70522

PRESSURE PSIA	CORRECTED PRESSURE PSIA	PORE DIAMETER um	CUM. INTR. VOLUME cc/g	CUM. PORE SURFACE AREA m2/g	DIFF. INTR. VOLUME dV/:dD cc/g um	INCR. INTR. VOLUME cc/g
50.0	54.3	3.3326	0.0029	0.5788	0.0003	-.0005
26.0	30.3	5.9734	0.0028	0.5787	0.0000	-.0001
13.0	17.3	10.4678	0.0028	0.5787	0.0000	0.0000

Received: 05/25/89

Results by Sample

SAMPLE ID SFE-3 8226 FT FRACTION 01A TEST CODE CLAY NAME Clay Type Analysis by XRD
 Date & Time Collected not specified Category _____

CLAY COMPONENTIAL ANALYSIS

CARBONATES (ACETIC ACID SOLUBLE) : 41
 SILICATES & ALUMINO-SILICATES : 58
 CLAYS-NORMALIZED TO 100% : 1
 Kaolinite + Chlorite : 2
 Illite-Montmorillonite : 10
 Expandable Clays : 88
 (Montmorillonite, Smectite, etc)

Note: N.D. = Not Detected

X-RAY DIFFRACTION PHASES PRESENT

Major: Quartz-SiO2 (5-490), Calcite-CaCO3 (5-586)
 Major-Minor: Albite-NaAl3Si3O8 (9-466)
 Minor:
 Minor-Trace: Clays

Note: All constituents were listed in a probable order of decreasing abundance.

Clays may include kaolinite, illite and montmorillonite.

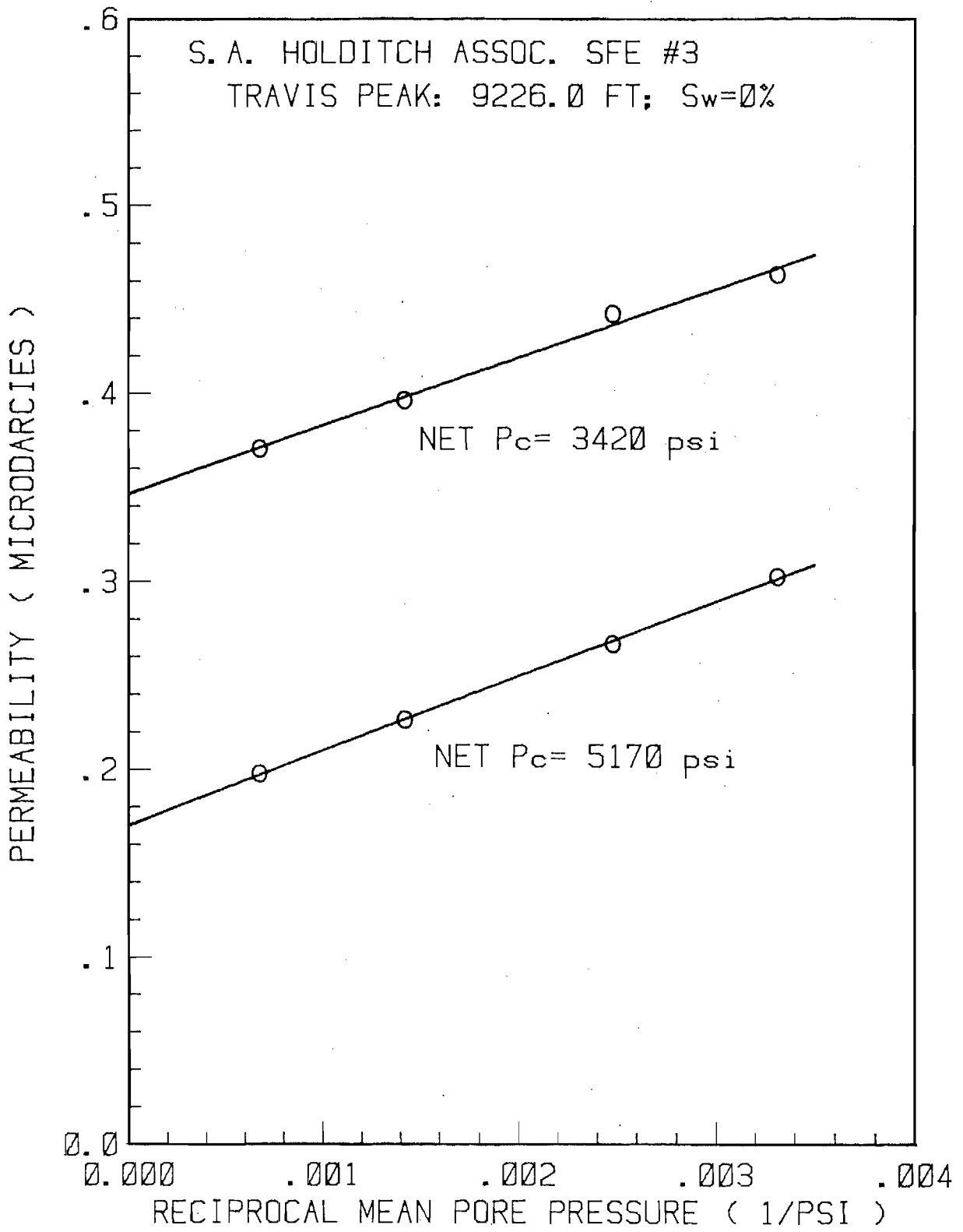
WELL NAME: S.A. HOLDITCH ASSOC. SFE #3

PLUG: TRAVIS PEAK: 9226.0 FT; Sw=0%

PLUG LENGTH: 5.204 CM

PLUG AREA: 5.032 CM²

TEST DATE (M-D)	BEGIN TIME (H:M)	DUR- ATION (H:M)	CONFINING PRESSURE (PSIA)	MEAN PORE P (PSIA)	DIFFERENTIAL PRESSURE (PSI)	FLOW RATE (SCC/S)	TEMPERATURE (DEG. F)	VISCOSITY (C POISE)	COMPRES- SIBILITY (Z)	PERMEABILITY VALUE (MICRODARCY)	STD. DEV. (%)
11-17	15:40	00:46	4866	1471.66	38.54	5.04E-003	98.00	0.02023	1.0099	4.35E-001	(1.1)
11-20	13:22	00:54	4885	1471.58	38.27	4.26E-003	98.00	0.02023	1.0099	3.71E-001	(.4)
11-21	11:26	01:32	4127	703.27	45.23	2.77E-003	98.00	0.01902	0.9990	3.96E-001	(.8)
11-22	13:36	01:08	3822	403.64	45.64	1.82E-003	98.00	0.01871	0.9981	4.42E-001	(.8)
11-27	13:26	01:14	3728	301.86	47.00	1.47E-003	98.00	0.01863	0.9983	4.63E-001	(.4)
11-29	10:12	01:17	5477	301.87	46.86	9.59E-004	98.00	0.01863	0.9983	3.02E-001	(1.2)
11-30	10:22	01:30	5582	403.53	49.58	1.19E-003	98.00	0.01871	0.9981	2.67E-001	(1.1)
12-01	14:30	01:22	5872	701.32	49.25	1.72E-003	98.00	0.01902	0.9990	2.26E-001	(1.3)
12-06	09:10	01:47	6646	1473.09	50.66	3.01E-003	98.00	0.02023	1.0099	1.98E-001	(1.5)



MICROMERITICS PORE SIZER 9310

V1.04

PAGE 1

890507602

6/8/89

SFE #3 9228

9

PENETROMETER NUMBER 70522

PRESSURE PSIA	CORRECTED PRESSURE PSIA	PORE DIAMETER um	CUM. INTR. VOLUME cc/g	CUM. PORE SURFACE AREA m2/g	DIFF. INTR. VOLUME dV/:dD cc/g um	INCR. INTR. VOLUME cc/g
1.3	1.3	136.7062	0.0000	0.0000	0.0000	0.0000
2.3	2.3	79.4301	0.0001	0.0000	0.0000	0.0001
3.4	3.4	53.5888	0.0004	0.0000	0.0000	0.0003
5.3	5.3	34.3518	0.0005	0.0000	0.0000	0.0001
8.3	8.3	21.8433	0.0008	0.0001	0.0000	0.0003
9.9	9.9	18.2689	0.0008	0.0001	0.0000	0.0000
13.1	13.1	13.8592	0.0010	0.0001	0.0000	0.0001
15.5	15.5	11.6972	0.0010	0.0001	0.0000	0.0000
18.1	18.1	10.0029	0.0010	0.0001	0.0000	0.0000
20.2	20.2	8.9474	0.0010	0.0001	0.0000	0.0000
22.2	22.2	8.1327	0.0010	0.0001	0.0000	0.0000
25.3	25.3	7.1388	0.0011	0.0002	0.0001	0.0001
40.0	44.4	4.0751	0.0012	0.0003	0.0000	0.0001
61.0	65.4	2.7662	0.0012	0.0003	0.0000	0.0000
65.0	69.4	2.6067	0.0012	0.0003	0.0000	0.0000
71.0	75.4	2.3993	0.0012	0.0003	0.0000	0.0000
75.0	79.4	2.2784	0.0012	0.0003	0.0000	0.0000
81.0	85.4	2.1183	0.0012	0.0003	0.0000	0.0000
86.0	90.4	2.0011	0.0012	0.0003	0.0000	0.0000
90.0	94.4	1.9163	0.0012	0.0003	0.0000	0.0000
108.0	112.4	1.6093	0.0012	0.0003	0.0000	0.0000
129.0	133.4	1.3560	0.0012	0.0003	0.0000	0.0000
142.0	146.4	1.2356	0.0014	0.0007	0.0011	0.0001
173.0	177.4	1.0197	0.0014	0.0007	0.0000	0.0000
180.0	184.4	0.9809	0.0014	0.0007	0.0000	0.0000
206.0	210.4	0.8597	0.0014	0.0007	0.0000	0.0000
224.0	228.4	0.7920	0.0014	0.0007	0.0000	0.0000
244.0	248.4	0.7282	0.0014	0.0007	0.0000	0.0000
263.0	267.4	0.6765	0.0015	0.0015	0.0026	0.0001
283.0	287.4	0.6294	0.0015	0.0015	0.0000	0.0000
303.0	307.4	0.5884	0.0015	0.0015	0.0000	0.0000
338.0	342.4	0.5283	0.0016	0.0025	0.0023	0.0001
360.0	364.4	0.4964	0.0016	0.0025	0.0000	0.0000
382.0	386.4	0.4681	0.0016	0.0025	0.0000	0.0000
404.0	408.4	0.4429	0.0018	0.0037	0.0054	0.0001
429.0	433.3	0.4174	0.0019	0.0049	0.0054	0.0001
452.0	456.3	0.3963	0.0021	0.0063	0.0065	0.0001
476.0	480.3	0.3765	0.0022	0.0077	0.0069	0.0001
500.0	504.3	0.3586	0.0025	0.0107	0.0153	0.0003
537.0	541.3	0.3341	0.0027	0.0139	0.0112	0.0003
558.0	562.3	0.3217	0.0032	0.0189	0.0330	0.0004
582.0	586.2	0.3085	0.0037	0.0258	0.0417	0.0005

MICROMERITICS PORE SIZER 9310

V1.04

PAGE 2

890507602

6/8/89

SFE #3 9228

9

PENETROMETER NUMBER 70522

PRESSURE PSIA	CORRECTED PRESSURE PSIA	PORE DIAMETER um	CUM. INTR. VOLUME cc/g	CUM. PORE SURFACE AREA m2/g	DIFF. INTR. VOLUME dV/:dD cc/g um	INCR. INTR. VOLUME cc/g
603.0	607.2	0.2978	0.0040	0.0294	0.0257	0.0003
626.0	630.2	0.2870	0.0047	0.0388	0.0632	0.0007
655.0	659.1	0.2744	0.0058	0.0545	0.0870	0.0011
678.0	682.1	0.2652	0.0064	0.0646	0.0742	0.0007
700.0	704.1	0.2569	0.0070	0.0730	0.0663	0.0005
733.0	737.0	0.2454	0.0081	0.0905	0.0955	0.0011
758.0	762.0	0.2374	0.0089	0.1041	0.1023	0.0008
777.0	780.9	0.2316	0.0097	0.1181	0.1427	0.0008
800.0	803.9	0.2250	0.0106	0.1325	0.1244	0.0008
834.0	837.8	0.2159	0.0114	0.1475	0.0902	0.0008
856.0	859.8	0.2104	0.0122	0.1629	0.1492	0.0008
896.0	899.7	0.2010	0.0130	0.1789	0.0880	0.0008
905.0	908.7	0.1990	0.0134	0.1871	0.2071	0.0004
930.0	933.7	0.1937	0.0141	0.2011	0.1288	0.0007
957.0	960.7	0.1883	0.0143	0.2040	0.0252	0.0001
984.0	987.7	0.1831	0.0145	0.2099	0.0533	0.0003
1012.0	1015.6	0.1781	0.0148	0.2159	0.0543	0.0003
1098.0	1101.6	0.1642	0.0155	0.2320	0.0493	0.0007
1200.0	1203.6	0.1503	0.0162	0.2494	0.0493	0.0007
1305.0	1308.5	0.1382	0.0167	0.2646	0.0455	0.0005
1396.0	1399.5	0.1292	0.0171	0.2769	0.0458	0.0004
1505.0	1508.5	0.1199	0.0175	0.2901	0.0440	0.0004
1596.0	1599.5	0.1131	0.0178	0.2995	0.0402	0.0003
1694.0	1697.5	0.1065	0.0181	0.3095	0.0420	0.0003
1795.0	1798.4	0.1006	0.0184	0.3201	0.0458	0.0003
1900.5	1903.9	0.0950	0.0186	0.3313	0.0492	0.0003
2000.0	2003.4	0.0903	0.0188	0.3372	0.0291	0.0001
4976.0	4979.3	0.0363	0.0218	0.5278	0.0559	0.0030
7960.0	7963.2	0.0227	0.0233	0.7321	0.1108	0.0015
9968.0	9971.2	0.0181	0.0237	0.8126	0.0899	0.0004
14960.0	14963.1	0.0121	0.0245	1.0303	0.1359	0.0008
19904.0	19907.1	0.0091	0.0252	1.2893	0.2283	0.0007
24984.0	24987.0	0.0072	0.0259	1.6251	0.3710	0.0007
29856.0	29859.0	0.0061	0.0263	1.8726	0.3482	0.0004
20016.0	20019.0	0.0090	0.0263	1.8726	0.0000	0.0000
9992.0	9995.0	0.0181	0.0263	1.8726	0.0000	0.0000
4968.0	4971.0	0.0364	0.0258	1.7921	0.0300	-.0005
1000.0	1003.2	0.1803	0.0237	1.7161	0.0143	-.0021
745.0	748.2	0.2417	0.0232	1.7057	0.0089	-.0005
481.0	484.2	0.3735	0.0226	1.6986	0.0042	-.0005
230.0	233.3	0.7752	0.0211	1.6881	0.0038	-.0015
93.0	96.4	1.8763	0.0193	1.6827	0.0016	-.0018

MICROMERITICS PORE SIZER 9310

V1.04

PAGE 3
6/8/89
9

890507602
SFE #3 9228
PENETROMETER NUMBER 70522

PRESSURE PSIA	CORRECTED PRESSURE PSIA	PORE DIAMETER um	CUM. INTR. VOLUME cc/g	CUM. PORE SURFACE AREA m2/g	DIFF. INTR. VOLUME dV:dD cc/g um	INCR. INTR. VOLUME cc/g
47.0	50.4	3.5873	0.0189	1.6821	0.0002	-.0004
23.0	26.5	6.8307	0.0178	1.6813	0.0003	-.0011
14.0	17.5	10.3481	0.0178	1.6813	0.0000	0.0000

Received: 05/25/89

Results by Sample

SAMPLE ID SFE-3 9228 FT FRACTION 02A TEST CODE CLAY NAME Clay Type Analysis by XRD
Date & Time Collected not specified Category _____

CLAY COMPONENTIAL ANALYSIS

CARBONATES (ACETIC ACID SOLUBLE) : 4

SILICATES & ALUMINO-SILICATES : 94

CLAYS-NORMALIZED TO 100% : 2

 Kaolinite + Chlorite : 14

 Illite-Montmorillonite : 33

 Expandable Clays : 53

 (Montmorillonite, Smectite, etc)

Note: N.D. = Not Detected

X-RAY DIFFRACTION PHASES PRESENT

Major: Quartz

Major-Minor:

Minor: Calcite, Albite, Microcline-KAlSi3O8 (19-932)

Minor-Trace: Clays

Note: All constituents were listed in a probable order of decreasing abundance.

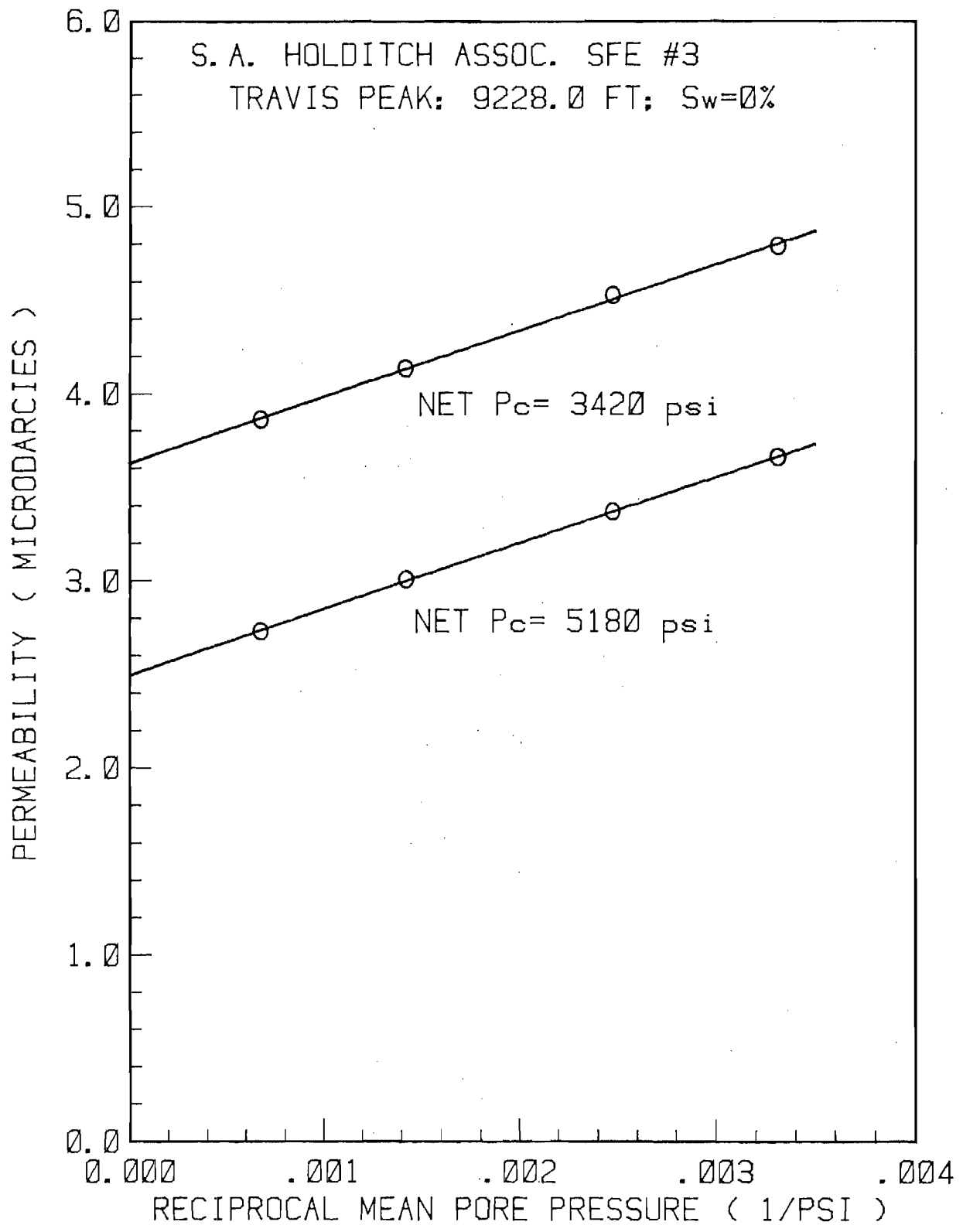
WELL NAME: S.A. HOLDITCH ASSOC. SFE #3

PLUG: TRAVIS PEAK: 9228.0 FT; Sw=0%

PLUG LENGTH: 5.076 CM

PLUG AREA: 5.037 CM²

TEST DATE (M-D)	BEGIN TIME (H:M)	DUR- ATION (H:M)	CONFINING PRESSURE (PSIA)	MEAN PORE P (PSIA)	DIFFERENTIAL PRESSURE (PSI)	FLOW RATE (SCC/S)	TEMPERATURE (DEG. F)	VISCOSITY (C POISE)	COMPRES- SIBILITY (Z)	PERMEABILITY VALUE (MICRODARCY)	STD. DEV. (%)
11-17	15:13	00:07	4874	1471.67	38.59	4.80E-002	98.00	0.02023	1.0099	4.03E+000	(.7)
11-20	12:55	00:08	4875	1471.58	38.33	4.57E-002	98.01	0.02023	1.0099	3.86E+000	(.3)
11-21	11:00	00:07	4120	703.27	45.30	2.97E-002	98.00	0.01902	0.9990	4.13E+000	(.3)
11-22	14:49	00:07	3819	403.66	45.55	1.91E-002	98.01	0.01871	0.9981	4.53E+000	(.3)
11-27	10:10	00:08	3723	301.84	47.11	1.57E-002	98.00	0.01863	0.9983	4.79E+000	(.2)
11-29	09:40	00:11	5482	301.87	46.95	1.19E-002	98.00	0.01863	0.9983	3.66E+000	(.1)
11-30	09:11	00:09	5586	403.56	49.66	1.55E-002	98.00	0.01871	0.9981	3.37E+000	(.1)
12-01	09:13	00:09	5884	701.32	49.36	2.35E-002	98.00	0.01902	0.9990	3.01E+000	(.3)
12-04	13:28	00:08	6645	1473.00	50.72	4.27E-002	98.00	0.02023	1.0099	2.73E+000	(.2)



MICROMERITICS PORE SIZER 9310

V1.04

PAGE 1

890507603

6/15/89

SFE #3 9234

3

PENETROMETER NUMBER 130201

PRESSURE PSIA	CORRECTED PRESSURE PSIA	PORE DIAMETER um	CUM. INTR. VOLUME cc/g	CUM. PORE SURFACE AREA m2/g	DIFF. INTR. VOLUME dV/:dD cc/g um	INCR. INTR. VOLUME cc/g
1.4	1.4	127.9988	0.0000	0.0000	0.0000	0.0000
2.1	2.1	84.7925	0.0000	0.0000	0.0000	0.0000
3.3	3.3	54.1666	0.0001	0.0000	0.0000	0.0001
5.4	5.4	33.2162	0.0003	0.0000	0.0000	0.0001
8.2	8.2	22.1564	0.0004	0.0000	0.0000	0.0001
10.2	10.2	17.7525	0.0004	0.0000	0.0000	0.0000
13.2	13.2	13.7454	0.0004	0.0000	0.0000	0.0000
15.2	15.2	11.8629	0.0004	0.0000	0.0000	0.0000
18.1	18.1	9.9781	0.0004	0.0000	0.0000	0.0000
20.3	20.3	8.9117	0.0006	0.0001	0.0001	0.0001
22.1	22.1	8.1957	0.0006	0.0001	0.0000	0.0000
25.3	25.3	7.1464	0.0006	0.0001	0.0000	0.0000
40.0	44.7	4.0507	0.0006	0.0001	0.0000	0.0000
61.0	65.7	2.7549	0.0006	0.0001	0.0000	0.0000
66.0	70.7	2.5600	0.0006	0.0001	0.0000	0.0000
71.0	75.6	2.3910	0.0007	0.0003	0.0008	0.0001
80.0	84.6	2.1368	0.0007	0.0003	0.0000	0.0000
80.0	84.6	2.1368	0.0007	0.0003	0.0000	0.0000
86.0	90.6	1.9953	0.0007	0.0003	0.0000	0.0000
90.0	94.6	1.9110	0.0007	0.0003	0.0000	0.0000
102.0	106.6	1.6960	0.0007	0.0003	0.0000	0.0000
129.0	133.6	1.3533	0.0007	0.0003	0.0000	0.0000
144.0	148.6	1.2168	0.0007	0.0003	0.0000	0.0000
160.0	164.6	1.0985	0.0007	0.0003	0.0000	0.0000
200.0	204.6	0.8838	0.0007	0.0003	0.0000	0.0000
199.0	203.7	0.8881	0.0006	-0.0003	0.0327	-0.0001
231.0	235.7	0.7675	0.0006	-0.0003	0.0000	0.0000
242.0	246.7	0.7333	0.0006	-0.0003	0.0000	0.0000
263.0	267.6	0.6758	0.0007	0.0005	0.0025	0.0001
286.0	290.6	0.6223	0.0007	0.0005	0.0000	0.0000
307.0	311.6	0.5804	0.0007	0.0005	0.0000	0.0000
332.0	336.6	0.5373	0.0007	0.0005	0.0000	0.0000
357.0	361.6	0.5001	0.0007	0.0005	0.0000	0.0000
382.0	386.6	0.4678	0.0007	0.0005	0.0000	0.0000
408.0	412.6	0.4383	0.0007	0.0005	0.0000	0.0000
437.0	441.6	0.4095	0.0007	0.0005	0.0000	0.0000
463.0	467.6	0.3868	0.0007	0.0005	0.0000	0.0000
491.0	495.6	0.3649	0.0007	0.0005	0.0000	0.0000
505.0	509.6	0.3549	0.0007	0.0005	0.0000	0.0000
533.0	537.6	0.3364	0.0007	0.0005	0.0000	0.0000
564.0	568.6	0.3181	0.0007	0.0005	0.0000	0.0000
592.0	596.6	0.3031	0.0007	0.0005	0.0000	0.0000

MICROMERITICS PORE SIZER 9310

V1.04

PAGE 2

890507603

6/15/89

SFE #3 9234

3

PENETROMETER NUMBER 130201

PRESSURE PSIA	CORRECTED PRESSURE PSIA	PORE DIAMETER um	CUM. INTR. VOLUME cc/g	CUM. PORE SURFACE AREA m2/g	DIFF. INTR. VOLUME dV/:dD cc/g um	INCR. INTR. VOLUME cc/g
606.0	610.6	0.2962	0.0007	0.0005	0.0000	0.0000
636.0	640.6	0.2823	0.0007	0.0005	0.0000	0.0000
666.0	670.6	0.2697	0.0007	0.0005	0.0000	0.0000
681.0	685.6	0.2638	0.0007	0.0005	0.0000	0.0000
710.0	714.6	0.2531	0.0007	0.0005	0.0000	0.0000
740.0	744.6	0.2429	0.0007	0.0005	0.0000	0.0000
756.0	760.6	0.2378	0.0007	0.0005	0.0000	0.0000
787.0	791.6	0.2285	0.0007	0.0005	0.0000	0.0000
802.0	806.6	0.2242	0.0007	0.0005	0.0000	0.0000
834.0	838.6	0.2157	0.0007	0.0005	0.0000	0.0000
867.0	871.6	0.2075	0.0007	0.0005	0.0000	0.0000
881.0	885.6	0.2042	0.0007	0.0005	0.0000	0.0000
915.0	919.6	0.1967	0.0007	0.0005	0.0000	0.0000
931.0	935.6	0.1933	0.0007	0.0005	0.0000	0.0000
962.0	966.6	0.1871	0.0008	0.0035	0.0228	0.0001
977.0	981.6	0.1842	0.0008	0.0035	0.0000	0.0000
1009.0	1013.6	0.1784	0.0008	0.0035	0.0000	0.0000
1114.0	1118.6	0.1617	0.0008	0.0035	0.0000	0.0000
1199.0	1203.6	0.1503	0.0008	0.0035	0.0000	0.0000
1305.0	1309.6	0.1381	0.0011	0.0113	0.0232	0.0003
1410.0	1414.6	0.1279	0.0016	0.0240	0.0413	0.0004
1517.0	1521.6	0.1189	0.0018	0.0331	0.0314	0.0003
1606.0	1610.6	0.1123	0.0020	0.0380	0.0215	0.0001
1696.0	1700.6	0.1064	0.0021	0.0432	0.0237	0.0001
1816.0	1820.6	0.0993	0.0024	0.0542	0.0402	0.0003
1907.0	1911.6	0.0946	0.0024	0.0542	0.0000	0.0000
2008.0	2012.6	0.0899	0.0024	0.0542	0.0000	0.0000
4984.0	4988.5	0.0363	0.0034	0.1168	0.0184	0.0010
7960.0	7964.5	0.0227	0.0041	0.2124	0.0520	0.0007
9968.0	9972.4	0.0181	0.0044	0.2676	0.0617	0.0003
14944.0	14948.4	0.0121	0.0049	0.4169	0.0934	0.0006
19912.0	19916.4	0.0091	0.0054	0.5767	0.1402	0.0004
24888.0	24892.4	0.0073	0.0056	0.7147	0.1553	0.0003
29856.0	29860.4	0.0061	0.0059	0.8840	0.2333	0.0003
20040.0	20044.4	0.0090	0.0059	0.8840	0.0000	0.0000
10000.0	10004.4	0.0181	0.0059	0.8840	0.0000	0.0000
4968.0	4972.4	0.0364	0.0056	0.8426	0.0154	-0.0003
1005.0	1009.4	0.1792	0.0045	0.8007	0.0079	-0.0011
739.0	743.5	0.2433	0.0042	0.7954	0.0044	-0.0003
487.0	491.5	0.3680	0.0039	0.7917	0.0023	-0.0003
234.0	238.5	0.7584	0.0038	0.7907	0.0004	-0.0001
78.0	82.5	2.1927	0.0037	0.7903	0.0001	-0.0001

MICROMERITICS PORE SIZER 9310

V1.04

PAGE 3

890507603

6/15/89

SFE #3 9234

3

PENETROMETER NUMBER 130201

PRESSURE PSIA	CORRECTED PRESSURE PSIA	PORE DIAMETER um	CUM. INTR. VOLUME cc/g	CUM. PORE SURFACE AREA m2/g	DIFF. INTR. VOLUME dV/:dD cc/g um	INCR. INTR. VOLUME cc/g
49.0	53.5	3.3796	0.0031	0.7895	0.0005	-.0006
29.0	33.5	5.3952	0.0030	0.7893	0.0001	-.0001
15.0	19.5	9.2641	0.0030	0.7893	0.0000	0.0000

Received: 05/25/89

Results by Sample

SAMPLE ID SFE-3 9234 FT FRACTION 03A TEST CODE CLAY NAME Clay Type Analysis by XRD
Date & Time Collected not specified Category _____

CLAY COMPONENTIAL ANALYSIS

CARBONATES (ACETIC ACID SOLUBLE) : 42

SILICATES & ALUMINO-SILICATES : 57

CLAYS-NORMALIZED TO 100% : 1

 Kaolinite + Chlorite : 11

 Illite-Montmorillonite : 32

 Expandable Clays : 57

 (Montmorillonite, Smectite, etc)

Note: N.D. = Not Detected

X-RAY DIFFRACTION PHASES PRESENT

Major: Quartz, Calcite

Major-Minor: Albite and/or Albite-potassium high (9-478)

Minor:

Minor-Trace: Clays

Note: All constituents were listed in a probable order of decreasing abundance.

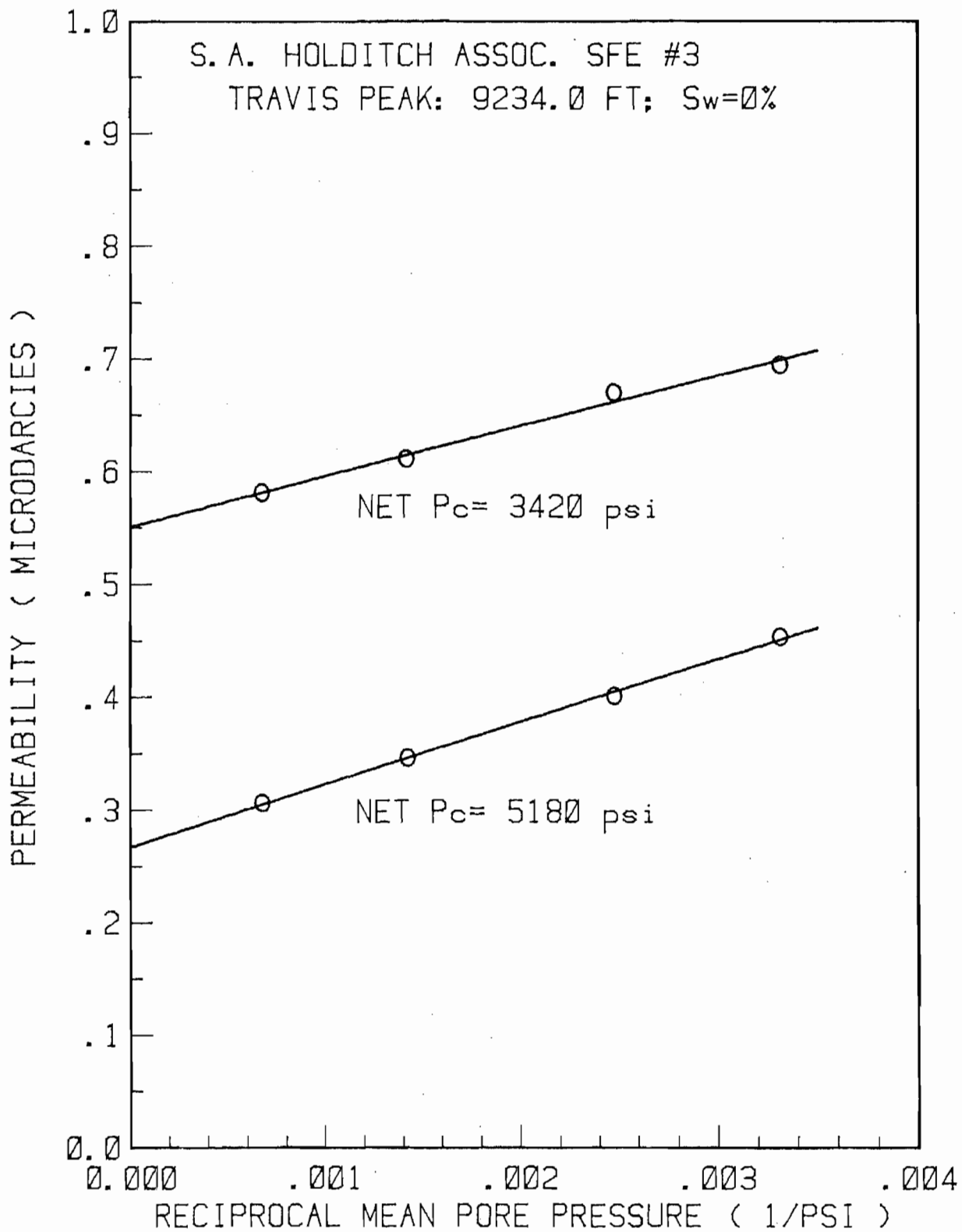
WELL NAME: S.A. HOLDITCH ASSOC. SFE #3

PLUG: TRAVIS PEAK: 9234.0 FT; Sw=0%

PLUG LENGTH: 5.122 CM

PLUG AREA: 5.034 CM²

TEST DATE (M-D)	BEGIN TIME (H:M)	DUR- ATION (H:M)	CONFINING PRESSURE (PSIA)	MEAN PORE P (PSIA)	DIFFERENTIAL PRESSURE (PSI)	FLOW RATE (SCC/S)	TEMPERATURE (DEG. F)	VISCOSITY (C POISE)	COMPRES- SIBILITY (Z)	PERMEABILITY VALUE (MICRODARCY)	STD. DEV. (%)
11-17	14:38	00:33	4877	1471.67	38.73	8.24E-003	98.00	0.02023	1.0099	6.96E-001	(.1)
11-20	11:55	00:53	4878	1471.58	38.47	6.83E-003	98.00	0.02023	1.0099	5.81E-001	(.6)
11-21	13:12	00:40	4122	703.27	45.16	4.33E-003	98.00	0.01902	0.9990	6.11E-001	(.4)
11-22	12:21	00:46	3826	403.64	45.67	2.80E-003	98.00	0.01871	0.9981	6.70E-001	(.2)
11-27	12:42	00:37	3723	301.86	47.01	2.25E-003	98.00	0.01863	0.9983	6.95E-001	(.5)
11-29	10:17	01:17	5477	301.85	46.90	1.46E-003	98.00	0.01863	0.9983	4.53E-001	(.9)
11-30	10:22	01:30	5582	403.54	49.56	1.82E-003	98.00	0.01871	0.9981	4.01E-001	(.8)
12-01	14:30	01:20	5872	701.32	49.23	2.67E-003	98.00	0.01902	0.9990	3.46E-001	(.8)
12-04	11:48	01:18	6647	1472.98	50.93	4.77E-003	98.00	0.02023	1.0099	3.06E-001	(.8)



MICROMERITICS PORE SIZER 9310

V1.04

PAGE 1
5/31/89
2

890507604

SFE #3 9237

PENETROMETER NUMBER 130163

PRESSURE PSIA	CORRECTED PRESSURE PSIA	PORE DIAMETER um	CUM. INTR. VOLUME cc/g	CUM. PORE SURFACE AREA m2/g	DIFF. INTR. VOLUME dV/:dD cc/g um	INCR. INTR. VOLUME cc/g
0.9	0.9	211.5349	0.0000	0.0000	0.0000	0.0000
2.1	2.1	86.9949	0.0006	0.0000	0.0000	0.0006
3.1	3.1	57.7466	0.0007	0.0000	0.0000	0.0001
5.2	5.2	34.8886	0.0009	0.0000	0.0000	0.0001
8.1	8.1	22.4034	0.0009	0.0000	0.0000	0.0000
10.4	10.4	17.3990	0.0010	0.0001	0.0000	0.0001
13.4	13.4	13.5325	0.0010	0.0001	0.0000	0.0000
15.3	15.3	11.8489	0.0010	0.0001	0.0000	0.0000
18.1	18.1	9.9979	0.0010	0.0001	0.0000	0.0000
20.5	20.5	8.8294	0.0010	0.0001	0.0000	0.0000
22.3	22.3	8.1031	0.0012	0.0001	0.0002	0.0001
25.3	25.3	7.1592	0.0012	0.0001	0.0000	0.0000
41.0	45.6	3.9645	0.0012	0.0001	0.0000	0.0000
62.0	66.6	2.7148	0.0012	0.0001	0.0000	0.0000
66.0	70.6	2.5611	0.0012	0.0001	0.0000	0.0000
71.0	75.6	2.3920	0.0013	0.0004	0.0009	0.0001
81.0	85.6	2.1126	0.0013	0.0004	0.0000	0.0000
80.0	84.6	2.1372	0.0010	-0.0002	0.0117	-.0003
86.0	90.6	1.9958	0.0012	0.0001	0.0010	0.0001
92.0	96.6	1.8719	0.0012	0.0001	0.0000	0.0000
101.0	105.6	1.7124	0.0012	0.0001	0.0000	0.0000
128.0	132.6	1.3638	0.0013	0.0005	0.0004	0.0001
143.0	147.6	1.2252	0.0013	0.0005	0.0000	0.0000
163.0	167.6	1.0790	0.0013	0.0005	0.0000	0.0000
183.0	187.6	0.9640	0.0013	0.0005	0.0000	0.0000
202.0	206.6	0.8754	0.0013	0.0005	0.0000	0.0000
223.0	227.6	0.7946	0.0013	0.0005	0.0000	0.0000
244.0	248.6	0.7275	0.0013	0.0005	0.0000	0.0000
266.0	270.6	0.6683	0.0013	0.0005	0.0000	0.0000
290.0	294.6	0.6139	0.0013	0.0005	0.0000	0.0000
303.0	307.6	0.5880	0.0013	0.0005	0.0000	0.0000
328.0	332.6	0.5438	0.0013	0.0005	0.0000	0.0000
356.0	360.6	0.5015	0.0013	0.0005	0.0000	0.0000
382.0	386.6	0.4678	0.0013	0.0005	0.0000	0.0000
410.0	414.6	0.4362	0.0013	0.0005	0.0000	0.0000
438.0	442.6	0.4086	0.0013	0.0005	0.0000	0.0000
467.0	471.6	0.3835	0.0013	0.0005	0.0000	0.0000
483.0	487.6	0.3709	0.0013	0.0005	0.0000	0.0000
511.0	515.6	0.3508	0.0013	0.0005	0.0000	0.0000
542.0	546.6	0.3309	0.0013	0.0005	0.0000	0.0000
558.0	562.6	0.3215	0.0013	0.0005	0.0000	0.0000
589.0	593.6	0.3047	0.0013	0.0005	0.0000	0.0000

MICROMERITICS PORE SIZER 9310

V1.04

PAGE 2

890507604

5/31/89

SFE #3 9237

2

PENETROMETER NUMBER 130163

PRESSURE PSIA	CORRECTED PRESSURE PSIA	PORE DIAMETER um	CUM. INTR. VOLUME cc/g	CUM. PORE SURFACE AREA m2/g	DIFF. INTR. VOLUME dV/:dD cc/g um	INCR. INTR. VOLUME cc/g
604.0	608.6	0.2972	0.0013	0.0005	0.0000	0.0000
634.0	638.6	0.2832	0.0013	0.0005	0.0000	0.0000
666.0	670.6	0.2697	0.0013	0.0005	0.0000	0.0000
682.0	686.6	0.2634	0.0013	0.0005	0.0000	0.0000
712.0	716.6	0.2524	0.0013	0.0005	0.0000	0.0000
729.0	733.6	0.2465	0.0013	0.0005	0.0000	0.0000
761.0	765.6	0.2362	0.0013	0.0005	0.0000	0.0000
779.0	783.6	0.2308	0.0013	0.0005	0.0000	0.0000
812.0	816.6	0.2215	0.0013	0.0005	0.0000	0.0000
844.0	848.6	0.2131	0.0013	0.0005	0.0000	0.0000
860.0	864.6	0.2092	0.0013	0.0005	0.0000	0.0000
894.0	898.6	0.2013	0.0014	0.0033	0.0182	0.0001
910.0	914.6	0.1977	0.0014	0.0033	0.0000	0.0000
942.0	946.6	0.1911	0.0014	0.0033	0.0000	0.0000
959.0	963.6	0.1877	0.0014	0.0033	0.0000	0.0000
1008.0	1012.6	0.1786	0.0014	0.0033	0.0000	0.0000
1004.0	1008.6	0.1793	0.0013	0.0001	0.2035	-0.0001
1112.0	1116.6	0.1620	0.0013	0.0001	0.0000	0.0000
1203.0	1207.6	0.1498	0.0014	0.0038	0.0118	0.0001
1315.0	1319.6	0.1371	0.0014	0.0038	0.0000	0.0000
1406.0	1410.6	0.1282	0.0014	0.0038	0.0000	0.0000
1501.0	1505.6	0.1201	0.0014	0.0038	0.0000	0.0000
1616.0	1620.6	0.1116	0.0014	0.0038	0.0000	0.0000
1710.0	1714.6	0.1055	0.0014	0.0038	0.0000	0.0000
1811.5	1816.1	0.0996	0.0014	0.0038	0.0000	0.0000
1908.5	1913.1	0.0945	0.0014	0.0038	0.0000	0.0000
2000.0	2004.6	0.0902	0.0014	0.0038	0.0000	0.0000
4976.0	4980.6	0.0363	0.0024	0.0674	0.0187	0.0010
7968.0	7972.5	0.0227	0.0039	0.2625	0.1056	0.0014
9984.0	9988.5	0.0181	0.0043	0.3472	0.0943	0.0004
14928.0	14932.4	0.0121	0.0052	0.5758	0.1440	0.0009
19912.0	19916.4	0.0091	0.0055	0.6844	0.0949	0.0003
24888.0	24892.4	0.0073	0.0058	0.8252	0.1585	0.0003
29856.0	29860.4	0.0061	0.0060	0.9980	0.2381	0.0003
19992.0	19996.4	0.0090	0.0060	0.9980	0.0000	0.0000
9992.0	9996.4	0.0181	0.0060	0.9980	0.0000	0.0000
4984.0	4988.4	0.0363	0.0060	0.9980	0.0000	0.0000
1003.0	1007.4	0.1795	0.0052	0.9660	0.0060	-0.0009
751.0	755.4	0.2394	0.0050	0.9633	0.0024	-0.0001
497.0	501.4	0.3607	0.0049	0.9614	0.0012	-0.0001
232.0	236.4	0.7649	0.0046	0.9593	0.0007	-0.0003
94.0	98.4	1.8373	0.0046	0.9593	0.0000	0.0000

MICROMERITICS PORE SIZER 9310

V1.04

PAGE 3

890507604

5/31/89

SFE #3 9237

2

PENETROMETER NUMBER 130163

PRESSURE PSIA	CORRECTED PRESSURE PSIA	PORE DIAMETER um	CUM. INTR. VOLUME cc/g	CUM. PORE SURFACE AREA m2/g	DIFF. INTR. VOLUME dv/:dD cc/g um	INCR. INTR. VOLUME cc/g
47.0	51.4	3.5159	0.0046	0.9593	0.0000	0.0000
30.0	34.5	5.2492	0.0043	0.9591	0.0002	-.0003
14.0	18.5	9.7999	0.0043	0.9591	0.0000	0.0000

Received: 05/25/89

Results by Sample

SAMPLE ID SFE-3 9237 FT FRACTION 04A TEST CODE CLAY NAME Clay Type Analysis by XRD
 Date & Time Collected not specified Category _____

CLAY COMPONENTIAL ANALYSIS

CARBONATES (ACETIC ACID SOLUBLE) : 19

SILICATES & ALUMINO-SILICATES : 79

CLAYS-NORMALIZED TO 100% : 2

 Kaolinite + Chlorite : 35

 Illite-Montmorillonite : 34

 Expandable Clays : 31

 (Montmorillonite, Smectite, etc)

Note: N.D. = Not Detected

X-RAY DIFFRACTION PHASES PRESENT

Major: Quartz

Major-Minor: Calcite

Minor: Albite

Minor-Trace: Clays

Note: All constituents were listed in a probable order of decreasing abundance.

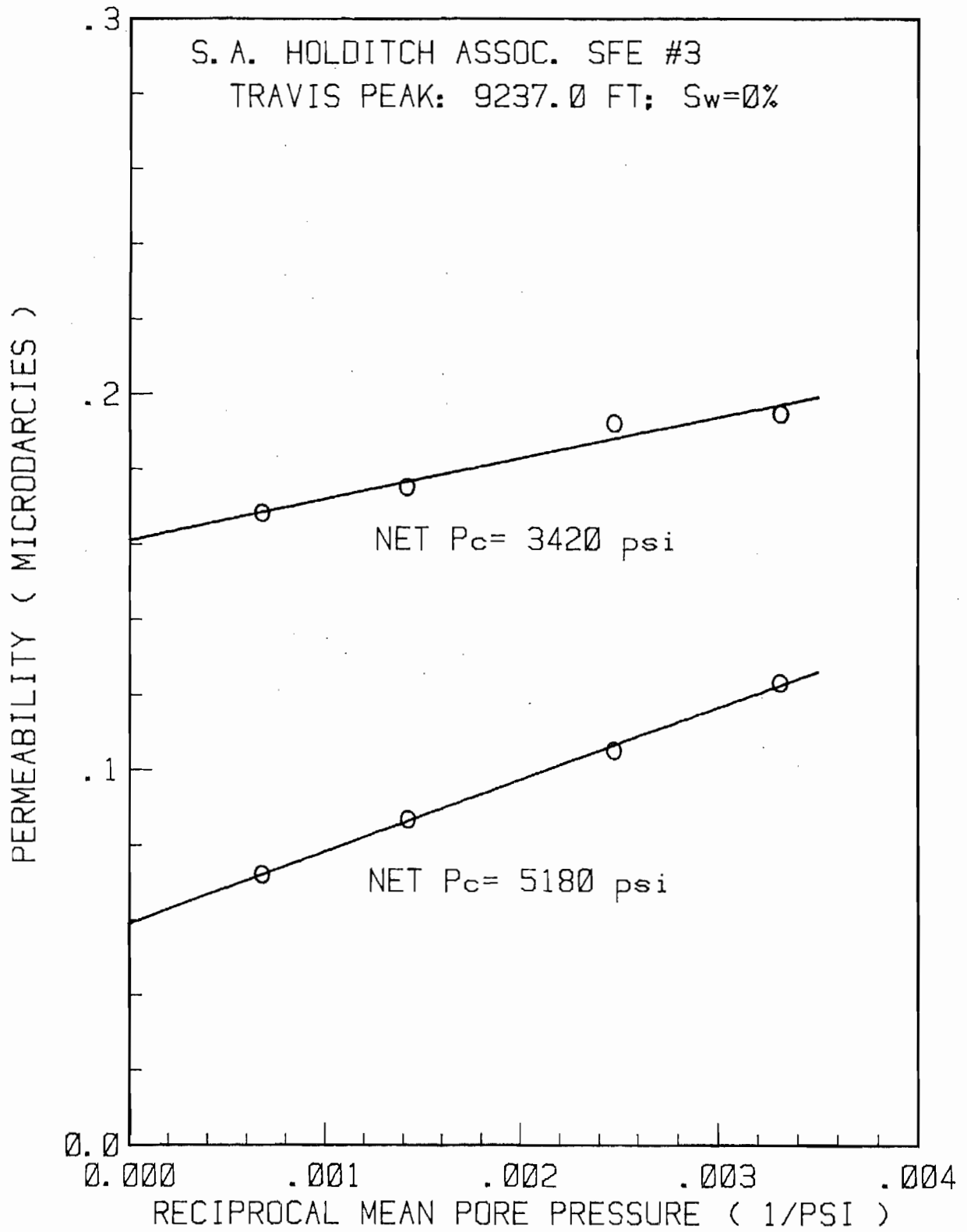
WELL NAME: S.A. HOLDITCH ASSOC. SFE #3

PLUG: TRAVIS PEAK: 9237.0 FT; Sw=0Z

PLUG LENGTH: 5.134 CM

PLUG AREA: 5.037 CM²

TEST DATE (M-D)	BEGIN TIME (H:M)	DUR-ATION (H:M)	CONFINING PRESSURE (PSIA)	MEAN PORE P (PSIA)	DIFFERENTIAL PRESSURE (PSI)	FLOW RATE (SCC/S)	TEMPERATURE (DEG. F)	VISCOSITY (C POISE)	COMPRES-SIBILITY (Z)	PERMEABILITY VALUE (MICRODARCY)	STD. DEV. (%)
11-17	13:21	01:09	4868	1471.68	38.77	2.82E-003	98.00	0.02023	1.0099	2.38E-001	(1.3)
11-20	10:20	01:28	4873	1471.56	38.59	1.98E-003	98.00	0.02023	1.0099	1.68E-001	(1.1)
11-21	09:28	01:28	4122	703.26	45.39	1.25E-003	98.00	0.01902	0.9990	1.75E-001	(.8)
11-22	10:40	01:32	3823	403.63	45.72	8.04E-004	98.00	0.01871	0.9981	1.92E-001	(.9)
11-27	10:55	01:40	3725	301.84	47.08	6.30E-004	98.00	0.01863	0.9983	1.95E-001	(.7)
11-29	11:45	03:30	5469	301.89	46.82	3.96E-004	98.00	0.01863	0.9983	1.23E-001	(.8)
11-30	12:07	03:00	5577	403.57	49.49	4.76E-004	98.00	0.01871	0.9981	1.05E-001	(1.5)
12-01	10:52	03:30	5878	701.32	49.35	6.70E-004	98.00	0.01902	0.9990	8.69E-002	(2.2)
12-04	13:54	02:42	6642	1473.02	50.71	1.12E-003	98.00	0.02023	1.0099	7.22E-002	(2.5)



MICROMERITICS PORE SIZER 9310

V1.04

PAGE 1

890507605

6/5/89

SFE #3 9237.7

9

PENETROMETER NUMBER 70522

PRESSURE PSIA	CORRECTED PRESSURE PSIA	PORE DIAMETER um	CUM. INTR. VOLUME cc/g	CUM. PORE SURFACE AREA m2/g	DIFF. INTR. VOLUME dV:dD cc/g um	INCR. INTR. VOLUME cc/g
1.0	1.0	174.7462	0.0000	0.0000	0.0000	0.0000
2.1	2.1	87.7546	0.0003	0.0000	0.0000	0.0003
3.4	3.4	52.8837	0.0008	0.0000	0.0000	0.0005
5.3	5.3	34.3518	0.0009	0.0000	0.0000	0.0001
7.9	7.9	22.9666	0.0009	0.0000	0.0000	0.0000
10.2	10.2	17.7682	0.0010	0.0001	0.0000	0.0001
13.5	13.5	13.4061	0.0010	0.0001	0.0000	0.0000
15.4	15.4	11.7177	0.0010	0.0001	0.0000	0.0000
18.0	18.0	10.0580	0.0010	0.0001	0.0000	0.0000
20.1	20.1	8.9834	0.0010	0.0001	0.0000	0.0000
22.1	22.1	8.1724	0.0010	0.0001	0.0000	0.0000
23.0	23.0	7.8745	0.0010	0.0001	0.0000	0.0000
24.1	24.1	7.5040	0.0010	0.0001	0.0000	0.0000
25.6	25.6	7.0735	0.0010	0.0001	0.0000	0.0000
40.0	44.4	4.0764	0.0012	0.0002	0.0001	0.0002
61.0	65.4	2.7675	0.0015	0.0005	0.0002	0.0002
70.0	74.4	2.4325	0.0015	0.0005	0.0000	0.0000
70.0	74.4	2.4325	0.0015	0.0005	0.0000	0.0000
76.0	80.4	2.2509	0.0015	0.0005	0.0000	0.0000
80.0	84.3	2.1443	0.0016	0.0007	0.0011	0.0001
86.0	90.3	2.0019	0.0016	0.0007	0.0000	0.0000
90.0	94.3	1.9170	0.0016	0.0007	0.0000	0.0000
100.0	104.3	1.7336	0.0018	0.0012	0.0012	0.0002
127.0	131.3	1.3772	0.0018	0.0012	0.0000	0.0000
141.0	145.3	1.2445	0.0018	0.0012	0.0000	0.0000
174.0	178.3	1.0142	0.0019	0.0016	0.0005	0.0001
181.0	185.3	0.9759	0.0019	0.0016	0.0000	0.0000
200.0	204.3	0.8852	0.0020	0.0021	0.0013	0.0001
220.0	224.3	0.8063	0.0020	0.0021	0.0000	0.0000
241.0	245.3	0.7373	0.0022	0.0027	0.0016	0.0001
262.0	266.3	0.6791	0.0022	0.0027	0.0000	0.0000
283.0	287.3	0.6295	0.0022	0.0027	0.0000	0.0000
307.0	311.3	0.5810	0.0023	0.0034	0.0023	0.0001
330.0	334.3	0.5410	0.0023	0.0034	0.0000	0.0000
355.0	359.3	0.5034	0.0024	0.0043	0.0030	0.0001
379.0	383.3	0.4719	0.0024	0.0043	0.0000	0.0000
405.0	409.3	0.4419	0.0024	0.0043	0.0000	0.0000
431.0	435.3	0.4155	0.0024	0.0043	0.0000	0.0000
459.0	463.3	0.3904	0.0024	0.0043	0.0000	0.0000
487.0	491.3	0.3681	0.0024	0.0043	0.0000	0.0000
514.0	518.3	0.3490	0.0025	0.0056	0.0059	0.0001
529.0	533.3	0.3391	0.0025	0.0056	0.0000	0.0000

MICROMERITICS PORE SIZER 9310

V1.04

PAGE 2

890507605

6/5/89

SFE #3 9237.7

9

PENETROMETER NUMBER 70522

PRESSURE PSIA	CORRECTED PRESSURE PSIA	PORE DIAMETER um	CUM. INTR. VOLUME cc/g	CUM. PORE SURFACE AREA m2/g	DIFF. INTR. VOLUME dV/:dD cc/g um	INCR. INTR. VOLUME cc/g
558.0	562.3	0.3217	0.0025	0.0056	0.0000	0.0000
586.0	590.3	0.3064	0.0025	0.0056	0.0000	0.0000
615.0	619.3	0.2921	0.0025	0.0056	0.0000	0.0000
628.0	632.3	0.2860	0.0025	0.0056	0.0000	0.0000
658.0	662.3	0.2731	0.0026	0.0072	0.0088	0.0001
689.0	693.3	0.2609	0.0026	0.0072	0.0000	0.0000
703.0	707.3	0.2557	0.0026	0.0072	0.0000	0.0000
732.0	736.3	0.2456	0.0026	0.0072	0.0000	0.0000
764.0	768.3	0.2354	0.0026	0.0072	0.0000	0.0000
779.0	783.3	0.2309	0.0026	0.0072	0.0000	0.0000
811.0	815.3	0.2218	0.0026	0.0072	0.0000	0.0000
844.0	848.3	0.2132	0.0026	0.0072	0.0000	0.0000
858.0	862.3	0.2098	0.0027	0.0093	0.0328	0.0001
891.0	895.3	0.2020	0.0027	0.0093	0.0000	0.0000
906.0	910.3	0.1987	0.0027	0.0093	0.0000	0.0000
939.0	943.3	0.1917	0.0027	0.0093	0.0000	0.0000
954.0	958.3	0.1887	0.0027	0.0093	0.0000	0.0000
987.0	991.3	0.1825	0.0027	0.0093	0.0000	0.0000
1003.0	1007.3	0.1796	0.0027	0.0093	0.0000	0.0000
1105.0	1109.3	0.1630	0.0027	0.0093	0.0000	0.0000
1213.0	1217.3	0.1486	0.0027	0.0093	0.0000	0.0000
1306.0	1310.3	0.1380	0.0030	0.0157	0.0215	0.0002
1418.0	1422.3	0.1272	0.0030	0.0157	0.0000	0.0000
1509.0	1513.3	0.1195	0.0030	0.0157	0.0000	0.0000
1603.0	1607.3	0.1125	0.0030	0.0157	0.0000	0.0000
1699.0	1703.3	0.1062	0.0030	0.0157	0.0000	0.0000
1811.5	1815.8	0.0996	0.0030	0.0157	0.0000	0.0000
1916.0	1920.2	0.0942	0.0031	0.0204	0.0209	0.0001
2000.0	2004.2	0.0902	0.0031	0.0204	0.0000	0.0000
4984.0	4988.2	0.0363	0.0034	0.0419	0.0063	0.0003
7960.0	7964.2	0.0227	0.0036	0.0727	0.0168	0.0002
9960.0	9964.2	0.0182	0.0036	0.0727	0.0000	0.0000
14936.0	14940.2	0.0121	0.0039	0.1328	0.0376	0.0002
19912.0	19916.2	0.0091	0.0039	0.1328	0.0000	0.0000
24888.0	24892.2	0.0073	0.0041	0.2439	0.1251	0.0002
29856.0	29860.2	0.0061	0.0042	0.3121	0.0939	0.0001
20000.0	20004.2	0.0090	0.0042	0.3121	0.0000	0.0000
10000.0	10004.2	0.0181	0.0042	0.3121	0.0000	0.0000
4992.0	4996.2	0.0362	0.0042	0.3121	0.0000	0.0000
1002.0	1006.2	0.1798	0.0042	0.3121	0.0000	0.0000
740.0	744.2	0.2430	0.0042	0.3121	0.0000	0.0000
502.0	506.2	0.3573	0.0041	0.3105	0.0010	-0.0001

MICROMERITICS PORE SIZER 9310

V1.04

PAGE 3

890507605

6/5/89

SFE #3 9237.7

9

PENETROMETER NUMBER 70522

PRESSURE PSIA	CORRECTED PRESSURE PSIA	PORE DIAMETER um	CUM. INTR. VOLUME cc/g	CUM. PORE SURFACE AREA m2/g	DIFF. INTR. VOLUME dV/:dD cc/g um	INCR. INTR. VOLUME cc/g
236.0	240.2	0.7530	0.0040	0.3097	0.0003	-.0001
98.0	102.2	1.7696	0.0037	0.3090	0.0002	-.0002
49.0	53.2	3.3971	0.0032	0.3081	0.0003	-.0006
27.0	31.2	5.7879	0.0031	0.3080	0.0000	-.0001
15.0	19.2	9.3964	0.0031	0.3080	0.0000	0.0000

Received: 05/25/89

Results by Sample

SAMPLE ID SFE-3 9237.7 FT FRACTION 05A TEST CODE CLAY NAME Clay Type Analysis by XRD
 Date & Time Collected not specified Category _____

CLAY COMPONENTIAL ANALYSIS

CARBONATES (ACETIC ACID SOLUBLE) : 52

SILICATES & ALUMINO-SILICATES : 47

CLAYS-NORMALIZED TO 100% : 1

 Kaolinite + Chlorite : 5

 Illite-Montmorillonite : 23

 Expandable Clays : 72

 (Montmorillonite, Smectite, etc)

Note: N.D. = Not Detected

X-RAY DIFFRACTION PHASES PRESENT

Major: Calcite

Major-Minor: Quartz

Minor:

Minor-Trace: Clays

Note: All constituents were listed in a probable order of decreasing abundance.

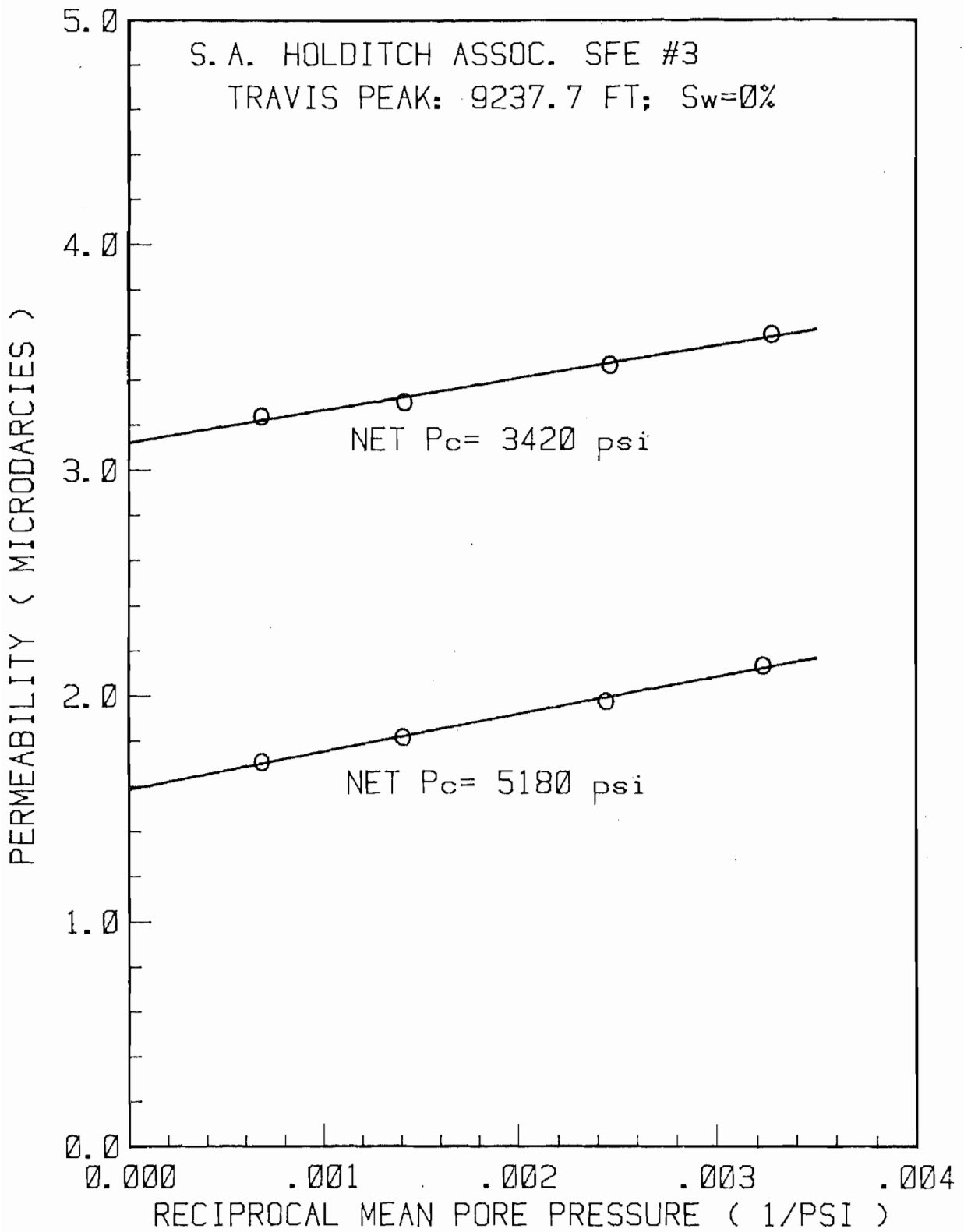
WELL NAME: S.A. HOLDITCH ASSOC, SFE #3

PLUG: TRAVIS PEAK: 9237.7 FT; Sw=0Z

PLUG LENGTH: 5.119 CM

PLUG AREA: 5.029 CM²

TEST DATE (M-D)	BEGIN TIME (H:M)	DUR- ATION (H:M)	CONFINING PRESSURE (PSIA)	MEAN PORE P (PSIA)	DIFFERENTIAL PRESSURE (PSI)	FLOW RATE (SCC/S)	TEMPERATURE (DEG. F)	VISCOSITY (C POISE)	COMPRES- SIBILITY (Z)	PERMEABILITY VALUE (MICRODARCY)	STD. DEV. (%)
11-06	13:51	00:12	4878	1464.14	22.06	2.17E-002	98.00	0.02022	1.0097	3.24E+000	(.9)
11-07	14:32	00:20	4121	704.24	20.98	1.09E-002	98.00	0.01902	0.9990	3.30E+000	(.4)
11-08	10:20	00:20	3828	405.47	21.77	6.94E-003	98.00	0.01871	0.9981	3.47E+000	(.3)
11-09	09:13	00:32	3726	305.07	22.78	5.71E-003	97.99	0.01863	0.9983	3.60E+000	(1.9)
11-10	15:31	00:22	5484	309.28	30.30	4.56E-003	98.00	0.01864	0.9983	2.13E+000	(.2)
11-13	11:34	00:24	5587	408.84	30.79	5.64E-003	98.00	0.01872	0.9981	1.97E+000	(.4)
11-14	11:03	00:23	5881	707.98	31.22	8.95E-003	98.00	0.01903	0.9990	1.82E+000	(2.5)
11-15	10:54	00:19	6634	1463.56	28.36	1.47E-002	98.00	0.02021	1.0097	1.71E+000	(.9)



MICROMERITICS PORE SIZER 9310

V1.04

PAGE 1
5/31/89
2

890507606

SFE #3 9242

PENETROMETER NUMBER 130201

PRESSURE PSIA	CORRECTED PRESSURE PSIA	PORE DIAMETER um	CUM. INTR. VOLUME cc/g	CUM. PORE SURFACE AREA m2/g	DIFF. INTR. VOLUME dV/:dD cc/g um	INCR. INTR. VOLUME cc/g
0.9	0.9	211.5349	0.0000	0.0000	0.0000	0.0000
2.1	2.1	86.9949	0.0006	0.0000	0.0000	0.0006
3.1	3.1	57.7466	0.0010	0.0000	0.0000	0.0003
5.2	5.2	34.8886	0.0011	0.0000	0.0000	0.0002
8.1	8.1	22.4034	0.0013	0.0001	0.0000	0.0002
10.4	10.4	17.3990	0.0014	0.0001	0.0000	0.0002
13.4	13.4	13.5325	0.0014	0.0001	0.0000	0.0000
15.3	15.3	11.8489	0.0014	0.0001	0.0000	0.0000
18.1	18.1	9.9979	0.0014	0.0001	0.0000	0.0000
20.5	20.5	8.8294	0.0016	0.0002	0.0001	0.0002
22.3	22.3	8.1031	0.0016	0.0002	0.0000	0.0000
25.3	25.3	7.1592	0.0016	0.0002	0.0000	0.0000
40.0	44.6	4.0547	0.0016	0.0002	0.0000	0.0000
60.0	64.6	2.7995	0.0016	0.0002	0.0000	0.0000
68.0	72.6	2.4910	0.0016	0.0002	0.0000	0.0000
70.0	74.6	2.4243	0.0016	0.0002	0.0000	0.0000
75.0	79.6	2.2720	0.0016	0.0002	0.0000	0.0000
85.0	89.6	2.0184	0.0016	0.0002	0.0000	0.0000
86.0	90.6	1.9962	0.0016	0.0002	0.0000	0.0000
90.0	94.6	1.9118	0.0016	0.0002	0.0000	0.0000
102.0	106.6	1.6966	0.0016	0.0002	0.0000	0.0000
128.0	132.6	1.3639	0.0016	0.0002	0.0000	0.0000
141.0	145.6	1.2421	0.0016	0.0002	0.0000	0.0000
197.0	201.6	0.8971	0.0016	0.0002	0.0000	0.0000
194.0	198.6	0.9107	0.0016	0.0002	0.0000	0.0000
203.0	207.6	0.8712	0.0016	0.0002	0.0000	0.0000
223.0	227.6	0.7946	0.0016	0.0002	0.0000	0.0000
241.0	245.6	0.7364	0.0016	0.0002	0.0000	0.0000
262.0	266.6	0.6784	0.0016	0.0002	0.0000	0.0000
293.0	297.6	0.6077	0.0017	0.0012	0.0022	0.0002
303.0	307.6	0.5880	0.0017	0.0012	0.0000	0.0000
327.0	331.6	0.5454	0.0017	0.0012	0.0000	0.0000
362.0	366.6	0.4934	0.0017	0.0012	0.0000	0.0000
385.0	389.6	0.4642	0.0017	0.0012	0.0000	0.0000
409.0	413.6	0.4373	0.0017	0.0012	0.0000	0.0000
435.0	439.6	0.4114	0.0017	0.0012	0.0000	0.0000
460.0	464.6	0.3893	0.0017	0.0012	0.0000	0.0000
488.0	492.6	0.3672	0.0017	0.0012	0.0000	0.0000
514.0	518.6	0.3488	0.0019	0.0029	0.0086	0.0002
529.0	533.6	0.3390	0.0019	0.0029	0.0000	0.0000
556.0	560.6	0.3226	0.0019	0.0029	0.0000	0.0000
584.0	588.6	0.3073	0.0021	0.0049	0.0103	0.0002

MICROMERITICS PORE SIZER 9310

V1.04

PAGE 2
5/31/89
2

890507606
SFE #3 9242
PENETROMETER NUMBER 130201

PRESSURE PSIA	CORRECTED PRESSURE PSIA	PORE DIAMETER um	CUM. INTR. VOLUME cc/g	CUM. PORE SURFACE AREA m2/g	DIFF. INTR. VOLUME dV/:dD cc/g um	INCR. INTR. VOLUME cc/g
611.0	615.6	0.2938	0.0021	0.0049	0.0000	0.0000
638.0	642.6	0.2815	0.0022	0.0071	0.0128	0.0002
651.0	655.6	0.2759	0.0024	0.0094	0.0284	0.0002
680.0	684.6	0.2642	0.0024	0.0094	0.0000	0.0000
707.0	711.5	0.2542	0.0029	0.0167	0.0474	0.0005
735.0	739.5	0.2446	0.0032	0.0218	0.0329	0.0003
762.0	766.5	0.2360	0.0035	0.0271	0.0368	0.0003
789.0	793.5	0.2279	0.0038	0.0326	0.0395	0.0003
801.0	805.5	0.2245	0.0041	0.0382	0.0934	0.0003
829.0	833.5	0.2170	0.0046	0.0468	0.0630	0.0005
855.0	859.4	0.2104	0.0052	0.0586	0.0966	0.0006
880.0	884.4	0.2045	0.0060	0.0739	0.1333	0.0008
906.0	910.4	0.1987	0.0067	0.0864	0.1086	0.0006
931.0	935.3	0.1934	0.0073	0.0994	0.1194	0.0006
956.0	960.3	0.1883	0.0081	0.1160	0.1575	0.0008
980.0	984.3	0.1838	0.0087	0.1296	0.1381	0.0006
1006.0	1010.2	0.1790	0.0097	0.1505	0.2012	0.0010
1098.0	1102.1	0.1641	0.0112	0.1875	0.1060	0.0016
1202.0	1206.1	0.1500	0.0128	0.2278	0.1120	0.0016
1294.0	1298.0	0.1393	0.0139	0.2584	0.1043	0.0011
1406.0	1410.0	0.1283	0.0150	0.2916	0.1002	0.0011
1510.0	1513.9	0.1195	0.0157	0.3120	0.0719	0.0006
1614.0	1617.9	0.1118	0.0163	0.3339	0.0825	0.0006
1702.0	1705.9	0.1060	0.0168	0.3514	0.0824	0.0005
1813.0	1816.9	0.0995	0.0173	0.3699	0.0734	0.0005
1927.5	1931.3	0.0936	0.0177	0.3895	0.0805	0.0005
2008.0	2011.8	0.0899	0.0179	0.3964	0.0423	0.0002
4976.0	4979.6	0.0363	0.0234	0.7477	0.1034	0.0055
7960.0	7963.5	0.0227	0.0258	1.0696	0.1745	0.0024
9968.0	9971.4	0.0181	0.0266	1.2246	0.1731	0.0008
14928.0	14931.3	0.0121	0.0283	1.6853	0.2891	0.0017
19904.0	19907.3	0.0091	0.0295	2.1036	0.3661	0.0011
24952.0	24955.2	0.0072	0.0306	2.6465	0.6031	0.0011
29856.0	29859.2	0.0061	0.0314	3.1225	0.6651	0.0008
20008.0	20011.2	0.0090	0.0314	3.1225	0.0000	0.0000
9960.0	9963.2	0.0182	0.0306	2.8896	0.0869	-0.0008
4976.0	4979.3	0.0363	0.0295	2.7268	0.0610	-0.0011
1001.0	1004.5	0.1801	0.0257	2.5863	0.0264	-0.0038
752.0	755.5	0.2394	0.0252	2.5773	0.0080	-0.0005
496.0	499.5	0.3621	0.0241	2.5625	0.0090	-0.0011
234.0	237.7	0.7610	0.0217	2.5456	0.0060	-0.0024
96.0	99.8	1.8126	0.0190	2.5372	0.0026	-0.0027

MICROMERITICS PORE SIZER 9310

V1.04

PAGE 3
5/31/89
2

890507606

SFE #3 9242

PENETROMETER NUMBER 130201

PRESSURE PSIA	CORRECTED PRESSURE PSIA	PORE DIAMETER um	CUM. INTR. VOLUME cc/g	CUM. PORE SURFACE AREA m2/g	DIFF. INTR. VOLUME dV:dD cc/g um	INCR. INTR. VOLUME cc/g
36.0	39.8	4.5412	0.0181	2.5360	0.0003	-.0010
30.0	33.9	5.3314	0.0160	2.5344	0.0026	-.0021
15.0	18.9	9.5496	0.0157	2.5342	0.0001	-.0003

Received: 05/25/89

Results by Sample

SAMPLE ID SFE-3 9242 FT FRACTION 06A TEST CODE CLAY NAME Clay Type Analysis by XRD
Date & Time Collected not specified Category _____

CLAY COMPONENTIAL ANALYSIS

CARBONATES (ACETIC ACID SOLUBLE) : 4

SILICATES & ALUMINO-SILICATES : 93

CLAYS-NORMALIZED TO 100% : 3

 Kaolinite + Chlorite : 14

 Illite-Montmorillonite : 29

 Expandable Clays : 57

 (Montmorillonite, Smectite, etc)

Note: N.D. = Not Detected

X-RAY DIFFRACTION PHASES PRESENT

Major: Quartz

Major-Minor: Albite

Minor: Calcite

Minor-Trace: Clays

Note: All constituents were listed in a probable order of decreasing abundance.

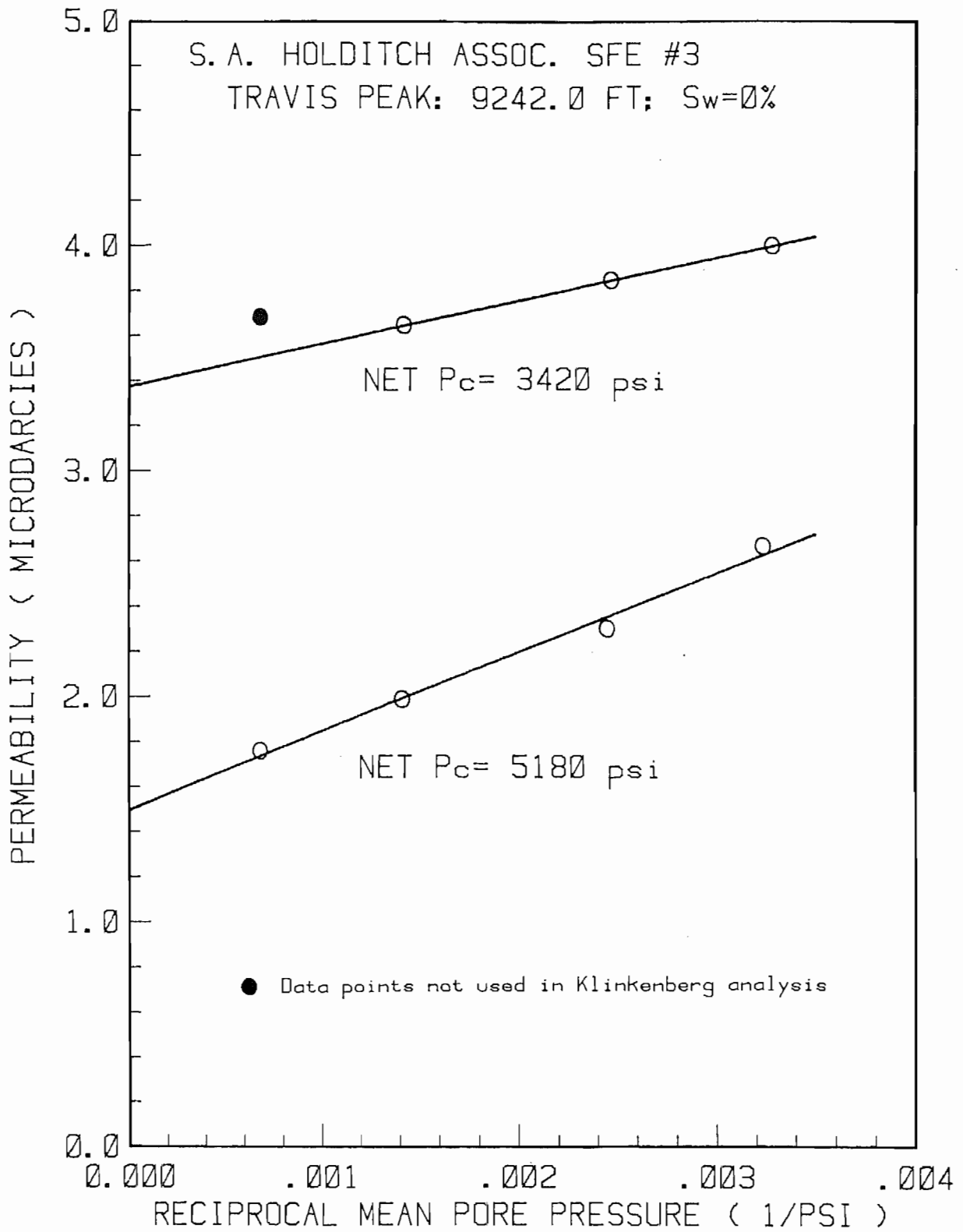
WELL NAME: S.A. HOLDITCH ASSOC. SFE #3

PLUG: TRAVIS PEAK: 9242.0 FT; Sw=0%

PLUG LENGTH: 4.968 CM

PLUG AREA: 5.032 CM²

TEST DATE (M-D)	BEGIN TIME (H:M)	DUR-ATION (H:M)	CONFINING PRESSURE (PSIA)	MEAN PORE P (PSIA)	DIFFERENTIAL PRESSURE (PSI)	FLOW RATE (SCC/S)	TEMPERATURE (DEG. F)	VISCOSITY (C POISE)	COMPRES-SIBILITY (Z)	PERMEABILITY VALUE (MICRODARCY)	STD. DEV. (%)
11-06	14:11	00:13	4876	1464.15	21.91	2.53E-002	98.00	0.02022	1.0097	3.68E+000	(.2)
11-07	15:00	00:15	4120	704.25	20.89	1.23E-002	98.00	0.01902	0.9990	3.65E+000	(.2)
11-08	10:45	00:18	3826	405.47	21.70	7.91E-003	98.00	0.01871	0.9981	3.84E+000	(.2)
11-09	09:56	00:18	3724	305.07	22.74	6.52E-003	98.00	0.01863	0.9983	4.00E+000	(.3)
11-10	16:04	00:16	5481	309.26	30.26	5.86E-003	98.00	0.01864	0.9983	2.67E+000	(.2)
11-13	12:20	00:45	5584	408.83	30.71	6.75E-003	98.00	0.01872	0.9981	2.30E+000	(.2)
11-14	08:46	00:31	5885	707.98	31.35	1.01E-002	98.00	0.01903	0.9990	1.99E+000	(1.7)
11-15	09:32	00:28	6636	1463.51	28.62	1.58E-002	98.00	0.02021	1.0097	1.76E+000	(.2)



MICROMERITICS PORE SIZER 9310

V1.04

PAGE 1
6/15/89
10

890507607

SFE #3 9246.5

PENETROMETER NUMBER 130163

PRESSURE PSIA	CORRECTED PRESSURE PSIA	PORE DIAMETER um	CUM. INTR. VOLUME cc/g	CUM. PORE SURFACE AREA m2/g	DIFF. INTR. VOLUME dV/:dD cc/g um	INCR. INTR. VOLUME cc/g
1.4	1.4	127.1887	0.0000	0.0000	0.0000	0.0000
2.5	2.5	72.0280	0.0002	0.0000	0.0000	0.0002
3.3	3.3	54.1666	0.0005	0.0000	0.0000	0.0003
5.1	5.1	35.5678	0.0005	0.0000	0.0000	0.0000
8.0	8.0	22.6815	0.0009	0.0001	0.0000	0.0005
10.3	10.3	17.5970	0.0009	0.0001	0.0000	0.0000
12.8	12.8	14.0826	0.0009	0.0001	0.0000	0.0000
15.0	15.0	12.0551	0.0009	0.0001	0.0000	0.0000
18.1	18.1	9.9979	0.0009	0.0001	0.0000	0.0000
20.1	20.1	8.9995	0.0011	0.0002	0.0002	0.0002
22.1	22.1	8.1923	0.0011	0.0002	0.0000	0.0000
25.2	25.2	7.1745	0.0011	0.0002	0.0000	0.0000
41.0	45.6	3.9639	0.0011	0.0002	0.0000	0.0000
61.0	65.6	2.7562	0.0013	0.0003	0.0001	0.0002
65.0	69.6	2.5978	0.0013	0.0003	0.0000	0.0000
71.0	75.6	2.3917	0.0013	0.0003	0.0000	0.0000
76.0	80.6	2.2434	0.0013	0.0003	0.0000	0.0000
80.0	84.6	2.1373	0.0013	0.0003	0.0000	0.0000
86.0	90.6	1.9958	0.0013	0.0003	0.0000	0.0000
90.0	94.6	1.9115	0.0013	0.0003	0.0000	0.0000
100.0	104.6	1.7288	0.0013	0.0003	0.0000	0.0000
127.0	131.6	1.3741	0.0013	0.0003	0.0000	0.0000
140.0	144.6	1.2507	0.0014	0.0008	0.0013	0.0002
175.0	179.6	1.0070	0.0014	0.0008	0.0000	0.0000
180.0	184.6	0.9797	0.0016	0.0015	0.0058	0.0002
203.0	207.6	0.8712	0.0016	0.0015	0.0000	0.0000
219.0	223.6	0.8088	0.0016	0.0015	0.0000	0.0000
244.0	248.6	0.7275	0.0017	0.0023	0.0019	0.0002
260.0	264.6	0.6835	0.0017	0.0023	0.0000	0.0000
279.0	283.6	0.6377	0.0017	0.0023	0.0000	0.0000
304.0	308.6	0.5861	0.0019	0.0033	0.0030	0.0002
332.0	336.6	0.5373	0.0019	0.0033	0.0000	0.0000
359.0	363.6	0.4974	0.0020	0.0045	0.0039	0.0002
377.0	381.6	0.4740	0.0022	0.0058	0.0067	0.0002
405.0	409.6	0.4416	0.0024	0.0072	0.0048	0.0002
433.0	437.6	0.4133	0.0027	0.0101	0.0111	0.0003
451.0	455.5	0.3970	0.0028	0.0117	0.0096	0.0002
478.0	482.5	0.3748	0.0035	0.0182	0.0283	0.0006
506.0	510.5	0.3543	0.0041	0.0250	0.0306	0.0006
532.0	536.5	0.3371	0.0047	0.0323	0.0366	0.0006
555.0	559.4	0.3233	0.0058	0.0456	0.0794	0.0011
581.0	585.4	0.3090	0.0066	0.0555	0.0547	0.0008

MICROMERITICS PORE SIZER 9310

V1.04

PAGE 2

890507607

6/15/89

SFE #3 9246.5

10

PENETROMETER NUMBER 130163

PRESSURE PSIA	CORRECTED PRESSURE PSIA	PORE DIAMETER um	CUM. INTR. VOLUME cc/g	CUM. PORE SURFACE AREA m2/g	DIFF. INTR. VOLUME dV/:dD cc/g um	INCR. INTR. VOLUME cc/g
603.0	607.3	0.2978	0.0078	0.0721	0.1124	0.0013
628.0	632.3	0.2861	0.0088	0.0850	0.0801	0.0009
655.0	659.2	0.2744	0.0099	0.1006	0.0939	0.0011
677.0	681.2	0.2655	0.0110	0.1169	0.1242	0.0011
704.0	708.1	0.2554	0.0119	0.1314	0.0931	0.0009
729.0	733.1	0.2467	0.0127	0.1439	0.0902	0.0008
759.0	763.0	0.2370	0.0135	0.1568	0.0810	0.0008
778.0	782.0	0.2313	0.0140	0.1649	0.0818	0.0005
797.0	801.0	0.2258	0.0143	0.1704	0.0572	0.0003
829.0	833.0	0.2171	0.0147	0.1789	0.0543	0.0005
851.0	855.0	0.2115	0.0147	0.1789	0.0000	0.0000
885.0	889.0	0.2035	0.0152	0.1879	0.0582	0.0005
908.0	911.9	0.1983	0.0155	0.1942	0.0612	0.0003
929.0	932.9	0.1939	0.0155	0.1942	0.0000	0.0000
951.0	954.9	0.1894	0.0160	0.2040	0.1055	0.0005
972.0	975.9	0.1853	0.0160	0.2040	0.0000	0.0000
998.0	1001.9	0.1805	0.0160	0.2040	0.0000	0.0000
1108.0	1111.9	0.1627	0.0168	0.2223	0.0439	0.0008
1206.0	1209.8	0.1495	0.0174	0.2384	0.0476	0.0006
1308.0	1311.8	0.1379	0.0177	0.2471	0.0270	0.0003
1398.0	1401.8	0.1290	0.0182	0.2612	0.0532	0.0005
1504.0	1507.8	0.1200	0.0187	0.2763	0.0519	0.0005
1597.0	1600.8	0.1130	0.0190	0.2871	0.0450	0.0003
1705.0	1708.8	0.1058	0.0193	0.2986	0.0439	0.0003
1809.5	1813.2	0.0997	0.0196	0.3108	0.0514	0.0003
1905.5	1909.2	0.0947	0.0198	0.3172	0.0313	0.0002
1990.0	1993.7	0.0907	0.0202	0.3375	0.1172	0.0005
4976.0	4979.6	0.0363	0.0223	0.4660	0.0375	0.0020
7960.0	7963.6	0.0227	0.0232	0.5935	0.0692	0.0009
9968.0	9971.6	0.0181	0.0234	0.6242	0.0343	0.0002
14944.0	14947.5	0.0121	0.0238	0.7487	0.0779	0.0005
19904.0	19907.5	0.0091	0.0243	0.9264	0.1561	0.0005
24944.0	24947.5	0.0072	0.0246	1.0801	0.1709	0.0003
29856.0	29859.5	0.0061	0.0249	1.2687	0.2631	0.0003
20016.0	20019.5	0.0090	0.0249	1.2687	0.0000	0.0000
9992.0	9995.5	0.0181	0.0249	1.2687	0.0000	0.0000
4992.0	4995.5	0.0362	0.0248	1.2456	0.0087	-.0002
994.0	997.6	0.1813	0.0237	1.2052	0.0076	-.0011
749.0	752.6	0.2403	0.0232	1.1963	0.0080	-.0005
494.0	497.6	0.3635	0.0226	1.1880	0.0051	-.0006
169.0	172.7	1.0473	0.0207	1.1773	0.0028	-.0019
96.0	99.8	1.8131	0.0195	1.1738	0.0016	-.0013

MICROMERITICS PORE SIZER 9310

V1.04

PAGE 3
6/15/89
10

890507607

SFE #3 9246.5

PENETROMETER NUMBER 130163

PRESSURE PSIA	CORRECTED PRESSURE PSIA	PORE DIAMETER um	CUM. INTR. VOLUME cc/g	CUM. PORE SURFACE AREA m2/g	DIFF. INTR. VOLUME dV/:dD cc/g um	INCR. INTR. VOLUME cc/g
36.0	39.8	4.5463	0.0188	1.1730	0.0002	-.0006
25.0	28.8	6.2806	0.0185	1.1727	0.0002	-.0003
14.0	17.8	10.1625	0.0185	1.1727	0.0000	0.0000

Received: 05/25/89

Results by Sample

SAMPLE ID SFE-3 9246.5 FT FRACTION Q7A TEST CODE CLAY NAME Clay Type Analysis by XRD
 Date & Time Collected not specified Category _____

CLAY COMPONENTIAL ANALYSIS

CARBONATES (ACETIC ACID SOLUBLE) : 5

SILICATES & ALUMINO-SILICATES : 94

CLAYS-NORMALIZED TO 100% : 1

 Kaolinite + Chlorite : 23

 Illite-Montmorillonite : 20

 Expandable Clays : 57

 (Montmorillonite, Smectite, etc)

Note: N.D. = Not Detected

X-RAY DIFFRACTION PHASES PRESENT

Major: Quartz

Major-Minor:

Minor: Calcite, Albite

Minor-Trace: Microcline, Clays

Note: All constituents were listed in a probable order of decreasing abundance.

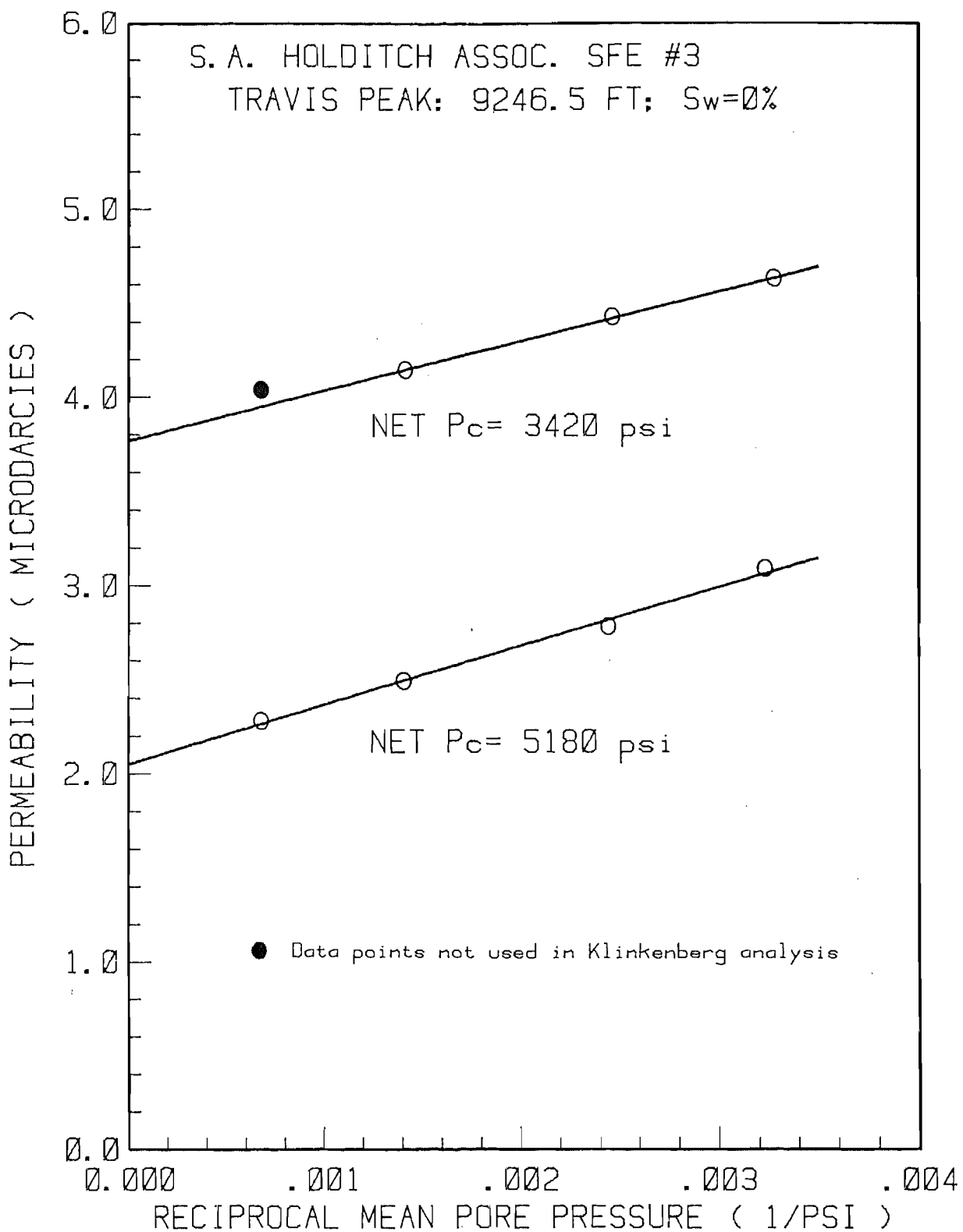
WELL NAME: S.A. HOLDITCH ASSOC. SFE #3

PLUG: TRAVIS PEAK: 9246.5 FT; Sw=0Z

PLUG LENGTH: 5.109 CM

PLUG AREA: 5.045 CM²

TEST DATE (M-D)	REGIN TIME (H:M)	DUR- ATION (H:M)	CONFINING PRESSURE (PSIA)	MEAN PORE P (PSIA)	DIFFERENTIAL PRESSURE (PSI)	FLOW RATE (SCC/S)	TEMPERATURE (DEG. F)	VISCOSITY (C POISE)	COMPRES- SIBILITY (Z)	PERMEABILITY VALUE (MICRODARCY)	STD. DEV. (%)
11-06	14:29	00:10	4874	1464.15	21.82	2.69E-002	98.00	0.02022	1.0097	4.04E+000	(.5)
11-07	15:22	00:13	4118	704.25	20.83	1.36E-002	98.00	0.01902	0.9990	4.14E+000	(.2)
11-08	11:11	00:23	3824	405.47	21.65	8.87E-003	97.99	0.01871	0.9981	4.43E+000	(2.4)
11-09	10:26	00:25	3722	305.08	22.66	7.34E-003	98.00	0.01863	0.9983	4.63E+000	(2.2)
11-10	16:25	00:18	5480	309.28	30.17	6.60E-003	98.01	0.01864	0.9983	3.09E+000	(.3)
11-13	13:15	00:23	5582	408.83	30.62	7.94E-003	98.00	0.01872	0.9981	2.78E+000	(.2)
11-14	09:31	00:13	5884	708.00	31.26	1.24E-002	98.00	0.01903	0.9990	2.49E+000	(.2)
11-15	10:19	00:22	6635	1463.54	28.49	1.98E-002	98.00	0.02021	1.0097	2.28E+000	(2.3)



MICROMERITICS PORE SIZER 9310

V1.04

PAGE 1
6/12/89
10

890507608
SFE #3 9248
PENETROMETER NUMBER 130163

PRESSURE PSIA	CORRECTED PRESSURE PSIA	PORE DIAMETER um	CUM. INTR. VOLUME cc/g	CUM. PORE SURFACE AREA m2/g	DIFF. INTR. VOLUME dV/:dD cc/g um	INCR. INTR. VOLUME cc/g
1.3	1.3	136.7062	0.0000	0.0000	0.0000	0.0000
2.4	2.4	74.7056	0.0000	0.0000	0.0000	0.0000
3.3	3.3	55.3604	0.0003	0.0000	0.0000	0.0003
5.0	5.0	36.0140	0.0005	0.0000	0.0000	0.0002
8.2	8.2	21.9867	0.0008	0.0001	0.0000	0.0003
10.3	10.3	17.5970	0.0009	0.0001	0.0000	0.0002
13.3	13.3	13.5783	0.0009	0.0001	0.0000	0.0000
15.0	15.0	12.0623	0.0009	0.0001	0.0000	0.0000
18.2	18.2	9.9141	0.0011	0.0002	0.0001	0.0002
20.3	20.3	8.9196	0.0011	0.0002	0.0000	0.0000
22.2	22.2	8.1393	0.0011	0.0002	0.0000	0.0000
25.3	25.3	7.1541	0.0011	0.0002	0.0000	0.0000
40.0	44.6	4.0527	0.0011	0.0002	0.0000	0.0000
61.0	65.6	2.7565	0.0014	0.0005	0.0002	0.0003
65.0	69.6	2.5981	0.0014	0.0005	0.0000	0.0000
70.0	74.6	2.4240	0.0014	0.0005	0.0000	0.0000
75.0	79.6	2.2720	0.0016	0.0008	0.0010	0.0002
81.0	85.6	2.1128	0.0016	0.0008	0.0000	0.0000
85.0	89.6	2.0184	0.0016	0.0008	0.0000	0.0000
90.0	94.6	1.9119	0.0017	0.0011	0.0015	0.0002
100.0	104.6	1.7292	0.0019	0.0015	0.0009	0.0002
125.0	129.6	1.3961	0.0027	0.0035	0.0024	0.0008
145.0	149.5	1.2097	0.0036	0.0064	0.0051	0.0009
160.0	164.5	1.0998	0.0047	0.0102	0.0101	0.0011
188.0	192.4	0.9403	0.0069	0.0189	0.0139	0.0022
199.0	203.3	0.8896	0.0079	0.0230	0.0187	0.0009
226.0	230.2	0.7856	0.0099	0.0329	0.0197	0.0021
240.0	244.1	0.7409	0.0118	0.0428	0.0423	0.0019
261.0	265.1	0.6823	0.0130	0.0490	0.0189	0.0011
279.0	283.0	0.6390	0.0139	0.0547	0.0219	0.0009
299.0	303.0	0.5970	0.0148	0.0609	0.0225	0.0009
337.0	340.9	0.5305	0.0161	0.0698	0.0190	0.0013
355.0	358.9	0.5040	0.0167	0.0747	0.0238	0.0006
375.0	378.9	0.4774	0.0172	0.0786	0.0178	0.0005
404.0	407.8	0.4435	0.0178	0.0841	0.0186	0.0006
423.0	426.8	0.4238	0.0185	0.0899	0.0321	0.0006
453.0	456.8	0.3960	0.0191	0.0961	0.0227	0.0006
474.0	477.8	0.3786	0.0196	0.1010	0.0273	0.0005
506.0	509.7	0.3548	0.0201	0.1061	0.0200	0.0005
528.0	531.7	0.3401	0.0204	0.1098	0.0215	0.0003
550.0	553.7	0.3266	0.0205	0.1117	0.0117	0.0002
585.0	588.7	0.3072	0.0212	0.1196	0.0326	0.0006

MICROMERITICS PORE SIZER 9310

V1.04

PAGE 2

890507608

6/12/89

SFE #3 9248

10

PENETROMETER NUMBER 130163

PRESSURE PSIA	CORRECTED PRESSURE PSIA	PORE DIAMETER um	CUM. INTR. VOLUME cc/g	CUM. PORE SURFACE AREA m2/g	DIFF. INTR. VOLUME dV/:dD cc/g um	INCR. INTR. VOLUME cc/g
607.0	610.7	0.2962	0.0215	0.1238	0.0286	0.0003
628.0	631.7	0.2863	0.0216	0.1260	0.0160	0.0002
652.0	655.6	0.2759	0.0221	0.1327	0.0452	0.0005
676.0	679.6	0.2661	0.0223	0.1351	0.0162	0.0002
710.0	713.6	0.2534	0.0226	0.1399	0.0249	0.0003
734.0	737.6	0.2452	0.0227	0.1425	0.0192	0.0002
757.0	760.6	0.2378	0.0231	0.1477	0.0426	0.0003
781.0	784.6	0.2305	0.0232	0.1504	0.0217	0.0002
805.0	808.6	0.2237	0.0234	0.1532	0.0231	0.0002
828.0	831.6	0.2175	0.0235	0.1560	0.0255	0.0002
853.0	856.6	0.2112	0.0237	0.1590	0.0249	0.0002
878.0	881.5	0.2052	0.0240	0.1651	0.0528	0.0003
903.0	906.5	0.1995	0.0240	0.1651	0.0000	0.0000
929.0	932.5	0.1939	0.0242	0.1683	0.0284	0.0002
954.0	957.5	0.1889	0.0243	0.1716	0.0312	0.0002
979.0	982.5	0.1841	0.0245	0.1750	0.0329	0.0002
1005.0	1008.5	0.1793	0.0245	0.1750	0.0000	0.0000
1102.0	1105.5	0.1636	0.0251	0.1897	0.0402	0.0006
1198.0	1201.5	0.1505	0.0254	0.1977	0.0242	0.0003
1300.0	1303.5	0.1388	0.0259	0.2108	0.0402	0.0005
1400.0	1403.4	0.1289	0.0262	0.2203	0.0320	0.0003
1505.0	1508.4	0.1199	0.0265	0.2304	0.0352	0.0003
1601.0	1604.4	0.1127	0.0265	0.2304	0.0000	0.0000
1696.0	1699.4	0.1064	0.0267	0.2362	0.0251	0.0002
1817.0	1820.4	0.0994	0.0270	0.2485	0.0447	0.0003
1898.0	1901.4	0.0951	0.0272	0.2550	0.0373	0.0002
2016.0	2019.4	0.0896	0.0275	0.2687	0.0568	0.0003
4984.0	4987.3	0.0363	0.0291	0.3691	0.0296	0.0016
7960.0	7963.3	0.0227	0.0295	0.4333	0.0350	0.0005
10032.0	10035.3	0.0180	0.0300	0.5264	0.1010	0.0005
14936.0	14939.2	0.0121	0.0305	0.6522	0.0801	0.0005
19912.0	19915.2	0.0091	0.0310	0.8311	0.1566	0.0005
24888.0	24891.2	0.0073	0.0311	0.9084	0.0870	0.0002
29856.0	29859.2	0.0061	0.0313	1.0032	0.1306	0.0002
20000.0	20003.2	0.0090	0.0313	1.0032	0.0000	0.0000
10008.0	10011.2	0.0181	0.0313	1.0032	0.0000	0.0000
4992.0	4995.2	0.0362	0.0313	1.0032	0.0000	0.0000
1001.0	1004.3	0.1801	0.0302	0.9623	0.0077	-.0011
732.0	735.3	0.2460	0.0300	0.9594	0.0024	-.0002
497.0	500.3	0.3615	0.0295	0.9531	0.0041	-.0005
222.0	225.4	0.8026	0.0280	0.9423	0.0036	-.0016
95.0	98.5	1.8369	0.0257	0.9356	0.0021	-.0022

MICROMERITICS PORE SIZER 9310

V1.04

PAGE 3

890507608

6/12/89

SFE #3 9248

10

PENETROMETER NUMBER 130163

PRESSURE PSIA	CORRECTED PRESSURE PSIA	PORE DIAMETER um	CUM. INTR. VOLUME cc/g	CUM. PORE SURFACE AREA m2/g	DIFF. INTR. VOLUME dV:dD cc/g um	INCR. INTR. VOLUME cc/g
47.0	50.5	3.5789	0.0242	0.9332	0.0009	-.0016
30.0	33.6	5.3860	0.0232	0.9324	0.0005	-.0009
15.0	18.6	9.7264	0.0229	0.9322	0.0001	-.0003

Received: 05/25/89

Results by Sample

SAMPLE ID SFE-3 9248 FT FRACTION 08A TEST CODE CLAY NAME Clay Type Analysis by XRD
 Date & Time Collected not specified Category _____

CLAY COMPONENTIAL ANALYSIS

CARBONATES (ACETIC ACID SOLUBLE) : 5

SILICATES & ALUMINO-SILICATES : 93

CLAYS-NORMALIZED TO 100% : 2

 Kaolinite + Chlorite : 25

 Illite-Montmorillonite : 19

 Expandable Clays : 56

 (Montmorillonite, Smectite, etc)

Note: N.D. = Not Detected

X-RAY DIFFRACTION PHASES PRESENT

Major: Quartz

Major-Minor:

Minor: Calcite, Albite

Minor-Trace: Microcline, Clays

Note: All constituents were listed in a probable order of decreasing abundance.

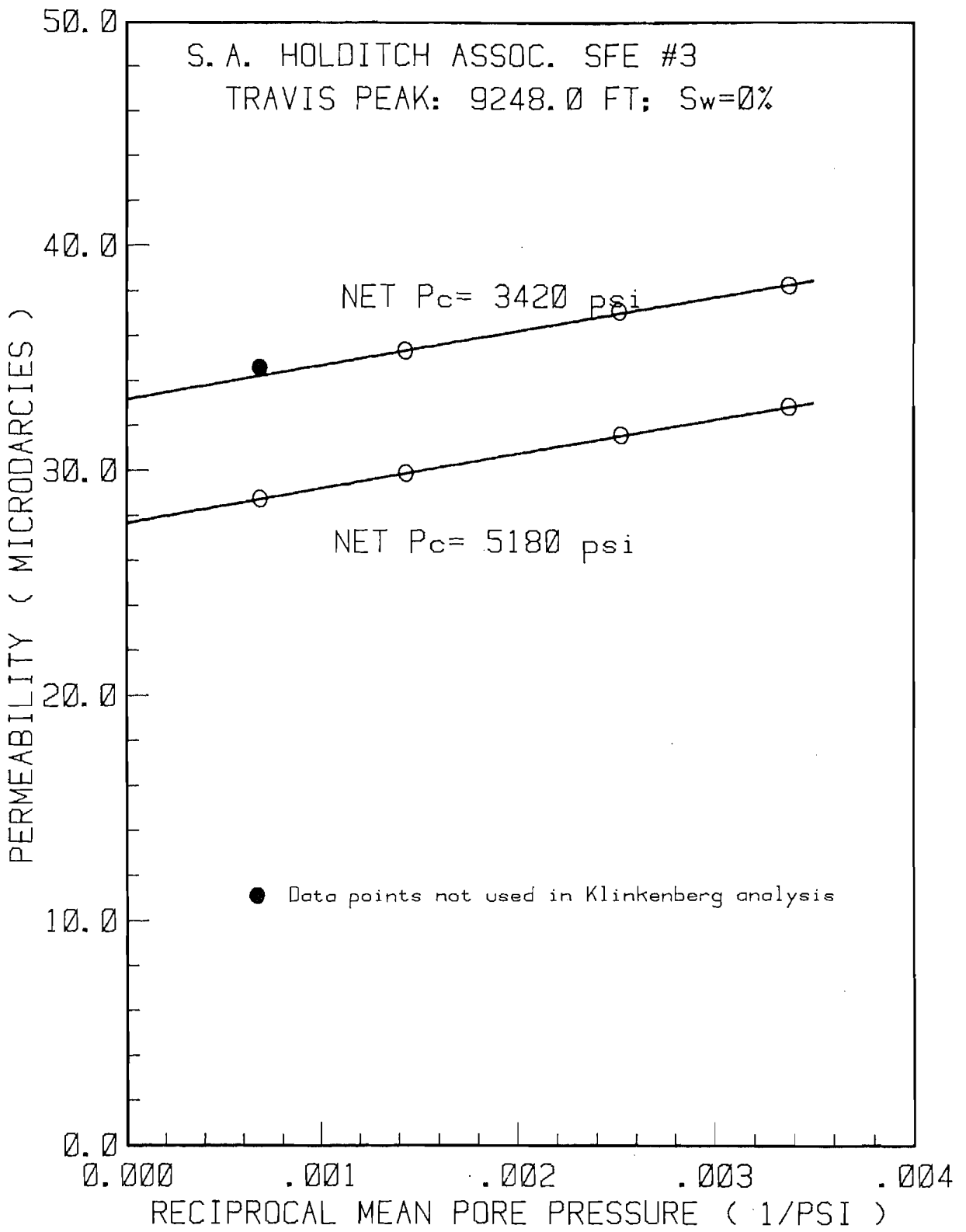
WELL NAME: S.A. HOLDITCH ASSOC. SFE #3

PLUG: TRAVIS PEAK: 9248.0 FT; Sw=0Z

PLUG LENGTH: 5.189 CM

PLUG AREA: 5.045 CM²

TEST DATE (M-D)	BEGIN TIME (H:M)	DUR- ATION (H:M)	CONFINING PRESSURE (PSIA)	MEAN PORE P (PSIA)	DIFFERENTIAL PRESSURE (PSI)	FLOW RATE (SCC/S)	TEMPERATURE (DEG. F)	VISCOSITY (C POISE)	COMPRES- SIBILITY (Z)	PERMEABILITY VALUE (MICRODARCY)	STD. DEV. (%)
11-06	11:19	00:06	4870	1455.59	5.80	6.00E-002	98.00	0.02020	1.0095	3.46E+001	(1.3)
11-07	16:12	00:06	4125	696.36	5.85	3.18E-002	98.00	0.01901	0.9989	3.53E+001	(.6)
11-08	13:07	00:10	3817	396.82	5.28	1.74E-002	98.00	0.01871	0.9981	3.71E+001	(5.1)
11-09	11:12	00:09	3720	296.07	5.69	1.45E-002	98.00	0.01863	0.9983	3.82E+001	(.4)
11-10	14:54	00:09	5473	296.11	5.67	1.24E-002	98.01	0.01863	0.9983	3.28E+001	(.3)
11-13	10:21	00:09	5582	395.46	5.76	1.62E-002	98.00	0.01870	0.9981	3.16E+001	(.3)
11-14	13:15	00:09	5875	694.51	5.70	2.61E-002	98.00	0.01901	0.9989	2.99E+001	(.4)
11-15	13:29	00:07	6630	1451.81	5.90	5.07E-002	98.00	0.02019	1.0095	2.87E+001	(1.0)



MICROMERITICS PORE SIZER 9310

V1.04

PAGE 1
6/15/89
10

890507609
SFE #3 9286
PENETROMETER NUMBER 130201

PRESSURE PSIA	CORRECTED PRESSURE PSIA	PORE DIAMETER um	CUM. INTR. VOLUME cc/g	CUM. PORE SURFACE AREA m2/g	DIFF. INTR. VOLUME dV/:dD cc/g um	INCR. INTR. VOLUME cc/g
1.4	1.4	127.1887	0.0000	0.0000	0.0000	0.0000
2.5	2.5	72.0280	0.0001	0.0000	0.0000	0.0001
3.3	3.3	54.1666	0.0003	0.0000	0.0000	0.0001
5.1	5.1	35.5678	0.0006	0.0000	0.0000	0.0003
8.0	8.0	22.6815	0.0010	0.0001	0.0000	0.0004
10.3	10.3	17.5970	0.0012	0.0001	0.0000	0.0001
12.8	12.8	14.0826	0.0012	0.0001	0.0000	0.0000
15.0	15.0	12.0551	0.0013	0.0002	0.0001	0.0001
18.1	18.1	9.9979	0.0015	0.0002	0.0001	0.0001
20.1	20.1	8.9995	0.0016	0.0003	0.0001	0.0001
22.1	22.1	8.1923	0.0016	0.0003	0.0000	0.0000
25.2	25.2	7.1745	0.0020	0.0005	0.0004	0.0004
40.0	44.6	4.0588	0.0023	0.0007	0.0001	0.0003
60.0	64.6	2.8014	0.0023	0.0007	0.0000	0.0000
66.0	70.6	2.5632	0.0023	0.0007	0.0000	0.0000
70.0	74.6	2.4257	0.0023	0.0007	0.0000	0.0000
75.0	79.6	2.2735	0.0025	0.0010	0.0010	0.0001
80.0	84.5	2.1392	0.0026	0.0012	0.0011	0.0001
86.0	90.5	1.9975	0.0026	0.0012	0.0000	0.0000
91.0	95.5	1.8929	0.0026	0.0012	0.0000	0.0000
110.0	114.5	1.5790	0.0026	0.0012	0.0000	0.0000
121.0	125.5	1.4408	0.0029	0.0020	0.0021	0.0003
149.0	153.5	1.1781	0.0031	0.0025	0.0006	0.0001
160.0	164.5	1.0993	0.0031	0.0025	0.0000	0.0000
195.0	199.5	0.9065	0.0032	0.0030	0.0008	0.0001
201.0	205.5	0.8801	0.0034	0.0037	0.0055	0.0001
220.0	224.5	0.8056	0.0035	0.0044	0.0020	0.0001
241.0	245.5	0.7367	0.0035	0.0044	0.0000	0.0000
264.0	268.5	0.6736	0.0035	0.0044	0.0000	0.0000
279.0	283.5	0.6380	0.0037	0.0053	0.0041	0.0001
303.0	307.5	0.5882	0.0037	0.0053	0.0000	0.0000
328.0	332.5	0.5440	0.0038	0.0063	0.0033	0.0001
354.0	358.5	0.5045	0.0040	0.0074	0.0037	0.0001
391.0	395.5	0.4573	0.0040	0.0074	0.0000	0.0000
400.0	404.5	0.4472	0.0040	0.0074	0.0000	0.0000
426.0	430.5	0.4201	0.0040	0.0074	0.0000	0.0000
453.0	457.5	0.3953	0.0040	0.0074	0.0000	0.0000
479.0	483.5	0.3741	0.0042	0.0105	0.0138	0.0003
506.0	510.5	0.3543	0.0042	0.0105	0.0000	0.0000
524.0	528.5	0.3422	0.0042	0.0105	0.0000	0.0000
554.0	558.5	0.3239	0.0044	0.0122	0.0080	0.0001
583.0	587.5	0.3079	0.0044	0.0122	0.0000	0.0000

MICROMERITICS PORE SIZER 9310

V1.04

PAGE 2
6/15/89
10

890507609

SFE #3 9286

PENETROMETER NUMBER 130201

PRESSURE PSIA	CORRECTED PRESSURE PSIA	PORE DIAMETER um	CUM. INTR. VOLUME cc/g	CUM. PORE SURFACE AREA m2/g	DIFF. INTR. VOLUME dv/:dD cc/g um	INCR. INTR. VOLUME cc/g
603.0	607.4	0.2977	0.0045	0.0142	0.0144	0.0001
633.0	637.4	0.2837	0.0045	0.0142	0.0000	0.0000
652.0	656.4	0.2755	0.0047	0.0163	0.0178	0.0001
673.0	677.4	0.2670	0.0047	0.0163	0.0000	0.0000
704.0	708.4	0.2553	0.0047	0.0163	0.0000	0.0000
724.0	728.4	0.2483	0.0047	0.0163	0.0000	0.0000
755.0	759.4	0.2382	0.0048	0.0187	0.0144	0.0001
775.0	779.4	0.2320	0.0048	0.0187	0.0000	0.0000
823.0	827.4	0.2186	0.0048	0.0187	0.0000	0.0000
831.0	835.4	0.2165	0.0048	0.0187	0.0000	0.0000
850.0	854.4	0.2117	0.0050	0.0214	0.0304	0.0001
883.0	887.4	0.2038	0.0050	0.0214	0.0000	0.0000
903.0	907.4	0.1993	0.0050	0.0214	0.0000	0.0000
925.0	929.4	0.1946	0.0050	0.0214	0.0000	0.0000
956.0	960.4	0.1883	0.0050	0.0214	0.0000	0.0000
978.0	982.4	0.1841	0.0051	0.0246	0.0347	0.0001
999.0	1003.4	0.1802	0.0051	0.0246	0.0000	0.0000
1108.0	1112.4	0.1626	0.0053	0.0280	0.0083	0.0001
1203.0	1207.4	0.1498	0.0053	0.0280	0.0000	0.0000
1301.0	1305.4	0.1385	0.0053	0.0280	0.0000	0.0000
1402.0	1406.4	0.1286	0.0054	0.0324	0.0147	0.0001
1500.0	1504.4	0.1202	0.0054	0.0324	0.0000	0.0000
1603.0	1607.4	0.1125	0.0056	0.0374	0.0190	0.0001
1714.0	1718.4	0.1053	0.0057	0.0428	0.0201	0.0001
1794.0	1798.4	0.1006	0.0057	0.0428	0.0000	0.0000
1898.5	1902.9	0.0950	0.0057	0.0428	0.0000	0.0000
1994.5	1998.9	0.0905	0.0057	0.0428	0.0000	0.0000
4984.0	4988.4	0.0363	0.0063	0.0797	0.0108	0.0006
7960.0	7964.3	0.0227	0.0067	0.1393	0.0324	0.0004
9960.0	9964.3	0.0182	0.0069	0.1680	0.0321	0.0001
14928.0	14932.3	0.0121	0.0070	0.2067	0.0242	0.0001
19904.0	19908.3	0.0091	0.0072	0.2620	0.0484	0.0001
24888.0	24892.3	0.0073	0.0073	0.3336	0.0805	0.0001

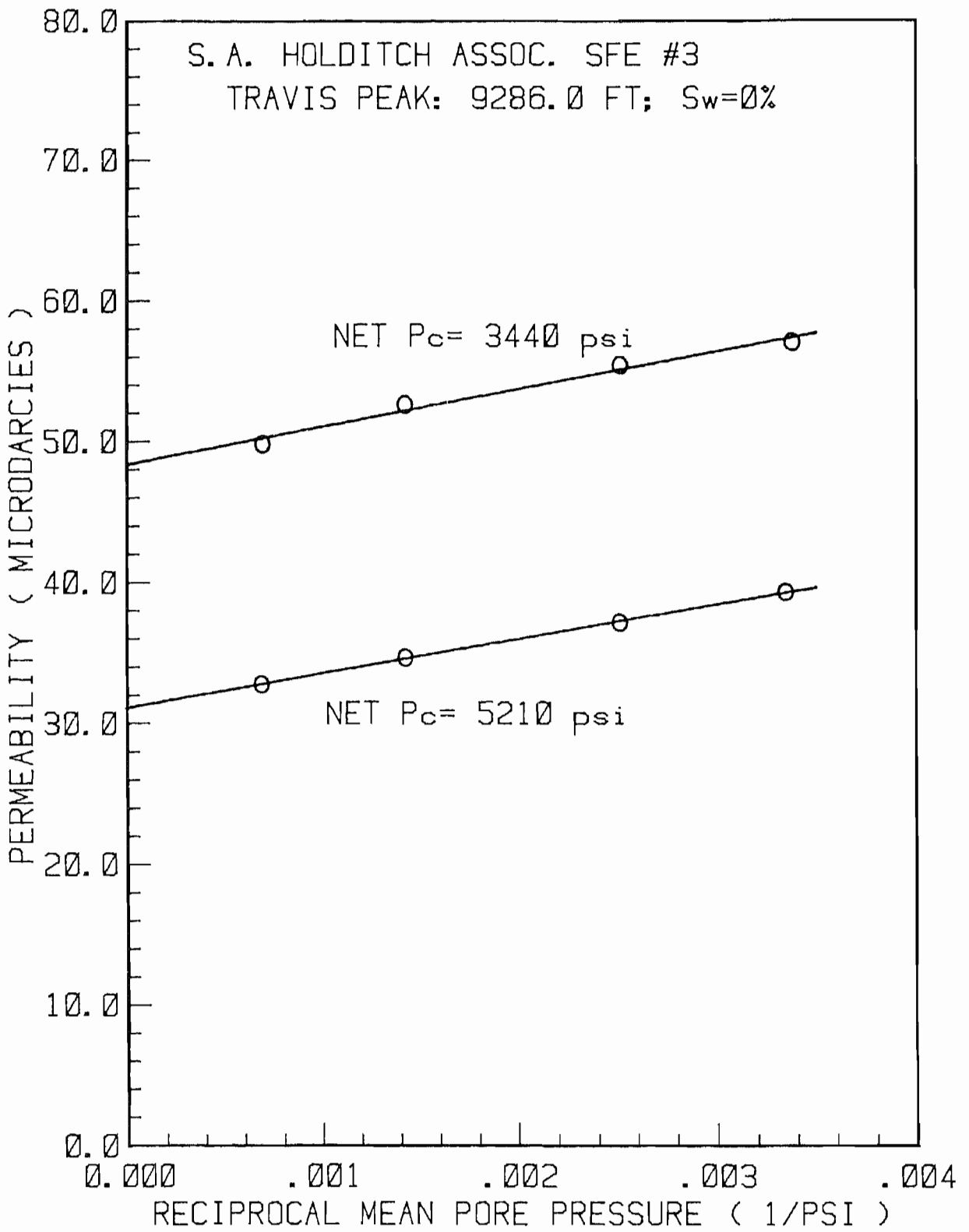
WELL NAME: S.A. HOLDITCH ASSOC. SFE #3

PLUG: TRAVIS PEAK: 9286.0 FT; Sw=0Z

PLUG LENGTH: 5.172 CM

PLUG AREA: 5.030 CM²

TEST DATE (M-D)	BEGIN TIME (H:M)	DUR-ATION (H:M)	CONFINING PRESSURE (PSIA)	MEAN PORE P (PSIA)	DIFFERENTIAL PRESSURE (PSI)	FLOW RATE (SCC/S)	TEMPERATURE (DEG. F)	VISCOSITY (C POISE)	COMPRES-SIBILITY (Z)	PERMEABILITY VALUE (MICRODARCY)	STD. DEV. (%)
10-20	13:38	00:02	4879	1437.22	10.18	1.52E-001	98.01	0.02016	1.0091	5.02E+001	(1.0)
10-23	11:49	00:05	4878	1435.14	6.25	9.22E-002	98.00	0.02016	1.0091	4.98E+001	(1.1)
10-24	09:51	00:08	4140	701.60	4.88	3.98E-002	97.99	0.01902	0.9990	5.26E+001	(1.1)
10-25	13:13	00:06	3831	397.74	5.38	2.67E-002	98.00	0.01871	0.9981	5.54E+001	(.5)
10-26	11:21	00:05	3742	296.38	5.53	2.11E-002	98.00	0.01863	0.9983	5.71E+001	(.3)
10-27	09:00	00:04	5516	299.34	11.00	2.92E-002	98.00	0.01863	0.9983	3.93E+001	(.3)
10-30	11:10	00:05	5609	398.37	9.49	3.16E-002	98.00	0.01871	0.9981	3.72E+001	(.3)
10-31	09:44	00:05	5915	701.03	8.22	4.41E-002	98.00	0.01902	0.9990	3.47E+001	(.6)
11-02	14:22	00:06	6657	1454.50	6.68	6.56E-002	98.00	0.02020	1.0095	3.28E+001	(1.1)



MICROMERITICS PORE SIZER 9310

V1.04

PAGE 1

890507610

SFE #3 9293

6/9/89

PENETROMETER NUMBER 130201

11

PRESSURE PSIA	CORRECTED PRESSURE PSIA	PORE DIAMETER um	CUM. INTR. VOLUME cc/g	CUM. PORE SURFACE AREA m2/g	DIFF. INTR. VOLUME dV/:dD cc/g um	INCR. INTR. VOLUME cc/g
0.9	0.9	202.9880	0.0000	0.0000	0.0000	0.0000
2.3	2.3	80.0630	0.0004	0.0000	0.0000	0.0004
3.3	3.3	55.0570	0.0006	0.0000	0.0000	0.0002
5.1	5.1	35.3800	0.0012	0.0001	0.0000	0.0006
8.1	8.1	22.2792	0.0012	0.0001	0.0000	0.0000
9.9	9.9	18.2192	0.0014	0.0001	0.0000	0.0002
13.0	13.0	13.8975	0.0014	0.0001	0.0000	0.0000
15.4	15.4	11.7657	0.0015	0.0002	0.0001	0.0002
18.2	18.2	9.9484	0.0015	0.0002	0.0000	0.0000
20.3	20.3	8.9235	0.0017	0.0003	0.0002	0.0002
22.5	22.5	8.0512	0.0017	0.0003	0.0000	0.0000
25.1	25.1	7.1951	0.0017	0.0003	0.0000	0.0000
40.0	44.6	4.0547	0.0019	0.0004	0.0001	0.0002
64.0	68.6	2.6363	0.0019	0.0004	0.0000	0.0000
65.0	69.6	2.5984	0.0019	0.0004	0.0000	0.0000
70.0	74.6	2.4243	0.0019	0.0004	0.0000	0.0000
75.0	79.6	2.2720	0.0019	0.0004	0.0000	0.0000
81.0	85.6	2.1128	0.0019	0.0004	0.0000	0.0000
92.0	96.6	1.8722	0.0019	0.0004	0.0000	0.0000
90.0	94.6	1.9118	0.0019	0.0004	0.0000	0.0000
101.0	105.6	1.7127	0.0021	0.0008	0.0010	0.0002
157.0	161.6	1.1193	0.0023	0.0014	0.0003	0.0002
150.0	154.6	1.1699	0.0023	0.0014	0.0000	0.0000
161.0	165.6	1.0922	0.0023	0.0014	0.0000	0.0000
198.0	202.6	0.8928	0.0027	0.0029	0.0019	0.0004
207.0	211.6	0.8548	0.0027	0.0029	0.0000	0.0000
226.0	230.6	0.7844	0.0027	0.0029	0.0000	0.0000
244.0	248.6	0.7276	0.0031	0.0050	0.0068	0.0004
260.0	264.6	0.6837	0.0033	0.0061	0.0044	0.0002
280.0	284.5	0.6357	0.0039	0.0096	0.0121	0.0006
299.0	303.5	0.5959	0.0046	0.0146	0.0194	0.0008
328.0	332.5	0.5440	0.0058	0.0227	0.0223	0.0012
353.0	357.4	0.5061	0.0073	0.0345	0.0407	0.0015
375.0	379.2	0.4769	0.0122	0.0738	0.1659	0.0048
405.0	409.2	0.4420	0.0133	0.0839	0.0332	0.0012
425.0	429.1	0.4215	0.0145	0.0946	0.0564	0.0012
454.0	458.1	0.3949	0.0162	0.1117	0.0653	0.0017
487.0	491.0	0.3684	0.0180	0.1299	0.0656	0.0017
509.0	513.0	0.3526	0.0187	0.1385	0.0490	0.0008
532.0	535.9	0.3375	0.0193	0.1452	0.0383	0.0006
557.0	560.9	0.3224	0.0199	0.1522	0.0386	0.0006
581.0	584.9	0.3092	0.0201	0.1547	0.0146	0.0002

MICROMERITICS PORE SIZER 9310

V1.04

PAGE 2

890507610

SFE #3 9293

6/9/89

PENETROMETER NUMBER 130201

11

PRESSURE PSIA	CORRECTED PRESSURE PSIA	PORE DIAMETER um	CUM. INTR. VOLUME cc/g	CUM. PORE SURFACE AREA m2/g	DIFF. INTR. VOLUME dv/:dD cc/g um	INCR. INTR. VOLUME cc/g
606.0	609.9	0.2966	0.0205	0.1598	0.0305	0.0004
631.0	634.9	0.2849	0.0211	0.1677	0.0497	0.0006
656.0	659.9	0.2741	0.0213	0.1705	0.0179	0.0002
682.0	685.8	0.2637	0.0214	0.1734	0.0186	0.0002
722.0	725.8	0.2492	0.0222	0.1854	0.0532	0.0008
735.0	738.8	0.2448	0.0224	0.1886	0.0441	0.0002
759.0	762.8	0.2371	0.0224	0.1886	0.0000	0.0000
784.0	787.8	0.2296	0.0226	0.1919	0.0257	0.0002
810.0	813.8	0.2222	0.0232	0.2021	0.0791	0.0006
836.0	839.8	0.2154	0.0232	0.2021	0.0000	0.0000
862.0	865.8	0.2089	0.0236	0.2094	0.0598	0.0004
875.0	878.8	0.2058	0.0236	0.2094	0.0000	0.0000
903.0	906.7	0.1995	0.0241	0.2209	0.0913	0.0006
931.0	934.7	0.1935	0.0241	0.2209	0.0000	0.0000
956.0	959.7	0.1884	0.0243	0.2249	0.0383	0.0002
983.0	986.7	0.1833	0.0243	0.2249	0.0000	0.0000
1025.0	1028.7	0.1758	0.0245	0.2292	0.0258	0.0002
1101.0	1104.7	0.1637	0.0251	0.2429	0.0479	0.0006
1210.0	1213.7	0.1490	0.0259	0.2626	0.0526	0.0008
1309.0	1312.7	0.1378	0.0265	0.2788	0.0516	0.0006
1412.0	1415.7	0.1278	0.0265	0.2788	0.0000	0.0000
1513.0	1516.6	0.1193	0.0272	0.3038	0.0909	0.0008
1598.0	1601.6	0.1129	0.0272	0.3038	0.0000	0.0000
1702.0	1705.6	0.1060	0.0276	0.3179	0.0561	0.0004
1832.5	1836.1	0.0985	0.0280	0.3331	0.0513	0.0004
1902.5	1906.1	0.0949	0.0280	0.3331	0.0000	0.0000
2008.0	2011.6	0.0899	0.0282	0.3414	0.0388	0.0002
4976.0	4979.5	0.0363	0.0311	0.5251	0.0541	0.0029
7960.0	7963.4	0.0227	0.0325	0.7083	0.0994	0.0014
9952.0	9955.4	0.0182	0.0330	0.8218	0.1275	0.0006
14936.0	14939.4	0.0121	0.0338	1.0260	0.1275	0.0008
19912.0	19915.3	0.0091	0.0346	1.3177	0.2555	0.0008
24896.0	24899.3	0.0073	0.0350	1.5068	0.2126	0.0004
29856.0	29859.3	0.0061	0.0355	1.8549	0.4803	0.0006
20024.0	20027.3	0.0090	0.0355	1.8549	0.0000	0.0000
10000.0	10003.3	0.0181	0.0355	1.8549	0.0000	0.0000
5000.0	5003.3	0.0361	0.0350	1.7694	0.0321	-0.0006
1001.0	1004.4	0.1801	0.0332	1.7051	0.0121	-0.0017
747.0	750.4	0.2410	0.0328	1.6977	0.0063	-0.0004
492.0	495.4	0.3651	0.0323	1.6901	0.0047	-0.0006
233.0	236.5	0.7648	0.0309	1.6805	0.0034	-0.0014
75.0	78.6	2.3012	0.0280	1.6729	0.0019	-0.0029

MICROMERITICS PORE SIZER 9310

V1.04

PAGE 3
6/9/89
11

890507610

SFE #3 9293

PENETROMETER NUMBER 130201

PRESSURE PSIA	CORRECTED PRESSURE PSIA	PORE DIAMETER um	CUM. INTR. VOLUME cc/g	CUM. PORE SURFACE AREA m2/g	DIFF. INTR. VOLUME dV/:dD cc/g um	INCR. INTR. VOLUME cc/g
50.0	53.7	3.3690	0.0257	1.6697	0.0022	-.0023
29.0	32.7	5.5297	0.0251	1.6691	0.0003	-.0006
13.0	16.7	10.8205	0.0249	1.6691	0.0000	-.0002

Received: 05/25/89

Results by Sample

SAMPLE ID SFE-3 9293 FT FRACTION 10A TEST CODE CLAY NAME Clay Type Analysis by XRD
 Date & Time Collected not specified Category _____

CLAY COMPONENTIAL ANALYSIS

CARBONATES (ACETIC ACID SOLUBLE) : 2

SILICATES & ALUMINO-SILICATES : 96

CLAYS-NORMALIZED TO 100% : 2

 Kaolinite + Chlorite : 11

 Illite-Montmorillonite : 38

 Expandable Clays : 51

 (Montmorillonite, Smectite, etc)

Note: N.D. = Not Detected

X-RAY DIFFRACTION PHASES PRESENT

Major: Quartz

Major-Minor:

Minor: Albite, Microcline, Calcite

Minor-Trace: Clays

Note: All constituents were listed in a probable order of decreasing abundance.

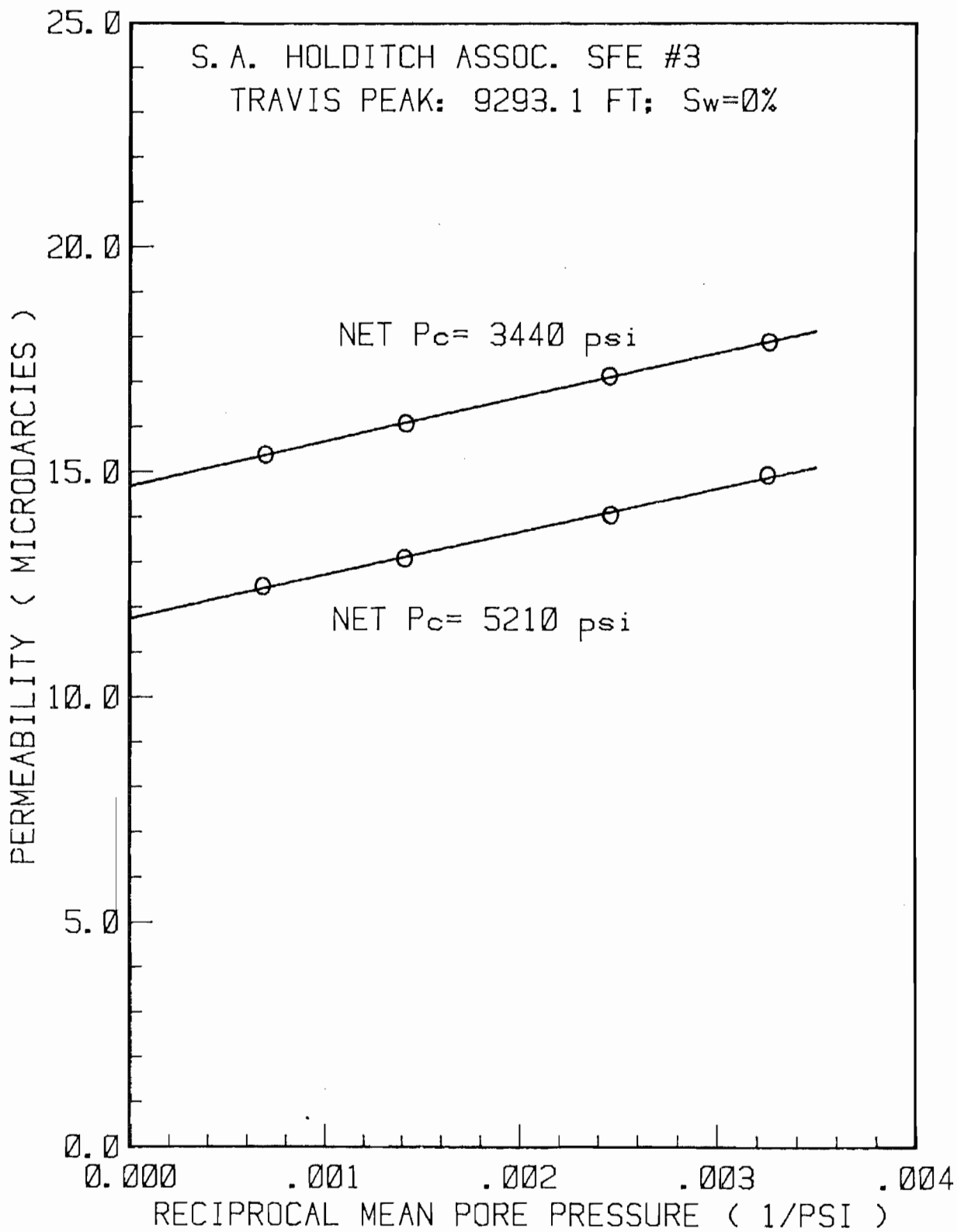
WELL NAME: S.A. HOLDITCH ASSOC. SFE #3

PLUG: TRAVIS PEAK: 9293.1 FT; Sw=0%

PLUG LENGTH: 5.074 CM

PLUG AREA: 5.044 CM²

TEST DATE (M-D)	BEGIN TIME (H:M)	DUR- ATION (H:M)	CONFINING PRESSURE (PSIA)	MEAN PORE P (PSIA)	DIFFERENTIAL PRESSURE (PSI)	FLOW RATE (SCC/S)	TEMPERATURE (DEG. F)	VISCOSITY (C POISE)	COMPRES- SIBILITY (Z)	PERMEABILITY VALUE (MICRODARCY)	STD. DEV. (%)
10-20	13:46	00:06	4877	1437.20	10.09	5.03E-002	98.01	0.02016	1.0091	1.65E+001	(.4)
10-23	10:38	00:07	4885	1436.95	10.01	4.67E-002	98.00	0.02016	1.0091	1.54E+001	(.4)
10-24	11:28	00:08	4133	704.12	9.51	2.43E-002	98.00	0.01902	0.9990	1.61E+001	(.2)
10-25	09:25	00:04	3844	406.81	22.60	3.62E-002	98.00	0.01871	0.9981	1.71E+001	(.2)
10-26	08:52	00:04	3748	306.48	24.67	3.12E-002	97.99	0.01864	0.9983	1.79E+001	(.1)
10-27	09:41	00:07	5513	307.10	25.52	2.70E-002	98.00	0.01864	0.9983	1.49E+001	(.6)
10-30	11:55	00:07	5607	405.75	23.32	3.05E-002	98.00	0.01871	0.9981	1.41E+001	(.8)
10-31	11:26	00:06	5913	707.14	19.69	4.11E-002	98.00	0.01903	0.9990	1.31E+001	(.5)
11-02	09:31	00:06	6660	1462.09	21.62	8.28E-002	98.00	0.02021	1.0097	1.25E+001	(1.0)



MICROMERITICS PORE SIZER 9310

V1.04

PAGE 1

890507611

SFE #3 9297

6/8/89

9

PENETROMETER NUMBER 130201

PRESSURE PSIA	CORRECTED PRESSURE PSIA	PORE DIAMETER um	CUM. INTR. VOLUME cc/g	CUM. PORE SURFACE AREA m2/g	DIFF. INTR. VOLUME dV/:dD cc/g um	INCR. INTR. VOLUME cc/g
1.3	1.3	136.7062	0.0000	0.0000	0.0000	0.0000
2.3	2.3	79.4301	0.0003	0.0000	0.0000	0.0003
3.4	3.4	53.5888	0.0004	0.0000	0.0000	0.0001
5.3	5.3	34.3518	0.0006	0.0000	0.0000	0.0001
8.3	8.3	21.8433	0.0007	0.0001	0.0000	0.0001
9.9	9.9	18.2689	0.0007	0.0001	0.0000	0.0000
13.1	13.1	13.8592	0.0007	0.0001	0.0000	0.0000
15.5	15.5	11.6972	0.0009	0.0001	0.0001	0.0001
18.1	18.1	10.0029	0.0009	0.0001	0.0000	0.0000
20.2	20.2	8.9474	0.0009	0.0001	0.0000	0.0000
22.2	22.2	8.1327	0.0009	0.0001	0.0000	0.0000
25.3	25.3	7.1388	0.0009	0.0001	0.0000	0.0000
40.0	44.6	4.0520	0.0009	0.0001	0.0000	0.0000
61.0	65.6	2.7556	0.0009	0.0001	0.0000	0.0000
66.0	70.6	2.5605	0.0009	0.0001	0.0000	0.0000
70.0	74.6	2.4233	0.0009	0.0001	0.0000	0.0000
75.0	79.6	2.2711	0.0009	0.0001	0.0000	0.0000
80.0	84.6	2.1370	0.0009	0.0001	0.0000	0.0000
86.0	90.6	1.9955	0.0009	0.0001	0.0000	0.0000
90.0	94.6	1.9112	0.0009	0.0001	0.0000	0.0000
100.0	104.6	1.7286	0.0010	0.0004	0.0008	0.0001
125.0	129.6	1.3952	0.0010	0.0004	0.0000	0.0000
148.0	152.6	1.1850	0.0010	0.0004	0.0000	0.0000
160.0	164.6	1.0986	0.0010	0.0004	0.0000	0.0000
194.0	198.6	0.9106	0.0010	0.0004	0.0000	0.0000
201.0	205.6	0.8796	0.0010	0.0004	0.0000	0.0000
219.0	223.6	0.8088	0.0012	0.0011	0.0021	0.0001
248.0	252.6	0.7160	0.0013	0.0019	0.0016	0.0001
265.0	269.6	0.6708	0.0013	0.0019	0.0000	0.0000
284.0	288.6	0.6267	0.0013	0.0019	0.0000	0.0000
304.0	308.6	0.5860	0.0013	0.0019	0.0000	0.0000
334.0	338.6	0.5341	0.0015	0.0030	0.0029	0.0001
355.0	359.6	0.5030	0.0016	0.0042	0.0048	0.0001
374.0	378.6	0.4777	0.0016	0.0042	0.0000	0.0000
418.0	422.6	0.4280	0.0021	0.0081	0.0090	0.0004
427.0	431.6	0.4191	0.0021	0.0081	0.0000	0.0000
458.0	462.6	0.3910	0.0025	0.0126	0.0160	0.0004
479.0	483.5	0.3740	0.0028	0.0157	0.0177	0.0003
501.0	505.5	0.3578	0.0030	0.0173	0.0092	0.0001
534.0	538.5	0.3359	0.0034	0.0225	0.0205	0.0004
552.0	556.5	0.3250	0.0039	0.0280	0.0415	0.0004
585.0	589.4	0.3068	0.0046	0.0375	0.0413	0.0007

MICROMERITICS PORE SIZER 9310

V1.04

PAGE 2

890507611

SFE #3 9297

6/8/89

PENETROMETER NUMBER 130201

9

PRESSURE PSIA	CORRECTED PRESSURE PSIA	PORE DIAMETER um	CUM. INTR. VOLUME cc/g	CUM. PORE SURFACE AREA m2/g	DIFF. INTR. VOLUME dV/:dD cc/g um	INCR. INTR. VOLUME cc/g
604.0	608.4	0.2973	0.0054	0.0474	0.0784	0.0007
623.0	627.4	0.2883	0.0058	0.0536	0.0500	0.0004
653.0	657.3	0.2751	0.0069	0.0685	0.0799	0.0010
672.0	676.3	0.2674	0.0075	0.0773	0.0777	0.0006
701.0	705.3	0.2564	0.0082	0.0888	0.0683	0.0007
729.0	733.2	0.2467	0.0090	0.1007	0.0767	0.0007
762.0	766.2	0.2361	0.0102	0.1206	0.1131	0.0012
780.0	784.1	0.2307	0.0109	0.1334	0.1387	0.0007
798.0	802.1	0.2255	0.0118	0.1492	0.1743	0.0009
829.0	833.1	0.2171	0.0126	0.1627	0.0895	0.0007
849.0	853.0	0.2120	0.0133	0.1767	0.1476	0.0007
881.0	885.0	0.2044	0.0141	0.1911	0.0979	0.0007
903.0	907.0	0.1994	0.0145	0.2000	0.0908	0.0004
926.0	929.9	0.1945	0.0148	0.2061	0.0608	0.0003
948.0	951.9	0.1900	0.0151	0.2124	0.0668	0.0003
973.0	976.9	0.1851	0.0154	0.2188	0.0617	0.0003
998.0	1001.9	0.1805	0.0156	0.2220	0.0325	0.0001
1106.0	1109.9	0.1630	0.0162	0.2360	0.0342	0.0006
1203.0	1206.8	0.1499	0.0169	0.2552	0.0573	0.0007
1301.0	1304.8	0.1386	0.0174	0.2677	0.0400	0.0004
1405.0	1408.8	0.1284	0.0178	0.2811	0.0440	0.0004
1494.0	1497.8	0.1208	0.0181	0.2908	0.0393	0.0003
1599.0	1602.8	0.1128	0.0183	0.2959	0.0190	0.0001
1702.0	1705.8	0.1060	0.0184	0.3014	0.0220	0.0001
1811.5	1815.2	0.0996	0.0187	0.3131	0.0469	0.0003
1919.0	1922.7	0.0941	0.0189	0.3192	0.0269	0.0001
2000.0	2003.7	0.0903	0.0192	0.3323	0.0789	0.0003
4976.0	4979.6	0.0363	0.0217	0.4934	0.0473	0.0025
7960.0	7963.5	0.0227	0.0228	0.6356	0.0771	0.0010
9976.0	9979.5	0.0181	0.0232	0.7238	0.0981	0.0004
14928.0	14931.5	0.0121	0.0240	0.9221	0.1247	0.0007
19912.0	19915.5	0.0091	0.0246	1.1486	0.1979	0.0006
24880.0	24883.4	0.0073	0.0249	1.2953	0.1654	0.0003
29856.0	29859.4	0.0061	0.0253	1.5654	0.3714	0.0004
19984.0	19987.4	0.0090	0.0253	1.5654	0.0000	0.0000
9992.0	9995.4	0.0181	0.0252	1.5212	0.0166	-.0001
4984.0	4987.4	0.0363	0.0247	1.4550	0.0248	-.0004
1001.0	1004.5	0.1800	0.0234	1.4051	0.0094	-.0013
749.0	752.5	0.2403	0.0229	1.3965	0.0075	-.0004
476.0	479.6	0.3772	0.0226	1.3926	0.0022	-.0003
235.0	238.6	0.7580	0.0216	1.3852	0.0028	-.0010
85.0	88.7	2.0399	0.0204	1.3818	0.0009	-.0012

MICROMERITICS PORE SIZER 9310

V1.04

PAGE 3

890507611

6/8/89

SFE #3 9297

9

PENETROMETER NUMBER 130201

PRESSURE PSIA	CORRECTED PRESSURE PSIA	PORE DIAMETER um	CUM. INTR. VOLUME cc/g	CUM. PORE SURFACE AREA m2/g	DIFF. INTR. VOLUME dV:dD cc/g um	INCR. INTR. VOLUME cc/g
48.0	51.7	3.4968	0.0192	1.3801	0.0008	-.0012
30.0	33.8	5.3562	0.0183	1.3792	0.0005	-.0009
13.0	16.8	10.7819	0.0181	1.3792	0.0000	-.0001

Received: 05/25/89

Results by Sample

SAMPLE ID SFE-3 9297 FT FRACTION 11A TEST CODE CLAY NAME Clay Type Analysis by XRD
 Date & Time Collected not specified Category _____

CLAY COMPONENTIAL ANALYSIS

CARBONATES (ACETIC ACID SOLUBLE) : 2
 SILICATES & ALUMINO-SILICATES : 97
 CLAYS-NORMALIZED TO 100% : 1
 Kaolinite + Chlorite : 10
 Illite-Montmorillonite : 18
 Expandable Clays : 72
 (Montmorillonite, Smectite, etc)

Note: N.D. = Not Detected

X-RAY DIFFRACTION PHASES PRESENT

Major: Quartz
 Major-Minor:
 Minor: Albite, Microcline, Calcite
 Minor-Trace: Clays

Note: All constituents were listed in a probable order of decreasing abundance.

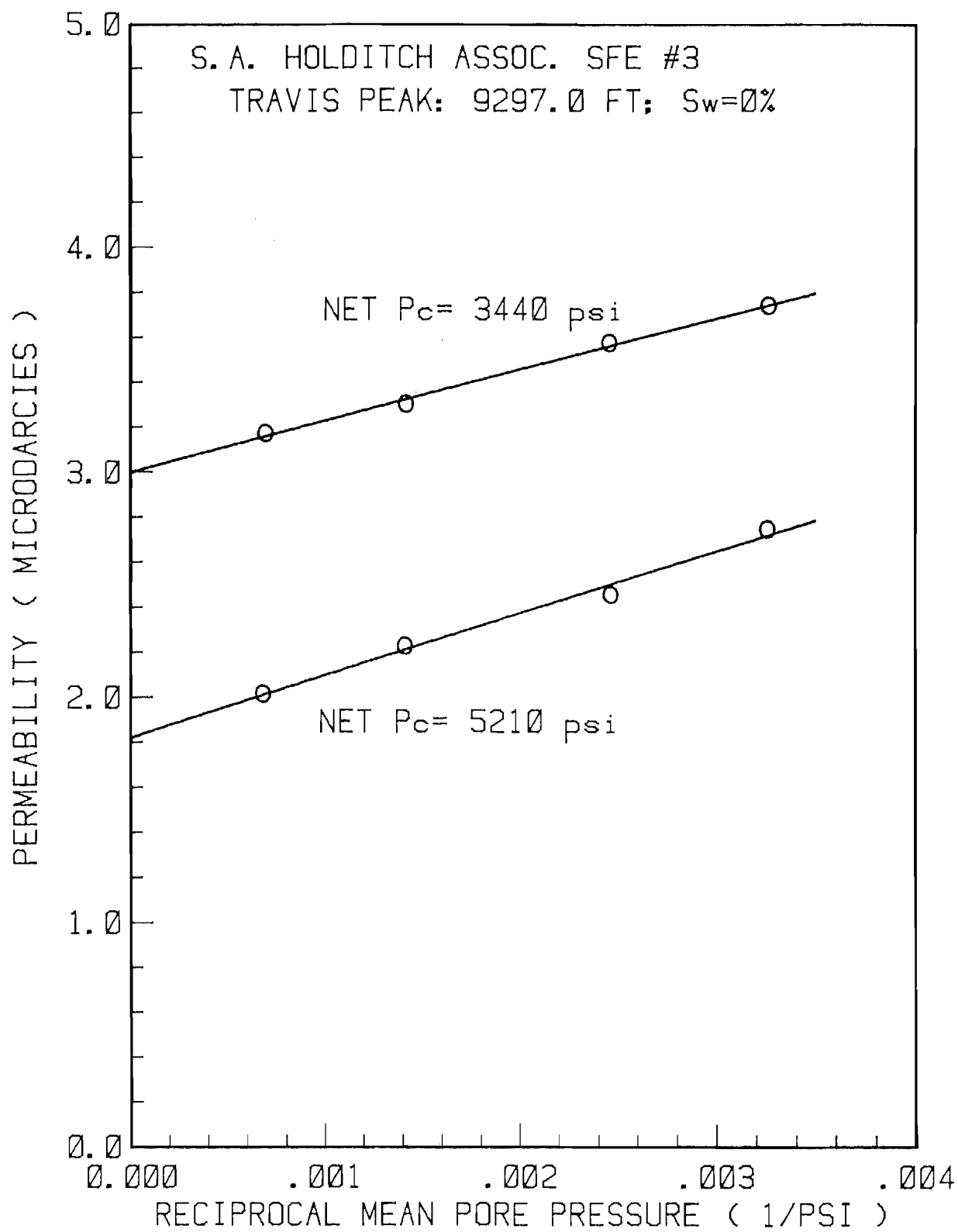
WELL NAME: S.A. HOLDITCH ASSOC. SFE #3

PLUG: TRAVIS PEAK: 9297.0 FT; Sw=0%

PLUG LENGTH: 5.111 CM

PLUG AREA: 5.040 CM²

TEST DATE (M-D)	BEGIN TIME (H:M)	DUR- ATION (H:M)	CONFINING PRESSURE (PSIA)	MEAN PORE P (PSIA)	DIFFERENTIAL PRESSURE (PSI)	FLOW RATE (SCC/S)	TEMPERATURE (DEG. F)	VISCOSITY (C POISE)	COMPRES- SIBILITY (Z)	PERMEABILITY VALUE (MICRODARCY)	STD. DEV. (%)
10-20	13:59	00:26	4871	1437.19	10.02	1.18E-002	98.00	0.02016	1.0091	3.93E+000	(1.3)
10-23	11:02	00:26	4881	1436.96	9.96	9.50E-003	98.00	0.02016	1.0091	3.17E+000	(1.4)
10-24	11:01	00:25	4135	704.11	9.57	4.98E-003	98.00	0.01902	0.9990	3.30E+000	(.5)
10-25	09:40	00:29	3843	406.79	22.58	7.48E-003	98.00	0.01871	0.9981	3.57E+000	(2.3)
10-26	09:04	00:24	3747	306.48	24.63	6.46E-003	98.00	0.01864	0.9983	3.74E+000	(.6)
10-27	09:59	00:24	5512	307.10	25.44	4.91E-003	98.00	0.01864	0.9983	2.75E+000	(2.0)
10-30	12:12	00:22	5607	405.75	23.24	5.27E-003	98.00	0.01871	0.9981	2.45E+000	(.6)
10-31	11:48	00:20	5913	707.13	19.65	6.93E-003	97.99	0.01903	0.9990	2.23E+000	(.2)
11-02	09:50	00:20	6661	1462.10	21.52	1.32E-002	97.99	0.02021	1.0097	2.02E+000	(.3)



MICROMERITICS PORE SIZER 9310

V1.04

PAGE 1
6/12/89
10

890507612

SFE #3 9306

PENETROMETER NUMBER 130163

PRESSURE PSIA	CORRECTED PRESSURE PSIA	PORE DIAMETER um	CUM. INTR. VOLUME cc/g	CUM. PORE SURFACE AREA m2/g	DIFF. INTR. VOLUME dV/:dD cc/g um	INCR. INTR. VOLUME cc/g
1.3	1.3	142.5235	0.0000	0.0000	0.0000	0.0000
2.3	2.3	78.1938	0.0001	0.0000	0.0000	0.0001
3.3	3.3	55.5133	0.0001	0.0000	0.0000	0.0000
5.1	5.1	35.2558	0.0004	0.0000	0.0000	0.0003
8.3	8.3	21.9147	0.0004	0.0000	0.0000	0.0000
10.3	10.3	17.5970	0.0006	0.0001	0.0000	0.0001
13.1	13.1	13.8211	0.0006	0.0001	0.0000	0.0000
15.2	15.2	11.8981	0.0006	0.0001	0.0000	0.0000
18.2	18.2	9.9337	0.0007	0.0001	0.0001	0.0001
20.2	20.2	8.9593	0.0007	0.0001	0.0000	0.0000
22.1	22.1	8.1690	0.0007	0.0001	0.0000	0.0000
25.2	25.2	7.1745	0.0007	0.0001	0.0000	0.0000
40.0	44.6	4.0513	0.0007	0.0001	0.0000	0.0000
61.0	65.6	2.7553	0.0007	0.0001	0.0000	0.0000
65.0	69.6	2.5970	0.0007	0.0001	0.0000	0.0000
70.0	74.6	2.4230	0.0007	0.0001	0.0000	0.0000
76.0	80.6	2.2428	0.0007	0.0001	0.0000	0.0000
82.0	86.6	2.0875	0.0007	0.0001	0.0000	0.0000
87.0	91.6	1.9736	0.0007	0.0001	0.0000	0.0000
93.0	97.6	1.8523	0.0007	0.0001	0.0000	0.0000
105.0	109.6	1.6496	0.0007	0.0001	0.0000	0.0000
133.0	137.6	1.3140	0.0007	0.0001	0.0000	0.0000
141.0	145.6	1.2419	0.0009	0.0006	0.0020	0.0001
176.0	180.6	1.0013	0.0009	0.0006	0.0000	0.0000
183.0	187.6	0.9639	0.0009	0.0006	0.0000	0.0000
202.0	206.6	0.8753	0.0009	0.0006	0.0000	0.0000
221.0	225.6	0.8016	0.0009	0.0006	0.0000	0.0000
241.0	245.6	0.7363	0.0009	0.0006	0.0000	0.0000
262.0	266.6	0.6783	0.0009	0.0006	0.0000	0.0000
283.0	287.6	0.6288	0.0009	0.0006	0.0000	0.0000
306.0	310.6	0.5822	0.0009	0.0006	0.0000	0.0000
329.0	333.6	0.5421	0.0009	0.0006	0.0000	0.0000
352.0	356.6	0.5071	0.0009	0.0006	0.0000	0.0000
376.0	380.6	0.4752	0.0010	0.0018	0.0046	0.0001
403.0	407.6	0.4437	0.0010	0.0018	0.0000	0.0000
428.0	432.6	0.4181	0.0010	0.0018	0.0000	0.0000
456.0	460.6	0.3926	0.0010	0.0018	0.0000	0.0000
483.0	487.6	0.3709	0.0010	0.0018	0.0000	0.0000
509.0	513.6	0.3521	0.0012	0.0034	0.0078	0.0001
537.0	541.6	0.3339	0.0012	0.0034	0.0000	0.0000
563.0	567.6	0.3186	0.0012	0.0034	0.0000	0.0000
590.0	594.6	0.3042	0.0013	0.0053	0.0102	0.0001

MICROMERITICS PORE SIZER 9310

V1.04

PAGE 2

890507612

6/12/89

SFE #3 9306

10

PENETROMETER NUMBER 130163

PRESSURE PSIA	CORRECTED PRESSURE PSIA	PORE DIAMETER um	CUM. INTR. VOLUME cc/g	CUM. PORE SURFACE AREA m2/g	DIFF. INTR. VOLUME dV/:dD cc/g um	INCR. INTR. VOLUME cc/g
603.0	607.6	0.2977	0.0015	0.0072	0.0226	0.0001
631.0	635.6	0.2846	0.0015	0.0072	0.0000	0.0000
657.0	661.6	0.2734	0.0016	0.0094	0.0132	0.0001
685.0	689.6	0.2623	0.0019	0.0138	0.0265	0.0003
713.0	717.6	0.2520	0.0021	0.0160	0.0144	0.0001
739.0	743.6	0.2432	0.0022	0.0184	0.0167	0.0001
751.0	755.6	0.2394	0.0024	0.0209	0.0381	0.0001
779.0	783.5	0.2308	0.0026	0.0259	0.0344	0.0003
806.0	810.5	0.2231	0.0029	0.0311	0.0383	0.0003
832.0	836.5	0.2162	0.0032	0.0364	0.0425	0.0003
858.0	862.5	0.2097	0.0035	0.0419	0.0452	0.0003
886.0	890.5	0.2031	0.0038	0.0476	0.0447	0.0003
923.0	927.5	0.1950	0.0043	0.0565	0.0545	0.0004
932.0	936.4	0.1931	0.0047	0.0656	0.2362	0.0004
958.0	962.4	0.1879	0.0050	0.0718	0.0564	0.0003
984.0	988.4	0.1830	0.0053	0.0781	0.0596	0.0003
1009.0	1013.4	0.1785	0.0059	0.0912	0.1306	0.0006
1113.0	1117.3	0.1619	0.0068	0.1119	0.0532	0.0009
1203.0	1207.3	0.1498	0.0077	0.1346	0.0732	0.0009
1295.0	1299.3	0.1392	0.0082	0.1509	0.0555	0.0006
1409.0	1413.2	0.1280	0.0091	0.1773	0.0787	0.0009
1506.0	1510.2	0.1198	0.0097	0.1963	0.0716	0.0006
1605.0	1609.2	0.1124	0.0100	0.2065	0.0400	0.0003
1706.0	1710.2	0.1058	0.0100	0.2065	0.0000	0.0000
1813.5	1817.7	0.0995	0.0103	0.2180	0.0471	0.0003
1904.5	1908.6	0.0948	0.0104	0.2240	0.0310	0.0001
2000.0	2004.1	0.0902	0.0106	0.2304	0.0326	0.0001
4976.0	4980.1	0.0363	0.0124	0.3420	0.0327	0.0018
7968.0	7972.0	0.0227	0.0128	0.4019	0.0324	0.0004
9976.0	9980.0	0.0181	0.0134	0.5173	0.1290	0.0006
14944.0	14948.0	0.0121	0.0137	0.5952	0.0489	0.0003
19912.0	19916.0	0.0091	0.0140	0.7063	0.0975	0.0003
24888.0	24892.0	0.0073	0.0143	0.8504	0.1621	0.0003
29896.0	29899.9	0.0060	0.0144	0.9388	0.1209	0.0001
19992.0	19995.9	0.0090	0.0144	0.9388	0.0000	0.0000
10000.0	10003.9	0.0181	0.0144	0.9388	0.0000	0.0000
4992.0	4995.9	0.0362	0.0144	0.9388	0.0000	0.0000
998.0	1002.0	0.1805	0.0134	0.9008	0.0071	-.0010
743.0	747.0	0.2421	0.0132	0.8980	0.0024	-.0001
501.0	505.0	0.3581	0.0130	0.8941	0.0025	-.0003
242.0	246.1	0.7350	0.0122	0.8887	0.0020	-.0007
94.0	98.1	1.8441	0.0119	0.8878	0.0003	-.0003

MICROMERITICS PORE SIZER 9310

V1.04

PAGE 3

890507612

6/12/89

SFE #3 9306

10

PENETROMETER NUMBER 130163

PRESSURE PSIA	CORRECTED PRESSURE PSIA	PORE DIAMETER um	CUM. INTR. VOLUME cc/g	CUM. PORE SURFACE AREA m2/g	DIFF. INTR. VOLUME dV/:dD cc/g um	INCR. INTR. VOLUME cc/g
49.0	53.1	3.4073	0.0118	0.8875	0.0001	-.0001
30.0	34.1	5.3021	0.0112	0.8870	0.0003	-.0006
12.0	16.1	11.2154	0.0109	0.8869	0.0000	-.0003

Received: 05/25/89

Results by Sample

SAMPLE ID SFE-3 9306 FT FRACTION 12A TEST CODE CLAY NAME Clay Type Analysis by XRD
 Date & Time Collected not specified Category _____

CLAY COMPONENTIAL ANALYSIS

CARBONATES (ACETIC ACID SOLUBLE) : 3
 SILICATES & ALUMINO-SILICATES : 95
 CLAYS-NORMALIZED TO 100% : 2
 Kaolinite + Chlorite : 9
 Illite-Montmorillonite : 14
 Expandable Clays : 77
 (Montmorillonite, Smectite, etc)

Note: N.D. = Not Detected

X-RAY DIFFRACTION PHASES PRESENT

Major: Quartz
 Major-Minor:
 Minor: Albite, Microcline, Calcite
 Minor-Trace: Clays

Note: All constituents were listed in a probable order of decreasing abundance.

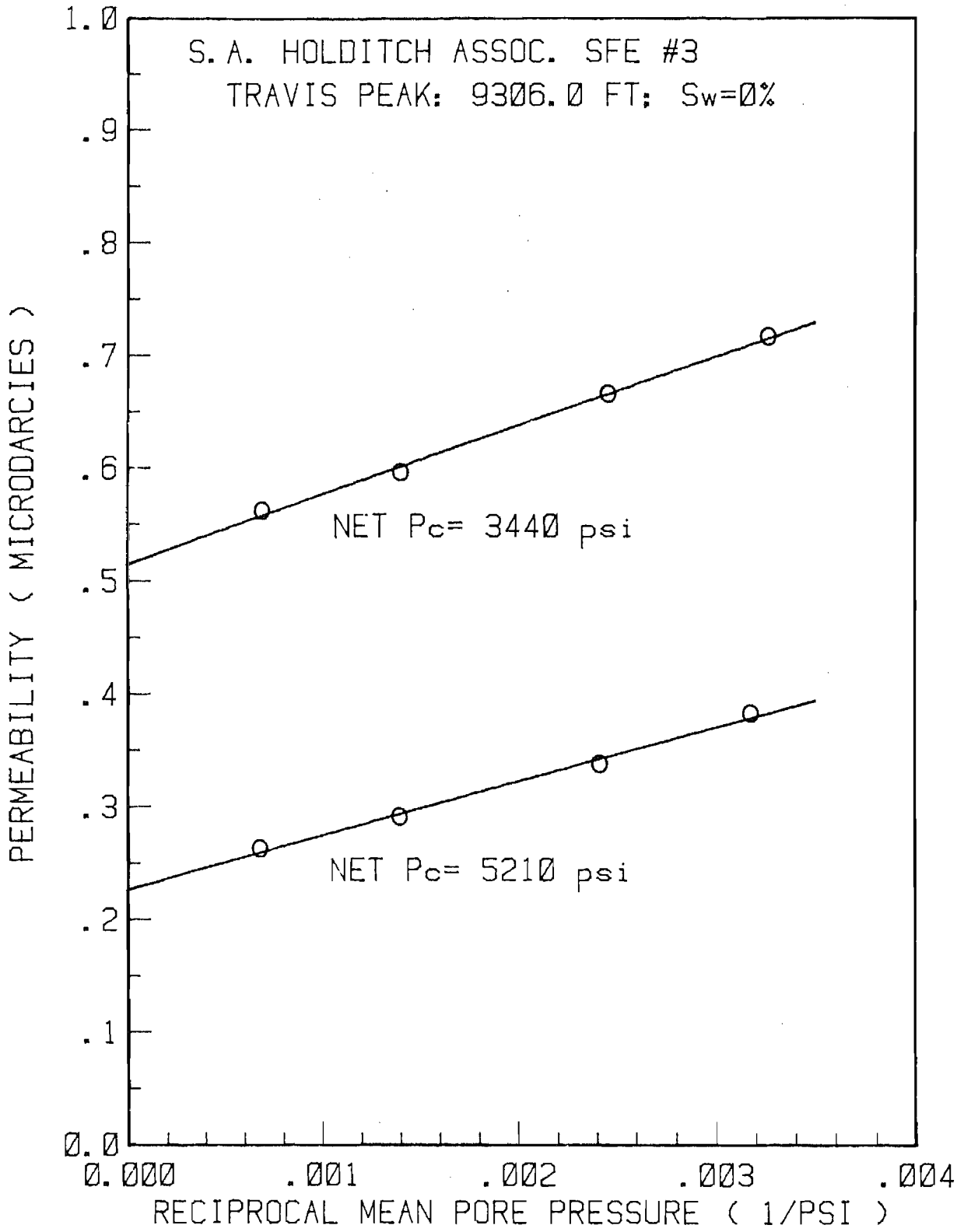
WELL NAME: S.A. HOLDITCH ASSOC. SFE #3

PLUG: TRAVIS PEAK: 9306.0 FT; Sw=0%

PLUG LENGTH: 5.135 CM

PLUG AREA: 5.050 CM²

TEST DATE (M-D)	BEGIN TIME (H:M)	DUR- ATION (H:M)	CONFINING PRESSURE (PSIA)	MEAN PORE P (PSIA)	DIFFERENTIAL PRESSURE (PSI)	FLOW RATE (SCC/S)	TEMPERATURE (DEG. F)	VISCOSITY (C POISE)	COMPRES- SIBILITY (Z)	PERMEABILITY VALUE (MICROBARCY)	STD. DEV. (%)
10-20	14:40	01:40	4853	1437.16	9.98	2.04E-003	98.00	0.02016	1.0091	6.82E-001	(1.5)
10-23	12:28	01:12	4871	1443.75	22.64	3.83E-003	98.00	0.02018	1.0093	5.62E-001	(1.0)
10-24	12:08	00:58	4143	712.80	25.81	2.45E-003	98.00	0.01903	0.9990	5.96E-001	(.6)
10-25	10:30	01:27	3839	406.80	22.51	1.39E-003	98.00	0.01871	0.9981	6.66E-001	(.5)
10-26	09:48	01:12	3744	306.50	24.58	1.23E-003	98.00	0.01864	0.9983	7.17E-001	(.5)
10-27	11:30	02:27	5503	315.03	40.10	1.10E-003	98.00	0.01864	0.9983	3.83E-001	(.5)
10-30	13:36	01:51	5611	414.24	38.98	1.24E-003	98.00	0.01872	0.9981	3.38E-001	(1.2)
10-31	12:48	01:33	5911	717.19	38.35	1.79E-003	98.00	0.01904	0.9991	2.91E-001	(.9)
11-02	10:45	01:22	6660	1470.96	38.16	3.07E-003	98.00	0.02023	1.0099	2.63E-001	(.9)



MICROMERITICS PORE SIZER 9310

V1.04

PAGE 1

890507613

6/12/89

SFE #3 9310.5

2

PENETROMETER NUMBER 130201

PRESSURE PSIA	CORRECTED PRESSURE PSIA	PORE DIAMETER um	CUM. INTR. VOLUME cc/g	CUM. PORE SURFACE AREA m2/g	DIFF. INTR. VOLUME dV/:dD cc/g um	INCR. INTR. VOLUME cc/g
1.3	1.3	136.7062	0.0000	0.0000	0.0000	0.0000
2.4	2.4	74.7056	0.0001	0.0000	0.0000	0.0001
3.3	3.3	55.3604	0.0003	0.0000	0.0000	0.0001
5.0	5.0	36.0140	0.0006	0.0000	0.0000	0.0003
8.2	8.2	21.9867	0.0006	0.0000	0.0000	0.0000
10.3	10.3	17.5970	0.0006	0.0000	0.0000	0.0000
13.3	13.3	13.5783	0.0006	0.0000	0.0000	0.0000
15.0	15.0	12.0623	0.0007	0.0001	0.0001	0.0001
18.2	18.2	9.9141	0.0009	0.0001	0.0001	0.0001
20.3	20.3	8.9196	0.0009	0.0001	0.0000	0.0000
22.2	22.2	8.1393	0.0009	0.0001	0.0000	0.0000
25.3	25.3	7.1541	0.0010	0.0002	0.0001	0.0001
41.0	45.6	3.9639	0.0010	0.0002	0.0000	0.0000
61.0	65.6	2.7559	0.0010	0.0002	0.0000	0.0000
66.0	70.6	2.5608	0.0010	0.0002	0.0000	0.0000
70.0	74.6	2.4235	0.0010	0.0002	0.0000	0.0000
75.0	79.6	2.2714	0.0010	0.0002	0.0000	0.0000
80.0	84.6	2.1372	0.0010	0.0002	0.0000	0.0000
85.0	89.6	2.0181	0.0012	0.0005	0.0012	0.0001
90.0	94.6	1.9115	0.0012	0.0005	0.0000	0.0000
102.0	106.6	1.6963	0.0012	0.0005	0.0000	0.0000
127.0	131.6	1.3741	0.0012	0.0005	0.0000	0.0000
141.0	145.6	1.2420	0.0012	0.0005	0.0000	0.0000
173.0	177.6	1.0183	0.0012	0.0005	0.0000	0.0000
180.0	184.6	0.9796	0.0012	0.0005	0.0000	0.0000
205.0	209.6	0.8628	0.0012	0.0005	0.0000	0.0000
221.0	225.6	0.8016	0.0012	0.0005	0.0000	0.0000
239.0	243.6	0.7424	0.0012	0.0005	0.0000	0.0000
271.0	275.6	0.6562	0.0012	0.0005	0.0000	0.0000
280.0	284.6	0.6355	0.0012	0.0005	0.0000	0.0000
299.0	303.6	0.5957	0.0012	0.0005	0.0000	0.0000
328.0	332.6	0.5438	0.0012	0.0005	0.0000	0.0000
358.0	362.6	0.4988	0.0012	0.0005	0.0000	0.0000
379.0	383.6	0.4715	0.0012	0.0005	0.0000	0.0000
401.0	405.6	0.4459	0.0013	0.0018	0.0056	0.0001
425.0	429.6	0.4210	0.0013	0.0018	0.0000	0.0000
460.0	464.6	0.3893	0.0013	0.0018	0.0000	0.0000
481.0	485.6	0.3724	0.0013	0.0018	0.0000	0.0000
505.0	509.6	0.3549	0.0013	0.0018	0.0000	0.0000
527.0	531.6	0.3402	0.0014	0.0034	0.0098	0.0001
550.0	554.6	0.3261	0.0017	0.0069	0.0205	0.0003
584.0	588.6	0.3073	0.0019	0.0087	0.0077	0.0001

MICROMERITICS PORE SIZER 9310

V1.04

PAGE 2

890507613

6/12/89

SFE #3 9310.5

2

PENETROMETER NUMBER 130201

PRESSURE PSIA	CORRECTED PRESSURE PSIA	PORE DIAMETER um	CUM. INTR. VOLUME cc/g	CUM. PORE SURFACE AREA m2/g	DIFF. INTR. VOLUME dV/:dD cc/g um	INCR. INTR. VOLUME cc/g
618.0	622.6	0.2905	0.0023	0.0145	0.0258	0.0004
629.0	633.6	0.2855	0.0025	0.0165	0.0287	0.0001
650.0	654.5	0.2763	0.0027	0.0206	0.0316	0.0003
686.0	690.5	0.2619	0.0029	0.0228	0.0100	0.0001
711.0	715.5	0.2528	0.0029	0.0228	0.0000	0.0000
734.0	738.5	0.2449	0.0030	0.0251	0.0184	0.0001
759.0	763.5	0.2369	0.0032	0.0275	0.0180	0.0001
787.0	791.5	0.2285	0.0032	0.0275	0.0000	0.0000
813.0	817.5	0.2212	0.0032	0.0275	0.0000	0.0000
825.0	829.5	0.2180	0.0033	0.0301	0.0452	0.0001
851.0	855.5	0.2114	0.0033	0.0301	0.0000	0.0000
878.0	882.5	0.2049	0.0033	0.0301	0.0000	0.0000
903.0	907.5	0.1993	0.0033	0.0301	0.0000	0.0000
929.0	933.5	0.1937	0.0033	0.0301	0.0000	0.0000
955.0	959.5	0.1885	0.0035	0.0331	0.0275	0.0001
984.0	988.5	0.1830	0.0035	0.0331	0.0000	0.0000
1013.0	1017.5	0.1778	0.0035	0.0331	0.0000	0.0000
1112.0	1116.5	0.1620	0.0035	0.0331	0.0000	0.0000
1213.0	1217.5	0.1486	0.0036	0.0369	0.0107	0.0001
1313.0	1317.5	0.1373	0.0039	0.0449	0.0256	0.0003
1414.0	1418.5	0.1275	0.0039	0.0449	0.0000	0.0000
1500.0	1504.5	0.1202	0.0039	0.0449	0.0000	0.0000
1604.0	1608.5	0.1124	0.0039	0.0449	0.0000	0.0000
1707.0	1711.5	0.1057	0.0039	0.0449	0.0000	0.0000
1817.5	1822.0	0.0993	0.0040	0.0506	0.0225	0.0001
1907.5	1912.0	0.0946	0.0040	0.0506	0.0000	0.0000
2000.0	2004.5	0.0902	0.0040	0.0506	0.0000	0.0000
4976.0	4980.4	0.0363	0.0045	0.0780	0.0080	0.0004
7984.0	7988.4	0.0226	0.0048	0.1172	0.0211	0.0003
9976.0	9980.4	0.0181	0.0049	0.1455	0.0320	0.0001
14936.0	14940.4	0.0121	0.0053	0.2602	0.0720	0.0004
19904.0	19908.4	0.0091	0.0055	0.3147	0.0478	0.0001
24888.0	24892.4	0.0073	0.0058	0.4560	0.1588	0.0003
29856.0	29860.4	0.0061	0.0059	0.5428	0.1195	0.0001
19984.0	19988.4	0.0090	0.0059	0.5428	0.0000	0.0000
10000.0	10004.4	0.0181	0.0059	0.5428	0.0000	0.0000
4984.0	4988.4	0.0363	0.0059	0.5428	0.0000	0.0000
1000.0	1004.4	0.1801	0.0055	0.5267	0.0030	-.0004
744.0	748.4	0.2417	0.0053	0.5240	0.0023	-.0001
493.0	497.4	0.3636	0.0051	0.5202	0.0024	-.0003
231.0	235.4	0.7682	0.0046	0.5171	0.0011	-.0004
95.0	99.5	1.8184	0.0042	0.5158	0.0004	-.0004

MICROMERITICS PORE SIZER 9310

V1.04

PAGE 3

890507613

6/12/89

SFE #3 9310.5

2

PENETROMETER NUMBER 130201

PRESSURE PSIA	CORRECTED PRESSURE PSIA	PORE DIAMETER um	CUM. INTR. VOLUME cc/g	CUM. PORE SURFACE AREA m2/g	DIFF. INTR. VOLUME dV/:dD cc/g um	INCR. INTR. VOLUME cc/g
50.0	54.5	3.3208	0.0042	0.5158	0.0000	0.0000
30.0	34.5	5.2435	0.0036	0.5152	0.0003	-.0006
14.0	18.5	9.7761	0.0035	0.5152	0.0000	-.0001

Received: 05/25/89

Results by Sample

SAMPLE ID SFE-3 9310.5 FT FRACTION 13A TEST CODE CLAY NAME Clay Type Analysis by XRD
 Date & Time Collected not specified Category _____

CLAY COMPONENTIAL ANALYSIS

CARBONATES (ACETIC ACID SOLUBLE) : 37

SILICATES & ALUMINO-SILICATES : 62

CLAYS-NORMALIZED TO 100% : 1

 Kaolinite + Chlorite : 15

 Illite-Montmorillonite : 29

 Expandable Clays : 56

 (Montmorillonite, Smectite, etc)

Note: N.D. = Not Detected

X-RAY DIFFRACTION PHASES PRESENT

Major: Quartz, Calcite

Major-Minor:

Minor: Albite

Minor-Trace: Clays

Note: All constituents were listed in a probable order of decreasing abundance.

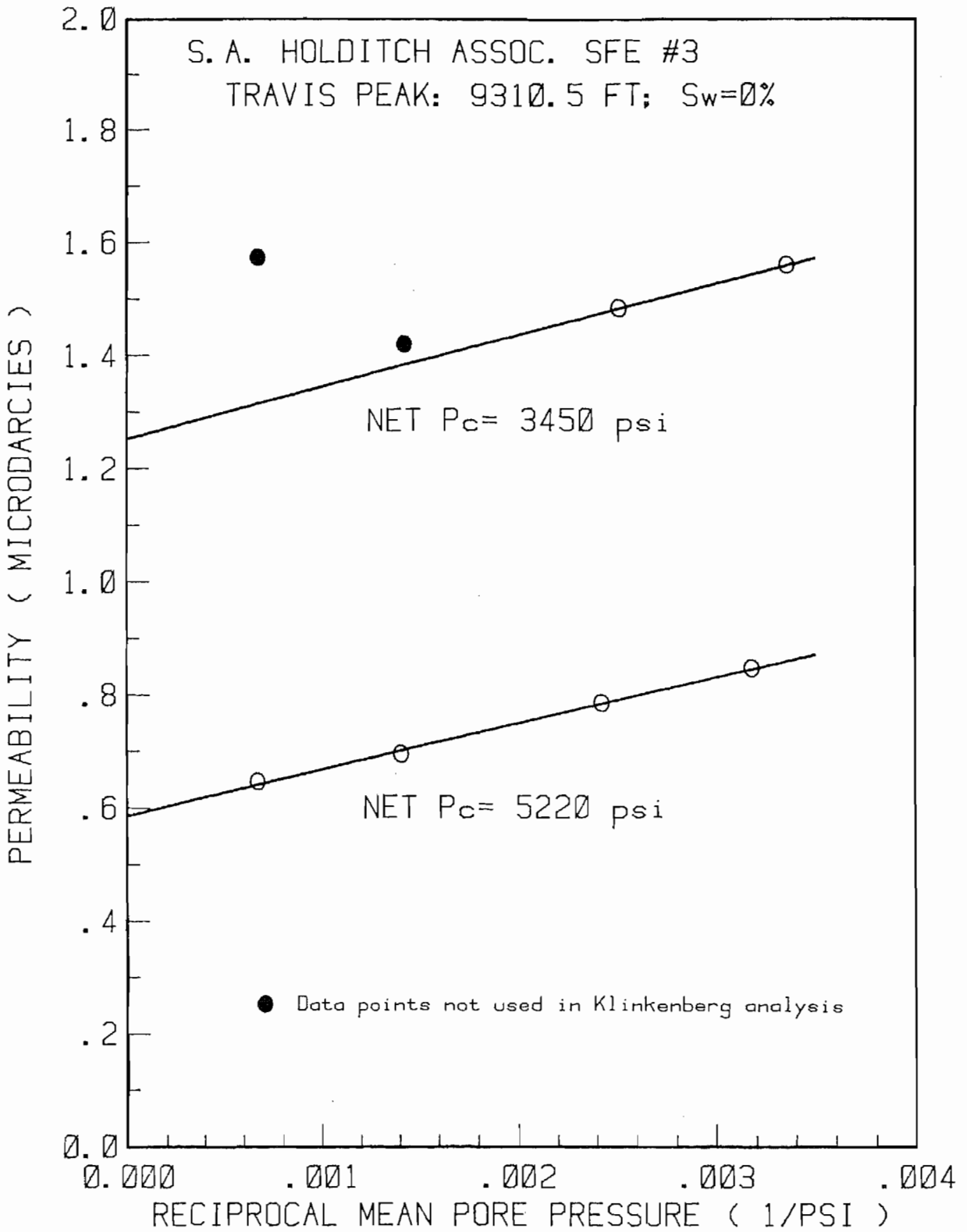
WELL NAME: S.A. HOLDITCH ASSOC. SFE #3

PLUG: TRAVIS PEAK: 9310.5 FT; Sw=0Z

PLUG LENGTH: 5.133 CM

PLUG AREA: 5.037 CM²

TEST DATE (M-D)	BEGIN TIME (H:M)	DUR- ATION (H:M)	CONFINING PRESSURE (PSIA)	MEAN PORE P (PSIA)	DIFFERENTIAL PRESSURE (PSI)	FLOW RATE (SCC/S)	TEMPERATURE (DEG. F)	VISCOSITY (C POISE)	COMPRES- SIBILITY (Z)	PERMEABILITY VALUE (MICRODARCY)	STD. DEV. (%)
08-02	15:06	01:19	4920	1485.49	9.54	5.55E-003	98.00	0.02026	1.0102	1.89E+000	(.8)
08-03	16:07	00:27	4935	1486.10	10.37	5.02E-003	98.00	0.02026	1.0102	1.57E+000	(.8)
08-07	13:39	01:06	4161	700.17	10.05	2.22E-003	98.00	0.01902	0.9990	1.42E+000	(.8)
08-09	09:33	01:15	3860	398.25	9.66	1.29E-003	98.00	0.01871	0.9981	1.48E+000	(.4)
08-10	10:00	01:18	3763	298.27	9.71	1.03E-003	98.00	0.01863	0.9983	1.56E+000	(.7)
08-11	15:24	00:39	5539	306.74	25.43	1.68E-003	98.00	0.01864	0.9983	9.47E-001	(.3)
08-14	09:48	00:54	5532	314.75	40.05	2.43E-003	98.00	0.01864	0.9983	8.47E-001	(.4)
08-15	10:51	00:38	5633	412.49	39.84	2.92E-003	98.00	0.01872	0.9981	7.85E-001	(.4)
08-17	13:30	00:40	5932	708.90	36.37	3.99E-003	98.00	0.01903	0.9990	6.95E-001	(1.3)
08-18	10:48	00:33	6710	1489.29	41.34	8.23E-003	98.00	0.02026	1.0103	6.47E-001	(.6)



MICROMERITICS PORE SIZER 9310

V1.04

PAGE 1

890507614

6/15/89

SFE #3 9317

3

PENETROMETER NUMBER 130163

PRESSURE PSIA	CORRECTED PRESSURE PSIA	PORE DIAMETER um	CUM. INTR. VOLUME cc/g	CUM. PORE SURFACE AREA m2/g	DIFF. INTR. VOLUME dV/:dD cc/g um	INCR. INTR. VOLUME cc/g
1.4	1.4	127.9988	0.0002	0.0000	0.0002	0.0002
2.1	2.1	84.7925	0.0002	0.0000	0.0000	0.0000
3.3	3.3	54.1666	0.0003	0.0000	0.0000	0.0002
5.4	5.4	33.2162	0.0005	0.0000	0.0000	0.0002
8.2	8.2	22.1564	0.0006	0.0000	0.0000	0.0002
10.2	10.2	17.7525	0.0006	0.0000	0.0000	0.0000
13.2	13.2	13.7454	0.0006	0.0000	0.0000	0.0000
15.2	15.2	11.8629	0.0008	0.0001	0.0001	0.0002
18.1	18.1	9.9781	0.0008	0.0001	0.0000	0.0000
20.3	20.3	8.9117	0.0008	0.0001	0.0000	0.0000
22.1	22.1	8.1957	0.0008	0.0001	0.0000	0.0000
25.3	25.3	7.1464	0.0008	0.0001	0.0000	0.0000
41.0	45.6	3.9626	0.0008	0.0001	0.0000	0.0000
61.0	65.6	2.7553	0.0008	0.0001	0.0000	0.0000
66.0	70.6	2.5602	0.0008	0.0001	0.0000	0.0000
71.0	75.6	2.3910	0.0008	0.0001	0.0000	0.0000
76.0	80.6	2.2428	0.0008	0.0001	0.0000	0.0000
80.0	84.6	2.1368	0.0008	0.0001	0.0000	0.0000
86.0	90.6	1.9953	0.0008	0.0001	0.0000	0.0000
91.0	95.6	1.8910	0.0008	0.0001	0.0000	0.0000
100.0	104.6	1.7284	0.0008	0.0001	0.0000	0.0000
127.0	131.6	1.3739	0.0008	0.0001	0.0000	0.0000
141.0	145.6	1.2418	0.0008	0.0001	0.0000	0.0000
178.0	182.6	0.9903	0.0009	0.0006	0.0006	0.0002
180.0	184.6	0.9796	0.0009	0.0006	0.0000	0.0000
200.0	204.6	0.8838	0.0009	0.0006	0.0000	0.0000
224.0	228.6	0.7911	0.0009	0.0006	0.0000	0.0000
250.0	254.6	0.7103	0.0009	0.0006	0.0000	0.0000
269.0	273.6	0.6610	0.0009	0.0006	0.0000	0.0000
289.0	293.6	0.6159	0.0009	0.0006	0.0000	0.0000
310.0	314.6	0.5748	0.0009	0.0006	0.0000	0.0000
332.0	336.6	0.5373	0.0009	0.0006	0.0000	0.0000
354.0	358.6	0.5043	0.0009	0.0006	0.0000	0.0000
378.0	382.6	0.4727	0.0009	0.0006	0.0000	0.0000
402.0	406.6	0.4448	0.0009	0.0006	0.0000	0.0000
425.0	429.6	0.4210	0.0009	0.0006	0.0000	0.0000
452.0	456.6	0.3961	0.0009	0.0006	0.0000	0.0000
477.0	481.6	0.3755	0.0009	0.0006	0.0000	0.0000
502.0	506.6	0.3570	0.0009	0.0006	0.0000	0.0000
529.0	533.6	0.3389	0.0009	0.0006	0.0000	0.0000
555.0	559.6	0.3232	0.0009	0.0006	0.0000	0.0000
581.0	585.6	0.3088	0.0009	0.0006	0.0000	0.0000

MICROMERITICS PORE SIZER 9310

V1.04

PAGE 2

890507614

6/15/89

SFE #3 9317

3

PENETROMETER NUMBER 130163

PRESSURE PSIA	CORRECTED PRESSURE PSIA	PORE DIAMETER um	CUM. INTR. VOLUME cc/g	CUM. PORE SURFACE AREA m2/g	DIFF. INTR. VOLUME dV/:dD cc/g um	INCR. INTR. VOLUME cc/g
607.0	611.6	0.2957	0.0009	0.0006	0.0000	0.0000
635.0	639.6	0.2828	0.0009	0.0006	0.0000	0.0000
662.0	666.6	0.2713	0.0009	0.0006	0.0000	0.0000
691.0	695.6	0.2600	0.0009	0.0006	0.0000	0.0000
703.0	707.6	0.2556	0.0009	0.0006	0.0000	0.0000
733.0	737.6	0.2452	0.0009	0.0006	0.0000	0.0000
761.0	765.6	0.2362	0.0009	0.0006	0.0000	0.0000
789.0	793.6	0.2279	0.0009	0.0006	0.0000	0.0000
804.0	808.6	0.2237	0.0009	0.0006	0.0000	0.0000
832.0	836.6	0.2162	0.0009	0.0006	0.0000	0.0000
862.0	866.6	0.2087	0.0009	0.0006	0.0000	0.0000
890.0	894.6	0.2022	0.0011	0.0036	0.0231	0.0002
905.0	909.6	0.1988	0.0011	0.0036	0.0000	0.0000
935.0	939.6	0.1925	0.0011	0.0036	0.0000	0.0000
976.0	980.6	0.1844	0.0011	0.0036	0.0000	0.0000
975.0	979.6	0.1846	0.0009	0.0003	0.8078	-.0002
1006.0	1010.6	0.1790	0.0009	0.0003	0.0000	0.0000
1107.0	1111.6	0.1627	0.0009	0.0003	0.0000	0.0000
1204.0	1208.6	0.1496	0.0009	0.0003	0.0000	0.0000
1302.0	1306.6	0.1384	0.0009	0.0003	0.0000	0.0000
1420.0	1424.6	0.1270	0.0009	0.0003	0.0000	0.0000
1503.0	1507.6	0.1200	0.0009	0.0003	0.0000	0.0000
1607.0	1611.6	0.1122	0.0012	0.0107	0.0390	0.0003
1707.0	1711.6	0.1057	0.0012	0.0107	0.0000	0.0000
1815.0	1819.6	0.0994	0.0014	0.0166	0.0241	0.0002
1907.0	1911.6	0.0946	0.0015	0.0228	0.0316	0.0002
2008.0	2012.6	0.0899	0.0018	0.0359	0.0636	0.0003
4976.0	4980.3	0.0363	0.0071	0.3709	0.0987	0.0053
7960.0	7964.3	0.0227	0.0085	0.5550	0.0998	0.0014
9960.0	9964.2	0.0182	0.0088	0.6141	0.0662	0.0003
14928.0	14932.2	0.0121	0.0092	0.7338	0.0750	0.0005
19920.0	19924.2	0.0091	0.0100	1.0188	0.2487	0.0008
24952.0	24956.2	0.0072	0.0104	1.2407	0.2474	0.0005

Received: 05/25/89

Results by Sample

SAMPLE ID SFE-3 9317 FT FRACTION 14A TEST CODE CLAY NAME Clay Type Analysis by XRD
 Date & Time Collected not specified Category _____

CLAY COMPONENTIAL ANALYSIS

CARBONATES (ACETIC ACID SOLUBLE) : 5

SILICATES & ALUMINO-SILICATES : 93

CLAYS-NORMALIZED TO 100% : 2

 Kaolinite + Chlorite : 16

 Illite-Montmorillonite : 43

 Expandable Clays : 41

 (Montmorillonite, Smectite, etc)

Note: N.D. = Not Detected

X-RAY DIFFRACTION PHASES PRESENT

Major: Quartz

Major-Minor:

Minor: Albite, Calcite

Minor-Trace: Microcline, Clays

Note: All constituents were listed in a probable order of decreasing abundance.

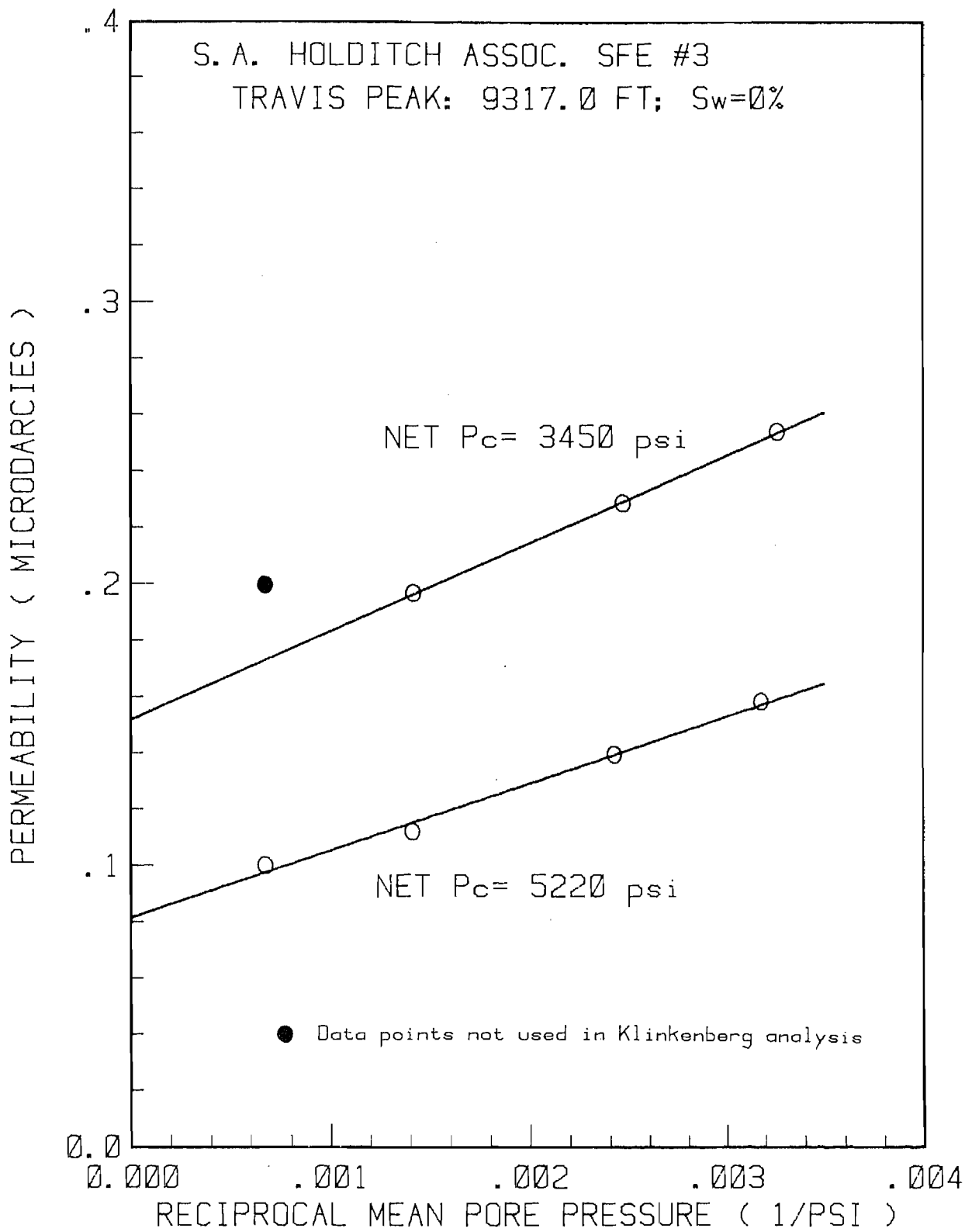
WELL NAME: S.A. HOLDITCH ASSOC. SFE #3

PLUG: TRAVIS PEAK: 9317.0 FT; Sw=0%

PLUG LENGTH: 5.098 CM

PLUG AREA: 5.040 CM²

TEST DATE (M-D)	BEGIN TIME (H:M)	DUR-ATION (H:M)	CONFINING PRESSURE (PSIA)	MEAN PORE P (PSIA)	DIFFERENTIAL PRESSURE (PSI)	FLOW RATE (SCC/S)	TEMPERATURE (DEG. F)	VISCOSITY (C POISE)	COMPRES-SIBILITY (Z)	PERMEABILITY VALUE (MICRODARCY)	STD. DEV. (%)
08-03	11:15	03:52	4928	1490.80	19.44	1.20E-003	98.00	0.02027	1.0103	2.00E-001	(2.0)
08-08	09:15	04:07	4162	705.39	19.78	6.15E-004	98.00	0.01902	0.9990	1.96E-001	(2.3)
08-09	14:00	02:37	3849	405.12	22.51	4.75E-004	98.00	0.01871	0.9981	2.28E-001	(1.3)
08-10	13:37	03:07	3755	306.73	25.51	4.55E-004	98.00	0.01864	0.9983	2.54E-001	(1.8)
08-11	16:10	00:30	5537	306.81	25.27	3.00E-004	98.00	0.01864	0.9983	1.69E-001	(1.9)
08-14	14:07	01:52	5529	314.76	39.92	4.55E-004	98.00	0.01864	0.9983	1.58E-001	(1.1)
08-15	14:12	01:48	5631	412.47	39.74	5.21E-004	98.00	0.01872	0.9981	1.39E-001	(1.3)
08-17	10:00	01:30	5934	708.92	36.50	6.50E-004	98.00	0.01903	0.9990	1.12E-001	(2.0)
08-18	13:20	01:40	6708	1489.25	41.20	1.28E-003	98.00	0.02026	1.0103	1.00E-001	(2.4)



MICROMERITICS PORE SIZER 9310

V1.04

PAGE 1

890507615

6/8/89

SFE #3 9321.1

2

PENETROMETER NUMBER 130163

PRESSURE PSIA	CORRECTED PRESSURE PSIA	PORE DIAMETER um	CUM. INTR. VOLUME cc/g	CUM. PORE SURFACE AREA m2/g	DIFF. INTR. VOLUME dV/:dD cc/g um	INCR. INTR. VOLUME cc/g
1.3	1.3	134.8712	0.0000	0.0000	0.0000	0.0000
2.3	2.3	77.5900	0.0002	0.0000	0.0000	0.0002
3.3	3.3	55.2083	0.0005	0.0000	0.0000	0.0003
5.0	5.0	35.9496	0.0005	0.0000	0.0000	0.0000
8.0	8.0	22.6815	0.0006	0.0000	0.0000	0.0002
10.2	10.2	17.7212	0.0006	0.0000	0.0000	0.0000
13.2	13.2	13.7454	0.0006	0.0000	0.0000	0.0000
15.0	15.0	12.0262	0.0008	0.0001	0.0001	0.0002
18.0	18.0	10.0429	0.0008	0.0001	0.0000	0.0000
20.2	20.2	8.9434	0.0008	0.0001	0.0000	0.0000
22.1	22.1	8.1724	0.0008	0.0001	0.0000	0.0000
25.1	25.1	7.2106	0.0008	0.0001	0.0000	0.0000
40.0	44.6	4.0513	0.0008	0.0001	0.0000	0.0000
61.0	65.6	2.7553	0.0008	0.0001	0.0000	0.0000
65.0	69.6	2.5970	0.0008	0.0001	0.0000	0.0000
70.0	74.6	2.4230	0.0008	0.0001	0.0000	0.0000
75.0	79.6	2.2709	0.0008	0.0001	0.0000	0.0000
80.0	84.6	2.1368	0.0008	0.0001	0.0000	0.0000
85.0	89.6	2.0176	0.0008	0.0001	0.0000	0.0000
90.0	94.6	1.9110	0.0008	0.0001	0.0000	0.0000
100.0	104.6	1.7284	0.0008	0.0001	0.0000	0.0000
125.0	129.6	1.3951	0.0008	0.0001	0.0000	0.0000
154.0	158.6	1.1401	0.0008	0.0001	0.0000	0.0000
160.0	164.6	1.0985	0.0008	0.0001	0.0000	0.0000
195.0	199.6	0.9059	0.0008	0.0001	0.0000	0.0000
202.0	206.6	0.8752	0.0008	0.0001	0.0000	0.0000
225.0	229.6	0.7876	0.0008	0.0001	0.0000	0.0000
242.0	246.6	0.7333	0.0008	0.0001	0.0000	0.0000
259.0	263.6	0.6860	0.0008	0.0001	0.0000	0.0000
279.0	283.6	0.6376	0.0008	0.0001	0.0000	0.0000
321.0	325.6	0.5554	0.0008	0.0001	0.0000	0.0000
330.0	334.6	0.5405	0.0008	0.0001	0.0000	0.0000
352.0	356.6	0.5071	0.0008	0.0001	0.0000	0.0000
385.0	389.6	0.4642	0.0008	0.0001	0.0000	0.0000
405.0	409.6	0.4415	0.0008	0.0001	0.0000	0.0000
428.0	432.6	0.4180	0.0009	0.0015	0.0064	0.0002
450.0	454.6	0.3978	0.0009	0.0015	0.0000	0.0000
500.0	504.6	0.3584	0.0009	0.0015	0.0000	0.0000
510.0	514.6	0.3514	0.0009	0.0015	0.0000	0.0000
534.0	538.6	0.3358	0.0009	0.0015	0.0000	0.0000
557.0	561.6	0.3220	0.0009	0.0015	0.0000	0.0000
581.0	585.6	0.3088	0.0009	0.0015	0.0000	0.0000

MICROMERITICS PORE SIZER 9310

V1.04

PAGE 2

890507615

5/8/89

SFE #3 9321.1

2

PENETROMETER NUMBER 130163

PRESSURE PSIA	CORRECTED PRESSURE PSIA	PORE DIAMETER um	CUM. INTR. VOLUME cc/g	CUM. PORE SURFACE AREA m2/g	DIFF. INTR. VOLUME dV:dD cc/g um	INCR. INTR. VOLUME cc/g
605.0	609.6	0.2967	0.0009	0.0015	0.0000	0.0000
629.0	633.6	0.2854	0.0009	0.0015	0.0000	0.0000
652.0	656.6	0.2754	0.0009	0.0015	0.0000	0.0000
678.0	682.6	0.2649	0.0009	0.0015	0.0000	0.0000
703.0	707.6	0.2556	0.0009	0.0015	0.0000	0.0000
731.0	735.6	0.2459	0.0009	0.0015	0.0000	0.0000
756.0	760.6	0.2378	0.0009	0.0015	0.0000	0.0000
781.0	785.6	0.2302	0.0009	0.0015	0.0000	0.0000
808.0	812.6	0.2226	0.0009	0.0015	0.0000	0.0000
833.0	837.6	0.2159	0.0011	0.0042	0.0226	0.0002
858.0	862.6	0.2097	0.0011	0.0042	0.0000	0.0000
884.0	888.6	0.2035	0.0011	0.0042	0.0000	0.0000
911.0	915.6	0.1975	0.0011	0.0042	0.0000	0.0000
935.0	939.6	0.1925	0.0011	0.0042	0.0000	0.0000
962.0	966.6	0.1871	0.0011	0.0042	0.0000	0.0000
989.0	993.6	0.1820	0.0012	0.0075	0.0296	0.0002
1001.0	1005.6	0.1799	0.0012	0.0075	0.0000	0.0000
1100.0	1104.6	0.1637	0.0014	0.0110	0.0093	0.0002
1202.0	1206.6	0.1499	0.0015	0.0148	0.0109	0.0002
1302.0	1306.6	0.1384	0.0020	0.0273	0.0393	0.0005
1402.0	1406.5	0.1286	0.0027	0.0499	0.0764	0.0008
1507.0	1511.5	0.1197	0.0032	0.0644	0.0505	0.0005
1597.0	1601.5	0.1129	0.0038	0.0851	0.0894	0.0006
1706.0	1710.5	0.1057	0.0044	0.1071	0.0836	0.0006
1804.5	1808.9	0.1000	0.0051	0.1363	0.1306	0.0008
1903.5	1907.9	0.0948	0.0060	0.1733	0.1739	0.0009
2000.0	2004.3	0.0902	0.0069	0.2123	0.1977	0.0009
4984.0	4988.1	0.0363	0.0123	0.5546	0.1003	0.0054
7976.0	7980.0	0.0227	0.0131	0.6566	0.0553	0.0008
9968.0	9972.0	0.0181	0.0137	0.7745	0.1328	0.0006
14928.0	14932.0	0.0121	0.0143	0.9335	0.0998	0.0006
19904.0	19907.9	0.0091	0.0147	1.1037	0.1490	0.0005
24896.0	24899.9	0.0073	0.0152	1.3244	0.2476	0.0005
29864.0	29867.9	0.0061	0.0153	1.4147	0.1244	0.0002
19984.0	19987.9	0.0090	0.0153	1.4147	0.0000	0.0000
9984.0	9987.9	0.0181	0.0153	1.4147	0.0000	0.0000
5000.0	5003.9	0.0361	0.0150	1.3704	0.0167	-0.0003
1004.0	1008.0	0.1794	0.0135	1.3146	0.0105	-0.0015
753.0	757.0	0.2389	0.0134	1.3117	0.0025	-0.0002
459.0	463.0	0.3906	0.0128	1.3041	0.0040	-0.0006
239.0	243.1	0.7441	0.0123	1.3009	0.0013	-0.0005
99.0	103.1	1.7546	0.0120	1.2999	0.0003	-0.0003

MICROMERITICS PORE SIZER 9310

V1.04

PAGE 3

890507615

6/8/89

SFE #3 9321.1

2

PENETROMETER NUMBER 130163

PRESSURE PSIA	CORRECTED PRESSURE PSIA	PORE DIAMETER um	CUM. INTR. VOLUME cc/g	CUM. PORE SURFACE AREA m2/g	DIFF. INTR. VOLUME dV:dD cc/g um	INCR. INTR. VOLUME cc/g
50.0	54.1	3.3415	0.0111	1.2985	0.0006	-.0009
23.0	27.1	6.6674	0.0111	1.2985	0.0000	0.0000
15.0	19.1	9.4562	0.0111	1.2985	0.0000	0.0000

Received: 05/25/89

Results by Sample

SAMPLE ID SFE-3 9321.1 FT FRACTION 15A TEST CODE CLAY NAME Clay Type Analysis by XRD
Date & Time Collected not specified Category _____

CLAY COMPONENTIAL ANALYSIS

CARBONATES (ACETIC ACID SOLUBLE) : 4
SILICATES & ALUMINO-SILICATES : 94
CLAYS-NORMALIZED TO 100% : 2
 Kaolinite + Chlorite : 12
 Illite-Montmorillonite : 36
 Expandable Clays : 52
 (Montmorillonite, Smectite, etc)

Note: N.D. = Not Detected

X-RAY DIFFRACTION PHASES PRESENT

Major: Quartz
Major-Minor:
Minor: Albite, Calcite
Minor-Trace: Clays

Note: All constituents were listed in a probable order of decreasing abundance.

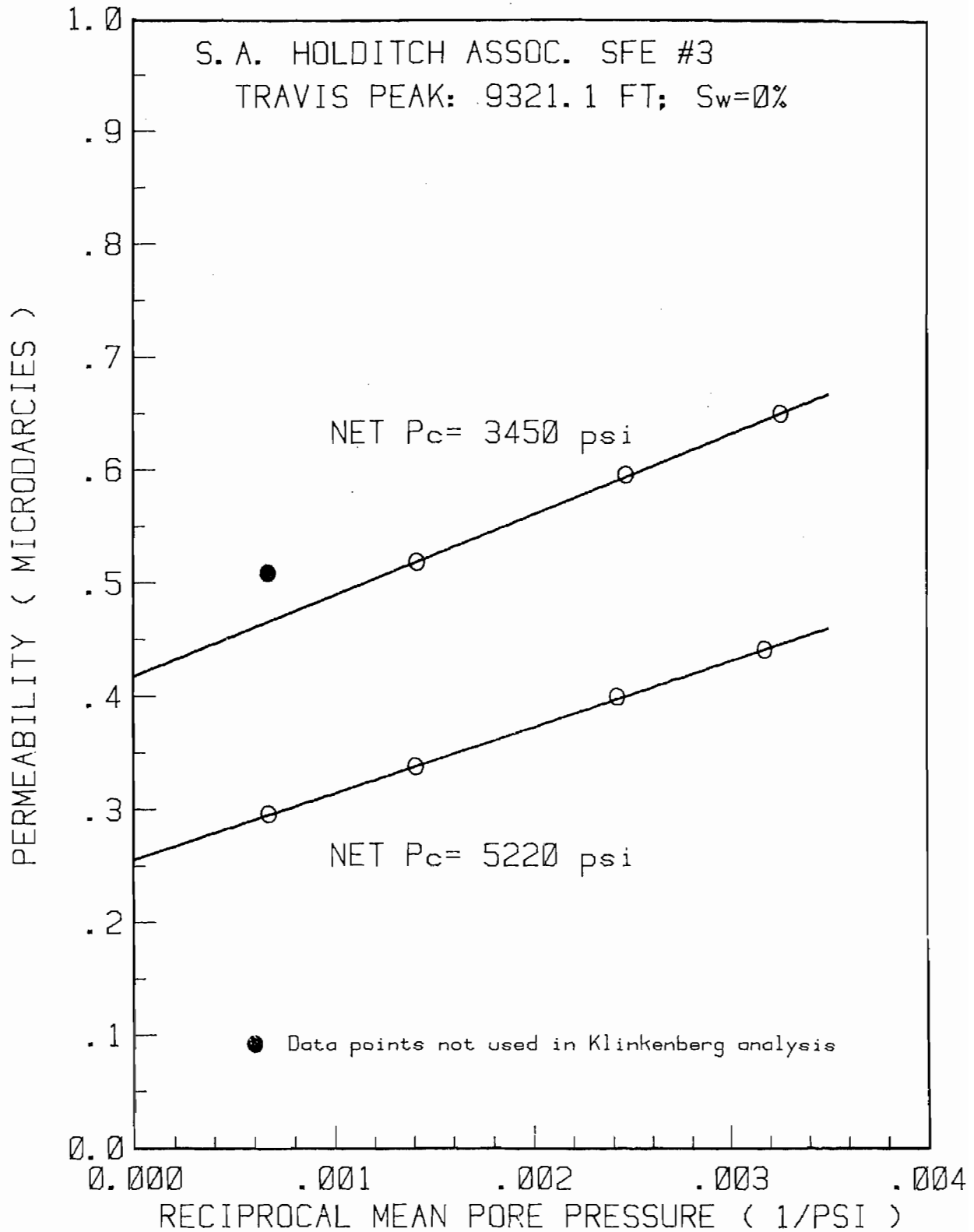
WELL NAME: S.A. HOLDITCH ASSOC. SFE #3

PLUG: TRAVIS PEAK: 9321.1 FT; Sw=0%

PLUG LENGTH: 5.174 CM

PLUG AREA: 5.044 CM²

TEST DATE (M-D)	BEGIN TIME (H:M)	DUR- ATION (H:M)	CONFINING PRESSURE (PSIA)	MEAN PORE P (PSIA)	DIFFERENTIAL PRESSURE (PSI)	FLOW RATE (SCC/S)	TEMPERATURE (DEG. F)	VISCOSITY (C POISE)	COMPRES- SIBILITY (Z)	PERMEABILITY VALUE (MICRODARCY)	STD. DEV. (Z)
08-03	09:55	01:07	4931	1490.79	19.50	3.04E-003	98.00	0.02027	1.0103	5.08E-001	(.9)
08-07	15:18	01:39	4161	705.40	19.82	1.60E-003	98.00	0.01902	0.9990	5.19E-001	(.7)
08-09	12:03	01:36	3854	405.12	22.53	1.22E-003	98.00	0.01871	0.9981	5.96E-001	(.6)
08-10	11:51	01:33	3760	306.73	25.56	1.15E-003	98.00	0.01864	0.9983	6.50E-001	(.6)
08-11	15:24	00:39	5539	306.74	25.44	7.84E-004	98.00	0.01864	0.9983	4.44E-001	(.7)
08-14	11:55	01:12	5531	314.75	39.98	1.26E-003	98.00	0.01864	0.9983	4.41E-001	(.5)
08-15	11:52	01:20	5633	412.49	39.76	1.48E-003	98.00	0.01872	0.9981	4.00E-001	(.7)
08-17	11:37	01:50	5933	708.92	36.43	1.93E-003	98.00	0.01903	0.9990	3.38E-001	(.8)
08-18	11:24	01:50	6709	1489.26	41.28	3.73E-003	98.00	0.02026	1.0103	2.96E-001	(1.0)



MICROMERITICS PORE SIZER 9310

V1.04

PAGE 1
6/12/89
10

890507616
SFE #3 9327
PENETROMETER NUMBER 130201

PRESSURE PSIA	CORRECTED PRESSURE PSIA	PORE DIAMETER um	CUM. INTR. VOLUME cc/g	CUM. PORE SURFACE AREA m2/g	DIFF. INTR. VOLUME dV/:dD cc/g um	INCR. INTR. VOLUME cc/g
1.3	1.3	142.5235	0.0000	0.0000	0.0000	0.0000
2.3	2.3	78.1938	0.0002	0.0000	0.0000	0.0002
3.3	3.3	55.5133	0.0002	0.0000	0.0000	0.0000
5.1	5.1	35.2558	0.0005	0.0000	0.0000	0.0003
8.3	8.3	21.9147	0.0005	0.0000	0.0000	0.0000
10.3	10.3	17.5970	0.0008	0.0001	0.0001	0.0003
13.1	13.1	13.8211	0.0008	0.0001	0.0000	0.0000
15.2	15.2	11.8981	0.0008	0.0001	0.0000	0.0000
18.2	18.2	9.9337	0.0008	0.0001	0.0000	0.0000
20.2	20.2	8.9593	0.0008	0.0001	0.0000	0.0000
22.1	22.1	8.1690	0.0010	0.0002	0.0002	0.0002
25.2	25.2	7.1745	0.0010	0.0002	0.0000	0.0000
40.0	44.6	4.0520	0.0010	0.0002	0.0000	0.0000
60.0	64.6	2.7982	0.0010	0.0002	0.0000	0.0000
65.0	69.6	2.5973	0.0010	0.0002	0.0000	0.0000
70.0	74.6	2.4233	0.0010	0.0002	0.0000	0.0000
75.0	79.6	2.2714	0.0012	0.0005	0.0011	0.0002
85.0	89.6	2.0179	0.0012	0.0005	0.0000	0.0000
86.0	90.6	1.9957	0.0012	0.0005	0.0000	0.0000
91.0	95.6	1.8913	0.0012	0.0005	0.0000	0.0000
101.0	105.6	1.7123	0.0012	0.0005	0.0000	0.0000
127.0	131.6	1.3740	0.0012	0.0005	0.0000	0.0000
140.0	144.6	1.2506	0.0013	0.0010	0.0013	0.0002
175.0	179.6	1.0069	0.0013	0.0010	0.0000	0.0000
181.0	185.6	0.9744	0.0013	0.0010	0.0000	0.0000
199.0	203.6	0.8882	0.0013	0.0010	0.0000	0.0000
225.0	229.6	0.7877	0.0013	0.0010	0.0000	0.0000
242.0	246.6	0.7334	0.0015	0.0018	0.0030	0.0002
259.0	263.6	0.6861	0.0015	0.0018	0.0000	0.0000
288.0	292.6	0.6181	0.0018	0.0038	0.0048	0.0003
307.0	311.6	0.5805	0.0021	0.0060	0.0087	0.0003
326.0	330.6	0.5471	0.0025	0.0084	0.0099	0.0003
352.0	356.5	0.5073	0.0033	0.0146	0.0207	0.0008
377.0	381.5	0.4741	0.0046	0.0254	0.0397	0.0013
401.0	405.4	0.4461	0.0063	0.0397	0.0588	0.0016
424.0	428.3	0.4223	0.0082	0.0579	0.0828	0.0020
450.0	454.2	0.3982	0.0114	0.0884	0.1301	0.0031
475.0	479.1	0.3775	0.0135	0.1104	0.1034	0.0021
498.0	502.0	0.3603	0.0153	0.1301	0.1051	0.0018
528.0	531.8	0.3401	0.0183	0.1639	0.1465	0.0030
555.0	558.8	0.3237	0.0201	0.1858	0.1105	0.0018
574.0	577.7	0.3131	0.0212	0.2002	0.1086	0.0012

MICROMERITICS PORE SIZER 9310

V1.04

PAGE 2
6/12/89
10

890507616

SFE #3 9327

PENETROMETER NUMBER 130201

PRESSURE PSIA	CORRECTED PRESSURE PSIA	PORE DIAMETER um	CUM. INTR. VOLUME cc/g	CUM. PORE SURFACE AREA m2/g	DIFF. INTR. VOLUME dV/:dD cc/g um	INCR. INTR. VOLUME cc/g
606.0	609.7	0.2967	0.0222	0.2132	0.0602	0.0010
630.0	633.6	0.2854	0.0232	0.2268	0.0881	0.0010
654.0	657.6	0.2750	0.0234	0.2291	0.0158	0.0002
679.0	682.6	0.2650	0.0240	0.2389	0.0655	0.0007
704.0	707.6	0.2556	0.0245	0.2465	0.0528	0.0005
730.0	733.5	0.2466	0.0250	0.2543	0.0546	0.0005
754.0	757.5	0.2388	0.0254	0.2598	0.0422	0.0003
780.0	783.5	0.2308	0.0257	0.2654	0.0416	0.0003
805.0	808.5	0.2237	0.0262	0.2741	0.0693	0.0005
831.0	834.5	0.2167	0.0267	0.2830	0.0709	0.0005
858.0	861.5	0.2099	0.0268	0.2861	0.0242	0.0002
885.0	888.5	0.2036	0.0270	0.2893	0.0258	0.0002
912.0	915.4	0.1976	0.0275	0.2992	0.0823	0.0005
925.0	928.4	0.1948	0.0277	0.3025	0.0595	0.0002
954.0	957.4	0.1889	0.0280	0.3094	0.0558	0.0003
981.0	984.4	0.1837	0.0283	0.3165	0.0636	0.0003
1010.0	1013.4	0.1785	0.0286	0.3237	0.0627	0.0003
1102.0	1105.3	0.1636	0.0293	0.3391	0.0443	0.0007
1211.0	1214.3	0.1489	0.0301	0.3602	0.0561	0.0008
1306.0	1309.3	0.1381	0.0305	0.3694	0.0305	0.0003
1407.0	1410.3	0.1282	0.0313	0.3941	0.0832	0.0008
1508.0	1511.2	0.1197	0.0316	0.4047	0.0384	0.0003
1610.0	1613.2	0.1121	0.0318	0.4104	0.0218	0.0002
1698.0	1701.2	0.1063	0.0323	0.4285	0.0852	0.0005
1810.0	1813.2	0.0997	0.0326	0.4413	0.0501	0.0003
1898.0	1901.2	0.0951	0.0328	0.4480	0.0357	0.0002
2000.0	2003.2	0.0903	0.0333	0.4693	0.1020	0.0005
4976.0	4979.0	0.0363	0.0362	0.6566	0.0549	0.0030
7968.0	7971.0	0.0227	0.0379	0.8798	0.1207	0.0016
9976.0	9978.9	0.0181	0.0382	0.9443	0.0721	0.0003
14976.0	14978.9	0.0121	0.0390	1.1624	0.1361	0.0008
19912.0	19914.9	0.0091	0.0397	1.4114	0.2201	0.0007
24888.0	24890.8	0.0073	0.0403	1.7337	0.3627	0.0007
29864.0	29866.8	0.0061	0.0408	2.0303	0.4080	0.0005
19992.0	19994.8	0.0090	0.0408	2.0303	0.0000	0.0000
10000.0	10002.8	0.0181	0.0407	1.9817	0.0182	-.0002
4984.0	4986.9	0.0363	0.0402	1.9090	0.0272	-.0005
1002.0	1004.9	0.1800	0.0382	1.8359	0.0137	-.0020
744.0	747.0	0.2421	0.0375	1.8234	0.0106	-.0007
481.0	484.0	0.3737	0.0370	1.8170	0.0038	-.0005
232.0	235.0	0.7695	0.0359	1.8090	0.0029	-.0012
96.0	99.1	1.8243	0.0339	1.8029	0.0019	-.0020

MICROMERITICS PORE SIZER 9310

V1.04

PAGE 3
6/12/89
10

890507616
SFE #3 9327
PENETROMETER NUMBER 130201

PRESSURE PSIA	CORRECTED PRESSURE PSIA	PORE DIAMETER um	CUM. INTR. VOLUME cc/g	CUM. PORE SURFACE AREA m2/g	DIFF. INTR. VOLUME dV/:dD cc/g um	INCR. INTR. VOLUME cc/g
49.0	52.3	3.4594	0.0308	1.7981	0.0019	-.0031
26.0	29.3	6.1721	0.0303	1.7977	0.0002	-.0005
13.0	16.3	11.0733	0.0296	1.7974	0.0001	-.0007

Received: 05/25/89

Results by Sample

SAMPLE ID SFE-3 9327 FT FRACTION 16A TEST CODE CLAY NAME Clay Type Analysis by XRD
Date & Time Collected not specified Category _____

CLAY COMPONENTIAL ANALYSIS

CARBONATES (ACETIC ACID SOLUBLE) : 3

SILICATES & ALUMINO-SILICATES : 95

CLAYS-NORMALIZED TO 100% : 2

Kaolinite + Chlorite : 21

Illite-Montmorillonite : 36

Expandable Clays : 43

(Montmorillonite, Smectite, etc)

Note: N.D. = Not Detected

X-RAY DIFFRACTION PHASES PRESENT

Major: Quartz

Major-Minor:

Minor: Albite, Calcite

Minor-Trace: Clays

Note: All constituents were listed in a probable order of decreasing abundance.

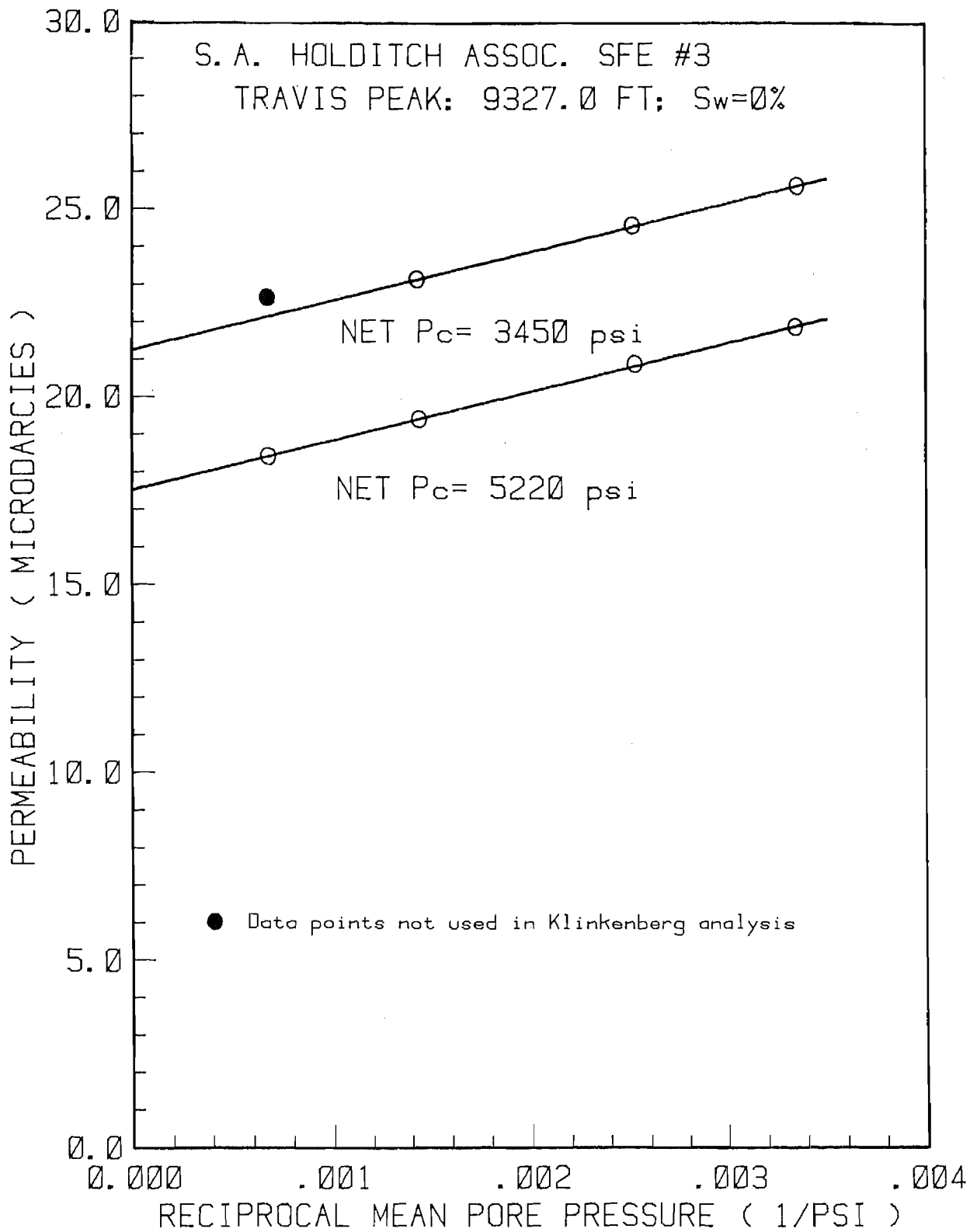
WELL NAME: S.A. HOLDITCH ASSOC. SFE #3

PLUG: TRAVIS PEAK: 9327.0 FT; Sw=0%

PLUG LENGTH: 5.093 CM

PLUG AREA: 5.047 CM²

TEST DATE (M-D)	BEGIN TIME (H:M)	DUR- ATION (H:M)	CONFINING PRESSURE (PSIA)	MEAN PORE P (PSIA)	DIFFERENTIAL PRESSURE (PSI)	FLOW RATE (SCC/S)	TEMPERATURE (DEG. F)	VISCOSITY (C POISE)	COMPRES- SIBILITY (Z)	PERMEABILITY	
										VALUE (MICRODARCY)	STD. DEV. (%)
08-02	14:54	00:07	4925	1485.50	9.69	6.99E-002	98.00	0.02026	1.0102	2.32E+001	(1.2)
08-03	16:35	00:09	4933	1486.10	10.18	7.16E-002	98.00	0.02026	1.0102	2.26E+001	(1.3)
08-07	13:26	00:08	4151	700.18	10.09	3.68E-002	98.00	0.01902	0.9990	2.31E+001	(.6)
08-09	09:05	00:15	3860	398.25	9.70	2.17E-002	98.00	0.01871	0.9981	2.45E+001	(.4)
08-10	08:54	00:12	3764	298.28	9.73	1.71E-002	98.00	0.01863	0.9983	2.56E+001	(.4)
08-11	16:46	00:05	5536	306.75	25.35	4.01E-002	98.00	0.01864	0.9983	2.24E+001	(.5)
08-14	16:25	00:10	5528	299.03	10.60	1.59E-002	98.00	0.01863	0.9983	2.18E+001	(.4)
08-15	09:57	00:10	5633	396.31	9.67	1.83E-002	98.00	0.01871	0.9981	2.09E+001	(.3)
08-17	14:53	00:05	5933	694.94	10.11	3.07E-002	98.00	0.01901	0.9989	1.94E+001	(.5)
08-18	15:45	00:06	6708	1473.04	10.34	5.87E-002	98.00	0.02023	1.0099	1.84E+001	(.8)



APPENDIX B.

Technical Papers and Journal Articles Published From This Project

SPE 17729

Comparison of Pore Geometry in High- and Low-Permeability Sandstones, Travis Peak Formation, East Texas

by D.J. Soeder and P. Chowdiah, Inst. of Gas Technology

Copyright 1988 Society of Petroleum Engineers

This paper was prepared for presentation at the SPE Gas Technology Symposium, held in Dallas, TX, June 13-15, 1988.

This paper was selected for presentation by an SPE Program Committee following review of information contained in an abstract submitted by the author(s). Contents of the paper, as presented, have not been reviewed by the Society of Petroleum Engineers and are subject to correction by the author(s). The material, as presented, does not necessarily reflect any position of the Society of Petroleum Engineers, its officers, or members. Papers presented at SPE meetings are subject to publication review by Editorial Committees of the Society of Petroleum Engineers. Permission to copy is restricted to an abstract of not more than 300 words. Illustrations may not be copied. The abstract should contain conspicuous acknowledgment of where and by whom the paper is presented. Write Publications Manager, SPE, P.O. Box 833836, Richardson, TX 75083-3836. Telex, 730989 SPEDAL.

ABSTRACT

Core analysis data have been correlated with petrographic observations of pore geometry for a number of sandstone samples from the Travis Peak Formation in East Texas. The results have also been compared with pore structure and core analysis data that had been obtained earlier for tight sands from Rocky Mountain basins.

Gas permeability for dry Travis Peak samples varied over a wide range, from less than 1 microdarcy to over 10 millidarcies. Some of the observed high permeabilities were due to fractures in the sample plugs, but most represented true matrix permeability. Samples with dry gas permeability of the order of 10 microdarcies or less contained secondary solution pores interconnected by narrow slots, much like pore structures observed in the Mesaverde and Frontier tight sands from the Rocky Mountains.

Higher permeability samples had a pore structure dominated by primary intergranular porosity, infilled and plugged up to a greater or lesser degree with authigenic clay minerals and carbonates. Intermediate stages of solution pore/slot pore development were observed in some of the Travis Peak samples. This had not been seen in earlier studies involving Rocky Mountain tight sands, where the development of secondary porosity is in an almost uniformly mature stage.

The higher permeability sandstones containing grain-supported pores were much less sensitive to stress. Also, plots of the "Swanson" parameter from mercury porosimetry data versus sample permeability are influenced significantly by the rock pore structure. Data for samples with grain-supported pores were in close agreement with available correlations for conventional sandstones. On the

other hand, data for lower permeability samples where flow is controlled by the slot pores showed significant deviations from these correlations. The results indicate that microscopic observations of pore structure combined with routine mercury porosimetry analyses can provide a useful tool for classifying and assessing tight sands.

INTRODUCTION

Over the past seven years, the Institute of Gas Technology (IGT) has been performing petrographic and petrophysical analyses on tight gas sandstone core aimed at trying to understand how the pore structure of these rocks influences properties such as pore volume compressibility, stress-dependence of permeability, and two-phase flow. These analyses are currently concentrated on the Cretaceous-age Travis Peak Formation in eastern Texas, which is the subject of a number of production and stimulation staged field experiments funded by the Gas Research Institute (GRI). Several piggyback coring operations were mounted a few years ago by GRI and, more recently, research has been performed on wells specifically drilled for the staged field experiments (SFE). IGT has analyzed approximately 40 samples from the piggyback cores and from the SFE cores, which cover a fairly wide range of depositional environments, diagenetic histories, petrophysical properties and pore morphologies.

The results of these analyses have convinced us that tight sandstone is a unique rock type, possessing distinct petrologic and petrophysical properties that separate it from "conventional" high permeability sandstones. As such, we have concluded that "tight sand" is more than just an F.E.R.C. designation for low permeability gas reservoirs, but refers to a recognizable petrology as well. IGT's research has shown that although many of these sands were deposited from different sources into different sedimentary environments, the resulting tight sands possess a number of remarkably similar petrological and petrophysical characteristics. Increased

References and illustrations at end of paper.

understanding is needed of the diagenetic alterations to grains and pores which change unconsolidated fluvial, deltaic and marine sands into similar, highly indurated, low permeability rocks.

Work on the Travis Peak Formation of eastern Texas over the past few years has given us the opportunity to analyze both tight sands and sands with conventional permeabilities from the same formation a few dozen miles apart. From these data it appears that a "transition zone" between conventional sands and tight sands can be recognized. This paper describes observations of these transitional sands, and details our perception of the petrologic differences between tight sands and sands with conventional permeabilities.

TECHNIQUES AND APPARATUS

Analyses of rock samples at IGT utilize a high-resolution permeameter, complimentary petrographic microscope observations, and a number of analytical chemistry procedures. These techniques are described in more detail below.

Tight sandstone core analysis at IGT is performed using a high-resolution, steady-state apparatus known as the Computer Operated Rock Analysis Laboratory, or CORAL. This device consists of four stainless-steel coreholders with associated tubing and fluid supplies in an isothermal chamber. The circulating air bath in the chamber is maintained at $\pm 0.01^\circ\text{F}$ [0.0056°C] of a selected setpoint. This accurate temperature control makes possible the high sensitivity of the CORAL system by allowing the use of reference pressures that are stable to about one part in 50,000. Steady-state flow rates, measured by sensitive differential pressure sensors on downstream lines, are averaged and recorded on magnetic disk by a microcomputer at operator-selected time intervals, together with temperature, confining pressure, and tank pressures. The computer-control and data logging features make CORAL extremely effective for measurement of ultra-low gas permeabilities, and it can measure actual gas flow with a resolution of 10^{-6} std. cm^3/sec . The device can also measure sample porosity under representative confining stress, and it collects pore volume compressibility data during routine net confining stress increases. Further details concerning the operation and capability of the CORAL can be found in Randolph's¹ 1983 paper.

Documentation of the pore structure of samples measured in the CORAL has been found to be a useful procedure for understanding some of the measured petrophysical properties.² This can be performed using both optical microscopy and scanning electron microscopy (SEM). We have found the optical microscope to be best for observing overall pore geometry and structure, while the SEM is better for identifying pore minerals and the nature of grain contacts in the sample.

Observation of rock samples with an optical microscope can be performed one of two ways: The light can either be reflected from the surface of the rock, or the sample can be sliced and ground thin enough so that the mineral components are capable of transmitting the light when the slice is illuminated from behind. Samples sliced in this

manner are known as "thin sections," so called because they are ground down to a standard thickness of only 30 micrometers. To observe the pore spaces in the thin section, the rock sample is first impregnated with a blue-dyed epoxy plastic before the section is prepared. The blue epoxy fills the pore space, making most larger pores visible under the microscope. However, in tight sands containing narrow, linear fracture porosity, microporous chert, clay, or organic materials, the blue dyed epoxy is difficult or impossible to see in a thin section. A solution to this problem was developed in 1984 by Robert Gies³ of Canadian Hunter Exploration, Ltd., in Calgary. Gies simply replaced the blue dye in the epoxy with a fluorescent dye, rhodamine-B, and studied the thin sections using incident-light fluorescence microscopy, a technique that has long had extensive medical, biological, and industrial applications. The rhodamine B dye in the pores fluoresces strongly when illuminated by an incident light beam of a specific exciter wavelength. A dichromatic interference filter allows only the rhodamine fluorescence to reach the eyepiece of the microscope, blocking all other wavelengths. This helps to make the pore structure even more visible by "blacking out" the mineral grains. The incident-light approach of fluorescent microscopy permits this technique to be applied to opaque materials such as shale and coal. In addition, the natural red color of rhodamine B shows up under transmitted light, preserving all of the features of the blue dye method. The fluorescent rhodamine dye in the pores and the blacked-out mineral grains also produce a very nice binary image, which requires little in the way of processing prior to image analysis.

Petrographic observations on tight sandstone cores have revealed that three main classes of pore geometry⁴ occur in these rocks:

- 1) Grain-supported primary pores, with the throats plugged by clay, calcite or other authigenic minerals, where the rock may or may not show some development of secondary solution pores. This is the classic type of tight sand described by Wilson,⁵ and is basically a conventional sand made tight by precipitation of minerals in the pore throats. These sands generally exhibit low pore volume compressibility, and equally low stress-dependence of permeability.
- 2) Highly-altered primary porosity, extensively filled-in with authigenic minerals, usually quartz overgrowths, coupled with significant amounts of secondary solution pore development, which makes up the bulk of the rock's porosity. Primary porosity is reduced to narrow, flat "slot" pores, which occur along the boundaries of adjoining quartz overgrowths. These slots are typically only about 0.1 micrometer in width under reservoir net stresses,² and are propped open by irregular bumps or "asperities" on the faces of the adjoining overgrowths.⁶ Although most of the porosity occurs in the solution pores, the only connection between individual secondary pores is commonly by way of the slots. Thus the narrow slots provide a bottleneck for movement of pore fluids and make the rock tight. The flat, poorly supported structure of

the slots is responsible for the high stress-dependence of permeability in these types of tight sands, and the narrow, uniform openings are highly susceptible to capillary blockage by imbibed water. Secondary solution pores interconnected by slots is the most common type of pore geometry observed by us in tight sands,² including the Travis Peak.

- 3) Ultrafine microporosity in an all-pervading matrix composed of clay, carbonate or silica, in which sand-sized quartz grains, which may or may not be honeycombed, are suspended. This is a relatively rare type of tight sand pore geometry that tends to exhibit a high degree of pore volume compressibility because of the lack of strong grain-to-grain support. Stress dependence of permeability may or may not be high, depending on the composition of the matrix. Calcite and silica matrices are much more stress resistant than clay, and the presence of honeycombed grains adds to the resistance by providing additional supported flowpaths. The effects of water imbibition on gas flow through this type of pore geometry are also somewhat variable; but, in general, pores of this nature are very small and easily plugged.

Individual tight sand samples often contain more than one class of pore geometry, although a single class usually predominates. Schematic drawings illustrating the differences between the three classes of pore geometry are shown in Figure 1.

Samples for the analyses described in this paper were obtained from two wells cored into the Travis Peak Formation in eastern Texas. The Travis Peak is Lower Cretaceous in age, and was deposited as a complex of delta lobes on a broad, shallow shelf in Texas, Louisiana, and Mississippi.⁷ Much of the initial delta deposits were reworked by fluvial and marine processes as the depocenters for the sediment shifted back and forth across the shelf. The uppermost part of the Travis Peak was deposited in a delta-fringe system that reflects the transition from terrestrial fluvial-deltaic deposition to nearshore, shallow marine shelf deposits.

The Travis Peak core utilized in this study came from two wells: Prairie Producing, #1 A.T. Mast et. al "A-1" well, Naconiche Creek field, Nacogdoches County, Texas, and S. A. Holditch & Associates, #5 Howell well, Waskom field, Harrison County, Texas. The Howell well was designated as GRI Staged Field Experiment (SFE) #1. The locations of both wells are shown on the map in Figure 2. The Travis Peak in the Howell well was significantly more porous and permeable than that in the Mast well. Sample plugs were cut from zones in the cores that consisted of uniform, unfractured, clean sandstone. Productive sands were sampled whenever possible, and about a dozen plugs were taken from each core.

The initial dry core measurements were made after the plug samples had been dried to constant weight at 60°C under 45% relative humidity. The controlled humidity drying removes all free pore water but retains proper clay mineral hydration, thereby avoiding significant damage to clay pore structures and the associated inaccuracies in permeability

measurement.⁸ The plugs were placed in thin lead sheaths after drying to prevent high pressure gas in the pores from diffusing into the rubber confining sleeves during core analysis. As part of the sample preparation procedure, rock slices one quarter of an inch (6.4 mm) in thickness were cut from the ends of each plug to provide samples for mercury porosimetry, scanning electron microscopy and thin sections.

Measurement of the reservoir properties of the humidity-oven dried cores consisted of the following standard procedures:

- Measure gas porosity and permeability at a mean pore pressure of 1500 psia [10.34 MPa] under a net confining stress of 1000 psi [6.89 MPa]. These are essentially "unconfined" measurements for comparison to "unstressed" core analysis data obtained by commercial labs on samples from this core.
- Raise cores to initial reservoir net stress while maintaining a pore pressure of 1500 psia [10.34 MPa]. Measure gas porosity at 1500 psia mean pore pressure. Measure permeability to gas at a variety of mean pore pressures between 1500 psia [10.34 MPa] and 300 psia [2.07 MPa].
- Increase net confining stress to 1/2 drawdown value while maintaining a pore pressure of 300 psia [2.07 MPa]. Pore volume compressibility was measured during this step.
- Measure gas permeability at 1/2 drawdown net confining stress at mean pore pressures from 300 to 1500 psia [2.07 to 10.34 MPa]. This measurement allowed the stress dependence of permeability to be determined.
- Maintain pore pressure at 1500 psia [10.34 MPa], but decrease the confining stress to initial reservoir net confining stress value. Rerun 1500 psia [10.34 MPa] gas permeability to check for hysteresis caused by the excursion to high net stress. Remove and weigh cores.

The pore pressure values were chosen to provide a uniform point spread on the Klinkenberg permeability plots, and the net confining stress values were determined from pressure measurements obtained during well testing.

Samples taken directly off the plug ends were used for mercury porosimetry, SEM, and optical microscopy studies to insure that there was no variation in lithology among these samples. Porosimetry was performed using a Micromeritics Model 9310 mercury porosimeter for semiautomated measurements of pore size distribution, pore volume and pore area for intrusion pressures of up to 30,000 psia [207 MPa].

Tight petrographic samples are impregnated at IGT using a two-stage process to insure that the epoxy works its way well into the pore volume. The rock sample is first placed under a vacuum in a small plastic beaker to remove air and other gases from the pores. Then, while still under vacuum, the small beaker is half-filled with degassed epoxy, completely covering the rock sample. In the second stage of the process, a rubber membrane is secured over the top of the plastic beaker and the epoxy-

covered sample is placed in a small pressure chamber. The epoxy is forced into the pore system under a hydraulic pressure of up to 2000 psia [13.8 MPa], well above the deduced highest capillary pressures for these rocks. After remaining under pressure for several hours, the rock is removed and the epoxy cured in an oven. We utilize a low-viscosity casting epoxy for impregnation to achieve the best results.

Once the rock has been impregnated, a flat-ground surface of the sample is glued to a flat-ground glass slide. The bulk of the sample is then trimmed away in a cut-off saw, and the thin slice remaining on the slide is ground and polished down to 30 micrometers, and then finished with a cover slip.

CORE ANALYSIS RESULTS

Tables 1 and 2 summarize the important dry core analysis results for samples from the SFE #1 and Prairie Mast A-1 wells, respectively. The tables list values measured at initial reservoir net stress, as well as at a net stress representative of the midpoint of reservoir drawdown. For some of the Mast A-1 samples, two sets of data at initial reservoir net stress are shown. The first of these corresponds to data measured during the first increase of net confining stress. The second set is data obtained along a decreasing net stress path following the measurement at midpoint drawdown net stress. The stress dependence of permeability is represented by the factor α , based on the empirical equation:

$$k = k_0 (P_{net})^{-\alpha} \quad (1)$$

Higher values of α indicate a greater effect of stress on permeability. The permeability values reported in Tables 1 and 2 are Klinkenberg permeabilities where gas slippage data could be measured. For high permeability samples ($k > 100 \mu d$) and some of the samples that contained fractures, the reported value is permeability measured at a high enough pore pressure to render gas slippage effects insignificant.

The Travis Peak data in this paper have been compared with data measured earlier by IGT on Mesaverde Group tight sandstone from the Rocky Mountains. Data on these 43 samples are available in references 10 and 11.

Porosity and Permeability

Figure 3 is a plot of porosity at half-drawdown net stress versus depth for the Travis Peak Sandstones. It is obvious from the plot that there is a strong drop-off in porosity with increasing depth, at least as deep as 9240 feet [2816.4 m]. Porosities are higher in the 9930 to 9960-foot [3026.7 to 3035.8 m] depth range. According to information supplied by Holditch Associates,⁹ the pore pressure gradients measured in the Mast well ranged from the approximately hydrostatic value of 0.44 psi/ft [9.96 kPa/m] at 8852 feet [2698.1 m] to the slightly overpressured gradient of 0.49 psi/ft [11.09 kPa/m] at a depth of 9602 feet [2926.7 m]. This slight overpressuring may have been responsible for the more complete dissolution of mineral grains to form solution pores, resulting in somewhat higher average porosity in this zone. Porosity of the

deepest sample, 9984.9 ft [3043.4 m], appears to fit into the porosity versus depth trend established by the cores in the upper part of the plot.

Figure 4 is a plot of permeability to gas at half-drawdown net stress as a function of depth for the samples from the Mast A-1 and SFE #1 wells. The plot shows a general trend of decreasing permeability with increasing depth, which is most evident when one traces the lowest permeability measured for each interval. The Mast A-1 samples show a large variation in permeability, primarily because some of the sample plugs supplied to us contained small fractures that contributed significantly to gas flow. The four highest permeability Mast A-1 samples (9935.5, 8666.2, 9937.7, and 9226.0) contained visible cracks. In addition, sample 9231.9 also contained a visible crack, but the core analysis results suggest that the crack closed off at high net stress.

Figure 5 is a plot of permeability to gas versus porosity at half drawdown net stress. Also included in this plot are data for 43 samples of the Mesaverde Group tight sand from the Multiwell Experiment (MWX) in Colorado, denoted by crosses. The plot displays only a fair correlation as is common with porosity-permeability plots, but shows a general trend of increasing permeability with increasing porosity. A significant feature of this plot is the dramatic difference between the SFE #1 data and the majority of the rest of the data. The MWX samples, which primarily had a slot-and-solution pore type of morphology (class 2, described earlier) lie within a fairly narrow range of porosity and permeability. Except for the four highest permeability samples, which contained fractures, the Mast A-1 data differ only slightly from the MWX data. The SFE #1 data, on the other hand, are distinctly different.

It appears that the observed variations in the range of petrophysical properties between the Travis Peak in the Mast A-1 core, and that in the SFE #1 core, are primarily related to fundamental differences in the pore geometry of these rocks. Nevertheless, as shown in Figures 3, 4, and 5, the much higher porosity and permeability values measured in the SFE #1 core dovetail neatly into the trends established by the earlier analyses on tighter rocks. This suggests to us that a continuity exists between the pore morphology of tight sands and that of conventional sands. Studies of sands in the "transition zone" between high and low permeability can provide insight into the processes which transform an unconsolidated sand deposit into a gas-bearing tight sandstone.

Pore Geometry of the Travis Peak Sandstone

Fresh, unconsolidated deposits of sand-sized sediment typically contain approximately 50% porosity. As the sand is buried and compacted by the weight of overlying sediment, this "primary porosity" is reduced to about 25%. Precipitation of minerals from solution in the pore waters may reduce the porosity still further, to 10% or less. Conversely, dissolution of sand grains by pore fluids may create additional pore volume. This "secondary porosity" generally occurs at sites occupied by sand grains composed of minerals which are unstable in a sedimentary environment, such as

orthoclase and plagioclase feldspars, amphiboles, pyroxenes and other mafic minerals. Dissolution of these minerals places many chemical species into solution in the pore fluids, which may later precipitate out as silica, clay minerals, carbonates, sulfides and others. Sandstones are made "tight" by these processes of grain compaction, dissolution, authigenic mineral precipitation, and other alterations to the pore morphology during burial and diagenesis.

Figure 6 is a pair of photomicrographs showing the grain and pore structure of a high permeability Travis Peak sandstone from a depth of 6122.8 ft (1866.2m) in the SPE #1 well. This core has a measured dry gas permeability of about 25 millidarcies, and a porosity of nearly 18%. The transmitted, plane-light view on the left shows that although some clays have precipitated in the pores and quartz overgrowths have formed on the grains, significant amounts of primary porosity remain, and the relatively open pore system is well interconnected. This is shown better in the epifluorescence view of the same field on the right, which indicates that many of the clayey areas are quite porous. Secondary porosity appears to be fairly common in this sample, accounting for the high porosity, and good interconnections of the secondary pores, either directly or by way of the open primary pores, are responsible for the high permeability of the sand.

For comparison, photomicrographs of a typical tight sandstone are shown in Figure 7 for the Travis Peak from a depth of 9954.9 ft. (3034.25m) from the Mast A-1 well. This sample has a measured dry gas permeability of approximately 13 microdarcies and a porosity of about 5%. The photo on the left, taken in transmitted light through crossed polars, shows the close, interlocking grain structure common in tight sandstones. This is usually caused by the precipitation of syntaxial quartz overgrowths on sand grains and is only very rarely a product of quartz pressure solution. The overgrowths expand into the primary pore spaces and form the flattened, interlocked grain network when the crystal faces join and grow against one another. Quartz precipitated as overgrowths generally fills most, if not all of the primary porosity, reducing it to narrow, flat, "sheet-like" or "slot-like" pores between abutting overgrowth faces. It is not known why the two adjoining overgrowths leave these narrow void spaces instead of completely suturing together, but it may be due to differences in orientation of the crystal axes, or to the inability of solution-bearing pore fluids to migrate into an opening smaller than a certain minimum size. SEM examination² shows that the slot-shaped voids between adjoining overgrowths are propped open by small surface irregularities on the faces of the overgrowths, referred to as "asperities" by Ostensen⁶ and assumed to have a Gaussian distribution. Slot pores are common in almost every tight sand examined by IGT, including the Mesaverde, Frontier, and Spirit River from Rocky Mountain basins, the Travis Peak from the Gulf Coast, and the Clinton from the Appalachian Basin. Such a widespread occurrence throughout time and space suggests that slot pores are a common denominator in tight sands, and provide a recognizable petrological feature by which to distinguish these rocks.

Since the quartz overgrowths fill up most of the primary porosity, tight sands would be non-economic as gas reservoirs unless significant additional pore volume was created in the rock. Fortunately, most of these sands contain a moderate amount of secondary solution porosity, as shown in the epifluorescent view in Figure 7. The secondary pores represent the sites of dissolved, unstable mineral grains, some of which still contain remnants of the original minerals. These secondary pores contain most of the sandstone's porosity (and gas), but compared to the pores visible in the permeable sandstone in Figure 6, they are not very well connected together. Gas must traverse the narrow slot pores to move between the solution pores in the Figure 7 sample, and the narrow slots, which are barely visible in the epifluorescence view, provide a bottleneck to flow and make the rock "tight." In addition, these narrow pores are easily plugged by capillary action at fairly low water saturations, and the flat, sheet-like morphology makes them quite susceptible to closing down at elevated net confining stress.

Although permeability is the main indicator of whether or not a sandstone is "tight," core analysis alone is sometimes not a reliable indicator. For example, the epifluorescent photomicrographs of the two samples in Figure 8 clearly show that the sample on the left (Mast-9935.1) contains a slot-pore/solution-pore morphology with a natural fracture cutting across the photograph. This fracture was barely visible to the unaided eye, although it is prominent in the thin section. Core analysis data show that the fractured sample has a permeability of about 10md. The sand on the right (SFE #1-6189.2) has very nearly the same permeability (9md), but obviously contains a "conventional" pore structure. Although routine core analysis may have missed the fracture in the Mast-9935.1 core and classed it as a non-tight sandstone, simple petrographic observation reveals the true pore morphology of the rock. Although this is a rather simple illustration of the complexities of tight sand, the two samples in Figure 8 can be used to demonstrate the effectiveness of another rapid, low-cost analytical technique for assessing pore geometry and reservoir quality in these rocks, namely, mercury porosimetry. Mercury porosimetry measures the amount of mercury metal intruded into the pores of a sample as a function of pressure. The median pore size determined from the porosimetry data for the sandstones shown in Figure 8 was 0.078 micrometers for Mast-9935.1, and 1.389 micrometers for SFE #1-6189.2. These data quickly and clearly indicate that the Mast sample has a much smaller average pore size than the SFE #1 sample and, therefore, it can easily be deduced that the similar permeabilities are probably due to the presence of a permeable pathway, such as a fracture, in the core with the smaller average pore size. More results from the mercury porosimetry work are given in a later section.

Core analysis work at IGT on a fairly large number of tight sandstone samples has shown that the dry permeability of slot-pore sandstone tends to range between 0.1 and 10 microdarcies.¹⁰ The more conventional sands, with flowpaths comprised of relatively open, grain-supported primary porosity, tend to have dry permeabilities above a millidarcy. A number of Travis Peak cores from the

SFE #1 well have dry gas permeabilities which fall between these two end member regions, and represent sands that are transitional between the slot-pore tight sands and the more conventional sands which contain significant primary porosity. Photomicrographs in epifluorescence of two of these samples from the SFE #1 core are shown in Figure 9. The left photomicrograph in this figure is SFE #1-7423.8, which has a measured porosity of about 10%, and a dry gas permeability of approximately 0.6 md. The photomicrograph on the right is SFE #1-7457.8, with a porosity of about 7.9% and a dry gas permeability of 0.55 md. Although the permeability values indicate that these sands fall into the transitional zone between "conventional" and "tight," we were excited to find that petrographic analysis also appears to show pore morphologies reflecting this transition. The pore geometry in SFE #1-7423.8, on the left side of Figure 9, is comprised mainly of compacted primary porosity, visible as the triangular or polygonal areas. A relatively small amount of solution porosity is visible; these pores appear fuzzy in epifluorescence, indicating that a significant quantity of microporosity is present, either within authigenic clays or in the dissolving, remnant mineral grains. The flat, angular sides on many of the grains represent the edges of syntaxial quartz overgrowths, some of which can be seen encroaching into primary pores. Linear porosity along grain boundaries is visible in much of the sample, especially between grains that show quartz overgrowth formation. More significant pore alteration is apparent in the companion photomicrograph of SFE #1-7457.8 on the right side of Figure 9. Solution pore development is more advanced, and most of the primary porosity has been reduced to remnants between quartz overgrowths. Linear porosity along grain boundaries is strikingly well-developed, and some of the grain surfaces contain irregular features that appear to prop the linear pores open. Whether or not these are Ostensen's⁶ "asperities" is debatable, but the presence of apparent partially-formed slots in a transitional sand is interesting and important. Although the linear, grain boundary pores in both photos in Figure 9 do not yet seem to represent the main flowpaths for gas through these rocks, it is not too difficult to imagine that continued alteration of the pores in samples like these could result in rocks with a pore morphology similar to that shown previously in Figure 7.

Finally, the photomicrographs in Figure 10 show what occurs when pore alteration proceeds beyond normal tight sandstone conditions. The samples shown in Figure 10, Mast-9229.3 on the left and Mast-9984.9 on the right, represent two of the tightest, lowest porosity slot-pore sands analyzed by IGT from the Travis Peak. The 9229.3 core has a measured porosity of about 4.3% and a dry gas permeability of about 1.3 microdarcy, and the 9984.9 core has a porosity of only 2.8% and a dry permeability of about 0.045 microdarcy. Porosity reduction in both of these samples to levels significantly lower than usual for productive tight sands appears to be mainly due to massive quartz precipitation into solution pores. Although the slot dimensions in these two cores are about the same as in the other tight sands, and permeabilities are comparable, the low porosities would strongly affect the economic viability of gas production from these sands.

Many of the features in tight sandstone pore morphology described above correlate well with a number of reservoir properties measured in the laboratory for these sandstones, as will be detailed in the following section. An important implication of this is that petrographic determination of pore morphology can serve as a useful tool, especially when combined with mercury porosimetry, for making rapid assessments of tight sandstone reservoir quality.

Stress Dependence

Figure 11 shows a plot of pore volume compressibility versus permeability for the Travis Peak and Mesaverde sandstones. The pore volume compressibilities were measured during net confining stress increase from initial reservoir conditions to half-drawdown conditions. The plot again emphasizes the narrow range of permeabilities encountered in the Mesaverde cores studied at IGT, and the large permeability range in the Travis Peak cores. The Travis Peak samples, in general, yielded lower values of pore volume compressibilities than the Mesaverde samples. A very slight tendency towards increasing pore volume compressibility with decreasing permeability is observable in the Travis Peak data. However, since pore volume compressibility depends not only on the geometry of the flow passages which move under compression, but also on the total porosity of the sample, it is not as directly relatable to the pore geometry. Stress-dependence of permeability, on the other hand, does correlate with pore morphology because any change at flow controlling apertures directly affects measured permeability.

Figure 12 shows the factor α for stress-dependence of permeability plotted against permeability. The plotted α values correspond to the first increase of net stress from initial reservoir conditions to half-drawdown conditions. The Mast A-1 samples which contained visible fractures are marked with the letter "F." These samples showed a larger stress-dependence of permeability due to closure of the fracture with increasing stress. Figure 12 shows a variation in stress-dependence that correlates with the variation in pore morphology within the Travis Peak. The extremely low stress-dependence of the high permeability SFE #1 samples is typical of media with grain supported pores, where the movement of grains under compression has little effect on the size of flow controlling apertures. As one moves to lower permeabilities, the Mast A-1 and MWX data show increasing stress-dependence, characteristic of flow controlled by narrow slots at grain boundaries. For this pore geometry, a small movement of the grains under compression affects the width of the slots considerably and can cause drastic reductions in permeability. The value of α in the neighborhood of 1.0 for the tight sandstones is consistent with the model developed by Ostensen⁶ for stress-dependence of permeability in slot pores propped open by asperities.

Swanson Parameter

The "Swanson parameter" $(S_b/P_c)_{max}$ is a parameter derived from unconfined sample mercury penetration data that was found by Swanson¹² to correlate very well with dry sample permeability for conventional

sandstones. The parameter is calculated as the maximum value of the ratio of mercury saturation (S_b) as a percent of bulk volume to the corresponding capillary pressure (P_c) along the capillary pressure curve. The same parameter has since been used to correlate tight sands data^{13,14} and has been found to correlate well, though differently from conventional sandstone.

Figure 13 shows the dry sample permeability at half-drawdown net stress for both Mesaverde and Travis Peak samples plotted against the Swanson Parameter. The Mast A-1 samples that contained visible fractures are marked by the letter "F" in Figure 13, since the measured permeabilities for these samples were anomalously high. A comparison of the pore morphology in the highest permeability "F" sample, with the pore geometry of the SFE #1 sample having a similar permeability, was shown in Figure 8. This comparison clearly indicates that the high permeability of the Mast core is due to a fracture. Also shown on the plot for comparison are the correlations developed by Swanson for routine air permeability (dashed line) and brine permeability of clean sandstones at 1000 psi [6.89 MPa] net stress (dotted line). Data for the high permeability SFE #1 samples are seen to agree extremely well with Swanson's correlation. The grain-supported pore morphology in these sandstones is typical of that in conventional sandstones. Furthermore, the low stress dependence of reservoir properties associated with such a pore geometry explains why Swanson's correlation, derived from data at a minimal confining stress, is also comparable to our data measured under several thousand psi net stress.

It is seen that as one moves to samples with lower permeability like the Mast A-1 samples, the gradual emergence of a slot pore/solution pore morphology results in larger deviations from Swanson's correlations. The lowest-permeability Mast A-1 samples with fully developed slot pores and secondary porosity behave in a manner similar to the Mesaverde sandstones, which also have well-developed secondary porosity connected by slots. It is possible that the observed deviation from Swanson's low net stress correlations in this permeability regime are a direct result of the high Klinkenberg effect and stress sensitivity that can be expected when narrow slots control the flow.

CONCLUSIONS

Although the correlations reported in this paper between pore morphology and petrophysical properties in sandstone are still somewhat preliminary in nature, we feel that the data are strong enough to conclude that the petrographic analysis does, indeed, show a fundamental change in the pore geometry between conventional sands and tight sands. This observation is somewhat contrary to the older view of tight sands, which proposed that virtually all contain grain-supported, primary porosity identical to conventional sands, but with the pore throats plugged by authigenic clay minerals.⁵ Our results indicate that primary porosity is actually quite low in typical tight sands, and has commonly been reduced to remnant "slot" pores between adjoining quartz overgrowths on sand grains. Much of the pore volume in tight sands is secondary in nature, although flowpaths between

the secondary pores often consist of slot pores.¹⁰ Observations of sands with intermediate permeabilities suggest that a "transitional zone" between tight sand and conventional sand can be recognized petrographically, with highly-altered, slot-pore tight sands as one end member, and conventional sands containing only slightly altered primary porosity as the other end member. "Transitional" sands contain aspects of both end members.

The petrologic aspects of sands intermediate between conventional and tight are reflected in the petrophysical properties measured by core analysis. Properties such as permeability, mean pore size, capillary entry pressure and stress-dependence of permeability show a smooth continuity from the tight sand region to the conventional sand region. With a sufficiently large data base of both high and low permeability sandstone core analyses, samples in the "transitional zone" can be easily recognized.

The degree of pore alteration, and hence the degree of "tightness" in the Travis Peak cores studied in this paper, varies directly as a function of depth. This leads us to conclude that the amount of diagenetic change in the Travis Peak is greater at increasing depths and, therefore, the processes which form secondary porosity, and quartz overgrowths in particular, are more significant at elevated temperatures and/or pressures. We speculate that at least some of the quartz overgrowth precipitation may be hydrothermal in nature, which neatly explains the increased volume of authigenic quartz at depth. In addition, our data clearly show that quartz overgrowth formation can and does continue into the late stages of diagenesis, partly filling the secondary porosity in some cases. It is difficult to reconcile our observations with Dutton and Finley's interpretation⁷ that formation of quartz overgrowths in the Travis Peak occurs mainly during the early stages of diagenesis, except to say that perhaps the overgrowths form in several different events.

Finally, the data collected and analyzed for this work leads us to conclude that fluorescent petrography and mercury porosimetry are useful techniques for rapidly and inexpensively assessing the quality of a tight sandstone reservoir. When compared against a data base of detailed petrophysical laboratory analyses, the combination of petrography and porosimetry quickly reveals which zones contain permeable, grain-supported primary porosity, which contain the tight, productive slot pore/solution pore morphology, and which contain a non-economic, highly altered, low-porosity pore structure. Further research and experimentation is needed to develop these procedures into routine well site measurements to help determine completion intervals in a tight gas sand well, but we believe such a role is possible in the future.

NOMENCLATURE

- k = permeability
- k_0 = constant in Equation 1
- P_{net} = net confining stress

α = stress dependence factor for permeability
 (Equation 1)

ACKNOWLEDGMENTS

The work reported in this paper was funded by the Gas Research Institute under contract No. 5086-211-1258. The financial support of GRI is gratefully acknowledged. Technical interactions with other GRI contractors in the area of tight gas sands research increased our understanding of the petrological and petrophysical characteristics of the Travis Peak. Special thanks are directed to Shirley Dutton and Karen Herrington of the Texas Bureau of Economic Geology, Brad Robinson and Bill Whitehead of S. A. Holditch and Associates, Ercill Hunt of ResTech, and D'Arcy Horner of GRI for their input and technical comments. We would also like to thank Susan Christensen of IGT for typing the manuscript, and our technician, John Hasenberg, for preparing the samples, maintaining the equipment, and manufacturing the thin sections.

REFERENCES

1. Randolph, P. L., "Porosity and Permeability of Mesaverde Sandstone Core From the U.S. DOE Multiwell Experiment, Garfield county, Colorado," SPE/DOE 11765 in Proceedings of the 1983 SPE/DOE Symposium on Low Permeability Gas Reservoirs, Denver, March 14-16, 1983, p. 449-460.
2. Soeder, D. J. and Randolph P. L., "Porosity, Permeability and Pore Structure of the Tight Mesaverde Sandstone, Piceance Basin, Colorado," SPE Formation Evaluation, Vol. 2, 129-36, June, 1987.
3. Gies, Robert M., "An Improved Method for Viewing Micropore Systems in Rocks With the Polarizing Microscope," SPE Formation Evaluation, Vol. 2, 209-214, June, 1987.
4. Soeder, D. J., "Reservoir Properties and the Pore Structure of Tight Gas Sands," (abstract) presented at the 1984 AAPG Annual Convention, San Antonio, Texas, May 21-23, 1984. AAPG Bulletin, Vol. 68, No. 4, p. 530, April, 1984.
5. Wilson, M. D., "Origins of Clays Controlling Permeability in Tight Gas Sands," J. Pet. Tech., Vol. 34, No. 12, 2871-76, December, 1982.
6. Ostensen, R. W., "Microcrack Permeability in Tight Gas Sandstone," Society of Pet. Engr. J., 919-926, December, 1983.

7. Dutton, S. P., and Finley, R. J., "Depositional and Diagenetic Controls on Reservoir Quality in Tight Sandstones of the Travis Peak (Hosston) Formation, East Texas," SPE Paper 15220, presented at the 1986 SPE Unconventional Gas Technology Symposium, Louisville, KY, May 18-21, 1986.
8. Soeder, D. J., "Laboratory Drying Procedures and the Permeability of Tight Sandstone Core," SPE Formation Evaluation, Vol. 1, 16-22, February, 1986.
9. Holditch, S. A., Robinson, B. M., and Whitehead, W. S., "Cooperative Well Report: Prairie Producing Company A. T. Mast "A" No. 1, Nacogdoches County, Texas," Report GRI 86/0041, prepared for Gas Research Institute by S. A. Holditch and Associates, Inc., February, 1986.
10. Randolph, P. L., Soeder, D. J. and Chowdiah, P., "Porosity and Permeability of Tight Sands," SPE/DOE Paper 12836, presented at the 1984 SPE/DOE/GRI Unconventional Gas Recovery Symposium, Pittsburgh, May 13-15, 1984.
11. Randolph, P. L., Soeder, D. J., and Chowdiah, P., "Effects of Water and Stress Upon Permeability to Gas of Paludal and Coastal Sands, U.S. DOE Multiwell Experiment," Topical Report DOE/MC/20342-1838 prepared for the U.S. Department of Energy, Morgantown Energy Technology Center, under Contract No. DE-AC21-83MC20342, Institute of Gas Technology, Chicago, February 1985.
12. Swanson, B. F., "A Simple Correlation Between Permeabilities and Mercury Capillary Pressures," J. Pet. Tech., 2498-2504 (1981) December.
13. Walls, J. D. and Amaefule, J. O., "Capillary Pressure and Permeability Relationships in Tight Gas Sands," paper SPE/DOE 13879 in Proceedings of the 1985 SPE/DOE Joint Symposium on Low Permeability Reservoirs, Denver, CO, May 19-22, 1985.
14. Chowdiah, P., "Effects of Pore Water Distribution and Stress on the Laboratory Measurement of Tight Sandstone Properties," paper SPE 15210 in Proceedings of the SPE Unconventional Gas Technology Symposium, Louisville, KY, May 18-21, 1986, 35-46.

Table 1. SUMMARY OF SFE #1 DRY CORE ANALYSIS

Plug Depth (ft)	Unconfined Sample Mercury Penetration Data				Net Confining Stress (psi)	Gas Porosity (%)	Klinkenberg Permeability (md)	Pore Volume Compressibility ($10^{-6}/\text{psi}$)	Stress Dependence Exponent for Permeability (a)	
	Entry Pressure (psi)	Porosity (%)	Median Pore Width (μm)	Swanson Parameter (S_b/P_c) _{max} (%/psi)					1st Increase of Net Stress	Decreasing Net Stress
6115.3	35	13.8	0.185	29.1×10^{-3}	2300 3900	13.02 12.89	0.31 0.28	6.8	0.18	—
6118.1	31	13.5	0.294	50.4×10^{-3}	2300 3900	14.19 14.07	2.1 2.0	5.4	0.07	—
6122.8	14.7	16.0	1.202	196.2×10^{-3}	2300 3900	17.92 17.79	25 25	4.7	—	—
6189.2	19.1	12.1	1.389	110.8×10^{-3}	2300 3400	13.53 13.46	9 9	5.3	—	—
6204.5	15.3	13.1	1.771	189.1×10^{-3}	2300 3400	15.07 15.01	18 17	3.5	—	—
7418.2	65	10.4	0.309	20.7×10^{-3}	2700 3400	9.38 9.34	0.024 0.019	5.4	1.01	—
7419.9	19.8	8.4	1.382	70.9×10^{-3}	2700 3400	8.97 8.95	4.3 4.2	3.9	—	—
7423.8	29.6	10.1	1.220	70.4×10^{-3}	2700 3400	10.10 10.06	0.59 0.57	5.3	0.12	—
7441.3	41	8.7	0.363	21.2×10^{-3}	2700 3500	10.54 10.51	2.4 2.4	3.4	0.06	—
7442.8	—	—	—	—	2700 3500	10.04 10.01	5 5	3.8	0.05	—
7457.8	41	8.2	0.579	38.5×10^{-3}	2700 3500	7.89 7.86	0.55 0.54	4.7	0.09	—

Table 2. SUMMARY OF MAST A-1 DRY CORE ANALYSIS

Plug Depth (ft)	Unconfined Sample Mercury Penetration Data				Net Confining Stress (psi)	Gas Porosity (%)	Klinkenberg Permeability (md)	Pore Volume Compressibility ($10^{-6}/\text{psi}$)	Stress Dependence Exponent for Permeability (a)	
	Entry Pressure (psi)	Porosity (%)	Median Pore Width (μm)	Swanson Parameter (S_b/P_c) _{max} (%/psi)					1st Increase of Net Stress	Decreasing Net Stress
8623.2	273	8.1	0.164	7.5×10^{-3}	3500 5500	7.57 7.50	0.0084 0.0071	4.2	0.36	—
8645.9	135	6.1	0.263	9.3×10^{-3}	3500 5500	7.46 7.39	0.049 0.035	4.9	0.75	—
8656.3	446	6.3	0.094	3.3×10^{-3}	3500 5500	6.13 6.06	0.0019 0.00093	6.0	1.38	—
8666.2	777	6.7	—	—	3500 5500	4.84 4.72	1.4 0.9	12.0	0.91	—
9203.3	42	4.8	0.392	10.8×10^{-3}	3800 5800 3800	4.81 4.74	0.025 0.015 0.019	6.6	1.24	0.63
9226.0	87	3.7	0.283	6.7×10^{-3}	3800 5800	3.75 3.70	0.068 0.039	7.7	1.30	—
9229.3	262	4.7	0.183	4.7×10^{-3}	3800 5800 3800	4.39 4.32	0.0027 0.0013 0.0019	7.8	1.66	0.87
9231.9	393	2.8	0.113	1.9×10^{-3}	3800 5800 3800	3.28 3.23	0.0036 0.00093 0.0013	6.6	3.17	0.86
9935.1	249	5.8	0.078	3.2×10^{-3}	3600 6000	5.76 5.62	10 10	9.7	—	—
9937.7	205	4.9	0.176	5.0×10^{-3}	3600 6000 3600	4.98 4.90	0.241 0.109 0.127	6.7	1.54	0.29
9954.9	70	5.0	0.215	6.5×10^{-3}	3600 6000 3600	5.27 5.17	0.0143 0.0128 0.0136	7.2	0.22	0.12
9984.9	407	2.7	0.067	1.0×10^{-3}	3600 6000 3600	2.82 2.71	0.00022 0.000045 0.00011	15.2	3.05	1.66

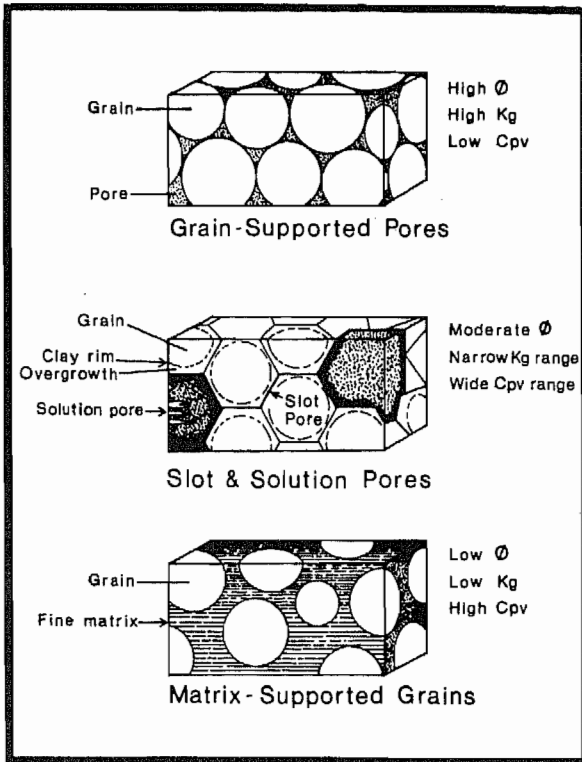


Fig. 1—The three main classes of pore geometry found in tight gas sandstones.

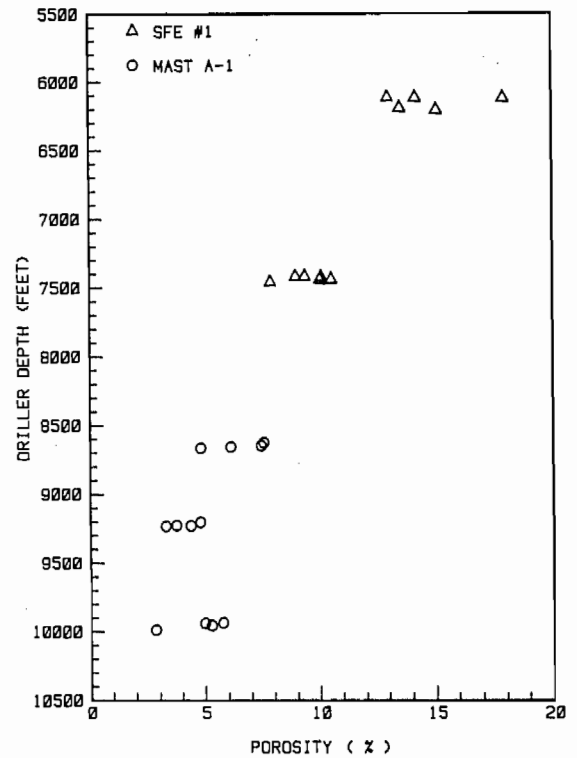


Fig. 3—Gas porosity measured from core vs. depth in the Travis Peak sandstones.

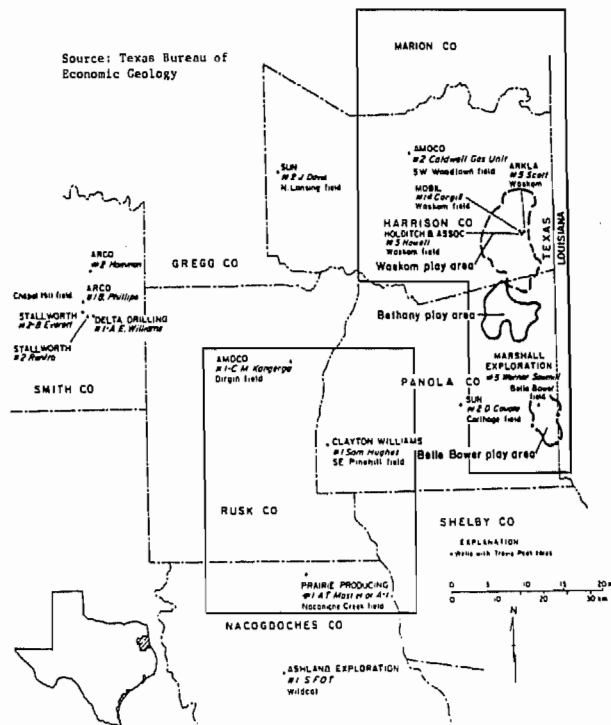


Fig. 2—Index map of cored Travis Peak wells in eastern Texas. The SFE No. 1 well (Holditch No. 5 Howell) is located at upper right, and the Mast A-1 well is at bottom center.

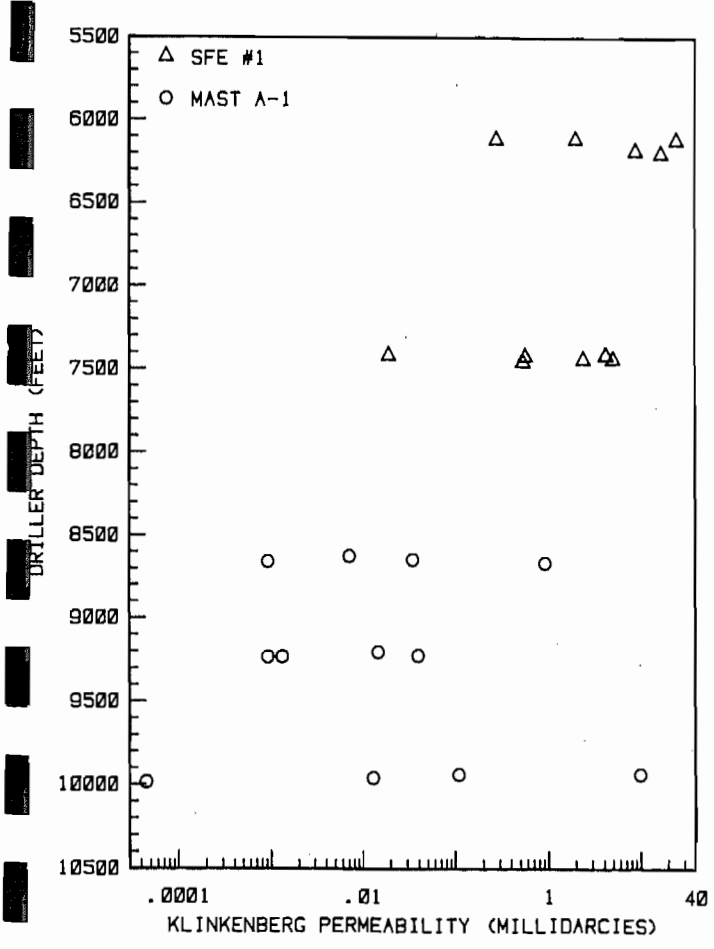


Fig. 4—Dry gas permeability from core analysis vs. depth in the Travis Peak sandstone.

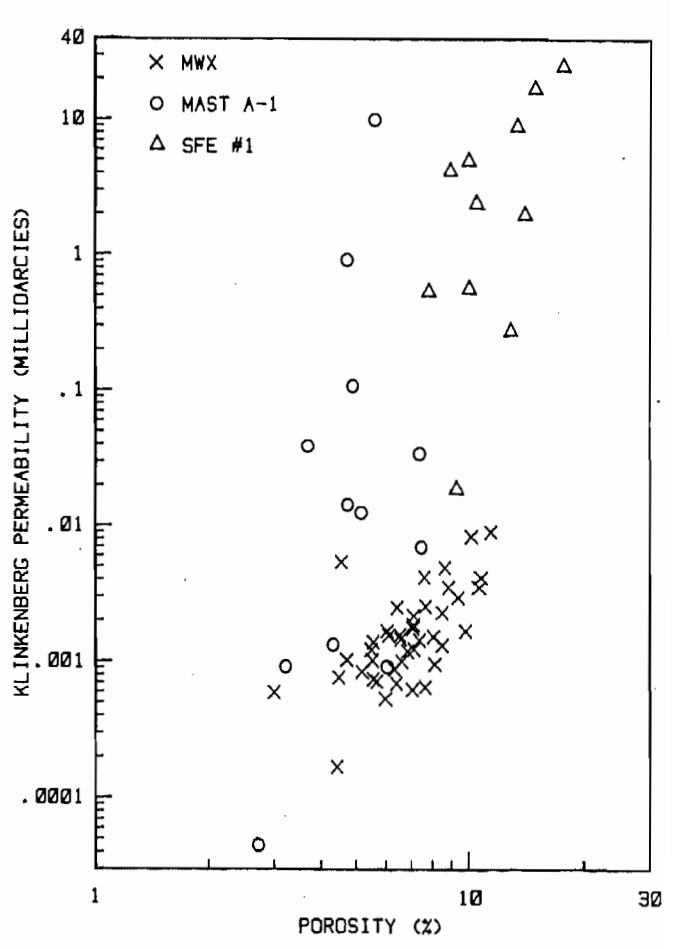


Fig. 5—Dry gas permeability vs. porosity for Travis Peak and Meeusarde cores.

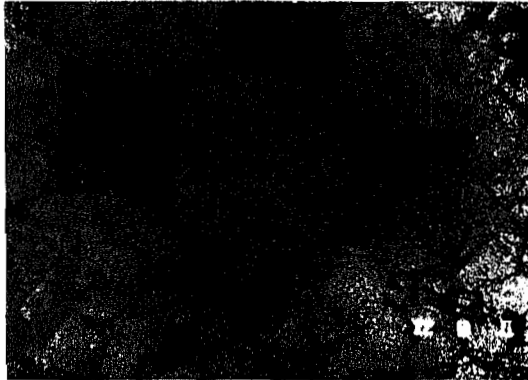


Fig. 6—Plane light and fluorescent views of a high-permeability Travis Peak core. SFE No. 1 well, 6,122.8 ft, 100x, short side of each photo = 0.77 mm.

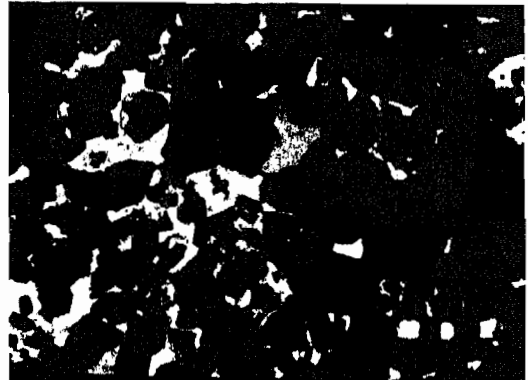


Fig. 7—Crossed-polar and fluorescent views of a low-permeability Travis Peak core. Mast A-1 well, 9,954 ft., 30x short side of each photo = 1.8 mm.

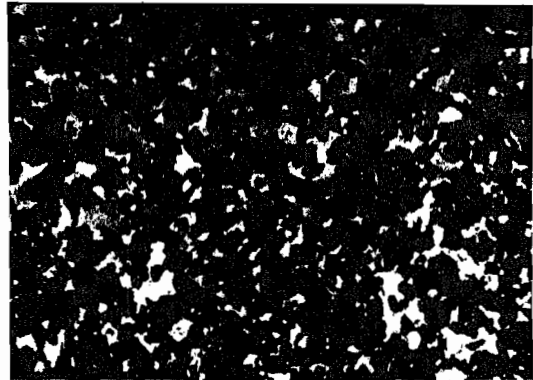
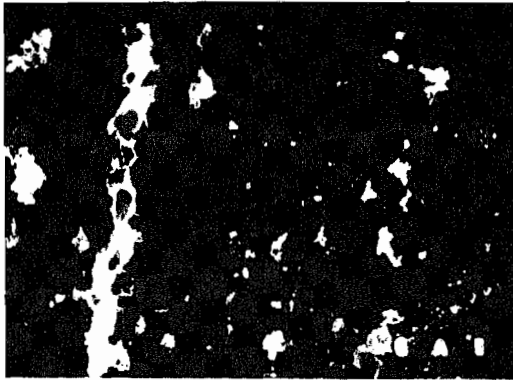


Fig. 8—High-permeability Travis Peak core with different pore morphologies. Mast A-1, 9,935.1 ft., 40 \times (left); SFE No. 1, 6,189.2, 40 \times (right), short side each photo = 1.85mm.

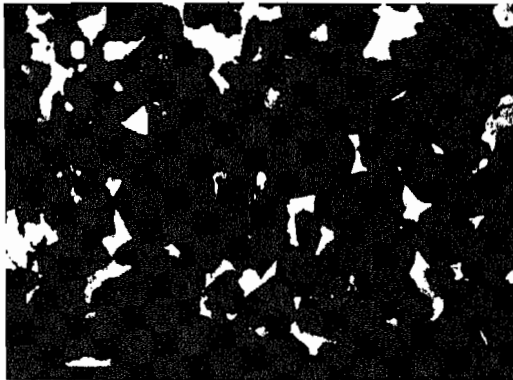


Fig. 9—Sub-millidarcy Travis Peak sands from the SFE No. 1 well, 7,423.8 ft (left) and 7,457.8 ft (right), both photos 100 \times , short side of each = 0.77 mm.

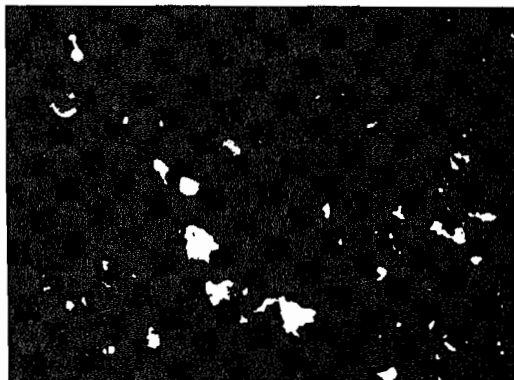


Fig. 10—Sub-microdarcy Travis Peak sands from the Mast A-1 well, 9,229.3 ft, 30 \times (left), short side = 1.6mm; 9,984.9 ft, 100 \times (right), short side = 0.8 mm.

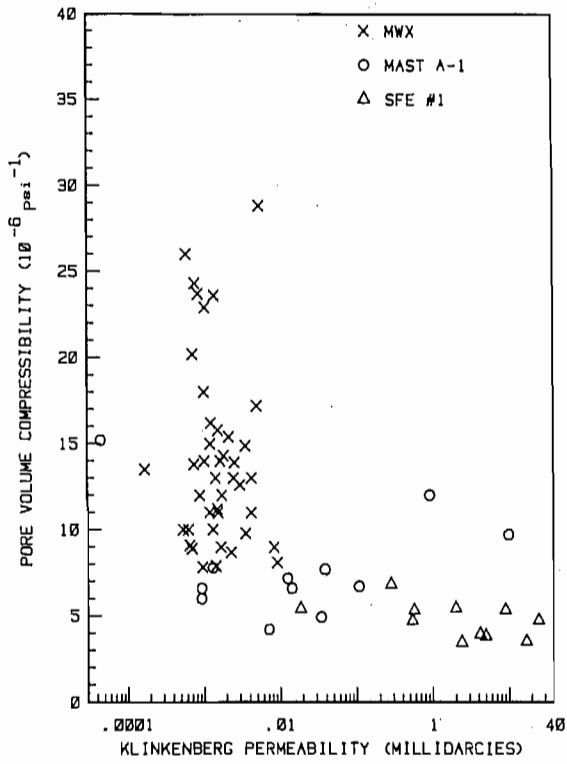


Fig. 11—Pore volume compressibility in Travis Peak and Mesaverde cores vs. permeability.

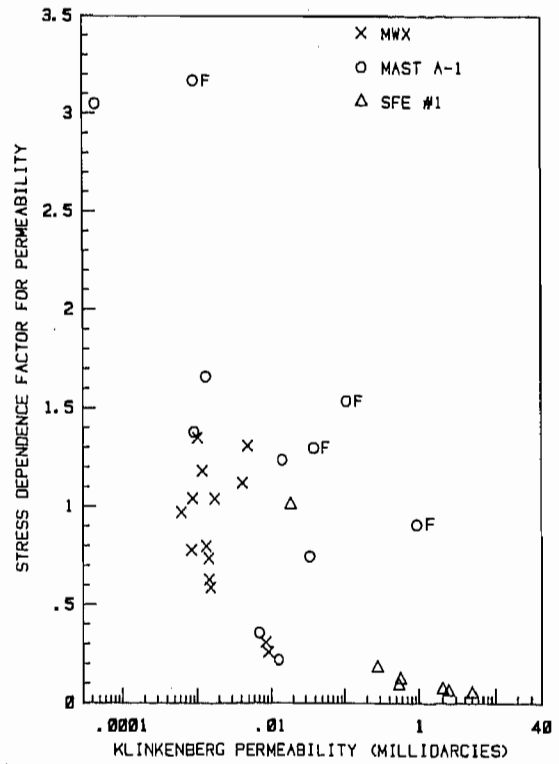


Fig. 12—Stress-dependence of permeability in the Travis Peak and Mesaverde cores (F=fractured).

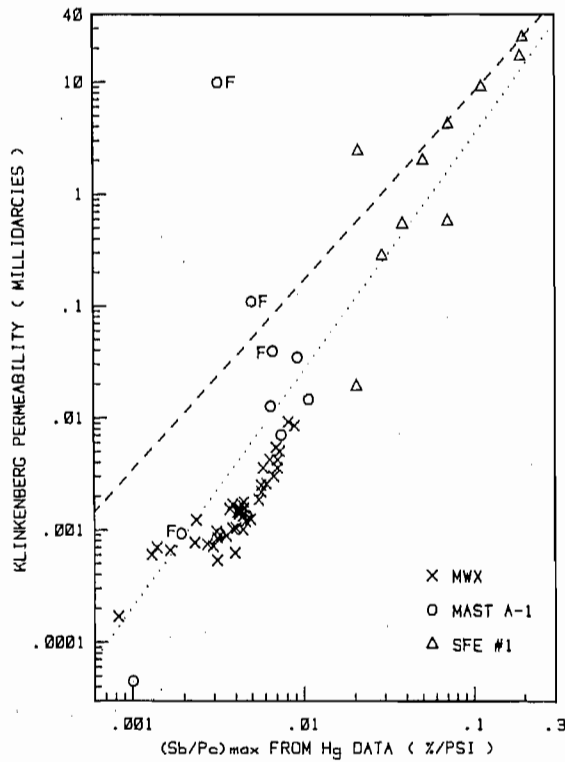


Fig. 13—Permeability vs. Swanson parameter for Travis Peak and Mesaverde cores (F=fractured).

Influence of Water-Desaturation Technique and Stress on Laboratory Measurement of Hydraulic Properties of Tight Sandstones

P. Chowdiah, Inst. of Gas Technology

Summary. Mercury porosimetry on unconfined sample chips and effective-gas-permeability measurements with evaporation used as the desaturating mechanism are two of the most common core-analysis measurements for tight sands. Data obtained with these two techniques have been compared with data on gas/water capillary pressure and effective gas permeability along a true drainage path at in-situ net confining stress. Results show that confining stress can have a significant effect on capillary pressure. Also, the use of evaporation to desaturate samples yields effective gas permeabilities much smaller than those obtained under true drainage conditions, suggesting that the evaporation method results in a pore-water distribution similar to that in an imbibition process.

Introduction

Permeabilities of most low-permeability, or tight, sandstones are extremely sensitive to confining stress and partial water saturation.¹⁻⁵ While this implies that measurements relating to two-phase flow in tight sands should be performed under carefully controlled conditions of stress and water saturation, such elaborate experiments are difficult and time-consuming because of the extremely small flow rates involved. Current laboratory practice has, therefore, come to rely on certain "short cuts." Two of the most common laboratory measurements used to obtain data relevant to two-phase flow in tight sands are (1) capillary-pressure measurements on unconfined samples and (2) permeability to gas under stationary-liquid conditions at various levels of water saturation established by evaporation.

In the capillary-pressure measurements, mercury porosimetry, a relatively fast and inexpensive measurement, is often used to obtain these data. A technique that uses a centrifuge to desaturate a water-saturated sample is also used.⁶ Neither of these measurements duplicates in-situ conditions exactly. Mercury data require the use of appropriate conversion factors to adapt the measured capillary-pressure curve to a gas/water system. In the centrifuge technique, the question of how adequately forces causing desaturation in the centrifuge represent reservoir mechanisms is debatable. In addition, a big uncertainty when such data are used for tight sands concerns applying data from unstressed samples to describe the reservoir matrix at in-situ stress.

In the permeability-to-gas measurements, gas permeability is measured by either the steady-state⁴ or the pulse technique³ at a net confining stress representative of in-situ conditions. However, the nature of water distribution resulting from evaporation cannot be related directly to either a drainage or imbibition saturation history.

The ultimate use of laboratory data is usually either as matrix property inputs in reservoir simulation or as an input to well-completion decisions. In either case, it is important to understand the conditions of stress and microscopic pore-water distribution relevant to the laboratory data so that the results may be applied meaningfully to the flow situation actually prevailing in the reservoir matrix. In this study, tight-sands data obtained with the two techniques listed above have been studied in conjunction with true drainage capillary-pressure and relative-permeability data, from the perspective of understanding the bearing that stress and microscopic pore-water distribution have on results from such experiments.

Equipment and Experimental Procedures

Mercury Porosimetry. An Aminco porosimeter capable of a maximum pressure of 15,000 psi [103.4 MPa] was used to obtain data

on mercury penetration into evacuated rock chips of about 1-cm³ volume. The raw data obtained were of pressure vs. volume of mercury entering the sample. When necessary to represent these data in terms of nonwetting phase (mercury) saturation of the sample, the total volume of mercury injected into the sample at 15,000 psi [103.4 MPa] was taken as the sample PV.

Dry-Sample Properties. Plug samples 1 in. [2.5 cm] in diameter and about 1 1/2 in. [3.8 cm] long were dried to a constant weight in a controlled-humidity oven at 140°F [60°C] and 45% relative humidity before all measurements. PV of the plug dried under these conditions was used as the basis for calculating water saturations for the partially water-saturated samples. Both PV and permeability were measured at net confining stresses representative of in-situ conditions. PV was obtained by the Boyle's-law technique, and permeability was measured by steady-state gas flow in an apparatus described in Ref. 4. Permeability to nitrogen was measured at mean pore pressures of 200, 500, and 1,000 psia [1379, 3447, and 6894 kPa], and a plot of permeability vs. reciprocal mean pore pressure was extrapolated to infinite pressure to obtain the Klinkenberg permeability of the sample.

Partially Water-Saturated Samples. Gas-phase permeability of partially water-saturated samples was also measured in a manner similar to that for the dry samples under conditions such that the water phase was stationary. Starting with a fully saturated sample, water saturation was successively decreased to desired levels by evaporating water. When the sample weight indicated that the right quantity of water had been removed, the sample was loaded in the core holder with a Viton™ rubber sleeve and subjected to the desired confining stress. Gas flow data were then obtained with a pressure drop generally 10 psi [69 kPa] or less and in no case > 20 psi [> 138 kPa]. The small pressure drop ensures that no water is pushed out of the sample by the gas and minimizes any capillary-pressure-related saturation gradients. The steady-state gas flow rate during these measurements was very small (as low as 10⁻⁶ cm³/s). Prehumidification of the nitrogen gas to prevent evaporation from the sample was therefore not necessary because the gas throughput during each permeability measurement was < 5 cm³. Steady-state gas flow rates of < 10⁻⁶ cm³/s are measured by monitoring the rate of pressure increase in a calibrated volume into which the gas flows. The pressure increase is measured relative to a reference pressure with a sensitive differential-pressure transmitter. The entire apparatus needs to be housed in a constant-temperature enclosure because a high degree of temperature stability is a key ingredient of this flow-measurement technique. All permeability measurements reported here were conducted at 90°F [32°C]. Details of the apparatus are available in Ref. 4.

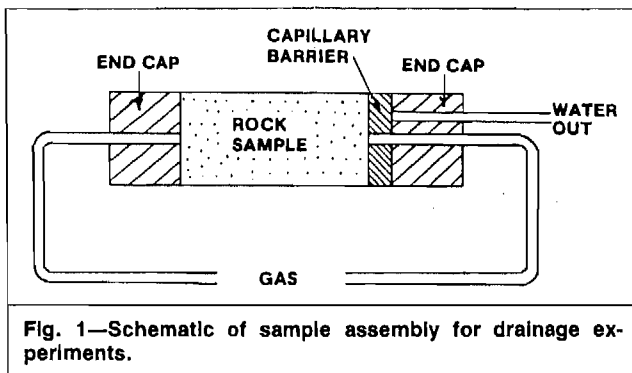


Fig. 1—Schematic of sample assembly for drainage experiments.

Drainage Capillary Pressure and Relative Permeability. In addition to the above equipment and procedures used to make measurements on most of the samples, a new apparatus was designed and built to permit gas-phase permeability measurements on tight sands along a true drainage path. The gas-flow-measurement system is similar to that described above, with saturation gradients within the sample minimized by the use of small gas pressure drops. The most important feature of the new apparatus, called the experimental tight rock apparatus (ExTRA), is that the sample plug is assembled in the core holder so that it is in contact with a water-saturated porous disk with a very high gas-entry pressure, as shown schematically in Fig. 1. When gas pressure on an initially water-saturated sample plug is increased above its threshold pressure, water displaced from the sample is permitted to exit through the "capillary barrier" into a pipette while the barrier blocks the gas as long as the gas pressure is below the gas threshold pressure for the disk. Gas distribution grooves between the sample and the capillary barrier serve to distribute the gas across the face of the sample. Capillary forces ensure that the water displaced from the sample exits preferentially through the capillary barrier into the pipette and that the gas lines remain free of water. Ideally, the capillary-barrier material should have a gas threshold pressure higher than the highest gas pressure that one expects to use during the capillary-pressure measurement. This is a difficult criterion to meet, particularly when the sample is a tight sand that has a high gas-entry pressure. Preliminary data have been obtained with two different barrier materials: a porous glass (Corning's Thirsty™ glass), which has a mean pore size of 0.004 μm , and Millipore™ filter membranes with a pore size of 0.025 μm . Of these, the glass was found to perform better. Diffusion of gas through the water-saturated capillary barrier was found to disrupt water-displacement measurements. This problem was overcome by providing a means of bleeding off this gas from the water flow system before taking pipette-level readings. Details of the experimental techniques are available in Ref. 7.

The procedure involved in making measurements starts with assembling the fully water-saturated sample and capillary barrier. Gas (nitrogen) pressure is then increased until it is above the entry pressure of the sample. Water displaced from the sample is monitored in a pipette downstream of the capillary barrier. It has been found that the sample may typically take anywhere from 4 days to 1 week to desaturate to equilibrium at each gas pressure step. Once capillary equilibrium has been established, a small pressure drop of 5 to 10 psi [34 to 69 kPa] is used to measure the gas-phase permeability. After this measurement, the gas pressure is increased to the next desired level to desaturate the sample further without removing it from the core holder. Thus, the experiment yields a capillary-pressure curve and permeability to gas as a function of water saturation along a true drainage path under a net confining stress representative of in-situ conditions. Owing to the small flow rates and long equilibrium times involved in such experiments on tight sands, a typical data set may take several weeks to obtain. A computerized data-acquisition unit is used to monitor the system during this period. Data from this apparatus reported in this paper have been found to be reproducible and are believed to be reliable, though they are among the first sets of tight-sand (<0.1 md) drainage data obtained.

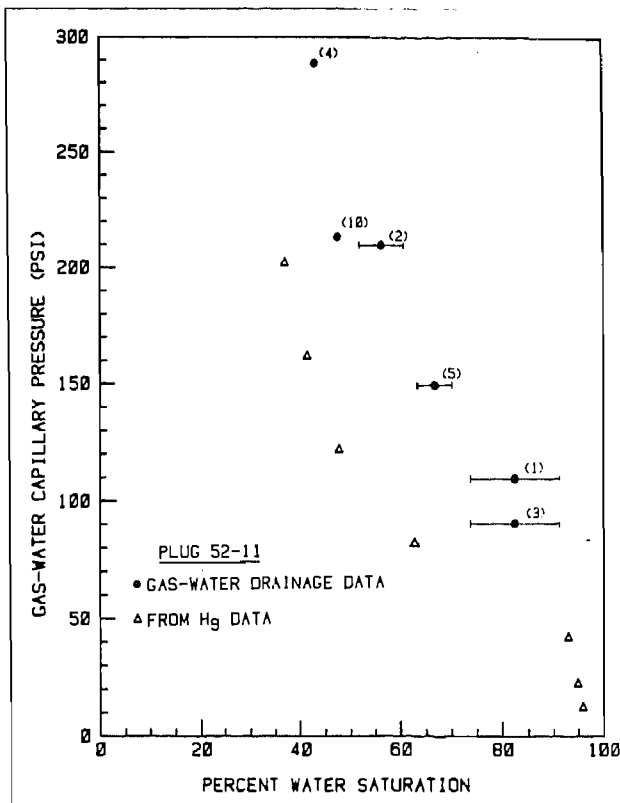


Fig. 2—Capillary-pressure data for Mesa Verde Sample 52-11.

Gas/Water Capillary Pressure at In-Situ Stress

Mercury-porosimetry capillary-pressure data have been the subject of several investigations⁸⁻¹⁰ and have been found to correlate well with dry-sample permeability. In view of the high stress sensitivity of tight sands, however, questions remain as to how well the mercury capillary-pressure curve represents gas/water capillary pressures at in-situ stress conditions in tight reservoirs. The reservoir gas/water capillary-pressure curve is an important input to two-phase flow simulators. The primary cause for concern is that mercury penetration data are obtained with unconfined rock chips and may not correctly represent pore-size distribution in a sample at reservoir net stress.

As a first move toward addressing this question, nitrogen/water drainage capillary-pressure data were obtained on two tight-sand samples at reservoir net stress and compared with mercury penetration data. Fig. 2 shows the comparison for Mesa Verde sample 52-11, which had a dry Klinkenberg permeability of 9.2 μm and a porosity of 11.4% at 4,440-psi [30.6-MPa] net stress. The filled circles in the plot are the gas/water data obtained at 4,440-psi [30.6-MPa] net confining stress, and the triangles are mercury data divided by a factor of five to account for differences in interfacial tension and contact angle between the mercury/vacuum and gas/water systems. The exact value of this conversion factor depends on the interfacial tension and contact angle values assumed for these systems. Five is a commonly used factor, based on interfacial tension in the range of 470 to 480 dynes/cm [470 to 480 mN/m] and contact angle in the range of 130° to 140° for the mercury/vacuum system, and corresponding values of 70 dynes/cm [70 mN/m] and 0° for the gas/water system. Water saturation values for the gas/water data are based on PV at reservoir net stress, whereas saturation values from the unconfined-sample mercury data are based on the total volume of mercury injected at 15,000 psi [103.4 MPa]. The number in parentheses beside each gas/water data point gives the number of days the gas pressure was held at that level before the water saturation was measured. The rather large error bars on the high-saturation data points are a result of difficulties experienced during this experiment in monitoring the extremely small (<10⁻⁶ cm³/s) water displacement rates. These difficulties

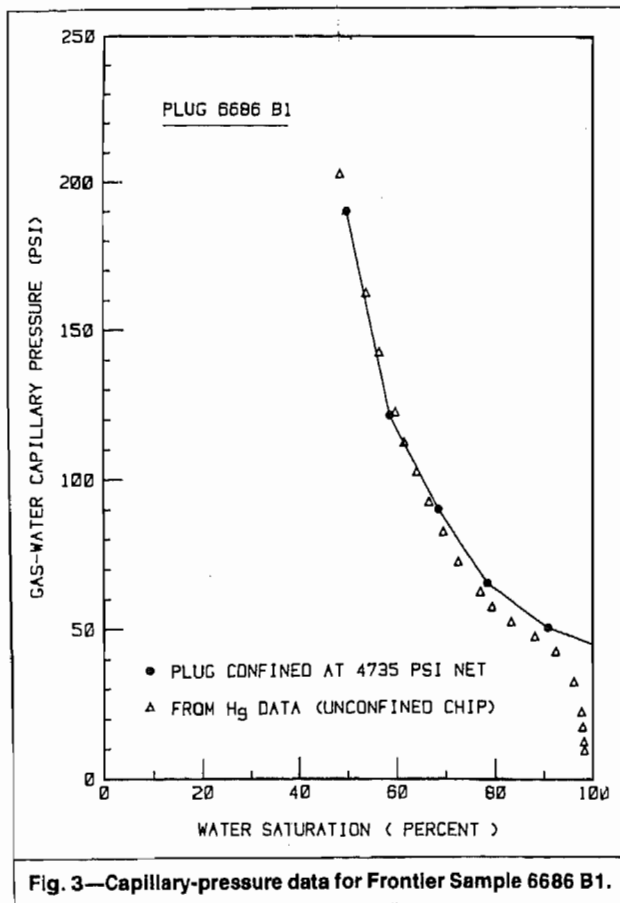


Fig. 3—Capillary-pressure data for Frontier Sample 6686 B1.

were caused by diffusion of nitrogen past the capillary barrier into the water line leading to the pipette. In subsequent experiments, this problem was overcome by providing a means for bleeding off the gas before taking pipette-level readings. In this experiment, however, water saturations were estimated from transient gas-flow data measured during the first few minutes after the imposition of a pressure drop across the sample. The data were fitted to a diffusivity equation solution for transient gas flow to estimate the PV available for gas flow. Details of this procedure are available in Ref. 7.

Some of the gas/water data points in Fig. 2 correspond to conditions before capillary equilibrium was established in the sample. Experience since these data were obtained has shown that desaturation to equilibrium after each gas-pressure increase takes several days. This is also evident in the data in Fig. 2 at the 210-psi [1448-kPa] capillary-pressure level, where a significant difference in water saturation was observed between data obtained 2 days after the gas pressure increase and that obtained 10 days after the increase.

Nevertheless, the difference between the gas/water and mercury data in Fig. 2 is large enough to warrant the qualitative conclusion that for this sample, the gas/water capillary pressures at reservoir net stress would be higher than expected from the mercury data, even after allowances are made for the incomplete desaturation at some of the gas/water data points.

Fig. 3 compares gas/water capillary-pressure data at 4,735-psi [32.6-MPa] net confining stress with estimates from unconfined-chip mercury-penetration data for a sample from the second Frontier formation in western Wyoming. This sample had a dry Klinkenberg permeability of $31.9 \mu\text{d}$ and a porosity of 13.7% at 4,735-psi [32.6-MPa] net stress. Fig. 3 shows that the gas/water capillary-pressure data for this sample agreed very well with estimates from mercury-penetration data.

Discussion. The data in Figs. 2 and 3 suggest that the effect of confining stress on the capillary-pressure curve was much more severe on Mesa Verde Sample 52-11 than on Frontier Sample 6686. This may be related to difference in pore morphology for these

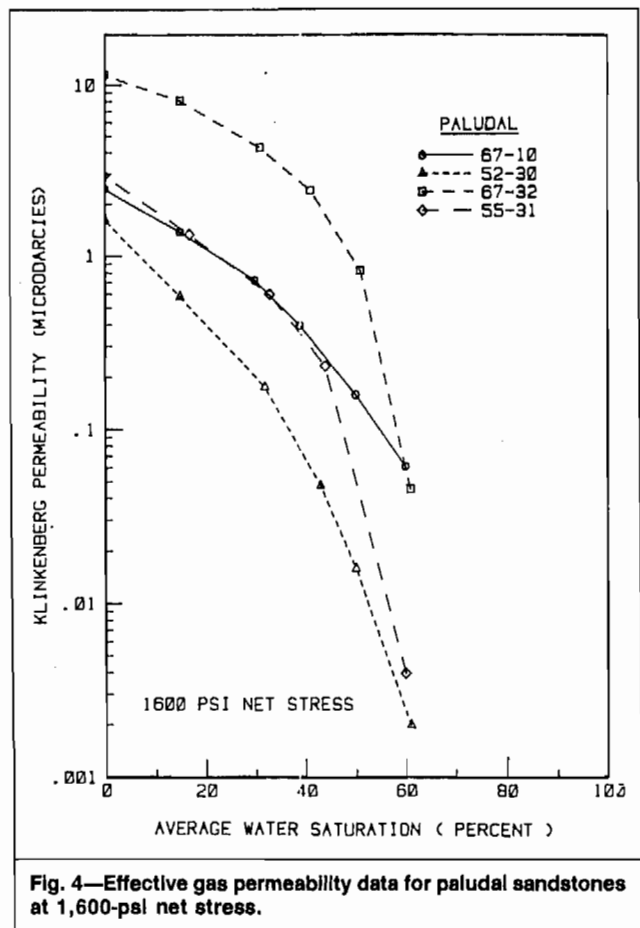


Fig. 4—Effective gas permeability data for paludal sandstones at 1,600-psi net stress.

rocks. Earlier thin-section and scanning electron microscope studies of paludal sandstones from the Mesa Verde formation have shown that these are dual-porosity rocks in which a substantial fraction of the void space occurs in the secondary pores and that the flow paths between these pores consist of intergranular slots.¹¹ On the other hand, Frontier Sample 6686 has a pore structure that may be classified as "grain-supported pores," where the pores consist of primary intergranular porosity propped open by contact points between individual rounded quartz sand grains.¹¹ This structure is similar to that of conventional (high-permeability) sandstones, with clogging of flow passages by secondary minerals, such as clays, being the main reason for the low permeability. While the amount of data at this stage is insufficient to permit any definite conclusions, microscopic studies of pore structure may provide a screening technique to determine the severity of confining-stress effect on the capillary-pressure curve. The need for such screening becomes obvious from the fact that the displacement rates in tight sands are so slow that it takes several weeks to measure a single gas/water capillary-pressure curve.

Gas-Phase Relative-Permeability Data

Figs. 4 through 7 show gas-phase permeability data as a function of water saturation for four coastal and four paludal (swamp deposit) Mesa Verde samples. The net confining stress on the samples is higher in Figs. 5 and 7 than in Figs. 4 and 6. The lower net stress corresponds to the initial reservoir pressure, while the higher net stress corresponds to the midpoint of reservoir drawdown. These data were obtained with steady-state gas-flow measurements with a stationary water phase and water saturations established by evaporation from a fully saturated condition. The water saturation values are based on sample PV at the net confining stress used and were determined gravimetrically. Water saturations are denoted as "average" values because the actual saturation distribution within the sample is unknown. Saturation gradients can develop within the sample during the evaporation process, as well as during the gas-phase permeability measurement, if large pressure drops are imposed. In these experiments, the gas-phase pressure drop was re-

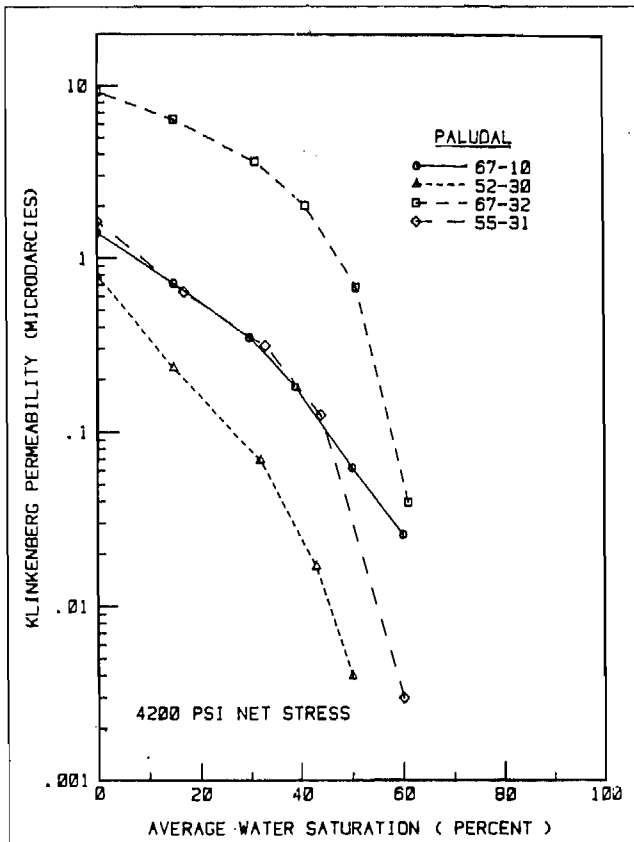


Fig. 5—Effective gas permeability data for paludal sandstones at 4,200-psi net stress.

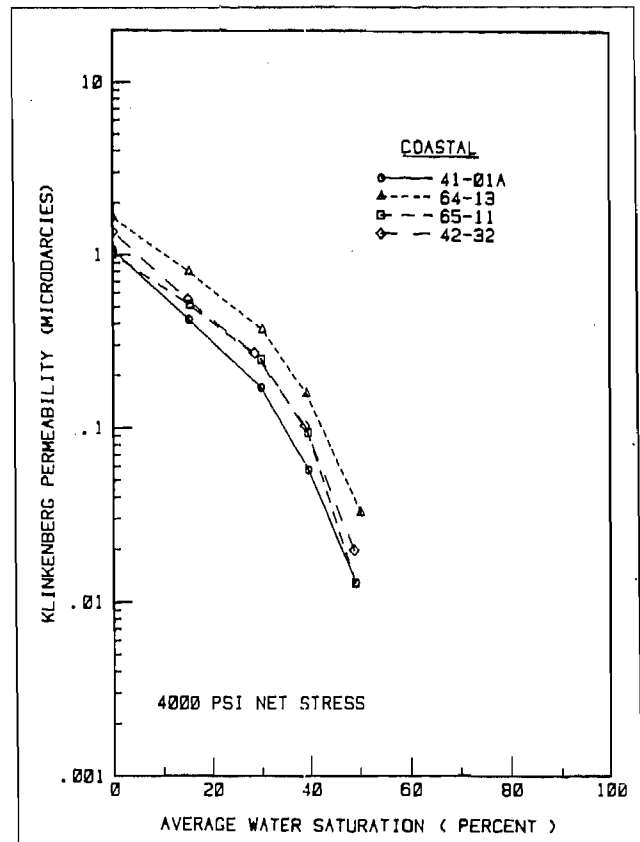


Fig. 7—Effective gas permeability data for coastal sandstones at 4,000-psi net stress.

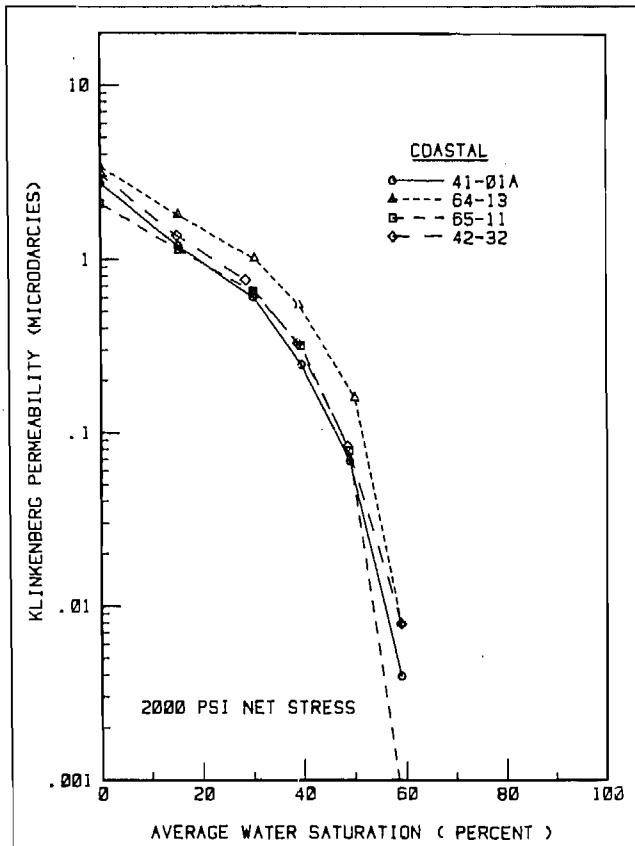


Fig. 6—Effective gas permeability data for coastal sandstones at 2,000-psi net stress.

stricted to values below 20 psi [138 kPa] to minimize water movement so that gradients resulting from the evaporation process were probably the predominant nonuniformity. Further details on the samples and experiments are available in Ref. 12.

Analysis With Corey's Equation. Analytical expressions describing the relative permeability data of Figs. 4 through 7 were obtained by fitting the data for each sample to the equation

$$k_{rg} = \left(\frac{1 - S_{gc} - S_w}{1 - S_{gc}} \right)^n (1 - S_w^2) \dots \dots \dots (1)$$

Nitrogen permeability of the dry rock was used as the basis for the relative permeability values. Eq. 1 has also been used in some earlier investigations^{6,13} to describe gas-phase relative-permeability behavior in tight sands. Eq. 1 is similar to the Corey¹⁴ equation but is conspicuous by the absence of an irreducible water saturation. This results because data obtained with evaporation to vary water saturation do not display an irreducible water saturation. (In fact, no measurements of irreducible water saturation under true drainage conditions are available for tight sands because the mercury-porosimetry capillary-pressure curves also do not yield an irreducible water saturation.) Note, however, that water saturations below irreducible are unrealistic from a reservoir perspective. There is some indirect evidence that irreducible water saturations in tight sands are on the order of 40%.¹⁵

The best-fit exponent, *n*, and critical gas saturations, *S_{gc}*, for each data set were determined by linear regression. The data points corresponding to 15% water saturation were not used in the regression fits because the measured permeability at 15% water saturation was found to be consistently lower than expected from the remaining data points for each sample. It is felt that the data at this low water saturation are anomalous because of nonuniform water distribution in the rock. Because warm air from a heat gun was used to enhance the extremely slow evaporation rates from 30 to 15% average water saturation, the samples were probably well be-

TABLE 1—PARAMETERS FOR EQ. 1 FIT TO RELATIVE-PERMEABILITY DATA

Plug	<i>n</i>		<i>S_{gc}</i>	
	High*	Low**	High*	Low**
	Net Stress	Net Stress	Net Stress	Net Stress
67-10†	3.32	2.64	0.096	0.19
52-30	3.42	4.13	0.35	0.25
67-32	1.27	1.32	0.38	0.39
55-31	2.04	1.95	0.36	0.40
41-01A	2.69	2.25	0.38	0.39
64-13	2.03	1.62	0.40	0.41
65-11	1.59	1.36	0.47	0.47
42-32	2.29	2.32	0.41	0.37

* Net stress = 4,200 psi for paludal samples and 4,000 psi for coastal.
 ** Net stress = 1,600 psi for paludal samples and 2,000 psi for coastal.
 † Sample contains coal laminae.

low 15% saturation near the surface and above 15% in the interior. At such low water saturations, the pore water is discontinuous, so rapid redistribution by liquid-phase transport is not possible.

Values of *n* and *S_{gc}* in Eq. 1 corresponding to both the high- and low-net-stress data for each sample are given in Table 1. The exponent, *n*, is indicative of the rate of decline of gas-phase permeability with water saturation. Higher values of *n* correspond to relative-permeability curves displaying a sharper decline in permeability with increased water saturation. The exponents in Table 1 show a significant variation, ranging from 1.3 to 4.1. The mean for all eight high-net-stress values is 2.33, with a standard deviation of 0.72, and that for the low-net-stress values is 2.20, with a standard deviation of 0.85. The variation in the exponent is much larger among the paludal samples, a fact that correlates with the wide variation in the paludal sample permeabilities (Figs. 4 and 5) compared with the coastal samples (Figs. 6 and 7). Also, the values of *n* in Table 1 show that higher-permeability samples tended to be less sensitive to water saturation.

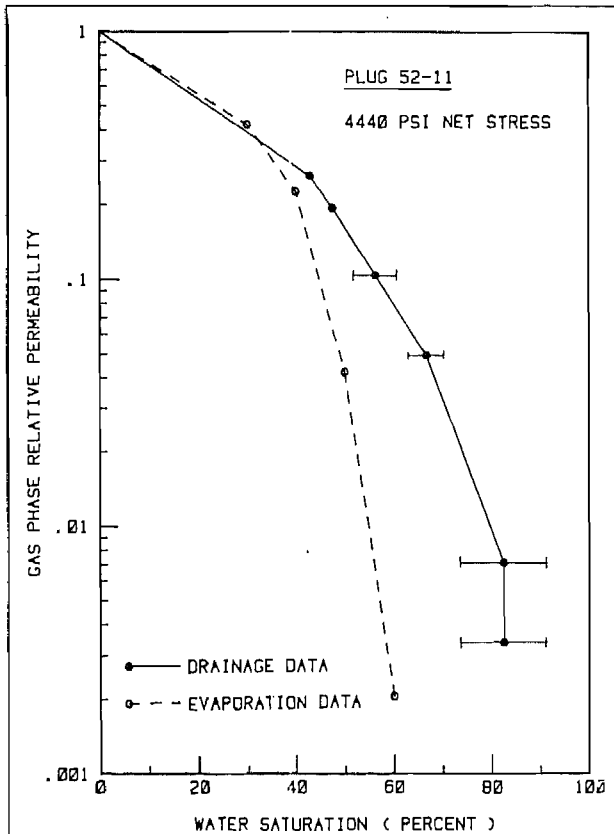


Fig. 8—Comparison of evaporation and drainage relative permeabilities.

TABLE 2—DRY-SAMPLE PROPERTIES

Sample	Net Confining Stress (psi)	Porosity (%)	Klinkenberg Permeability <i>k_∞</i> (μd)	Pore-Size Parameter <i>b</i> (psi)
52-11	4,440	11.43	9.23	63
6686 B1	4,735	13.67	31.9	43

Sample 67-10, which contained coaly laminations, yielded significantly lower values of *S_{gc}* than the rest of the samples. This is probably typical of behavior that can be expected of samples that contain heterogeneities consisting of high-permeability streaks. The presence of such heterogeneities can result in unexpectedly high permeabilities to gas at high water saturations and an extremely low (near zero) critical gas saturation under drainage conditions.¹⁵

It is interesting to compare the present results with those from some earlier studies. In their study of tight sands, Byrnes *et al.*¹⁶ concluded that gas-phase relative permeabilities could be described by Eq. 1 with *n* = 1.1 to 1.3 and *S_{gc}* = 0.2 to 0.3. However, their conclusion was based on measurements made at a net confining stress of only 120 psi [827 kPa]. In view of this fact, the significantly higher values for *n* and *S_{gc}* in the present study probably reflect the higher confining stress used. Sampath and Keighin¹³ were able to fit tight-sands data at high confining stress to Eq. 1 with *S_{gc}* = 30% and *n* ranging from 1.1 to 1.6. Ward and Morrow⁶ also arrived at values of *S_{gc}* = 30% and *n* = 1.5 for a high-net-stress correlation using tight-sands data from various sources, including Sampath and Keighin. The samples used by Sampath and Keighin spanned a permeability range of 10 to 200 μd, compared with the 1- to 10-μd range for the present data. Interestingly, the parameters *n* and *S_{gc}* for Sample 67-32, the highest-permeability sample in this study, are in good agreement with those reported by Sampath and Keighin.

Pore-Water Distribution. Laboratory measurements of relative permeabilities like those described above are of little significance unless the nature of water distribution in the pore network is well defined. In a reservoir, initial water saturations are generally established by drainage as gas accumulates and displaces water. When the reservoir is drawn down, water saturation increases by imbibition of water. Thus, conditions corresponding to both imbibition and drainage can exist in a reservoir at different locations and at different stages of production. It is well known that relative permeabilities along drainage and imbibition paths can differ considerably, particularly at high water saturations. The effect of pore-throat blockage by water and gas entrapment in isolated pockets during imbibition can be especially severe on tight sands, which often have a pore structure consisting of large solution pores interconnected by narrow, flow-controlling slots.

Unfortunately, the use of evaporation to vary core water saturation in the laboratory results in neither true drainage nor true imbibition pore-water distribution. However, a review of the laboratory procedure reveals that this method provides distinct possibilities for imbibition-type water movement. The evaporation process is very complex, with water movement from the interior of the sample to its surface occurring by a combination of vapor and liquid transport that may involve significant water movement by imbibition. The increase of confining pressure on the rock sample in the core holder subsequent to evaporation to the desired saturation causes further redistribution of the water in the pore space because of the decrease in PV of the sample. This movement of water could also result in the blockage of pore throats, as in an imbibition process.

The above discussion suggests that the pore-water distribution resulting from the use of evaporation to vary water saturation is likely to be closer to that in an imbibition cycle than to that in a drainage cycle. The high critical gas saturations of around 40% (see Table 1) resulting from measurements made with the evaporation method support this conclusion. In contrast, results presented in the following section show that critical gas saturations are much lower when water saturation is varied along a true drainage path.

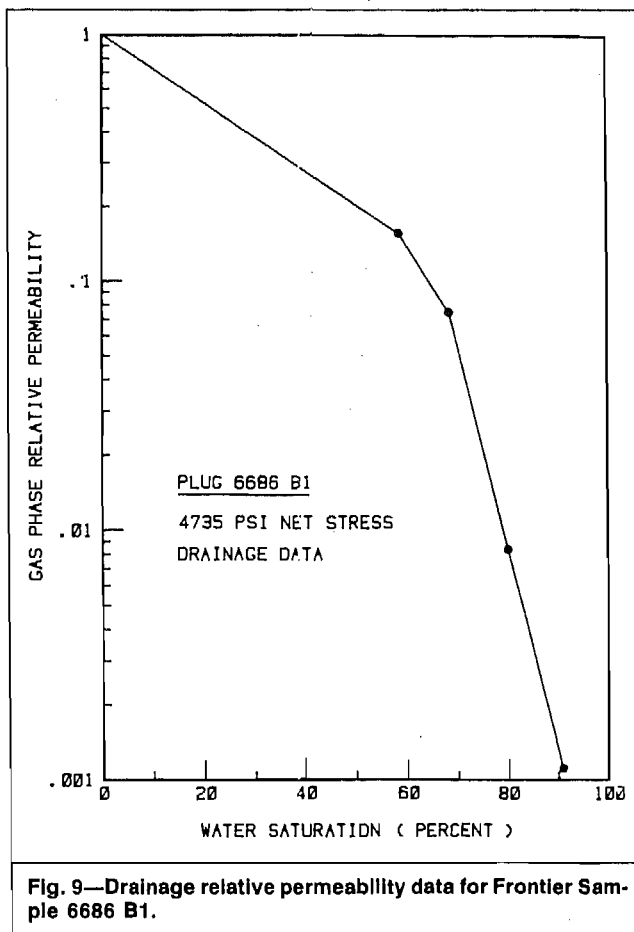


Fig. 9—Drainage relative permeability data for Frontier Sample 6686 B1.

Drainage Relative Permeabilities

Some gas-phase relative-permeability measurements were made along a true drainage path in the apparatus illustrated in Fig. 1. Gas permeabilities were measured by the steady-state, stationary-liquid technique in conjunction with drainage capillary-pressure measurements. Dry-sample properties for the two samples used are given in Table 2. The Klinkenberg permeability, k_{∞} , and the pore-size parameter, b , are the parameters in the Klinkenberg equation:

$$k = k_{\infty} \left(1 + \frac{b}{\bar{p}} \right), \dots \dots \dots (2)$$

which relates permeability to the mean pore pressure of the gas. The net confining stresses used in the relative-permeability determinations for these samples were the same as those listed in Table 2.

Fig. 8 shows gas-phase relative-permeability data as a function of water saturation for the paludal Mesa Verde Sample 52-11. The filled circles are data along a true drainage path, and the open circles are data that had been measured earlier with evaporation as the desaturating mechanism. The water saturation values for both data sets are based on sample PV's measured at a net confining stress of 4,440 psi [30.6 MPa]. The procedure for calculating the relative-permeability ratios differed slightly for the two data sets. Because Klinkenberg permeability to gas at various water saturations was available in the evaporation data set, these values were divided by the dry Klinkenberg permeability from Table 2 to obtain relative permeabilities. For the drainage data set, the pore pressure at which gas permeability was measured was different for each saturation and corresponded to the gas pressure required to maintain capillary equilibrium at that saturation. For the present data, because water was being displaced into pipettes open to the atmosphere, the gas pressure at each saturation was atmospheric pressure plus the capillary pressure at that saturation. The measured gas permeabilities were divided by the dry-sample permeability at the same gas pressure to calculate relative-permeability ratios. Eq.

TABLE 3—COMPARISON OF DRAINAGE AND EVAPORATION DATA

Sample	Desaturation Technique	Parameters in Eq. 1	
		n	S_{gc}
52-11	Evaporation	1.40	0.39
	Drainage	1.85	0.094
6686 B1	Drainage	1.71	0.047

2, along with data from Table 2, was used to estimate the dry-sample permeability.

The large error bars in the drainage data at high water saturations were a result of problems experienced in the measurement of water displaced during this experiment, as discussed in an earlier section in relation to the capillary-pressure data of Fig. 2. Fig. 8 shows that the drainage data yielded higher gas relative permeabilities than the evaporation data. While gas flow in the evaporation data set was nearly shut off at 60% water saturation, the true drainage data showed significant gas permeability at water saturations as high as 80%.

Fig. 9 shows gas-phase relative-permeability data along a true drainage path for a Frontier sandstone sample (Sample 6686 B1) at a net confining stress of 4,735 psi [32.6 MPa]. Data with evaporation as the desaturating mechanism have not been measured for this sample. The drainage data of Fig. 9 showed measurable permeability to gas at a water saturation as high as 90%.

Table 3 shows values of the exponent, n , and critical gas saturation, S_{gc} , calculated from the data of Figs. 8 and 9 by a regression fit to Eq. 1. The two lowest-permeability data points for the drainage data set in Fig. 8 (Sample 52-11) were excluded from the regression analysis because of the large uncertainty in water saturation for these points. Critical gas saturation from the evaporation data for Sample 52-11 was a high 39%, similar to the values listed in Table 1. On the other hand, both data sets obtained along a true drainage path yielded critical gas saturations of <10%.

A slightly modified experimental technique has been used recently to measure critical gas saturation directly. Results of such measurements on several tight-sand samples have been presented elsewhere¹⁵ and have confirmed the observation made here that under true drainage conditions, critical gas saturations are <10%.

Conclusions

1. Measurements of gas/water capillary pressure and gas-phase effective permeability along a true drainage path have been made at in-situ net stress for tight sandstones.

2. Comparison of measured gas/water values with mercury porosimetry data on unconfined samples shows that confining stress can significantly affect capillary-pressure data. The magnitude of the effect probably is largely dependent on pore morphology.

3. The evaporation method commonly used to establish saturation levels for gas-phase permeability measurements in tight sandstones yields effective gas permeabilities significantly lower than that obtained along a true drainage path. Critical gas saturations estimated from evaporation data were around 40%, while true drainage data gave values of around 10% or less.

4. Laboratory procedures involved in making measurements by the evaporation method provide opportunity for water movement in the rock in a manner that can block some pore throats and trap gas in isolated pockets. Permeability data obtained by this procedure are therefore likely to be closer to that along an imbibition path. This conclusion is supported by the large difference observed between evaporation and true drainage data. Because both drainage and imbibition conditions can be present in a reservoir at different stages during drawdown, it is important to use data appropriate to the conditions being simulated. Because laboratory techniques for conducting true imbibition relative-permeability measurements on tight sands are not currently available, the evaporation method provides the best available approximation to gas-phase relative permeability under imbibition conditions.

Nomenclature

- b = pore-size parameter in Klinkenberg equation, psi [kPa]
 k = permeability, μd
 k_{rg} = gas-phase relative permeability
 k_{∞} = Klinkenberg permeability, μd
 n = exponent in Eq. 1
 \bar{p} = mean gas pressure in pores, psi [kPa]
 S_{gc} = critical gas saturation, fraction
 S_w = water saturation, fraction

Acknowledgments

This work was supported in part by the Gas Research Inst. under Contract No. 5082-260-0711 and by the U.S. DOE under Contract Nos. DE-AC21-83MC20342 and DE-FG21-85MC22000. Philip Randolph of the Inst. of Gas Technology (IGT) contributed many useful suggestions and ideas on two-phase flow in tight sands, and his help is gratefully acknowledged. In addition, discussions with Dan Soeder of IGT proved very useful in the understanding of sandstone geology and pore morphology. Finally, I thank John Hasenberg of IGT for his valuable contribution in the design, construction, and maintenance of the laboratory equipment.

References

1. Thomas, R.D. and Ward, D.C.: "Effect of Overburden Pressure and Water Saturation on Gas Permeability of Tight Sandstone Cores," *JPT* (Feb. 1972) 120-24.
2. Jones, F.O. and Owens, W.W.: "A Laboratory Study of Low-Permeability Gas Sands," *JPT* (Sept. 1980) 1631-40.
3. Walls, J.D., Nur, A.M., and Bourbie, T.: "Effects of Pressure and Partial Water Saturation on Gas Permeability in Tight Sands," *JPT* (April 1982) 930-36.
4. Randolph, P.L.: "Porosity and Permeability of Mesaverde Sandstone Core From the U.S. DOE Multiwell Experiment, Garfield County, Colorado," paper SPE 11765 presented at the 1983 SPE/DOE Low-Permeability Gas Reservoirs Symposium, Denver, March 13-16.
5. Randolph, P.L., Soeder, D.J., and Chowdiah, P.: "Porosity and Permeability of Tight Sands," paper SPE 12836 presented at the 1984 SPE/DOE/GRI Unconventional Gas Recovery Symposium, Pittsburgh, May 13-15.
6. Ward, J.S. and Morrow, N.R.: "Capillary Pressures and Gas Relative Permeabilities of Low-Permeability Sandstones," *SPEFE* (Sept. 1987) 345-56.

7. Chowdiah, P.: "Measurement and Analysis of Two-Phase Flow Through Low Permeability Media. Task 2. Experimental Research," final report No. GRI-86/0123-1 prepared for Gas Research Inst., Contract No. 5082-260-0711, Inst. of Gas Technology, Chicago (March 1987).
8. Swanson, B.F.: "A Simple Correlation Between Permeabilities and Mercury Capillary Pressures," *JPT* (Dec. 1981) 2498-2504.
9. Walls, J.D. and Amaefule, J.O.: "Capillary Pressure and Permeability Relationships in Tight Gas Sands," paper SPE 13879 presented at the 1985 SPE/DOE Low-Permeability Gas Reservoirs Symposium, Denver, May 19-22.
10. Chowdiah, P.: "Effects of Pore Water Distribution and Stress on the Laboratory Measurement of Tight Sandstone Properties," *Proc.* SPE Unconventional Gas Technology Symposium, Louisville, KY (May 18-21, 1986) 35-46.
11. Soeder, D.J. and Randolph, P.L.: "Porosity, Permeability, and Pore Structure of the Tight Mesaverde Sandstone, Piceance Basin, Colorado," *SPEFE* (June 1987) 129-36.
12. Randolph, P.L., Soeder, D.J., and Chowdiah, P.: "Effects of Water and Stress Upon Permeability to Gas of Paludal and Coastal Sands, U.S. DOE Multiwell Experiment," topical report DOE/MC/20342-1838, U.S. DOE (Feb. 1985).
13. Sampath, K. and Keighin, C.W.: "Factors Affecting Slippage in Tight Sandstone," *JPT* (Nov. 1982) 2715-20.
14. Corey, A.T.: "The Interrelation Between Gas and Oil Relative Permeabilities," *Prod. Monthly* (Nov. 1954) 38-41.
15. Chowdiah, P.: "Laboratory Measurements Relevant to Two-Phase Flow in a Tight Gas Sand Matrix," paper SPE 16945 presented at the 1987 SPE Annual Technical Conference and Exhibition, Dallas, Sept. 27-30.
16. Byrnes, A.P., Sampath, K., and Randolph, P.L.: "Effect of Pressure and Water Saturation on Permeability of Western Tight Sandstones," *Proc.* U.S. DOE 5th Annual Symposium on Enhanced Oil and Gas Recovery and Improved Drilling Technology, Tulsa (Aug. 22-24, 1979) 34, L-5/1-L-6/16.

SI Metric Conversion Factor

$$\text{psi} \times 6.894757 \text{ E}+00 = \text{kPa}$$

SPEFE

Original SPE manuscript received for review May 18, 1986. Paper accepted for publication April 5, 1988. Revised manuscript received March 31, 1988. Paper (SPE 15210) first presented at the 1986 SPE Unconventional Gas Technology Symposium held in Louisville, May 18-21.

READINESS THROUGH RESEARCH

**ASSESSING TIGHT GAS RESERVOIR
QUALITY USING PETROGRAPHY
AND CORE ANALYSIS**

**EVALUATION DE LA QUALITE DES
RESERVOIRS GAZEIFERES COLMATES
PAR PETROGRAPHIE ET ANALYSE
DES CAROTTES**

by
Daniel J. Soeder

Prepared for
1989 International Gas Research Conference

Tokyo, Japan

November 6-9, 1989

**INSTITUTE OF GAS TECHNOLOGY
3424 South State Street Chicago Illinois 60616**

IGT

ASSESSING TIGHT GAS RESERVOIR QUALITY USING
PETROGRAPHY AND CORE ANALYSIS

EVALUATION DE LA QUALITE DES RESERVOIRS GAZEIFERES COLMATES PAR
PETROGRAPHIE ET ANALYSE DES CAROTTES

Daniel J. Soeder
Institute of Gas Technology, USA

ABSTRACT

The transport of liquids and gas through the pore systems of low-permeability reservoir rocks is difficult to measure using standard core analysis techniques. Very low flow rates and high capillary pressures force the analyses to take so much time that the data cannot be used for completion decisions. Several approaches have been taken in recent years to provide reservoir quality assessments of tight formations on a time scale applicable to well completion decision-making. A data base of high-precision, steady-state permeability measurements on tight gas reservoir samples has been combined with quantitative petrographic image analysis to correlate rock matrix flow properties with pore size and pore geometry in the samples. The goal of this research is to utilize petrography on chips and cuttings to assess tight gas reservoir quality, in conjunction with the fast-turnaround, unsteady-state permeabilities measured commercially on tight core samples.

RESUME

Le transport de liquides et gaz à travers le réseau de pores de roches-réservoir de faible perméabilité est difficile de mesurer à l'aide des techniques classiques d'analyses des carottes. A cause des très faibles débits et des fortes pressions capillaires, les analyses nécessitent trop de temps pour être utilisées lors des décisions de completion. Plusieurs approches ont été utilisées récemment afin d'évaluer la qualité des formations colmatées dans des temps permettant son utilisation lors des décisions de completion des puits. Une banque de données très précises pour la perméabilité à l'état stationnaire d'échantillons de réservoirs gazéifères colmatés a été utilisée avec des analyses quantitatives d'images pétrographiques afin d'établir les propriétés d'écoulement des fluides dans la matrice rocheuse en fonction de la taille et de la géométrie des pores des échantillons. Cette recherche a pour but l'utilisation de la pétrographie sur des éclats et tranches de roche afin d'évaluer la qualité des réservoirs gazéifères colmatés. L'analyse pétrographique est complétée par des mesures commerciales rapides et non stationnaires de la perméabilité des carottes de roches colmatées.

INTRODUCTION

The most common tight gas reservoirs are low permeability sandstones, organic-rich shales, and methane-bearing coal seams. Commercial gas production from these formations requires the presence of permeable pathways into the reservoir to collect the gas from a large surface area of the tight matrix and channel it to a wellbore. Natural permeable pathways, such as coarse sedimentary interbeds or natural fractures, are often supplemented with man-made fractures or horizontal boreholes to improve production rates and total recovery of the gas. Although permeable pathways and reservoir stimulation technology are important aspects of gas reservoir engineering, an understanding of the properties of the tight rock matrix is also required to accurately assess, model and predict tight gas reservoir performance. Virtually all of the reservoir's long-term performance is controlled by the rate at which gas from the tight matrix moves out to replenish gas produced from the permeable pathways. Properties of the tight rock matrix which influence total reservoir gas production include porosity, adsorbed gas, pore volume compressibility, pore size distribution, capillary entry pressure, flow path tortuosity, relative permeability, and permeability under drawdown net stress. Most of these are considerably more difficult to measure accurately in tight rocks than in conventional reservoir samples. Low cost, fast turnaround "unsteady state" core analysis offered by commercial laboratories can provide some of this information on tight rocks, although a number of the measurements which are important to tight gas reservoir engineering, such as adsorption or relative permeability, may not be readily available.

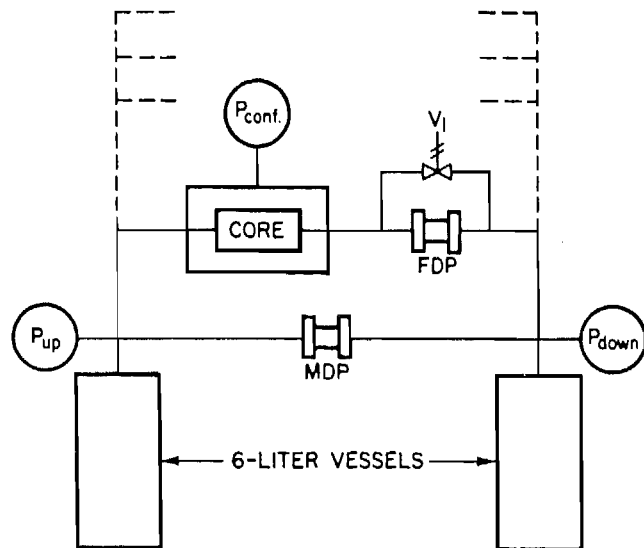
Since 1981, the Institute of Gas Technology (IGT) has been performing high precision analyses on tight gas reservoir core samples to try to improve the understanding of gas movement on a pore-to-pore scale within the rock matrix. These analyses have been made under carefully reproduced, in-situ reservoir conditions, including representative net confining stress, water saturation and steady-state gas flow. Data from these measurements were combined with pore morphology studies, made using special petrographic techniques, to begin to develop an understanding of the relationships between pore geometry and petrophysical properties of the tight rock matrix. Measurements on significant numbers of tight gas sandstone samples have created a data base and made it possible to assess the matrix properties of these low permeability rocks using simpler, faster and less expensive techniques. Similar detailed analyses have also contributed to the understanding of the reservoir properties of coal and gas shale, including trapping mechanisms, sensitivity of production to increased net stress, and the significance of adsorbed gas in these formations. The goal of the work reported in this paper is to provide an improved understanding of reservoir properties in tight gas resources, so that a combination of fast, inexpensive techniques, including unsteady-state core analysis, petrography, and porosimetry can be utilized to better assess tight gas reservoir quality.

MATERIALS AND METHODS

Tight rock samples are analyzed at IGT in a computerized, temperature-controlled, steady-state permeameter. A drawing of the various components in the apparatus is shown in Figure 1. The device contains four coreholders, plumbed in parallel with respect to the two main 6-liter gas tanks (only one coreholder is shown in the drawing for simplicity). The coreholders are a standard, hydrostatic, Hassler-type design, constructed of 316 stainless steel and rated for a hydraulic confining pressure of up to 70 MPa (10,000 psi). All of the components are enclosed in an insulated wooden chamber, and stable temperatures are maintained by an isothermal air bath

circulating inside the unit. The internal temperature of the chamber is kept about 3° - 5°C above ambient room temperature. This permits dynamic control of heat input to correct for internal and environmental temperature changes encountered during the course of operation. Power to the heating coils is controlled by a microcomputer using a proportional integral and derivative (PID) algorithm. The temperature inside the chamber is held constant to better than $\pm 0.01^\circ\text{C}$ of the nominal operating temperature of 310°K, allowing shut-in gas pressures to be stable to about one part in 30,000. For typical reference pressures of 7MPa (about 1000 psi), fluctuations due to temperature amount to less than 240 Pa (0.03 psi). This extraordinary degree of temperature control permits the apparatus to measure actual gas flow rates through rock samples as low as 10^{-6} standard $\text{cm}^3/\text{second}$.

As shown in Figure 1, the permeameter contains two 6-liter gas vessels, which apply a differential pressure across the cores, as well as supplying stable elevated pore pressures to the samples. Differential pressure is measured by the electronic transducer labeled "MDP" in Figure 1. As gas flows from the upstream tank, through the core and into the downstream tank, it must pass through the electronically actuated valve labeled "VI." At the start of a permeability measurement, gas pressure in the sample pores and downstream lines is equal to the pressure in the downstream tank. Higher pressure gas from the upstream tank is then introduced into the core, and the computer closes valve VI, isolating the downstream line from the downstream tank. Gas from the higher pressure upstream tank flows through the core, and the pressure in the downstream line volume gradually increases at a rate proportional to the permeability. The pressure increase in the downstream line with respect to the original pressure in the downstream tank is measured by the very sensitive differential pressure transmitter labeled "FDP" in Figure 1. When the downstream line pressure reaches 5kPa (0.7 psi) above the downstream tank reference pressure, it is at the maximum scale for the "FDP" sensor, and the microcomputer then opens valve VI for about 30 seconds. This allows the downstream line pressure to



A8300038

FIGURE 1. SCHEMATIC DRAWING OF PRECISION STEADY-STATE GAS PERMEAMETER USED AT IGT

equilibrate with the reference pressure, after which the valve is closed and another pressure build-up begins. The downstream line volumes for each coreholder are very accurately known (they average about 30cm³) and gas flow rates are calculated on the basis of a measured pressure increase over time in a known volume. Although the pressure on the downstream side of the core fluctuates by 5kPa with each measurement cycle, when compared to absolute gas pressures in the sample pores of 7 to 10 MPa, flow of gas through the cores can be considered essentially steady-state. Data for the flow rate calculations are generally taken from the central portion of each pressure build-up measurement to help eliminate transient pressure phenomena. The core analysis apparatus is also capable of measuring Boyle's Law (gas expansion) porosity on samples, as well as pore volume compressibility during increases in net confining pressure. The theory and operational characteristics of the high-precision, steady-state permeameter at IGT were described by Randolph (1983). The device has proven capable of measuring permeabilities to gas of less than 10⁻⁹ μm² (nanodarcy).

Other permeameter devices have also been developed at IGT to measure single-phase water permeabilities on tight rocks under reservoir net stress, as well as relative permeability to gas and water under various saturation paths (Chowdiah, 1987). The apparatus uses a capillary barrier in an attempt to perform the classic "Hassler"-type two-phase flow measurement on tight rocks, and it also directly measures a gas-water capillary pressure curve on samples held under conditions of restored in-situ reservoir net stress.

A better understanding of the relationship the core analysis data have to an actual low-permeability gas reservoir can be obtained by looking at the porosity and flow data with respect to the pore geometry and internal pore morphology of the samples (Soeder and Chowdiah, 1988). The contents of the pores are best observed with a scanning electron microscope on a sliced section of the rock sample. Overall pore geometry is seen better in optical thin sections at fairly low magnification.

A thin section is made from a piece of rock which is mounted to a glass slide, and ground and polished to a transparent, standard thickness of 30 micrometers. Prior to the thin section preparation process, the rock pores are commonly filled with blue-dyed, liquid plastic, which is then hardened. The plastic impregnation serves to hold the sample together during processing, and the blue color helps to distinguish the pores from clear mineral grains under the microscope.

In tight gas reservoir samples with very small pores, the blue-colored plastic can be difficult to see under a microscope. A modified impregnation technique was developed by Gies (1987) which employs a fluorescent dye in the plastic, rather than the standard blue material. Thin sections are observed using epifluorescence to make the fluorescent-dyed pores visible. An example of this in a tight gas sandstone is shown in Figure 2. The left photomicrograph shows clear sand grains and dark pores filled with the dyed plastic in transmitted light. The right photomicrograph is the same field of view in epifluorescence, showing only the fluorescent wavelengths from the dyed pores. The solid mineral grains are non-fluorescent, and therefore appear dark. Much more detail with respect to pore interconnections and matrix flowpath morphology can be observed in the fluorescent view of this tight sand. The fluorescent dye impregnation technique also works very well on coal, revealing phyteral porosity, porous macerals and microcleat structure as shown in Figure 3. The high-contrast image produced from the epifluorescent technique is very well suited to quantitative image analysis, since it is already in the binary form required by image



FIGURE 2. OBSERVATION OF PORES IN TIGHT GAS SANDSTONE USING TRANSMITTED LIGHT (LEFT) AND EPIFLUORESCENCE (RIGHT), TRAVIS PEAK SANDSTONE, SFE #2 WELL, 100X

analysis computers. Correlating the data produced from pore structure studies and petrographic image analysis with data obtained from high-precision core analysis has made great strides toward placing tight gas reservoir properties in the context of reservoir geology. This has produced a powerful and useful new tool for understanding the nature of productive versus non-productive tight gas reservoirs, in a manner that recognizes the influence of geological factors in controlling reservoir quality.



FIGURE 3. OBSERVATION OF PHYTERAL POROSITY, MICROCLEATS AND FLOWPATHS IN COAL, 40X, PRATT SEAM, ALABAMA WIDTH OF PHOTO = 2mm

RESULTS AND DISCUSSION

Analyses of low-permeability sandstone, shale, and coal have revealed that these tight materials have a number of properties in common. The flowpaths through these rocks often consist of narrow, linear cracks or "slots" rather than well-supported, triangular pores (refer back to Figures 2 and 3). Slot-like pore structures are much more susceptible to being squeezed shut under increased net confining stress than rounded or triangular pores (Ostensen, 1983). Net confining stress is always increased in a gas reservoir during production because the removal of gas lowers the pore pressure in the rocks, while the overburden pressure remains constant. Permeability reduction under stress is important in tight gas reservoirs, which have low permeabilities under even the best conditions. As shown in Figure 4, three different types of tight gas core samples show a significant reduction in permeability under increases in stress that are typical of reservoir drawdown. The narrow, uniform size of the cracks or slot pores also makes these rocks highly susceptible to flowpath blockage by liquids held under capillary pressure. As a result, permeability to gas tends to fall off rather steeply with fairly small increases in partial water saturation (Chowdiah, 1987).

Studies on tight gas sandstone have revealed that the pore geometry can be broken down into three main groups based on petrographic observations and core analysis data (Soeder and Randolph, 1987). These are shown schematically in Figure 5.

- 1) Grain-supported primary pores, with pore throats restricted to a greater or lesser degree by authigenic minerals, is the classic, earliest recognized tight sand pore geometry (Wilson, 1982). These rocks tend to have the highest matrix permeability of the tight sands, as well as the lowest pore volume compressibility.
- 2) The most common tight sandstone pore geometry, with permeabilities in the microdarcy range, contains secondary solution pores as the bulk of

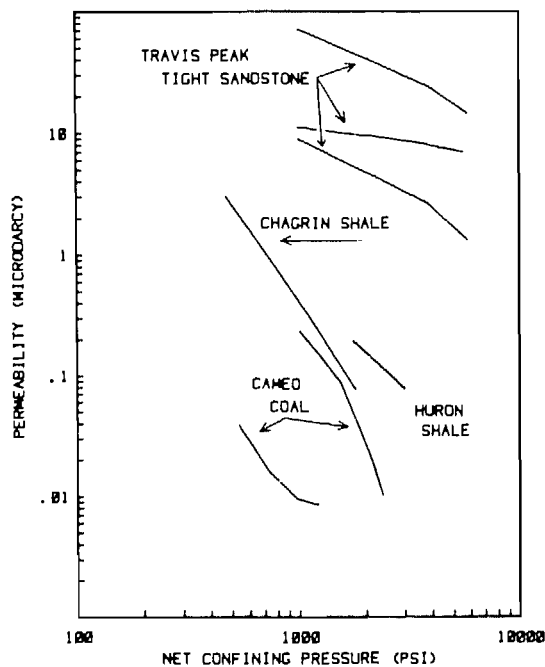


FIGURE 4. EXAMPLES OF THE EFFECT OF NET CONFINING STRESS ON SINGLE-PHASE PERMEABILITY IN TIGHT SAMPLES

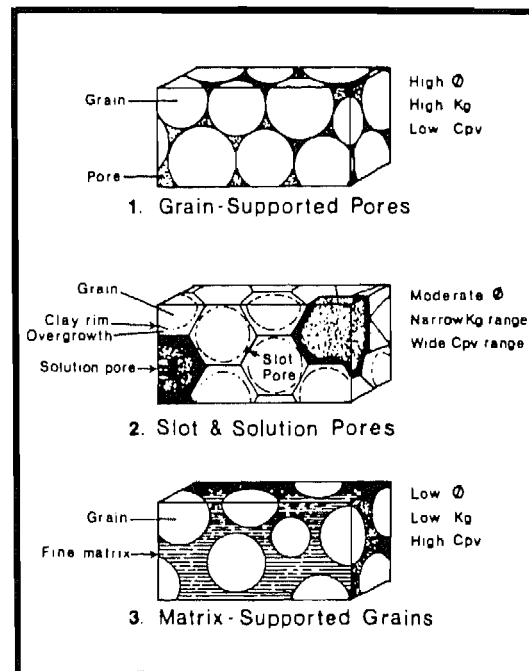


FIGURE 5. THE THREE MAIN CLASSES OF PORE GEOMETRY IN TIGHT SANDSTONE BASED ON PETROGRAPHIC AND CORE ANALYSIS DATA

the porosity; they are interconnected by primary porosity which has been reduced to narrow, linear cracks or "slots" by abutting, syntaxial quartz overgrowths on grains (Ostensen, 1983). The flat, crack-like slot flowpaths give the rock a high degree of stress-sensitivity, as well as being easily blocked with imbibed water held by high capillary pressures. 3) Sand grains supported in an ultra-fine, microporous matrix, which usually consists of clay or carbonate, is the third and least common tight sand pore geometry. These rocks tend to have a high pore volume compressibility, as well as a strong drop in permeability under increased stress, and they are also very sensitive to imbibed water. The three main tight sand pore morphologies described above can be readily identified under the petrographic microscope, and pore sizes can be easily determined with the mercury porosimeter. When this information is compared to that in a core analysis data base, the petrophysical parameters of the samples can be estimated and used to assess the quality of production potential from the tight gas sandstone matrix.

Current research at IGT, funded by the Gas Research Institute, is addressing the problem of reservoir quality prediction in the Travis Peak Sandstone of East Texas (Soeder and Chowdiah, 1988). Permeabilities measured on Travis Peak cores varied by over four orders of magnitude from about $10^{-2} \mu\text{m}^2$ to less than $10^{-6} \mu\text{m}^2$ (10 millidarcies to 1 microdarcy). This is a much greater range of permeability than the values typically measured in tight sands from the Rocky Mountains of the U.S. and Canada (Soeder and Randolph, 1987). The wide range of permeability in the Travis Peak suggested that a variety of pore geometries might be found in these samples which could be correlated to the permeability values. Results have shown that clearly visible differences in pore geometry are present between high-permeability and low-permeability core samples from the formation, as expected, and that these differences are distinctive enough to possibly permit reservoir quality assessments to be performed with reasonable accuracy using petrographic techniques (Soeder and Chowdiah, 1988). Current research on this project is investigating the practical aspects of utilizing petrographic reservoir assessment assisted by an image analysis computer, in conjunction with rapid, low cost mercury porosimetry to help quantify pore structure to the point of predicting reservoir parameters.

The reservoir properties of methane-rich coal seams and gas shales could also be assessed using petrographic and porosimetry analyses, provided there is a significant data base of detailed core analyses against which a comparison can be made. Although such extensive data bases do not currently exist at IGT for coal and shale as they do for tight sand, our limited number of core analyses revealed important and interesting reservoir properties which suggest that useful correlations may be possible in the future when more data are accumulated. Analysis of only nine cores of black, organic-rich and organic-lean gray shale from the Appalachian Basin revealed a number of important factors which may potentially control gas productivity of these rocks (Soeder, 1988). Black shale from the western, less thermally mature part of the basin contains significant amounts of liquid hydrocarbons. This petroleum is held in the shale pores under high capillary pressures, making the core samples virtually impermeable to gas. Organic-lean, gray shales with permeabilities comparable to tight sand, but highly stress-sensitive, are intertongued with the oil-bearing, black organic-rich shales in the western part of the Appalachian Basin. It appears that the impermeable black shales may act as reservoir seals, stratigraphically trapping gas in the permeable, gray shales beneath. A black shale sample from the more thermally mature, eastern part of the basin did not contain liquid hydrocarbons, and exhibited fairly high porosity and permeability. It also appears to contain a significant adsorbed component of gas, similar to coal.

Some recent work along these same lines by David K. Davies and Associates found similar permeability differences that correlate with the microscopic structure or fabric of shale (Davies et al., 1989). They determined that shales containing a "chaotic" microfabric had an overall larger pore size and higher permeability than shales composed of an ordered or layered microfabric. These fabrics correlate well with shale lithology, where gray shales deposited in an aerobic environment typically exhibit a chaotic fabric due to the activities of burrowing organisms in the soft mud, and black shales from an anoxic environment often contain an ordered, undisturbed fabric (Soeder, 1988). Understanding the relationships between gas productivity, shale microfabric and depositional environments could provide a new and useful geological tool for shale gas exploration and reservoir quality assessment.

Core analysis on a small number of coal samples revealed that one of the major causes of reduced gas permeability is elevated net confining stress (Rose and Foh, 1989). This is primarily due to the nature of coal as a plastic material, as well as to the fact that most flowpaths through the matrix consist of highly stress-sensitive flat, linear, narrow cracks or cleats (refer back to Figure 3). Calculations from core analysis data indicated that although all of the cleats narrowed in width to some degree under stress, the smaller size cracks were closed off completely. The main cause of reduced permeability in the coal was not a narrower average cleat size, but a greatly increased flowpath tortuosity caused by the closing of the smaller, interconnecting cracks. This was confirmed in petrographic observations of cleat systems in stressed and unstressed coal samples.

SUMMARY AND CONCLUSIONS

High-precision, steady-state core analysis under restored in-situ conditions can provide valuable measurements on low-permeability gas reservoir samples that cannot, in many cases, be obtained any other way. Unfortunately, the length of time required to collect data on these tight rocks is frequently far too long to permit the information to be used as a reservoir quality assessment technique prior to making a well completion. Fast turnaround, unsteady-state core measurements can provide significant amounts of reservoir property data, but it is often difficult to relate these measurements to specific aspects of the reservoir geology. The accumulation of a sizable data base of tight gas reservoir core measurements at IGT has permitted the development of correlations between petrophysical properties of tight rocks and the geological features of these formations. It appears that many of the fluid flow properties can be related, unsurprisingly, to certain aspects of the pore morphology and structure.

The combination of precision core analysis with petrographic study of pore geometry is a powerful technique for understanding the matrix properties which are critical to production in tight gas reservoirs. Identifying matrix parameters in terms of the pore morphology makes it possible to use low cost, rapid analysis techniques, such as mercury porosimetry and petrography, to assess tight gas reservoir quality prior to stimulation and completion. This could help to improve the selection of target horizons, and increase the efficiency of gas production from low-permeability formations.

REFERENCES CITED

Chowdiah, P. (1987), "Laboratory Measurements Relevant to Two-Phase Flow in Tight Gas Sand Matrix," paper SPE 16945 in Proceedings of the 1987 SPE Annual Technical Conference, Dallas, Texas, September 27-30, 1987, Society of Petroleum Engineers, Richardson, Texas.

Davies, D. K., et al. (1989), "Pore Geometry and Microfabrics of Gas-Bearing Devonian Shales," Abstract of presentation at 1989 American Association of Petroleum Geologists Annual Convention, San Antonio, Texas, April 23-26, 1989, AAPG Bulletin, v. 73, No. 3, p. 348, March 1989.

Gies, R. M. (1987), "An Improved Method for Viewing Micropore Systems in Rocks with the Polarizing Microscope," SPE Formation Evaluation, v. 2, No. 2, p. 209-214, June, 1987.

Ostensen, R. W. (1983), "Microcrack Permeability in Tight Gas Sandstone," Society Petroleum Engineers Journal, 919-926, December, 1983.

Randolph, P. L. (1983), "Porosity and Permeability of Mesaverde Sandstone Core From the U.S. DOE Multiwell Experiment, Garfield County, Colorado," paper SPE/DOE 11765 in Proceedings of the 1983 SPE/DOE Low Permeability Reservoirs Symposium, Denver, Colorado, March 14-16, 1983, p. 449-460, Society Petroleum Engineers, Richardson, Texas.

Rose, R. E. and Foh, S. E. (1984), "Liquid Permeability of Coal as a Function of Net Stress," SPE paper 12856 in Proceedings of the 1984 Unconventional Gas Recovery Symposium, Pittsburgh, PA, May 13-15, 1984, p. 253-259, Society Petroleum Engineers, Richardson, Texas.

Soeder, D. J. and Chowdiah, P. (1988), "Comparison of Pore Geometry in High and Low Permeability Sandstones, Travis Peak Formation, East Texas," paper SPE 17729 in Proceedings of SPE Gas Technology Symposium, Dallas, Texas, June 13-15, 1988, Society of Petroleum Engineers, Richardson, Texas.

Soeder, D. J. and Randolph P. L. (1987), "Porosity, Permeability and Pore Structure of the Tight Mesaverde Sandstone, Piceance Basin, Colorado," SPE Formation Evaluation, v. 2, No. 2, p. 129-136, June 1987.

Soeder, D. J. (1988), "Porosity and Permeability of Eastern Devonian Gas Shale," SPE Formation Evaluation, v. 3, p. 116-124, March, 1988.

Wilson, M. D. (1982), "Origins of Clays Controlling Permeability in Tight Gas Sands," Journal Petroleum Technology, v. 34, No. 12, p. 2871-76, December, 1982.

16WP/RPP/japan

Applications of Fluorescence Microscopy to Study of Pores in Tight Rocks¹

DANIEL J. SOEDER²

ABSTRACT

Observation of pore structures in thin section by traditional impregnation with blue-dyed epoxy becomes difficult when the pores are smaller than about 1 μm and/or linear in shape. These types of pores are common in many low-permeability gas reservoirs, such as coal, shale, and tight sandstone.

Incident-light fluorescence microscopy can be used to observe small, narrow pore structures in tight rocks. This common medical technique can be adapted to petrography by staining the impregnation epoxy with fluorescent rhodamine B dye along with the usual blue dye, and using an incident-light microscope equipped for epifluorescence to observe the prepared thin section.

Under excitation of green light at a wavelength of 5,400 \AA , rhodamine fluoresces a brilliant reddish orange, clearly showing impregnated pore spaces. A dichromatic interference filter in the light path passes the reddish orange light and blocks nonfluorescing mineral grains so that only the pore structure is visible. Fluorescing epoxy behaves as an emission source, and even submicron-size pores, which may be narrower than the wavelengths of visible light, become visible if they are impregnated. The incident-light configuration of the microscope also allows the observation of impregnated pore spaces in opaque materials such as coal. Fluorescence microscopy not only has potential for studying pore structures in tight sedimentary rocks, but also can be applied to crystalline rocks and other materials with narrow, linear, or small pores.

INTRODUCTION AND BACKGROUND

Rock pore structures typically are made visible in a thin section by impregnating the void spaces with a blue-dyed epoxy plastic prior to mounting and sectioning. The

traditional blue epoxy has limitations, however, when used on rocks with narrow, cracklike pores or microporosity, and on opaque materials such as coal. In pore diameters of 1 μm or less, the blue-dyed plastic commonly is too pale to see. Narrow, fracturelike pores, such as those in granite (Kowallis and Wang, 1983) and in many tight sandstones (Soeder and Randolph, 1987) also are difficult to observe when impregnated with blue plastic.

An inexpensive and clever solution to the problem of observing small pores through an optical microscope was devised by Canadian Hunter Exploration Ltd. (Gies, 1987) for use on tight gas sandstones in the Elmworth field of Alberta. Instead of the blue coloration, a bright-red fluorescent dye, rhodamine B, was added to the impregnation epoxy. A thin section so impregnated can be observed with an incident-light epifluorescence microscope equipped with proper illumination and filters. The microscope filter configuration passes only fluorescent wavelengths to the eyepiece; unimpregnated solid mineral grains appear black. This arrangement gives a high-contrast image of cracks and fine micropores and can be adapted for observing porosity in opaque materials, such as coal.

This paper is not intended as a review of the history of fluorescent microscopy in the study of rocks. It is apparent from the literature that many workers began impregnating microporous low-permeability rocks with fluorescent-dyed epoxy in the mid-1980s. About the time of Gies' (1987) findings, Yanguas and Dravis (1985) described a similar fluorescent pore-impregnation technique using a different dye and epoxy. Although neither paper referenced any earlier results, at least some workers probably have used similar procedures in the past. Nevertheless, impregnation with fluorescent dye has not been widely adopted by geologists and hydrologists because of a lack of publicity concerning its applications and because of a perceived difficulty in obtaining exotic fluorescent dyes.

One advantage of Gies' (1987) technique is that rhodamine B is a common low-cost material available from virtually any science supply house. Second, because rhodamine fluoresces a bright reddish orange in mid-range visible light (green) frequencies, it requires none of the expensive, special optics necessary for fluorescence using ultraviolet light. On the less desirable side, rhodamine is a dry powder that is strongly hydrophylic, and can be somewhat difficult to handle. Rhodamine also is a low-level toxic substance, and common-sense precautions must be exercised when working with it in the laboratory. Standard procedure at the Institute of Gas Technology (IGT) calls for latex gloves and lab coats when handling

©Copyright 1990. The American Association of Petroleum Geologists. All rights reserved.

¹Manuscript received, February 25, 1988; accepted, August 10, 1989.

²Institute of Gas Technology, 3424 South State Street, Chicago, Illinois 60616-3896.

Much of the work described in this paper was funded by the Gas Research Institute (GRI) under Contract No. 5086-211-1258. The financial support of GRI is gratefully acknowledged. Special thanks for help and encouragement are directed to Richard E. Wyman and Robert M. Gies of Canadian Hunter Exploration Ltd. in Calgary, Alberta. Thanks are also directed to the author's colleagues at the Institute of Gas Technology (IGT), including Susan Christensen for typing the manuscript, and John R. Hasenberg for preparing the samples.

Reference to trade names or specific commercial products in this article is for informational purposes only and does not constitute an endorsement, recommendation, or opinion of suitability by IGT or GRI.

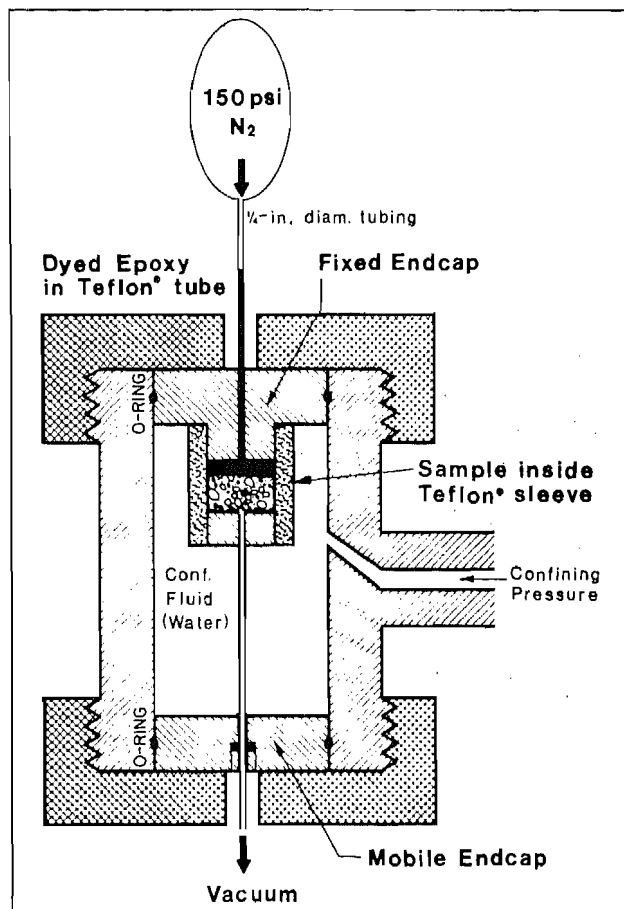


Figure 1—Apparatus for epoxy impregnation of samples under confining pressure.

the epoxy components and the powdered rhodamine; mixing is performed under a vented hood. After the dye compound is dissolved in the epoxy and cured, the material becomes inert and can be handled like any other colored plastic.

Anyone preparing to work with rhodamine B should be aware that it has been identified as both a mutagen and an equivocal tumorigenic agent (possible carcinogen) at high levels of exposure in laboratory animals (Sax, 1984). Although not particularly dangerous to humans in the small quantities used to dye batches of epoxy, prudence dictates that laboratory personnel should avoid skin contact and ingestion of the dye. Compared to standard petrographic laboratory procedures such as hydrofluoric acid etching, working with rhodamine is relatively safe, and its hazardous properties should not be overstated. In fact, until recently, it was a common food coloring known as FD&C Red Dye No. 19.

The advantages of using rhodamine impregnation on tight rocks outweigh any drawbacks related to possible toxicity at high levels of exposure, which can be avoided by exercising care in the laboratory. IGT has found this technique to be a powerful tool for observing pore structures and flow paths in tight gas reservoir samples, such as coal, shale, and tight sandstone. The combination of fluorescent petrography and high-resolution, steady-state core analysis has given us a better understanding of

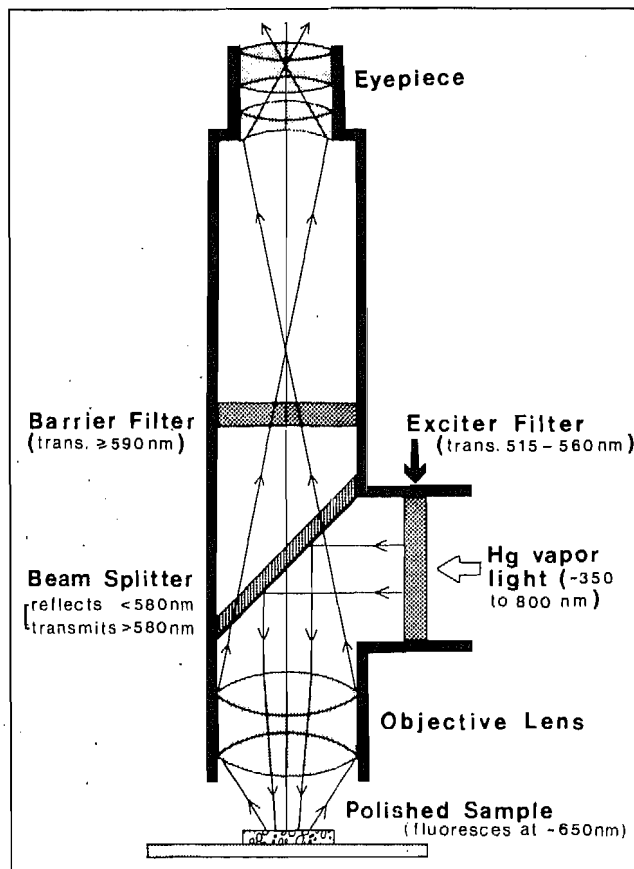


Figure 2—Microscope optical configuration for observing rhodamine fluorescence under incident light.

the mechanics of gas transport through pore systems of low-permeability formations.

MATERIALS AND TECHNICAL PROCEDURES

Tight rock samples at IGT normally are impregnated with Maraglas® 655 resin and 555 hardener, a low-viscosity clear-casting epoxy able to penetrate very small pores. (Manufacturers of all materials mentioned in the text are listed in Appendix 1). Maraglas is endothermic and must be cured in an oven, allowing impregnations to proceed for much longer periods than can be achieved with exothermic epoxies having preset curing times.

One useful aspect of the fluorescent-dye impregnation technique is that pore structures can be viewed in both epifluorescence and transmitted light simply by changing the illumination and filters without moving the sample. However, strongly fluorescent rhodamine B, when added to epoxy in concentrations sufficient for transmitted-light observations, results in overly bright fluorescence and a loss of fine detail. To avoid this problem, rhodamine is added to the epoxy in small amounts designed for optimal fluorescence. Then, a second, nonfluorescing dye is dissolved in the epoxy so that the pores are visible in transmitted light. One such nonfluorescing dye is Intraplast Brilliant Blue GN®, the original dye used at IGT for blue epoxy impregnation. A dry powder mixture

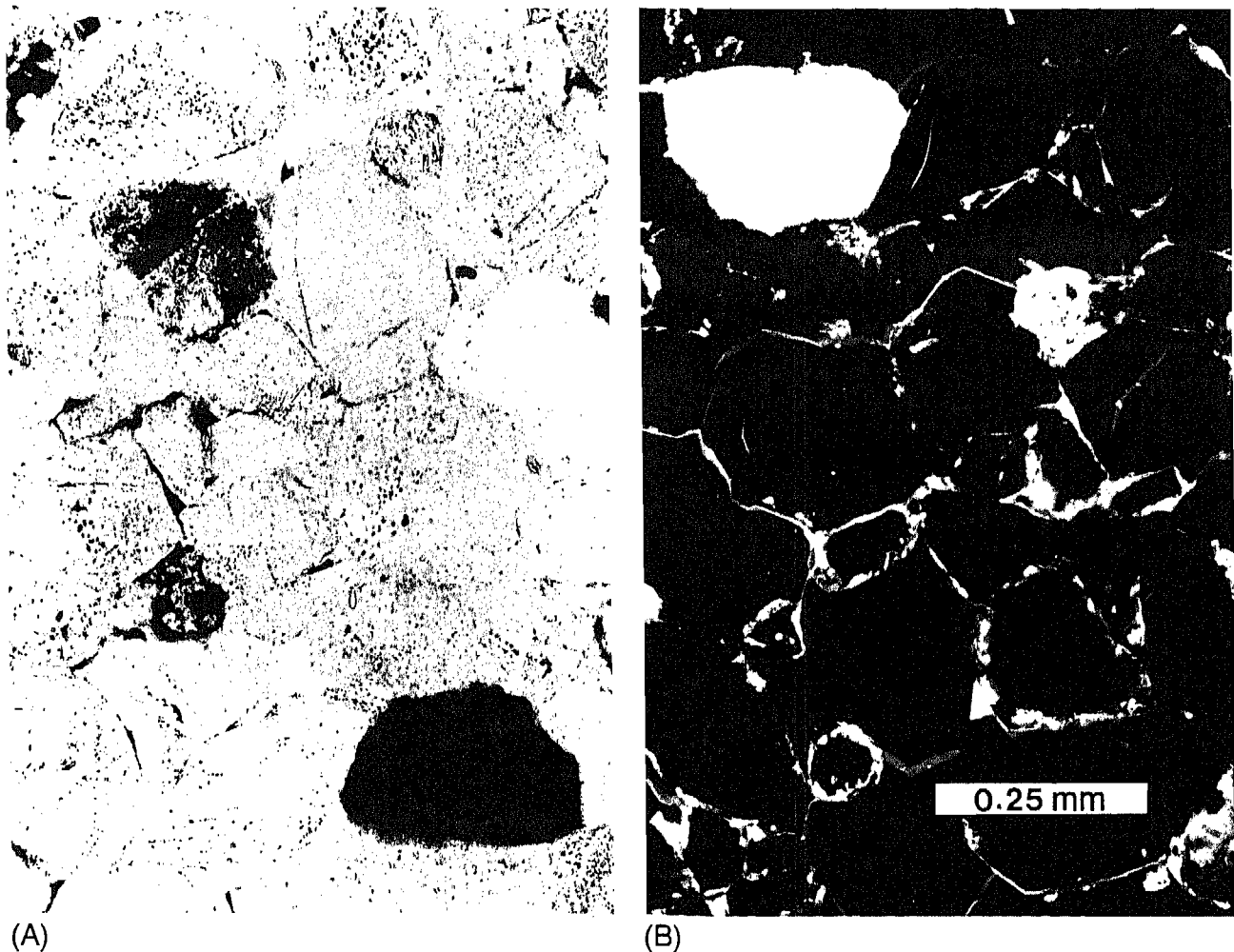


Figure 3—Photomicrographs of Travis Peak Sandstone core sample, S.A. Holditch and Associates 2 Staged Field Experiment well, North Appleby field, Nacogdoches County, Texas, 8,275 ft (2,522.2 m). (A) Sample in transmitted plane light, (B) same view in rhodamine epifluorescence.

of 30% rhodamine B and 70% blue by weight gives epoxy-impregnated pores a pleasant, indigo-violet color in transmitted light and a bright reddish orange glow in epifluorescence.

Before the Maraglas epoxy is mixed, the powdered dye mixture is dissolved in the solventlike hardener component at a nominal rate of 0.081 g of dye per gram of hardener. The epoxy is then mixed at a ratio of 100 parts 655 resin to 7.56 parts 555 hardener by weight, which is about 8% more hardener than called for by the manufacturer to compensate for the weight of the dye. The material is placed in a disposable beaker and mixed for at least one hour on a magnetic stir plate.

Samples are impregnated in a conventional vacuum apparatus. Rock chips in small (50-mL) disposable plastic beakers are placed inside a bell jar with a container of prepared epoxy, and both are exposed to a vacuum of about 50 mtor (6.67 Pa) for several hours. In the bell jar, the epoxy container is attached to a metal shaft above the beakers of sample chips. The shaft, which extends outside the bell jar through an O-ring seal, can be rotated to pour the epoxy into the sample beakers while maintain-

ing the vacuum. Epoxy is added to the beakers of chips until each sample is completely submerged.

As air is introduced into the bell jar, atmospheric pressure forces the epoxy into the pore spaces. To fully impregnate tight rocks usually requires additional pressure to overcome capillary forces because epoxy behaves as a nonwetting fluid phase in most rocks. Failure to recognize this phenomenon is a common cause of unsatisfactory impregnation in tight rocks. Workers at IGT impregnate tight samples by fastening a flexible membrane over the top of the plastic beaker (small rubber balloons work well) and placing the covered beakers into a hydraulic chamber where pressure of up to 8,000 psi (55.2 MPa) is applied for several hours to drive the epoxy into the tiniest pores. Pressure is increased slowly to avoid creating a differential pressure gradient between the inside and outside of the sample. Impregnation times as long as overnight can be used with Maraglas, although the material has a finite pot life and should be cured within 24 hr after mixing. Yanguas and Dravis (1985) also recommend using pressure impregnation on microporous rock samples.

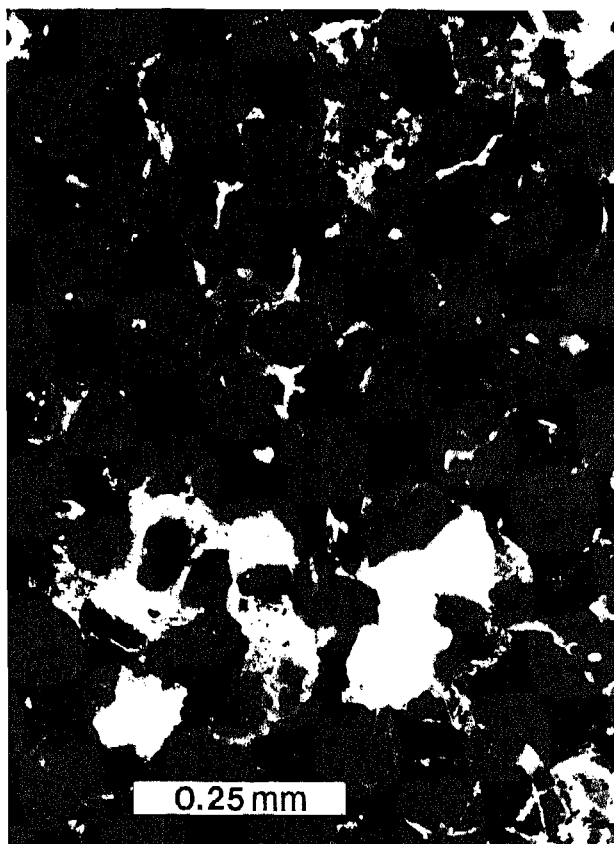


Figure 4—Photomicrograph of Spirit River Formation core sample, Canadian Hunter well 11-12-71-13W6, Elmworth field, Alberta, 6,786 ft (2,068.4 m), epifluorescence. Sample impregnated with epoxy under 5,000-psi (34.5 MPa) net confining pressure.

Maraglas 655 epoxy is oven cured at 167 °F (75 °C) for about 16 hr. The impregnated samples then are ground flat on one side for mounting with the final grinding done gently by hand. Vigorous polishing generates frictional heat that melts the epoxy and allows it to coat the mineral grains. Incident light then passes through the clear mineral grains and causes the thin coating of rhodamine-dyed epoxy on the back surface of the grains to fluoresce, giving a background glow to the thin section.

The smoothed surfaces are mounted onto ground-glass slides with Epo-Tech® 301-2 epoxy and placed in a spring-loaded mounting jig until a firm bond is formed. A different epoxy is used for mounting to reduce the possibility of dye migration from the pore epoxy to an identical bonding medium behind the grains. The thin sections then are ground and polished normally.

An alternative method to rhodamine-dye impregnation was used by Cather et al. (1989), wherein the sample's pores are filled with clear epoxy, a thin section is made, and the finished surface is stained with fluorescent dye. This procedure, adapted from Ruzyla and Jezek (1987), enables older thin sections, impregnated only with undyed or clear epoxy, to be stained for pore-morphology studies. The dye is carried in a solvent, such as toluene, that stains the epoxy plastic, but does not

attack the inorganic mineral grains. IGT has experimented with this technique and uses it occasionally. By surface-staining the epoxy, pores appear more two-dimensional than those fully impregnated with fluorescent dye, but the method has some drawbacks. In rocks of variable pore sizes, the solvent attacks the plastic such that proper staining of the small pores commonly occurs at the expense of overstaining the larger pores. Because of its larger surface area for solution action, plastic in large pores also can lose adhesion and fall out of the slide. Another problem is that solvents that stain epoxy plastic also may stain some of the organic material in a sample. Nevertheless, this technique can produce sharp fluorescent images of pores in rocks composed of transparent mineral grains. Its principal advantage is that older thin sections impregnated with only blue-dyed or clear epoxy can be stained for fluorescence.

Impregnation Under Effective Stress

Core-analysis measurements on low-permeability samples at IGT (Soeder and Randolph, 1987; Rose and Foh, 1984) and elsewhere have shown that the permeabilities of tight rocks and coals are sensitive to increases in net confining pressure. Permeability reduction results from adjustments in matrix flow paths to higher levels of effective stress, but previous attempts to observe these changes petrographically met with limited success (Brower and Morrow, 1985).

The apparatus in Figure 1 was assembled at IGT for sample impregnation under net confining stress. The unit consists of a triaxial, Hassler-type coreholder mounted vertically, with a short length of 0.25-in. (6.4-mm) diameter Teflon® tubing extending through the fixed, upstream endcap to the sample face. Both endcaps, which are coated with a mold-release compound prior to assembly, are arranged to enclose and seal a 1-in. (25.4-mm) diameter by 1-in. (25.4-mm) long rock sample inside a tight-fitting Teflon sleeve, which prevents the impregnation epoxy from bonding to the coreholder's parts. Hydraulic pressure supplies a uniform confining force equivalent to reservoir effective-stress conditions on all sides of the sample. The 0.25-in. (6.4-mm) tubing is filled with fluorescent-dyed epoxy, and an applied gas pressure of about 150 psia (1,034 kPa) forces the epoxy into the pores of the confined sample. A 50-mtor (6.67-Pa) vacuum applied to the downstream endcap simultaneously removes air from the pores. Stress is maintained until the epoxy has cured. It is important to apply the confining force before beginning impregnation to insure closure of any fractures that may have opened as a result of stress relaxation in the core. A conventional thin section is prepared from the cured sample.

Observation and Photomicrography

The optical configuration of the microscope used to observe the epoxy-impregnated samples in epifluorescence is shown schematically in Figure 2. Bright light from a mercury-vapor lamp enters from the side and

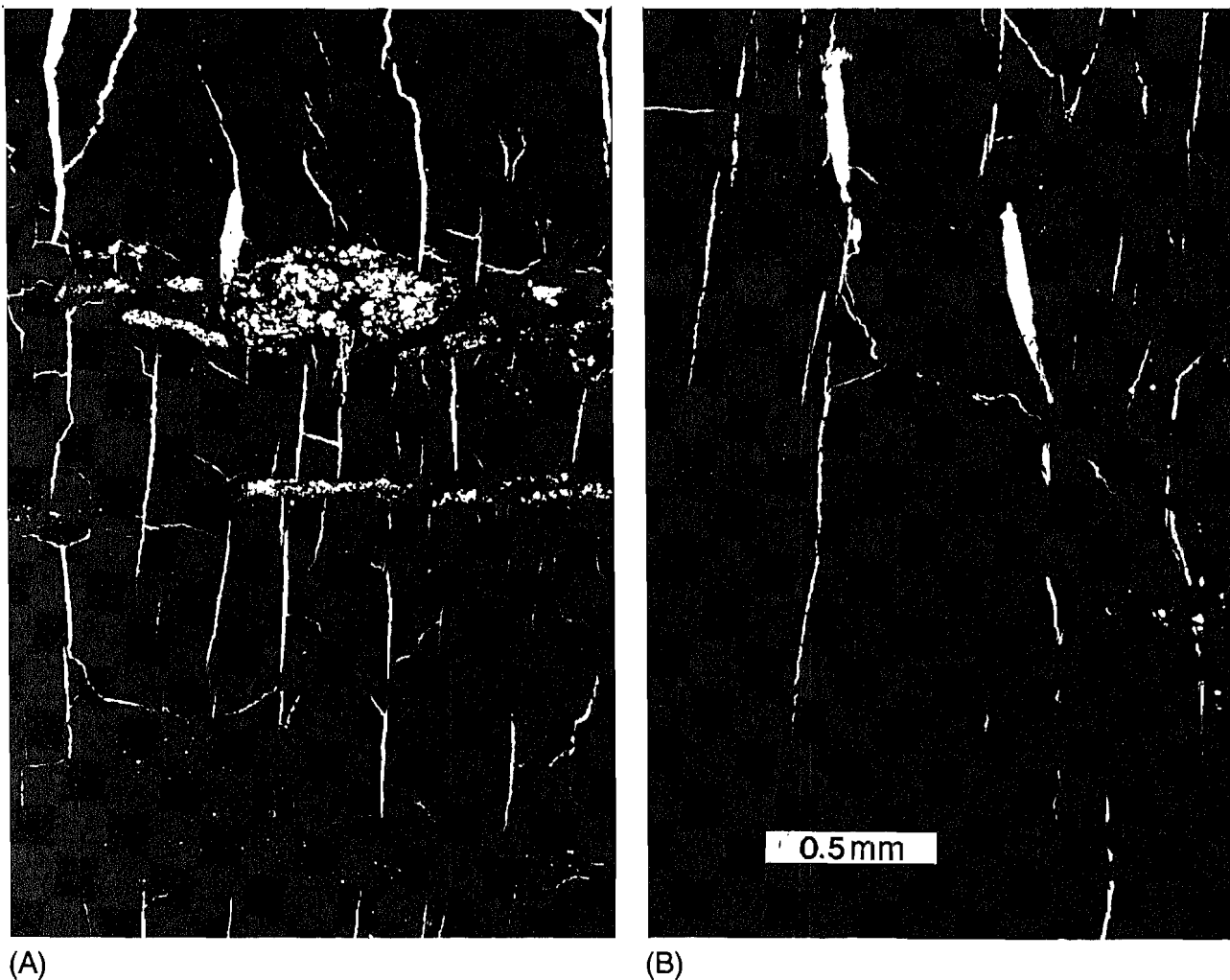


Figure 5—Photomicrographs of Pratt coal, Pottsville Formation core sample, from USX Corporation, Oak Grove mine, Warrior basin, Alabama. (A) Sample impregnated with rhodamine-dyed epoxy unconfined, (B) sample impregnated under 1,000-psi (6.895 MPa) effective stress, epifluorescence. Bar scale is same for (A) and (B).

passes through an exciter filter, which transmits green light between 5,150 and 5,600 Å wavelength. The light encounters a dichromatic beam splitter that reflects all wavelengths shorter than 5,800 Å and transmits all longer wavelengths. The beam splitter is mounted at a 45° angle to reflect the green light down through the objective lens and focus it onto the polished sample surface.

Light from the sample is collected by the objective lens and directed toward the eyepiece. Although the reddish orange fluorescent light passes through the beam splitter and barrier filter, green light reflected from the sample is effectively blocked. This prevents the mineral grains from being viewed and creates a high-contrast image in which only epoxy-impregnated pores are visible. The effect is shown in Figure 3 for a specimen of Lower Cretaceous Travis Peak sandstone from a depth of 8,275 ft (2,522.2 m) in the S.A. Holditch and Associates 2 Staged Field Experiment well, North Appleby field, Nacogdoches County, Texas. This core sample has gas porosity of 6.1% and dry gas permeability of 8.27 μ d. Figure 3A was taken in transmitted plane light, and Figure 3B was

taken with the incident-light rhodamine-epifluorescence arrangement. Because the pores under fluorescent light appear reddish orange between the darkened grains, more details of porosity can be distinguished visually than can be conveyed in a black and white photograph. Still, Figure 3 does demonstrate the nature of pore enhancement obtained from rhodamine impregnation.

Acceptable photomicrography of rhodamine-fluorescent pores requires some experimentation. Because of the high contrast of the fluorescent image, it is difficult to obtain photographs representative of the sample's visual appearance. Acceptable results have been obtained by using high-speed film (ISO 400 or faster) and bracketing the exposure widely. Camera metering systems generally do not accurately read these high-contrast images. Inasmuch as image brightness is directly proportional to magnification, it is sometimes difficult to see to focus at low powers. Accurate focusing for low-power fluorescence photographs can be done with transmitted light as long as the beam splitter and filters are mounted in the optical path of the microscope. High-contrast fluorescent

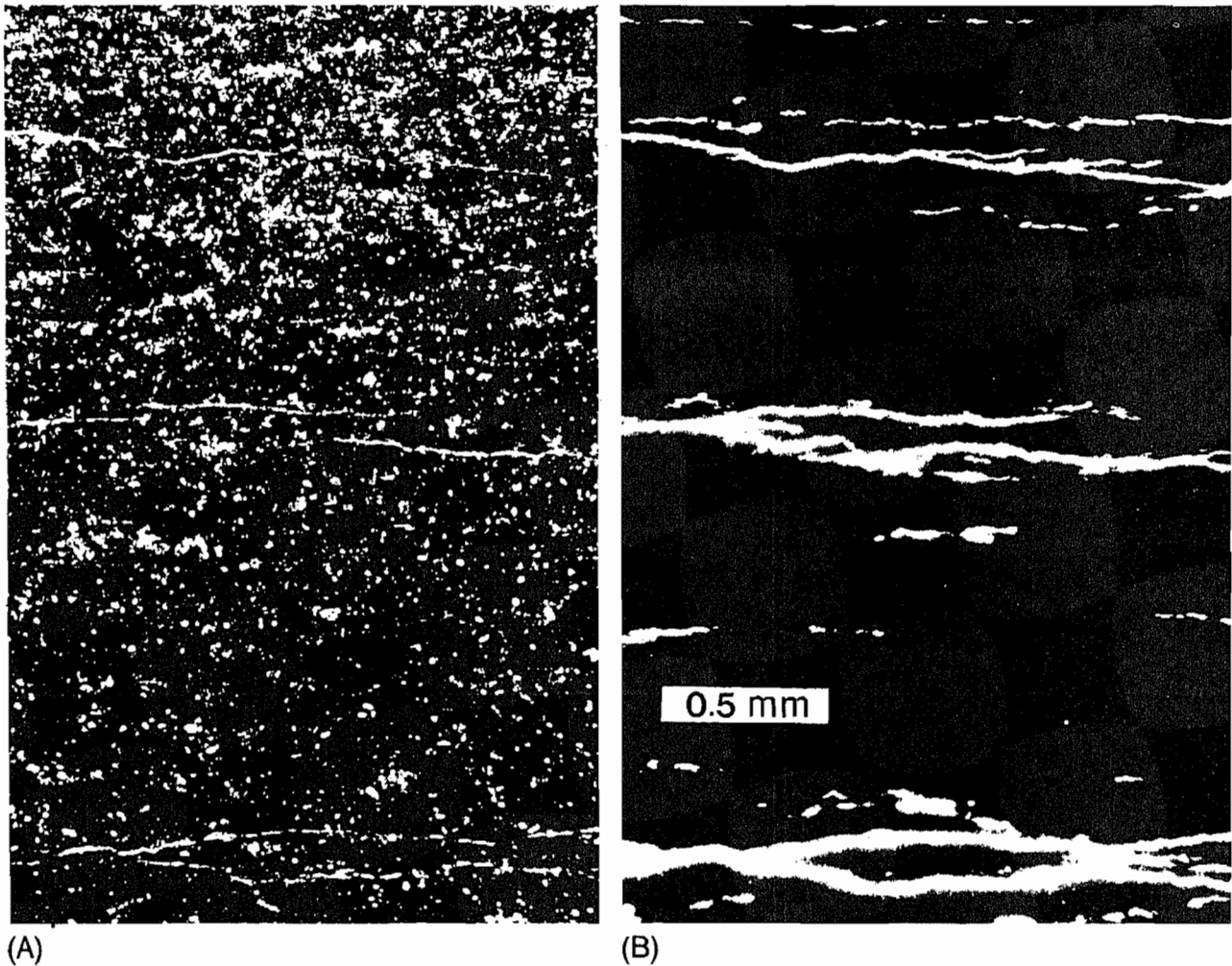


Figure 6—Photomicrographs showing fissility in black shale sample enhanced by fluorescence. Marcellus Shale, M.E.R.C. 1 well, Morgantown, West Virginia, 7,440.5 ft (2,270.3 m). (A) Sample in transmitted-light view, (B) sample in epifluorescence view.

images are well adapted to image analysis because they are essentially binary images that require little or no enhancement.

Cost Considerations

The costs involved in setting up a laboratory for epifluorescence microscopy of rhodamine-impregnated rock samples depend upon the facilities and equipment that are available and can be modified. IGT already had a Zeiss Universal® microscope equipped with a mercury lamp and filter holder for ultraviolet epifluorescence of biological specimens and facilities for epoxy impregnation and thin-section preparation. Setting up for fluorescence petrography, therefore, required only the purchases of a 100-g bottle of rhodamine B dye for impregnation (about \$70 U.S.) and the proper filter/beam splitter combination for rhodamine epifluorescence on the Zeiss microscope (about \$700 U.S.). A check of three brand-name microscope dealers (Zeiss, Nikon, and Olympus) in the Chicago area showed no dif-

ficulty in obtaining proper filter combinations. According to the instrument literature, one should be able easily to modify most modular microscopes for rhodamine epifluorescence.

RESULTS AND DISCUSSION

Observations of rhodamine-impregnated rocks under epifluorescence reveal features difficult or impossible to see in transmitted light. For example, as shown in Figure 3, the tight Travis Peak sandstone has narrow crack or slotlike pore interconnections visible along grain boundaries in the fluorescent view. Not apparent in the transmitted-light photo is that these slotlike pores (slot pores) are open flow paths through the rock and whose presence is critically important to permeability of this tight sandstone. The pore geometry of this sample is typical of that found in many tight gas sandstones (Soeder, 1984) and consists of relatively large grain-size secondary solution pores. These are interconnected through remnant primary intergranular porosity, which has been

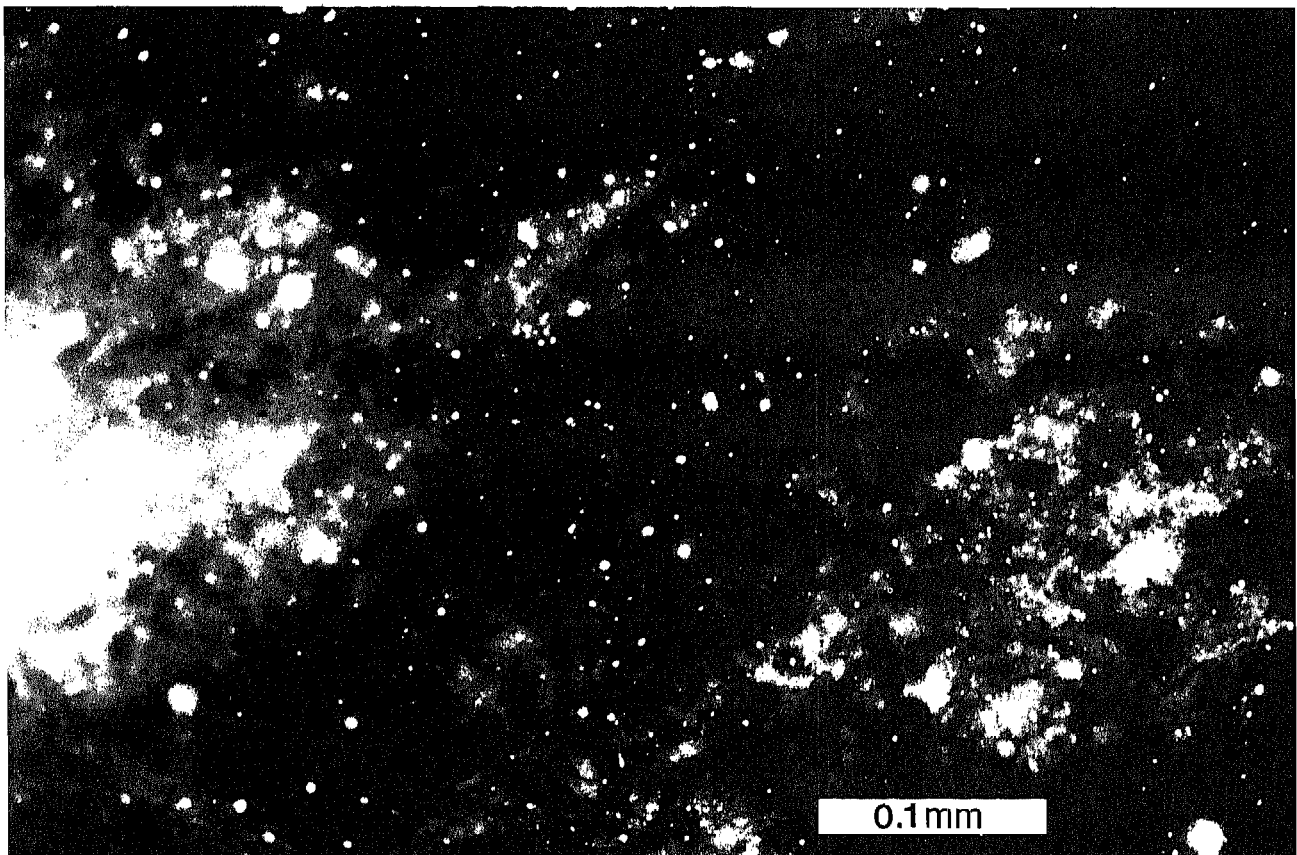


Figure 7—Photomicrograph showing fine details of porosity in gray shale sample under epifluorescence. Chagrin Member of Ohio Shale, Columbia Gas well 20143, Gallia County, Ohio, 2,170 ft (661 m).

reduced to narrow, linear slot pores by extensive quartz overgrowths. Solution pores provide tight gas sandstones with reasonable porosity and commercially significant gas contents. To be produced, however, gas must travel through the narrow slot-pore flow paths, which are responsible for low permeabilities of these rocks, as well as for the high sensitivity of gas production to reservoir stress and water saturation.

Pore Morphology and Stress

Calculations from core analysis data had indicated that the characteristic aperture of slot-shaped gas flow paths in western tight sandstones under effective stress representative of the midpoint of reservoir drawdown is on the order of $0.1 \mu\text{m}$ (Soeder and Randolph, 1987). Because this is smaller than wavelengths of visible light (0.4 to $0.7 \mu\text{m}$), these flow paths normally cannot be seen with an optical microscope. However, if these narrow pores are impregnated with fluorescent-dyed epoxy, the exciter beam causes the fluorescing rhodamine to emit light as a point source, making the pores visible.

Earlier attempts by Brower and Morrow (1985) to observe slot pores impregnated with epoxy under stress required the removal of mineral grains with hydrofluoric acid prior to scanning electron microscopy (SEM) of the epoxy pore casts. The absence of definitive slot-pore

casts in their stressed samples left open the question of whether slot pores truly exist as gas flow paths in the reservoir or are mere artifacts of stress relaxation as deep core is brought to the surface. Brower and Morrow (1985) were unable to ascertain whether the absence of slot-pore casts was due to damage by acid etching or to the possibility that the slots indeed are not flow paths at reservoir effective stress.

Successful fluorescent-epoxy impregnation of slot pores in a tight sandstone at representative reservoir effective stress is shown in Figure 4, a photomicrograph of Cretaceous Spirit River Formation sandstone from a depth of 6,786 ft (2,068.4 m) in Canadian Hunter 11-12-71-13W6 well, Elmworth field, Alberta. This core had a dry-gas permeability of $4.68 \mu\text{d}$ at 5,000-psi (34.5 MPa) net confining stress, the midpoint of drawdown, and dry effective gas porosity of 6.7%. The photomicrograph indicates that a number of narrow, impregnated slot pores are present at 5,000-psi (34.5 MPa) net confining stress. SEM observations of these and other tight sandstones showed slot pores containing clay minerals, clear evidence that the slot pores existed as open flow paths in the reservoir (Soeder and Randolph, 1987).

Coal, which is more stress sensitive than tight sandstone, shows more obvious changes when impregnated with fluorescent epoxy under confining pressure. Figure 5 shows epifluorescent photomicrographs of a mine sample of Pennsylvanian Pratt coal from the Pottsville For-

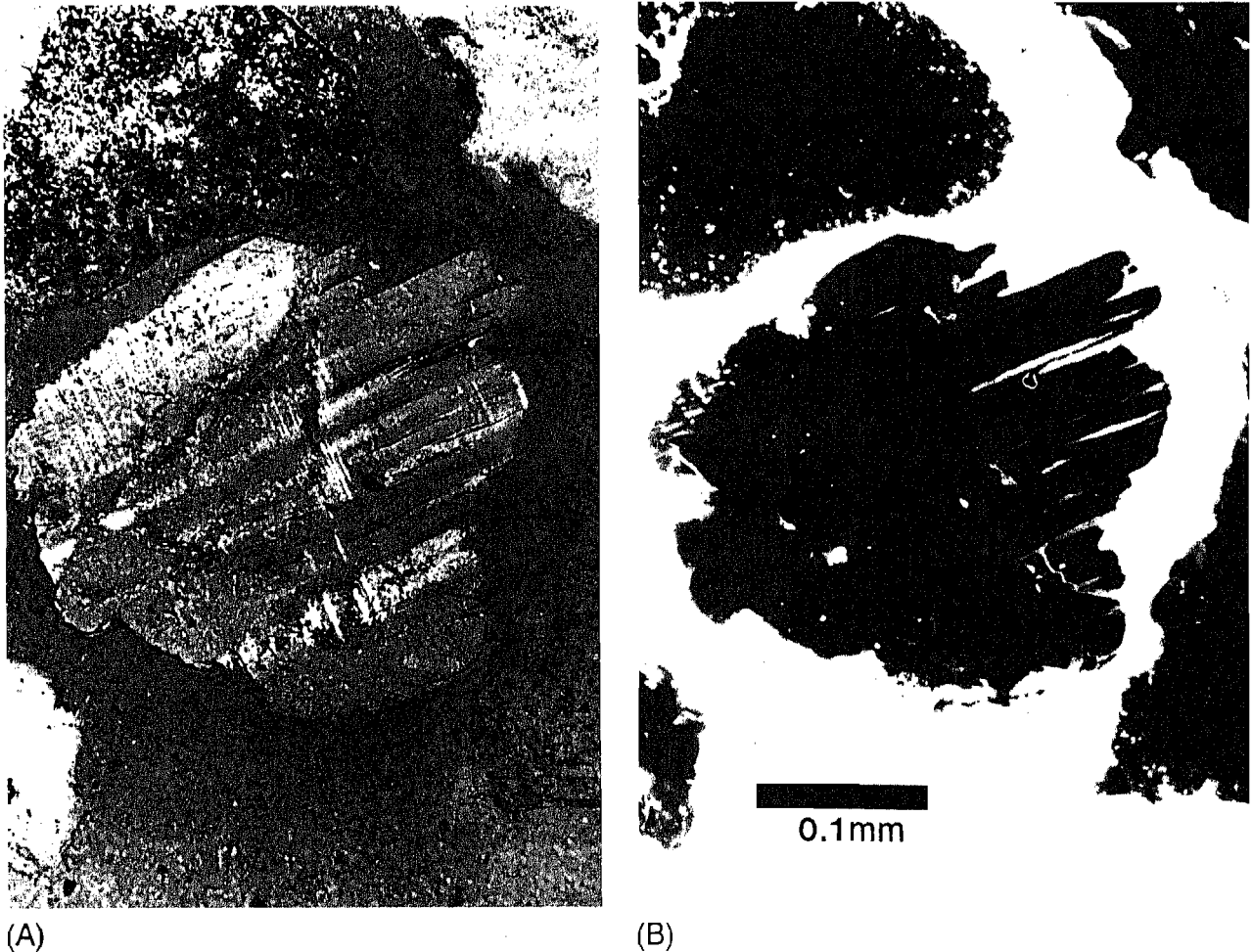


Figure 8—Microporosity in feldspar-rich sand from Cape Cod, Massachusetts. (A) Photomicrograph is through crossed polars with 1° red plate, (B) photomicrograph is same view in epifluorescence. Sample courtesy of Warren Wood, U.S. Geological Survey.

mation, Alabama, impregnated with rhodamine-dyed epoxy at (A) zero net stress and (B) under 1,000-psi (6.895 MPa) net confining stress. The two samples in Figure 5 were cut from the same bedding plane, less than 1 in. (2.54 cm) apart, and are reasonably similar in composition and microstructure. The amount of fine detail visible in the coal cleat network with rhodamine impregnation is astounding. The photographs show not only distinct narrowing of the major cleats under stress, as expected, but also show many tiny cleats visible in the unstressed sample disappear at 1,000-psi (6.895 MPa) effective stress.

Gas-permeability measurements can be used to calculate characteristic aperture and tortuosity of flow paths in a rock sample under stress (Randolph et al., 1984). For many low-permeability rocks, measurements commonly indicate that characteristic flow-path apertures increase under higher effective stress rather than decrease. For example, high-quality gas-permeability data from a core sample of Devonian Marcellus Shale revealed that the characteristic aperture of a flow path under 3,000 psi (20.69 MPa) effective stress is $0.05 \mu\text{m}$ (Soeder, 1988a). Doubling the effective stress to 6,000 psi (41.37 MPa)

increased the flow-path aperture to $0.35 \mu\text{m}$ but reduced permeability by nearly 70%. Calculated flow-path tortuosity increased more than ten times when effective stress was doubled.

These data are interpreted to mean that smaller pores and pathways in some tight gas formations close preferentially as effective stress increases, leaving only larger flow paths open to gas. This leads not only to larger characteristic flow-path aperture at high stress but also to greater flow-path tortuosity due to a reduction in the degree of pore interconnections. Although this phenomenon was discovered and described several years ago from calculations based on core-analysis data (Randolph et al., 1985), the coal photomicrographs in Figure 5 mark its first physical observation in a tight gas reservoir.

Impregnation of Coal and Shale

Fracture width, size distribution, and cleat spacing in coal are critical input parameters to mathematical models of coal-bed methane production (Wyman, 1984).

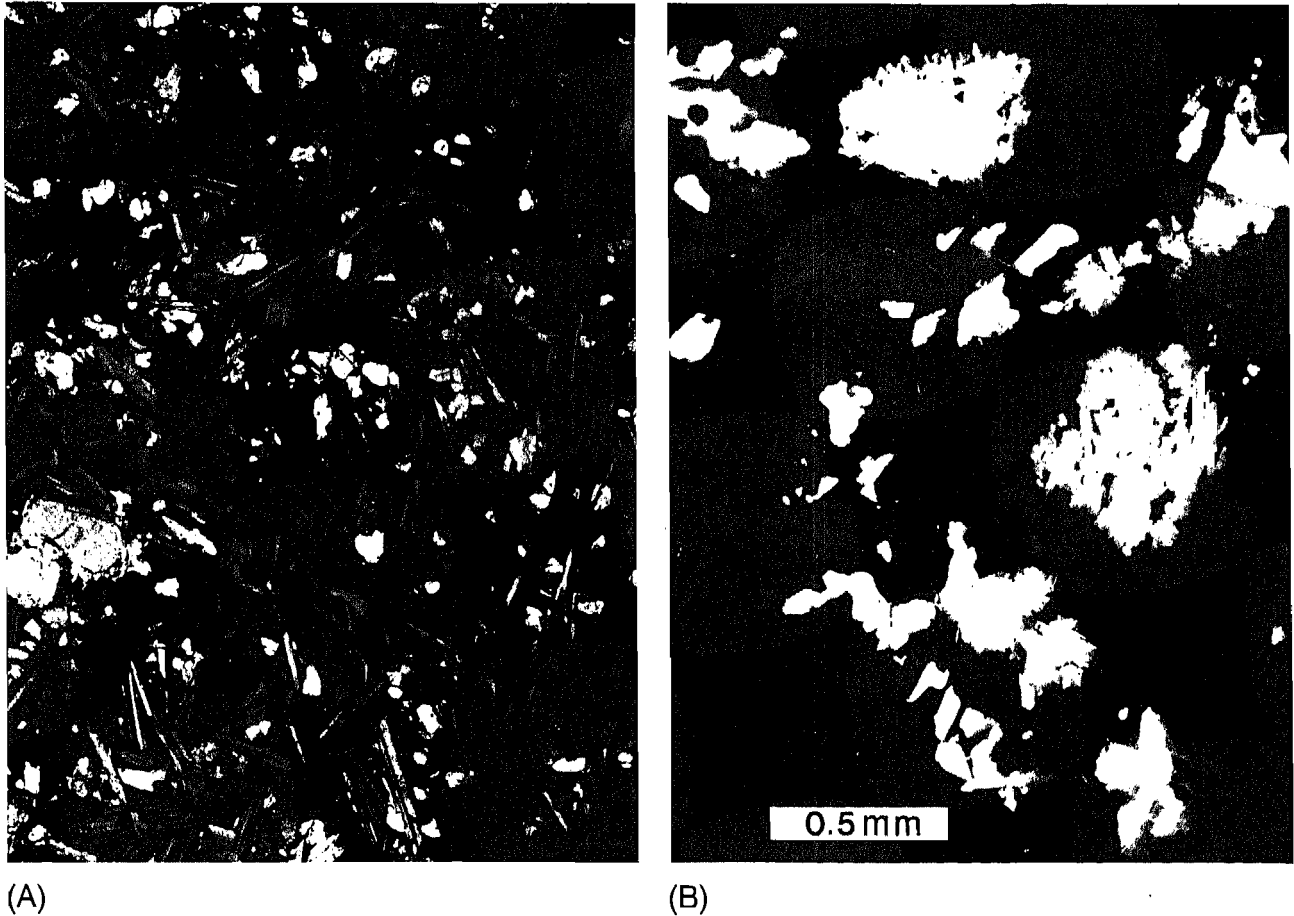


Figure 9—Porosity in Montana basalt (Geoscience Resources catalog 3520). (A) Photomicrograph through crossed polars with 1° red plate, (B) photomicrograph of same view in epifluorescence shows vesicles connected by network of fine cracks.

The epifluorescent impregnation technique appears to be useful in obtaining much of this information petrographically from polished optical sections. Careful microscopic examination of unimpregnated coal samples with the rhodamine filter configuration revealed that some coal components that fluoresce under ultraviolet light will also fluoresce faintly under the green exciter beam. The fluorescence of natural coal materials under green illumination is several orders of magnitude less than that of rhodamine dye, however, and the rhodamine-impregnated porosity can be distinguished with little difficulty.

Impregnating shale with rhodamine-dyed epoxy was significantly more difficult than the sandstone or coal impregnations. Apparently this arises from the nature of clay minerals, which strongly resist penetration of the oil-like epoxy resin into the matrix. Figure 6 shows the result of an epoxy impregnation by the vacuum/pressure method on the previously described Marcellus Shale from a depth of 7,448.5 ft (2,270.3 m) in the Department of Energy 1 Morgantown Energy Research Center well at Morgantown, West Virginia. In this wildcat Devonian gas-shale test, the Marcellus at this depth showed potential as a gas producer. Core-analysis measurements gave a porosity of about 10% and permeability of 19.6 μd at ini-

tial reservoir stress and 5.9 μd at midpoint of drawdown (Soeder, 1988a). As shown in the overexposed epifluorescent view in Figure 6B, epoxy remained primarily in bedding plane cracks in the fissile shale, with very little penetrating the matrix itself.

Impregnation of shale matrix was successful with a wetting-phase material, rhodamine-dyed shellac, an alcohol-based compound miscible in water. A shellac-impregnated sample of the Chagrin Member of the Upper Devonian Ohio Shale is shown in epifluorescence in Figure 7. This sample is from a depth of 2,170 ft (661 m) in Columbia Gas 20143 well, Gallia County, Ohio. Void spaces in the gray shale are visible both as small, isolated bright spots or pinpoint porosity, and as larger, glowing areas with silhouetted clay flakes in the foreground. Shales of this type generally have porosities of about 4% (Davies et al., 1989), and this sample has a measured permeability of about 1 μd at initial reservoir stress. Although successful impregnation was achieved with the shellac, it is not as hard as the epoxy and is more difficult to polish into a thin section.

Rhodamine impregnation of shales could be a useful tool for investigating relationships among shale fabric, pore structure, organic content, and depositional environment. Organic-rich black shales, which were depos-

ited in anoxic bottom environments, tend to be nonburrowed and possess a microfabric of parallel, oriented clay flakes, whereas organic-lean gray shales, which were bioturbated in aerobic environments, commonly exhibit jumbled, randomly piled clay flakes in their microfabrics (O'Brien, 1987). The degree of clay orientation has implications with respect to pore geometry, flow-path interconnectivity, and gas permeability (Davies et al., 1989) and is important in understanding the reservoir geology of Devonian gas shales. Ultrathin sections impregnated with fluorescent dye could provide data on shale pore structures complementary to that collected by SEM.

Other Applications

Studies of modern Cape Cod beach sand indicate that fluorescent-dye impregnation is useful for observing intragranular microporosity in individual sand grains. An example of this is shown in Figure 8, a feldspar-rich sand sample from Cape Cod. Formation of internal microporosity by weathering along twinned crystal boundaries in the center feldspar grain is apparent in epifluorescence (Figure 8B). The microcrystalline chert grain above the feldspar also shows porosity developed where individual crystals have been dissolved from the matrix. Observing and quantifying intragranular microporosity such as this is critical to modeling fluid flow through natural porous media, especially if diffusion or dispersion phenomena are important.

Igneous rocks also were impregnated with rhodamine-dyed epoxy to determine if crystalline rocks possess pore structures observable by this technique. Porosity in these kinds of rocks, although of little interest to most petroleum geologists, is important to geoscientists in the fields of nuclear and hazardous-waste disposal, where crystalline rocks are considered possible repository formations. Vesicular porosity was easily detected with epifluorescence in extrusive igneous rocks, such as basalt (Figure 9). A delicate weblike network of intercrystalline cracks can be seen connecting vesicles to one another and creating flow paths through the matrix. This basalt had measured porosity of about 5% and dry gas permeability of about 2 μ d. Successful impregnations also were obtained on diabase, welded tuff, gabbro, and granite (Soeder, 1988b). Although the granite had porosity of less than 0.6%, the network of pores noted by Kowallis and Wang (1983) in SEM studies of granites was clearly visible with fluorescent-dye impregnation.

SUMMARY AND CONCLUSIONS

Fluorescent rhodamine B dye can be used in epoxy impregnations of petrographic samples to enhance pore-structure visibility. When observed in thin section with a properly equipped incident-light microscope, rhodamine dye fluoresces strongly, creating a bright, high-contrast image in which only impregnated pores are visible. All other components, such as mineral grains, appear black.

Optimum image quality is obtained by using standard blue impregnation dye with rhodamine so that pores appear indigo/violet in transmitted light and glow reddish orange in epifluorescence. Another useful technique is staining the epoxy surface of a finished thin section with rhodamine dissolved in a solvent.

Advantages of rhodamine B over other fluorescent dyes include wide availability, relatively low cost, brilliant fluorescent response, and the fact that its excitation frequency is in visible light, so no expensive ultraviolet lenses are required. Disadvantages of rhodamine include its dry powder form and hydrophilic nature. Rhodamine is a slightly hazardous material but can be handled safely with common-sense laboratory precautions, such as gloves and lab coats.

Observation of rhodamine-impregnated pores can be done at minimum expense by adapting a universal-type microscope to epifluorescence with proper filters, beamsplitter, and illuminator. Photographing epifluorescent images can be done using conventional equipment with careful focusing and exposure.

IGT's experience indicates that epifluorescent-impregnation microscopy can be applied to rocks with small or cracklike pores, such as tight sandstones, and is particularly useful with opaque materials such as coal. Various pore features in tight rocks, such as slot pores or cracklike flow paths, microporosity, and changes in pore geometry under stress, which are not normally visible through an optical microscope, can be observed by using rhodamine-dye impregnation. Undoubtedly, other fields concerned with investigation of pore structures, such as ceramics and materials engineering, could benefit from this technology as well.

REFERENCES CITED

- Brower, K. R., and N. R. Morrow, 1985, Fluid flow in cracks as related to low-permeability gas sands: Society of Petroleum Engineers Journal, v. 25, p. 191-201.
- Cather, M. E., N. R. Morrow, and I. Klich, 1989, Applications of fluorescent dye staining techniques to reservoir studies of tight gas sands, Mesaverde Group, southwestern Colorado (abs.): AAPG Bulletin, v. 73, p. 342.
- Davies, D. K., W. R. Bryant, R. K. Vessell, and P. J. Burkett, 1989, Pore geometry and microfabrics of gas-bearing Devonian shales (abs.): AAPG Bulletin, v. 73, p. 348.
- Gies, R. M., 1987, An improved method for viewing micropore systems in rocks with the polarizing microscope: SPE Formation Evaluation, v. 2, p. 209-214.
- Kowallis, B. J., and H. F. Wang, 1983, Microcrack study of granitic cores from Illinois deep borehole UPH-3: Journal of Geophysical Research, v. 88, p. 7373-7380.
- O'Brien, N. R., 1987, The effects of bioturbation on the fabric of shale: Journal of Sedimentary Petrology, v. 57, p. 449-455.
- Randolph, P. L., D. J. Soeder, and P. Chowdiah, 1984, Porosity and permeability of tight sands, in Unconventional gas recovery symposium proceedings: Society of Petroleum Engineers, SPE Paper 12836, p. 57-66.
- , 1985, Effects of water and stress upon permeability to gas of paludal and coastal sands, U.S. DOE Multiwell Experiment: U.S. Department of Energy Report DOE/MC/20342-1838 (DE85008607), 199 p.
- Rose, R. E., and S. E. Foh, 1984, Liquid permeability of coal as a function of net stress, in Unconventional Gas Recovery Symposium Proceedings: Society of Petroleum Engineers, Paper SPE 12856, p. 253-260.

- Ruzyla, K., and D. I. Jezek, 1987, Staining method for recognition of pore space in thin and polished sections: *Journal Sedimentary Petrology*, v. 57, p. 777-778.
- Sax, N. I., 1984, *Dangerous properties of industrial materials*, 6th ed.: New York, Van Nostrand Reinhold, 1,251 p.
- Soeder, D. J., 1984, Reservoir properties and the pore structure of tight gas sands (abs.): *AAPG Bulletin*, v. 68, p. 530.
- 1988a, Porosity and permeability of eastern Devonian gas shale: *SPE Formation Evaluation*, v. 3, p. 116-124.
- 1988b, Laboratory measurements of permeability in igneous and pyroclastic rocks (abs.): *GSA Abstracts with Program*, v. 20, p. A310.
- and P. L. Randolph, 1987, Porosity, permeability, and pore structure of the tight Mesaverde sandstone, Piceance basin, Colorado: *SPE Formation Evaluation*, v. 2, p. 129-136.
- Wyman, R. E., 1984, Gas resources in Elmworth coal seams, in J. A. Masters, ed., *Elmworth case study of a deep basin gas field: AAPG Memoir 38*, p. 173-187.
- Yanguas, J. E., and J. J. Dravis, 1985, Blue fluorescent dye technique for recognition of microporosity in sedimentary rocks: *Journal of Sedimentary Petrology*, v. 55, p. 600-602.

APPENDIX 1

Materials Mentioned in This Paper and Their Suppliers

Maraglas® 655: 4-qt case of resin with appropriate quantity of 555 hardner	Registered trademark of Acme Chemicals & Insulation Co., P.O. Box 1404, New Haven, CT 06505; (203) 562-2171
Epo-Tech® 301-2: approximately 250 g of resin with hardner	Registered trademark of Epoxy Technology, Inc., 14 Fortune Drive, Billerica, MA 01821; distributed by Geoscience Resources, Inc., 2990 Anthony Road, Burlington, NC 27215; (919) 227-8300
Intraplast Brilliant Blue GN® : 2-lb can of powdered blue dye	Registered trademark of Crompton & Knowles Corp., 7535 Lincoln Avenue, Skokie, IL 60076; (312) 675-5510
Rhodamine B dye: 100-g bottle of powder, special for tungsten determination	Fisher Scientific Co., Chemical Manufacturing Division, Fair Lawn, NJ 07410; also available from Sargent-Welch, VWR Scientific, and other science supply houses; quantities and grades may vary
Teflon® tubing: registered trademark of E.I. Dupont de Nemours Company	Available from variety of suppliers, including Fisher Scientific Co., Chemical Manufacturing Division, Fair Lawn, NJ 07410

This list of supplies and their suppliers does not constitute an endorsement of these products by IGT, but is intended for information only.